UNIVERSIDADE FEDERAL DO RIO DE JANEIRO

LANA MONTEIRO MEUREN

Disfunção mitocondrial e produção de ROS induzidos pelo vírus da dengue em células endoteliais afetam a replicação viral, viabilidade celular e permeabilidade do endotélio

RIO DE JANEIRO
DEZEMBRO DE 2021

Lana Monteiro Meuren

DISFUNÇÃO MITOCONDRIAL E PRODUÇÃO DE ROS INDUZIDOS PELO VÍRUS DA DENGUE EM CÉLULAS ENDOTELIAIS AFETAM A REPLICAÇÃO VIRAL, VIABILIDADE CELULAR E PERMEABILIDADE DO ENDOTÉLIO

Tese de doutorado apresentado ao Programa de Pós-Graduação em Ciências (Microbiologia), Instituto de Microbiologia Paulo de Góes da Universidade Federal do Rio de Janeiro, como parte dos requisitos necessários à obtenção do título de Doutora em Ciências (Microbiologia).

Orientadora: Luciana Barros de Arruda
Coorientadora: Andrea Thompson Da Poian

RIO DE JANEIRO
DEZEMBRO DE 2021

Dedico esse trabalho

à minha família e amigos.

AGRADECIMENTOS

O desenvolvimento desta tese de doutorado contou com a ajuda de diversas pessoas, dentre as quais agradeço:

A minha orientadora, que durante esses 10 anos de trabalho, por sempre estar disponível para compartilhar sua sabedoria, ensinamentos, broncas e até mesmo os puxões de orelha. Não poderia de deixar de agradecer por toda empatia comigo durante esta pandemia, o caminho não foi fácil, mas graças a você, Lu, foi possível.

A minha coorientadora, pelas reuniões que tivemos, por deixar sempre seu laboratório de portas para mim e acima de tudo, pelos ensinamentos compartilhados.

A professora Luciana Costa, pela ajuda nesses anos de laboratório.

A turma do LAGIIVIR por todas as gargalhadas e discussões científicas.

Agradeço aos amigos Carolina Lucas, Michelle Papa, Natália Caetana, Pedro Gomes e Yasmin Mucunã pela amizade, pela companhia nos congressos, pelos conselhos, por toda ajuda que vocês sempre me proporcionaram dentro e fora do laboratório.

A professora Juliana Echevarria por aceitar revisar este trabalho.

Agradeço à banca avaliadora pela disponibilidade.

Agradeço também a minha família, aos meus pais e ao meu irmão, por sempre me apoiarem as minhas escolhas.

Ao meu avô, que sempre foi meu maior incentivador ao me chamar de doutora. - É Vô, finalmente este dia chegou.

Ao meu namorado Bruno, por ser estar ao meu lado e ser um porto seguro.

Aos meus amigos de faculdade Caroline e Levy que sempre estiveram ao meu lado durante esses anos de vida acadêmica.

As minhas amigas do Colégio Pedro II, Raíssa, Camila, Adriana e Vívian; e aos meus amigos de Jacarepaguá Brenda, Erick, Júlia e Kaique, por sempre estarem ao meu lado, mesmo quando eu preciso sumir para resolver algo da pós-graduação.

Ao Ronaldo pelo apoio técnico.

À todos que colaboraram para a execução deste trabalho.

Ao CNPq e FAPERJ, pelo suporte financeiro.

“O único homem que está isento de erros é aquele que não arrisca acertar”.

Albert Einstein

RESUMO

Meuren, Lana Monteiro. Disfunção mitocondrial e produção de ROS induzidos pelo vírus da dengue em células endoteliais afetam a replicação viral, viabilidade celular e permeabilidade do endotélio. Rio de Janeiro, 2021. Tese (Doutorado em Ciências - Microbiologia), Instituto de Microbiologia Paulo de Góes, Universidade Federal do Rio de Janeiro, Rio de Janeiro, 2021.

O aumento da permeabilidade vascular é descrito como um dos fatores de complicação da doença da dengue. A produção de espécies reativas de oxigênio induz mudanças na fisiologia celular e pode atuar como molécula sinalizadora para a morte celular. Nosso grupo já havia demonstrado que a infecção de células endoteliais com DENV resulta na ativação de sensores de RNA, produção de interferon e citocinas pró-inflamatórias, morte celular e permeabilidade. Também relatamos que a infecção por DENV promoveu a produção de ROS, mas a sinalização associada a este evento e suas consequências para a replicação do vírus e fisiologia das células endoteliais ainda não haviam sido investigadas. No presente estudo, avaliamos o papel da função mitocondrial e da ativação da NADPH oxidase (NOX) na produção de ROS e investigamos como esses mediadores afetam as células do endotélio microvascular cerebral humano (HBMEC) infectadas pelo vírus da dengue (DENV). Observamos que HBMECs infectadas com DENV2, com M.O.I. de 1 apresentam um aumento na produção de ROS de forma dependente de NAPH-oxidase e da via mitocondrial (mitROS). A fim de analisar o consumo de oxigênio, foi utilizado a respirometria de alta resolução e observado que a infecção por DENV nas HBMECs induziu uma diminuição da capacidade máxima respiratória. Além disso, nossos resultados mostraram alteração no potencial de membrana, indicando mudanças funcionais na mitocôndria, o que pode estar relacionado à produção de mitROS. Identificamos que a inibição específica de mitROS promoveu a diminuição da replicação do vírus, através de ensaio de plaque, e da morte celular verificada por citometria de fluxo. Por outro lado, a inibição da produção de ROS dependente de NOX inibiu a replicação do vírus, morte celular, aumento da permeabilidade, e a secreção de citocinas inflamatórias, incluindo IL-8 e CCL5. Esses dados indicam que a replicação do DENV em células endoteliais induziu a produção de ROS por diferentes vias. Desta forma, os eventos desencadeados pela produção de ROS estão associados à ativação endotelial e lesão vascular na infecção por DENV.

Palavras-chave: DENV, HBMECs, ROS, Mitocôndria, NADH oxidase, Morte celular

ABSTRACT

Meuren, Lana Monteiro. Disfunção mitocondrial e produção de ROS induzidos pelo vírus da dengue em células endoteliais afetam a replicação viral, viabilidade celular e permeabilidade do endotélio. Tese (Doutorado em Ciências - Microbiologia), Instituto de Microbiologia Paulo de Góes, Universidade Federal do Rio de Janeiro, Rio de Janeiro, 2021.

Increased vascular permeability has been described as one of the factors for dengue disease complication. Reactive Oxygen Species production induces changes in cell physiology and can act as signaling molecule for cell death. Our group had previously demonstrated that infection of endothelial cells with DENV results in the activation of RNA sensors, production of interferon and proinflammatory cytokines, cell death and permeability. We have also reported that DENV infection promoted ROS production, but the signaling associated to this event and its consequences for virus replication and endothelial cell physiology had not been investigated yet. In the present study, we evaluated the role of mitochondrial function and NADPH oxidase activation for ROS production and investigated how these mediators affected brain microvascular cells (HBMEC) infected by dengue virus (DENV). We observed that HBMECs infected with DENV2, with M.O.I. of 1 showed an increase in ROS production in a NAPH-oxidase and mitochondrial (mitROS)-dependent manner. A final analysis of oxygen consumption, high-resolution respirometry was used and observed that DENV infection in HBMECs induced a decrease in maximal respiratory capacity. Furthermore, our results in membrane potential, suggested that alteration in mitochondrial function, which may be related to mitROS production. We identified that the specific inhibition of mitROS promoted a decrease in virus replication, through plaque assay, and cell death verified by flow cytometry. On the other hand, inhibition of NOX-dependent ROS production inhibited virus replication, cell death, increased permeability, and the secretion of inflammatory cytokines, including IL-8 and CCL5. These data indicate that DENV replication in endothelial cells induced ROS production by different pathways. Thus, the events triggered by the production of ROS are associated with endothelial activation and vascular damage in DENV infection.

Keywords: DENV, HBMECs, ROS, Mitochondria, NADH oxidase, cell death

LISTA DE FIGURAS

Figura 1 - Distribuição mundial dos casos de Dengue. Em verde, está demarcado os países ou as áreas com risco de transmissão de dengue.	**1**
Figura 2 - Mapa da distribuição da taxa de incidência de dengue por município em 2020.	**2**
Figura 3 - Representação esquemática da partícula de DENV e sua organização genômica.	**3**
Figura 4 - Replicação dos Flavivirus.	**5**
Figura 5 - Reconhecimento dos vírus de RNA por sensores citoplasmáticos.	**11**
Figura 6 - Representação esquemática da ativação da via apoptótica através da ligação de receptores transmembranar.	**14**
Figura 7 - Indução de morte por apoptose através da ativação por capazes, via intrínseca.	**15**
Figura 8 - Ativação da NADPH oxidase. O complexo NADPH oxidase permanece em repouso quando as subunidades se encontram separadas.	**18**
Figura 9 - Cadeia transportadora de elétrons (STE).	**19**
Figura 10 - Reações catalisadas pelas enzimas Superoxido dismutase (SOD), catalase (CAT) e glutationa peroxidase (GPx), respectivamente.	**20**
Figura 11 - Ativação da via Nrf2 após indução do estresse oxidativo ocasionado por infecção viral.	**21**

Figura 12 - DENV induz aumento da produção de ROS em HBMECs.	**36**
Figura 13 - DENV não induz aumento da produção de ROS em tempos iniciais em HBMECs.	**37**
Figura 14 - Relação de ROS com replicação e morte celular.	**38**
Figura 15 - Avaliação da infecção viral e produção de ROS imunofluorência.	**39**
Figura 16 - A expressão de SOD não sofre alteração nos tempos iniciais da infecção.	**40**
Figura 17 - Curva de concentração de MitoTEMPO (MitoT) para determinar a concentração não tóxica em HBMECs.	**41**
Figura 18 - DENV induz aumento da produção de ROS em HBMECs via NADPH oxidade e via mitocôndria.	**42**
Figura 19 - DENV induz aumento na produção de mitROS em HBMECs.	**43**
Figura 20 - Análise da bioenergética mitocondrial em HBMECs infectadas com DENV.	**46**
Figura 21 - O aumento da produção de ROX dependente de NOX ocorre de forma independente.	**48**
Figura 22 - A inibição de ROS reduz a morte celular.	**49**
Figura 23 - A inibição de ROS reduz a replicação viral.	**50**
Figura 24 - DENV induz a autofagia em HBMECs.	**52**

Figura 25 - ROS parece ser importante na indução da autofagia.	**53**
Figura 26 - ROS mitocondrial está associado com o aumento da permeabilidade das HBMECs infectadas com DENV, mas o ROS produzido via NADPH-oxidase não está associada com este aumento.	**54**
Figura 27: O aumento na produção de ROS via NADPHox é essencial para a secreção de citocinas inflamatórias induzidas pela infecção por DENV em HBMECs.	**56**
Figura 28 - Confirmação do silenciamento de RIG-I.	**57**
Figura 29: O aumento na produção de ROS via mitocondrial pode acontecer de forma dependente de ativação de RIG-I.	**58**
Figura 30 - O aumento da produção de ROS pode ser importante para a ativação de RIG-I.	**58**
Figura 31 - A infecção por DENV em células endoteliais induz aumento na produção de ROS.	**66**

LISTA DE SIGLAS E ABREVIATURAS

A549	Linhagem celular carcinoma de pulmão humano
ADE	Potencialização mediada por anticorpos ("*Antibody-dependent enhancement*")
Apo	Apocininca
ATP	Trifosfato de adenosina
BHK	Linhagem celular de fibroblasto de *Mesocricetus auratus*
BSA	Albumina sérica bovina
C6/36	Linhagem celular da glândula do mosquito *Aedes albopictus*
CARD	Domínios de recrutamento e ativação de caspases
CAT	Catalase
CMC	Carboxi-metil-celulose
CO_2	Gás carbonico
DC-SIGN	Molécula ligada à adesão intercelular tipo 3 grambina não-ntegrina, do inglês "*Dendritic Cell-Specific Intercellular adhesion molecule-3-Grabbing Non-integrin*"
DENV	Vírus da dengue ("*Dengue virus*")
DHL	Enzima desidrogenase láctica

E	Glicoproteína do envelope viral
ECs	Células endoteliais
Fc	Porção constante da imunoglobulina (“*Fragment crystallizable*”)
FcgR	Receptores para porção Fc de imunoglobulinas
GPX	Glutationa peroxidase
GSH	Glutationa
h p.i.	Horas após infecção
H_2O_2	Peróxido de hidrogênio
HBMECs	Células do endotélio microvascular cerebral humano
HCV	Vírus da hepatite C
HepG2	Linhagem derivada de carcinoma hepatocelular humano
HUVEC	Células endoteliais da veia umbilical humana
IBqM	Instituto de Bioquímica Médica Leopoldo de Meis
ICAM	Moléculas de adesão
iDENV	Vírus da dengue inativado
IFN	Interferon

IKK	Complexo IkB quinase
IL-	Interleucina
LPS	Lipopolissacarídeo
M	Proteína de membrana viral
MAVS	Adaptador de sinalização antiviral mitocondrial
MDA-5	Gene 5 associado à diferenciação do melanoma, do inglês "*Melanoma differentiation-associates gene 5*"
MFI	Intensidade média de fluorêncencia
MitoT	MitoTEMPO
mitROS	ROS mitocondrial
Mock	Controle das condições de infecção viral sem a presença da partícula viral
MOI	Multiplicidade de infecção ("Multiplicity of infection")
NAC	N-Acetilcisteína
NAD-	Difosfopirido nucleótido
NADH	Dinucleótido de nicotinamida e adenina
NO	Óxido nítrico (NO)

NOX	NADPH oxidase
Nrf2	Fator de transcrição
NS	Proteína não estrutural (“*Nonstructural protein*”)
O_2-	Ânion de superóxido
OCR	Taxa de Consumo de Oxigênio
OH.	Radicais hidroxilas
Oligo	Oligomicina
OMS	Organização mundial de saúde
ORF	Fase aberta de leitura (“*Open Reading Frame*”)
PBS	Tampão fosfato-salino
PI	Iodeto de propídeo
PKR	Proteína quinase
prM	Receptores de reconhecimento padrão (“*Pattern recognition receptors*”)
PRR	Receptores de reconhecimento padrão (“*Pattern recognition receptors*”)
qRT PCR	PCR quantitativo (“*quantitative PCR*”)

RE	Retículo endoplasmático
RIG-I	Gene I induzido por ácido retinoico, do inglês "*Retinoic Acid-Inducible Gene 1*"
RLR-	Receptores do tipo RIG-I
RNAfd	RNA de fita dupla
RNAg	RNA genômico
RNAm	RNA mensageiro
RNS	Espécies reativas de nitrogênio
ROS	Espécies reativas de oxigênio
SFB	Soro fetal bovino
SOD	Superóxido dismutase
STS	Estaurosporina
TBK	"*TANK binding kinase*"
TLR-	"*Toll-like receptors*"
TNF-α	Fator de necrose tumoral ("*Tumor necrosis fator α*")
TRAIL	Ligante indutor de apoptose relacionado a TNF

TRIF	Adaptador contend domínio TIR inductor de interferon β (“*TIR-domain-containing adapter-inducing interferon-β*”)
U.I/L	Indica uma Unidade Internacional
UFRJ	Universidade Federal do Rio de Janeiro
UTR	Regiões não codificantes (“*Unstranlated Region*”)
UV	Ultravioleta

SUMÁRIO

RESUMO I

ABSTRACT II

LISTA DE FIGURAS III

LISTA DE SIGLAS E ABREVIATURAS VI

1. Introdução 1

1.1. Epidemiologia 1

1.2. Estrutura e Replicação do vírus da Dengue 2

1.3. Manifestações clínicas da dengue 5

1.2. Células endoteliais: função e papel em doenças inflamatórias e virais 8

1.2.1. Células endoteliais na dengue 8

1.3. Reconhecimento viral e seu papel na ativação e morte celular 10

1.4. Morte celular em resposta as infecções virais 12

1.4.1. Apoptose 12

1.4.2. Necroptose 16

1.5. Espécies Reativas de Oxigênio (ROS) 17

1.6. Produção de ROS em resposta a infecção viral 21

2. Racional 25

3. Objetivos 26

3.1. Objetivo Geral 26

3.2. Objetivos Específicos 26

3.2.1. Confirmar se a infecção por DENV induz a produção de ROS em HBMECs; 26

3.2.2. Caracterizar a via envolvida na produção de ROS por HBMECs infectadas por DENV, particularmente, avaliando o papel da ativação de NADPH oxidase e da mitocôndria no processo; 26

3.2.3. Avaliar a função e bioenergética mitocondrial em HBMECs infectadas com DENV; 26

3.2.4. Avaliar o papel de ROS na morte de células endoteliais induzida por DENV; 26

3.2.5. Avaliar o papel de ROS na replicação viral; 26

3.2.6. Avaliar o papel da produção de ROS e os fenômenos associados na permeabilidade endotelial; 26

3.2.7. Avaliar o papel da produção de ROS no aumento da produção de citocinas pró-inflamatórias e Interferon-β; 26

3.2.8. Investigar o papel da ativação da via RIG-I/MAVS na indução da produção de ROS. 26

4. Material e Métodos 27

4.1. Cultura de células 27

4.2. Vírus ... 27
4.3. Infecção de células endoteliais com DENV ... 28
4.4. Análise da replicação viral por ensaio de plaque e qRTPCR ... 28
4.5. Avaliação da produção de ROS por citometria de fluxo e por imunofluorescência ... 29
4.6. Determinação do consumo de oxigênio e caracterização dos parâmetros respiratórios ... 30
4.7. Análise da expressão de SOD, LC3, P62, pAKT e AKT durante a replicação do DENV ... 30
4.8. Avaliação da secreção de citocinas por ELISA ... 31
4.9. Avaliação da expressão de RNAm de IFN-β por qRT PCR ... 31
4.10. Avaliação da viabilidade celular por ensaio de metabolização de XTT ... 32
4.11. Avaliação da viabilidade celular por citometria de fluxo ... 32
4.12. Análise da viabilidade celular pela medida de atividade da enzima lactato desidrogenase (LDH) ... 33
4.13. Avaliação do papel de ROS na permeabilidade de células endoteliais ... 33
4.14. Análise da ativação da via RIG-I na indução da produção de ROS ... 33
4.15. Análise estatística ... 34
5. Resultados ... 36
5.1. Avaliação da produção de ROS durante a infecção por DENV em células HBMECs ... 36
5.2. Avaliação da expressão de enzimas antioxidantes ... 40
5.3. Caracterização da fonte de geração de ROS ... 41
5.4. Confirmação que a infecção por DENV induz produção de ROS mitocondrial em HBMECs ... 42
5.5. Avaliação da bioenergética mitocondrial e do potencial da membrana ... 44
5.6. Avaliação entre a relação da produção de ROS total e de mitROS ... 47
5.7. A inibição das principais vias de produção de ROS reduzem a morte celular. ... 48
5.8. A inibição das principais vias de produção de ROS reduzem a replicação viral. ... 50
5.9. A infecção por DENV induz autofagia em HBMECs, que pode ser regulada por ROS ... 51
5.10. Indução de ROS mitocondrial por DENV induz permeabilidade de HBMECs ... 53
5.11. ROS via NADPHox é essencial para a secreção de citocinas inflamatórias induzidas durante a infecção de HBMECs por DENV ... 55
5.12. Ativação de RIG-I pode ser importante para induzir o aumento de ROS ... 56
6. Discussão ... 59
7. Conclusões ... 67
8. Referências Bibliográficas ... 68
9. Anexos ... 84

1. Introdução

1.1. Epidemiologia

Atualmente, a Dengue é uma das mais importantes doenças tropicais do mundo e estima-se que cerca de 390 milhões de pessoas sejam infectadas pelo vírus da Dengue (DENV) anualmente (Guzman *et al*., 2016; Teixeira *et al*., 2013). Além disso, cerca de 40% da população mundial vive em áreas consideradas de risco de infecção por DENV e, nas últimas 5 décadas, o número de casos teve um aumento de 30 vezes globalmente (OMS, 2017) (Figura 1). A transmissão ocorre por mosquitos vetores do gênero Aedes, principalmente pelo *Aedes Stegomyia aegypti* e *Aedes alpopictus* (Ferreira-de-Lima, e Lima-Camara, 2018).

Figura 1: Distribuição mundial dos casos de Dengue. Em verde, estão demarcados os países ou as áreas com risco de transmissão de dengue (Adaptado OMS, 2015).

A dengue é endêmica no Brasil, que apresenta co-circulação dos 4 sorotipos virais (Figura 2). Em 2020, foram registrados 979.764 casos prováveis, com a taxa de incidência de 466,2 casos por 100 mil habitantes (Ministério da Saúde, 2020). Até outubro de 2021 foram notificados 477.209 casos prováveis, com a taxa de incidência de 223,7 casos de dengue por 100 mil habitantes no Brasil (Ministério da Saúde, 2020).

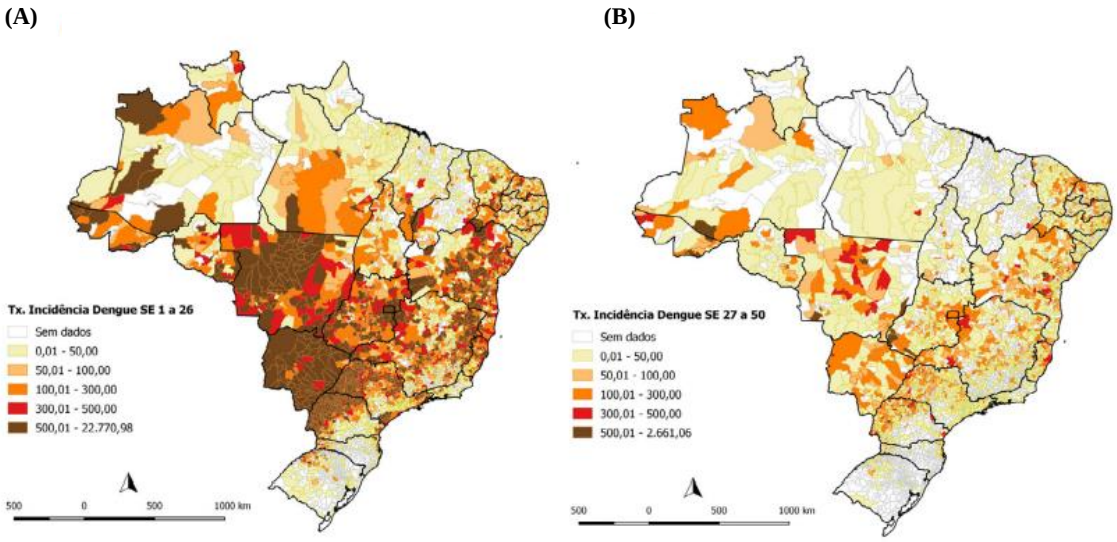

Figura 2: Mapa da distribuição da taxa de incidência de dengue por município em 2020. (A) SE 1 a 26. (B) 27 a 50 (Ministério da Saúde, 2020).

1.2. Estrutura e Replicação do vírus da Dengue

O vírus da dengue pertence à família Flaviviridae e ao gênero *Flavivirus*. Foram descritos 4 sorotipos, nomeados de DENV 1-4 (Guzman *et al*., 2010). O vírus é envelopado e possui cerca de 50 nm de diâmetro (Kuhn *et al*., 2002). No envelope viral estão inseridas as glicoproteínas E e M. O capsídeo do DENV dispõe de um formato icosaédrico formado pela proteína C e pelo genoma, que é constituído de fita simples de RNA, polaridade positiva e com 11kb, aproximadamente. O RNA genômico possui apenas uma fase aberta de leitura (ORF), flanqueada por regiões não codificantes (UTR), apresenta na extremidade 5’ a 5-metil guanosina (CAP), mas não apresenta a extremidade 3’ poliadenilada (HARRIS *et al*., 2006). O genoma codifica uma única poliproteína, que ao ser clivada forma 10 proteínas virais, sendo 3 estruturais - capsídeo (C), envelope (E) e de membrana (M), e 7 proteínas não estruturais - NS1, NS2A, NS2B, NS3, NS4A, NS4B e NS5 (Mukhopadhyay, Kuhn e Rossmann, 2005) (Figura 3)

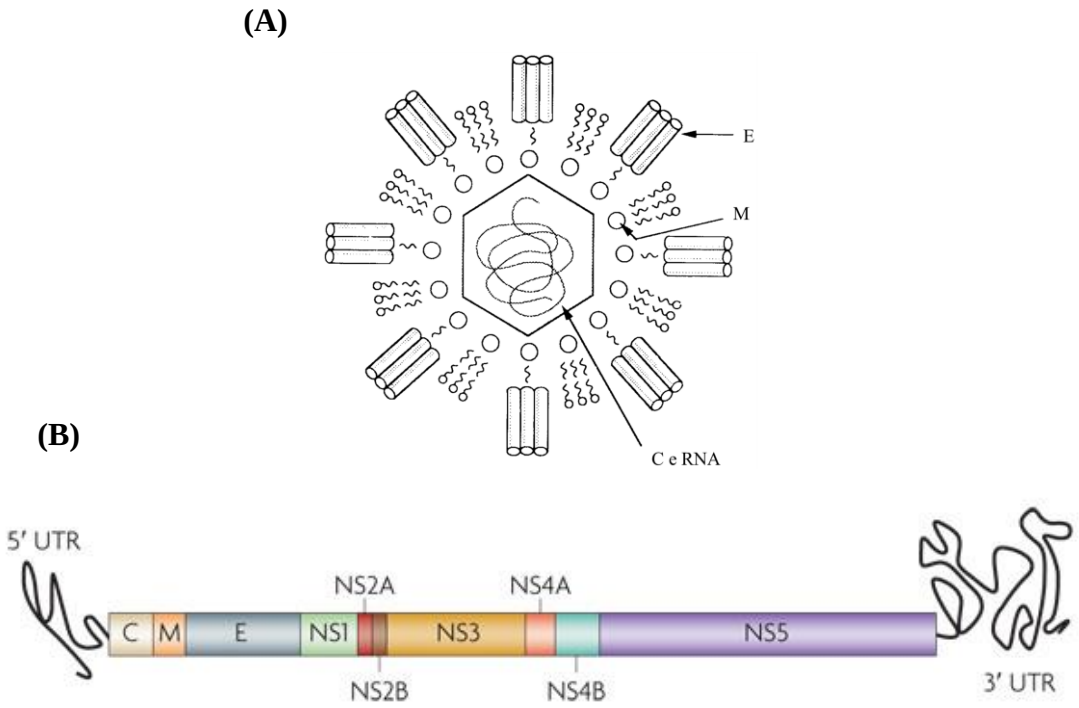

Figura 3: Representação esquemática da partícula de DENV e sua organização genômica. (A) Partícula viral madura. Proteína do envelope - E, Proteína de membrana- M e proteína do Core - C. (B) Genoma viral com 5' CAP, a região de proteínas estruturais e as regiões codificantes de proteína não estrutural e a região 3' UTR (Guzman *et al*., 2010; Henchal e Putnak, 1990).

Para que haja infecção de uma célula-alvo, a proteína E do vírus precisa se ligar a alguns tipos de receptores celulares, tais como: heparan sulfato, receptor de manose, e DC-SIGN (CD209, receptor de lectina do tipo C) (Shah *et al*., 2013), dependendo do tipo celular (Pereira e Kuhn, 2008; Hidari e Suzuki, 2011). Após a ligação, o vírus entra na célula hospedeira por endocitose de forma dependente de clatrina (Acosta *et al*., 2008; Peng *et al*., 2009). Em seguida, há uma acidificação do meio intraendossomal e a proteína E sofre um processo de trimerização, que promove a fusão entre a membrana do endossomo e a membrana do envelope viral (Mukhopadhyay *et al*., 2005; Zheng *et al*., 2010). Após a fusão, o nucleocapsídeo sofre desnudamento no citoplasma, levando a liberação do RNA genômico (RNAg). Como o DENV é um vírus de RNA fita simples polaridade positiva, este RNA mensageiro (RNAm) é traduzido, formando uma única poliproteína, que sofre clivagem por proteases virais e celulares posteriormente (Shiryaev *et al*., 2007).

A replicação do vírus só acontece após a liberação das proteínas estruturais e não estruturais a partir da clivagem da poliproteína. Assim, se forma o complexo de replicação viral,

a partir da interação das regiões complementares da região 3’ UTR com 5’ UTR e a circularização do RNAg (Filomatori *et al*., 2011). A RNA polimerase dependente de RNA se associa à extremidade 5’ do genoma e pode ser deslocada em direção a região 3’ UTR. Desta forma, o RNA viral é usado como molde para a formação do RNA de fita simples negativo, formando o intermediário de RNA dupla fita (RNAfd) (Murray *et al*., 2008). O RNA fita simples polaridade negativa serve como o molde para a formação de RNA fita simples polaridade positiva (Friebe e Harris, 2010). A formação desses RNA fita simples polaridade positiva possibilita a síntese de novas poliproteínas ou a formação de novos genomas virais (Schmaljohn e Mcclain, 1996).

Com a realização desses processos, a montagem da partícula viral pode ser iniciada. A montagem dos vírions ocorre no retículo endoplasmático (RE) (Sampath e Pasmanabhan, 2009) com montagem do nucleocapsídeo (NC). Em seguida, ocorre o brotamento do nucleocapsídeo para o lúmen do retículo, sendo adicionado a proteína de envelope (E) e a proteína precursora de membrana (prM) (Wengler e Wengler, 1989). A proteína prM é, então, clivada por proteases do hospedeiro e a liberação da partícula viral madura ocorre por exocitose (Clyde, Jennifer e Harris, 2006) (Figura 4).

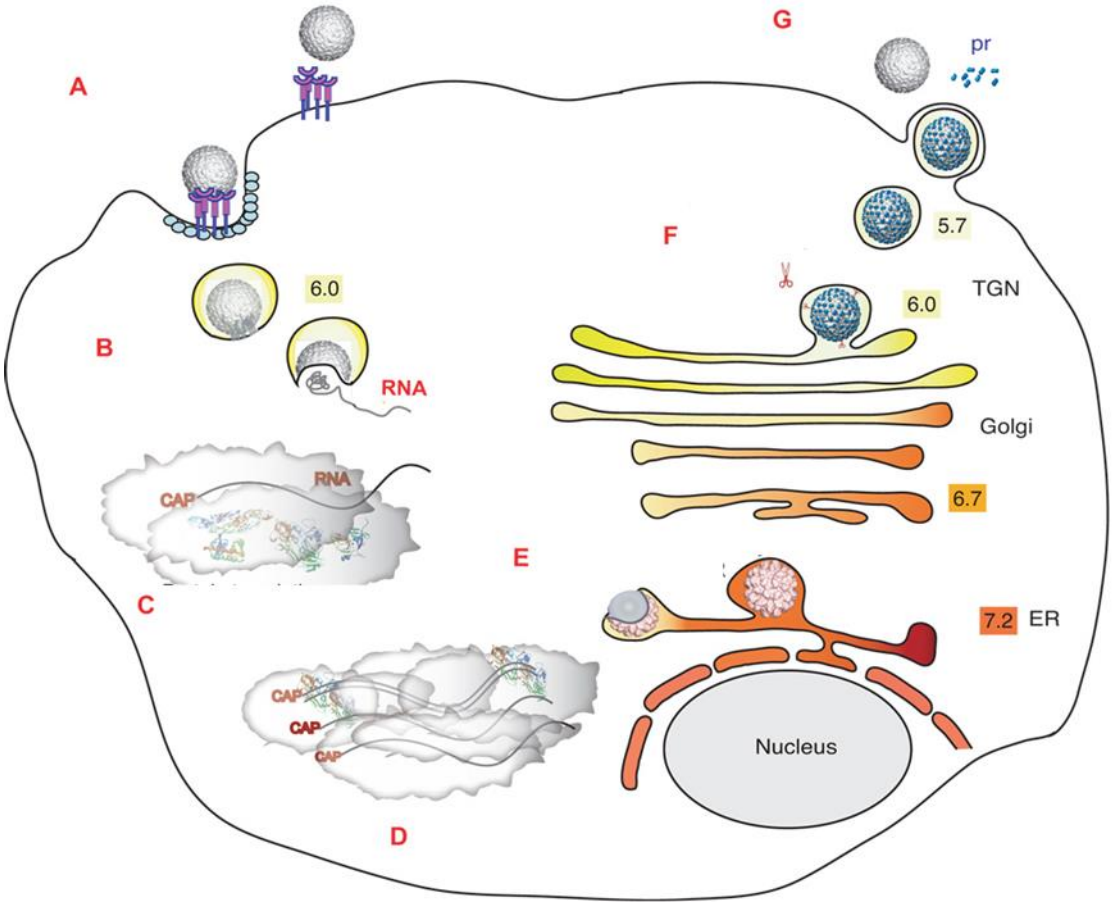

Figura 4: Replicação dos Flavivirus. A- Adsorção e endocitose; B- Fusão do envelope viral com a membrana da vesícula e, em seguida, liberação do nucleocapsídeo e desnudamento do ácido nucleico; C- Tradução da poliproteína e endereçamento para o RE; D- Replicação do genoma; E- Montagem das partículas virais no RE e aquisição do envelope e manutenção da forma viral e transporte por vesículas; F- Maturação; G- Liberação da partícula viral infecciosa (Sampath e Padmanabhan, 2009).

1.3. Manifestações clínicas da dengue

A dengue é uma doença com amplo espectro clínico e é considerada autolimitante na maioria dos indivíduos (Malavige e Ogg, 2017). A infecção pode ser assintomática, branda (anteriormente chamada dengue clássica), ou evoluir para formas graves (anteriormente chamadas de febre hemorrágica ou síndrome do choque da dengue) (Lee *et al*, 2016; Fernando *et al*, 2016). Atualmente, a OMS classifica a doença como: dengue com presença ou ausência de sinais de alerta e dengue grave. A doença é considerada grave, quando há pelo menos uma das seguintes manifestações: disfunção grave de órgãos, ou sangramento grave, ou extravasamento de plasma que pode levar ao choque (OMS, 2009). Os pacientes com dengue podem progredir através de três fases clínicas conhecidas como: fase febril, fase crítica e fase

de recuperação (Malavige e Ogg, 2017). Os sintomas da dengue clássica são relativamente brandos e são caracterizados por febre, cefaleia, anorexia, náuseas, dor retroorbital, mal-estar, congestão conjuntival, dor lombossacral, prostração, sensação de paladar alterado, podendo ocorrer erupção maculopapular. Na maioria dos indivíduos, esses sintomas duram de 2-7 dias, após os quais há recuperação (OMS, 2017; Malavige e Ogg, 2017). No entanto, alguns indivíduos após a fase febril, entram em uma fase crítica, que dura 24 a 48 horas, e está associada à plaquetopenia, aumento da permeabilidade vascular, extravasamento de plasma e hipotensão, podendo evoluir e desenvolver as formas graves da doença. A dengue grave está, então, associada a um aumento transitório da permeabilidade vascular, e extravasamento de plasma, resultando em acúmulo de líquido nas cavidades pleurais e peritoneais, hipotensão, podendo levar ao choque e óbito (Malavige e Ogg, 2017; Lei *et al*., 2001).

A doença é multifatorial e diversos mecanismos têm sido associados ao seu agravamento (Carvalho e Moreira, 2017). Dentre esses, a dengue grave já foi associada a fatores genéticos virais como o sorotipo e o genótipo viral, e fatores do hospedeiro, como a idade e o estado imune dos indivíduos infectados (Carvalho e Moreira 2017; Clyde, Jennifer e Harris, 2006). A infecção por um sorotipo confere imunidade a longo prazo somente contra aquele próprio sorotipo (Henchal, Henchal e Schlesinger, 1988). Entretanto, pode ocorrer uma resposta inespecífica contra os demais. Assim, a teoria do "pecado antigênico original" sugere que as células T de memória produzidas durante a infecção primária possam reagir, durante uma infecção secundaria, de forma mais imediata, mas com menos eficácia quando comparadas as células *naive*, o que resultaria em uma resposta imune ineficiente e com produção desregulada de citocinas (Mongkolsapaya *et al*., 2006). Outra hipótese é a da teoria da potencialização da infecção dependente de anticorpos (ADE). Segundo essa teoria, durante uma infecção secundária anticorpos neutralizantes produzidos a partir da primeira infecção reagem com os vírus da segunda infecção. Apesar disso, a neutralização não ocorre de forma eficiente, o que resultaria no aumento da circulação de imunocomplexos (Halstead *et al*., 1970; Haltead *et al*., 1976). A formação desses imunocomplexos facilitaria a entrada do vírus, inclusive de vírus imaturos que são formados durante a infecção em células do hospedeiro, que expressam receptores para porção Fc das imunoglobulinas (FcgR), como monócitos e macrófagos, resultando em maior replicação viral (Haltead *et al*., 1976).

Todavia, essas hipóteses não suportam todas as ocorrências observadas na dengue. Além disso, há casos de complicações em infecções primárias em crianças e em adultos (Clyde,

Jennifer e Harris, 2006), indicando a possibilidade de outros processos estarem relacionados à gravidade da doença.

Um fator preponderante na patogênese da dengue é a intensa resposta inflamatória com produção de mediadores, que atuam sobre o endotélio e contribuem para o aumento da permeabilidade vascular (Commins, Borish e Steinke, 2010). Foi amplamente demonstrado que os soros obtidos de pacientes com manifestação grave da doença apresentam níveis mais elevados de IFN-γ (Interferon gama), TNF-α (Fator de necrose tumoral), IL-2 (Interleucina-2), IL-10 (Interleucina-10), IL-6 (Interleucina-6), IL-8 (Interleucina-8), CCL5 e VEGF-α (Phanthanawiboon *et al*., 2016, Povoa *et al*., 2016; Zhao, *et al*., 2016; Her *et al.*, 2017; Chen *et al*., 2006). Acredita-se que o aumento dessas citocinas e quimiocinas ocorra, principalmente, devido à indução da sua produção por monócitos e macrófagos infectados (Borish e Steinke, 2003; Medin *et al.*, 2005). Por outro lado, estudos mostraram que hepatócitos e células endoteliais (EC) são também permissivos ao DENV, cuja a infecção poderia contribuir com o processo inflamatório, através da produção de quimiocinas e citocinas. Esses mediadores podem contribuir para o recrutamento de células inflamatórias e atuar sobre o próprio endotélio, colaborando para a lesão endotelial (Her *et al*., 2017; Nasirudeen *et al*., 2011; Conceição *et al*., 2013).

Outro fator importante descrito para a patogênese da dengue foi a própria proteína viral NS1. Experimentos *in vitro* demonstraram que níveis elevados de NS1 purificada ativam diretamente macrófagos de camundongos e células mononucleares do sangue periférico humano (PBMC). Esse fenômeno ocorre através do receptor Toll-like (TLR-4), culminando na produção de citocinas proinflamatórias e quimicionas. Além disso, ainda foi observado que o tratamento com NS1 resultou no aumento de permeabilidade de culturas de ECs *in vitro* (Modhiran *et al*., 2015; Beatty *et al*., 2015). Esses estudos mostraram que esses efeitos são dependentes do reconhecimento do receptor do tipo TLR-4, mas não de TLR-2 e TLR-6, o que tem sido comparado com o choque séptico induzido por lipopolissacarídeo (LPS) (Modhiran *et al*., 2015; Modhiran *et al*., 2017).

Finalmente, a própria infecção de células endoteliais pode contribuir para a lesão vascular, com aumento de permeabilidade e extravasamento de plasma, como será discutido a seguir.

1.2. Células endoteliais: função e papel em doenças inflamatórias e virais

As células endoteliais revestem os vasos sanguíneos formando uma barreira com permeabilidade baixa e seletiva para fluidos e solutos em condições fisiológicas normais (Félétou, 2011; Baldwin e Thurston, 2001). A desregulação da barreira endotelial pode ocorrer devido à uma variedade de fatores como agentes inflamatórios, trombose, traumatismo, bem como durante uma infecção por agentes infecciosos (Yuan e Rigor, 2018).

As células endoteliais representam também um elemento crítico no desenvolvimento de uma resposta inflamatória porque quando ativadas, aumentam a expressão de moléculas de adesão como VCAM-1, ICAM-1 e E-selectina. O aumento dessas moléculas pode ser responsável por recrutar leucócitos para a região da infecção, levando a potencialização da resposta inflamatória (Anderson *et al*., 1997; Cardier *et al*., 2005; Peyrefitte *et al*., 2006; Conceição *et al*., 2013).

1.2.1. Células endoteliais na dengue

O aumento da permeabilidade vascular é um dos principais fatores associado a patogênese da dengue, e uma série de evidências sugere que esse aumento pode ser consequência da ação de mediadores inflamatórios e/ou vasoativos produzidos, principalmente, por monócitos. Estudos clínicos demonstraram o aumento de TNF-α, IL-1β e IFN- α em pacientes que possuem a forma grave da doença (Azeredo *et al*., 2001; Suharti *et al*., 2003). Além disso, também já foi descrito que monócitos infectados *in vitro* com DENV produzem esses mesmos mediadores inflamatórios e que eles atuam sobre o endotélio contribuindo com a lesão vascular (Espina *et al*., 2003; Carr *et al*., 2003). Em um modelo de infecção murina com DENV-3 foi demonstrado que os animais apresentavam grande aumento de TNF-α, IL-6 e MCPI, associados a um aumento na permeabilidade vascular, sinais hemorrágicos, lesão hepática e intestinal e morte (Phanthanawiboon *et al*., 2016). O tratamento dos camundongos com um anticorpo anti-TNF-α murino reduziu os níveis plasmáticos de citocinas e os danos hepáticos, mas não afetou a carga viral. Por outro lado, o tratamento com angiopoietina recombinante, molécula que inibe o extravasamento vascular, retardou a morte dos animais. Esses achados sugerem que a inflamação e a lesão hemorrágica se somam no desenvolvimento da patogênese da dengue grave (Singh *et al*., 2018; Ong, Ng, Chu, 2013).

Como já mencionado, além do impacto de mediadores inflamatórios circulantes, a própria infecção do endotélio pode contribuir para a lesão vascular. Tem sido largamente demonstrado que linhagens de células endoteliais e células endoteliais primárias são permissivas ao DENV em modelos *in vitro* (Avirutnan *et al*., 1998; Basu *et al*., 2011; Conceição *et al*., 2013; Bunyaratvej *et al*., 1997; Huang *et al*., 2000; Arevalo *et al*, 2009; Dalrymple e Mackow 2011), e *in vivo* (Kyle *et al*., 2008; Zellweger, Prestwood e Sheresta, 2010). Além disso, análises *post-mortem* detectaram presença de vírus nas células endoteliais em diferentes tecidos de pacientes infectados com DENV (Jessie *et al*., 2004; Kyle *et al*., 2008; Povoa *et al*., 2014). Análises de autópsias evidenciaram apoptose de células endoteliais em diferentes tecidos (Ramos *et al*., 1998; Limonta *et al*., 2007) e pontos de necrose próximos a vasos sanguíneos (Povoa *et al*., 2016; Limonta *et al*., 2007). Esses achados sugerem que a morte de células endoteliais pode ser um dos elementos envolvidos no aumento da permeabilidade vascular observada na doença.

A ativação das células endoteliais está associada principalmente, com o reconhecimento viral e ativação de receptores de reconhecimento padrão (PRR). A ativação de RIG-I, MDA-5 e TLR-3 por DENV foi demonstrada em células mielóides, hepáticas e células endoteliais, sendo associada à liberação de citocinas pró-inflamatórias como: IL-1β, IL-6, IL-8, IFN e TNF-α (Loo *et al*., 2008; Tan e Chu, 2013; Conceição *et al*., 2013). Além disso, o vírus da dengue reduz a expressão de proteínas de junções como a ZO-1, Claudina-1, PECAM-1 e VE-caderina em células endoteliais, o que também contrubui para as alterações de permeabilidade do tecido, ainda que não haja morte celular (Soe *et al*., 2017).

Dados do nosso grupo mostraram que as células do endotélio microvascular cerebral humano (HBMECs) são permissivas ao DENV. Essa infecção induziu o aumento de expressão de sensores de RNA fita dupla citoplasmáticos: RIG-I (Gene I induzido por ácido retinóico) e MDA-5 (Gene 5 associado à diferenciação do melanoma) o que está relacionado com o aumento da produção de IFN-β (Interferon-β), IL6, IL8, CCL5, e da expressão de ICAM (Conceição *et al*., 2013). Também foi observado pelo nosso grupo que a infecção de HBMECs por DENV leva a morte celular, associada a perda de integridade da membrana plasmática, e consequentemente, induz aumento na permeabilidade das monocamadas celulares (Papa, 2014). Dados preliminares do nosso grupo sugeriram que células *bystander* presentes nas culturas com DENV apresentaram maior taxa de morte celular em relação às células infectadas. A morte das células *bystander* foi inibida ou retardada, parcialmente, pela adição de inibidores

de RIPK1 (Proteína cinase de interação com o receptor 1), sugerindo a indução de necroptose nessas culturas (Papa, 2014).

1.3. Reconhecimento viral e seu papel na ativação e morte celular

A ativação celular e as respostas de estresse em células infectadas por vírus podem ser geradas pela detecção de macromoléculas virais; incluindo o próprio genoma viral, intermediários de fita dupla de RNA e proteínas virais. Essa detecção ocorre através de receptores de reconhecimento de padrões (PRRs). O engajamento desses leva ao recrutamento de moléculas adaptadoras, que culmina na estimulação de fatores de transcrição, consequentemente, induzindo a expressão de IFN do tipo I e citocinas pró-inflamatórias (Chang *et al.,* 2006; Kato *et al*., 2006; Boo e Yang, 2010; Muñoz-Jordán e Fredericksen, 2010).

Os vírus de RNA podem ser reconhecidos por diferentes tipos de PRRs, incluindo sensores de RNA citossólicos ou endossomais. A ativação do receptor endossomal TLR3 inicia após o reconhecimento de moléculas de RNAs de fita dupla em vesículas endossomais. Esse reconhecimento induz uma via de transdução de sinal que se inicia pelo recrutamento da molécula adaptadora contento domínio TIR indutor de IFN-β (TRIF). Esse recrutamento induz a ativação de TBK (*TANK binding kinase*) e do complexo IkB cinase (IKK), que culmina na ativação de IRFs (*Interferon regulatory transcription factor*) e NF-kB (Fator de transcrição), respectivamente. O complexo formado é translocado para o núcleo, ativando a transcrição de genes e produção de mediadores (Valadão, 2016).

Os sensores citoplasmáticos RIG-I e MDA5 reconhecem moléculas de RNAfd no citoplasma celular. Esse reconhecimento provoca uma alteração conformacional nesses receptores com a exposição do domínio CARD (Domínios de recrutamento e ativação de caspases), permitindo o recrutamento da proteína adaptadora MAVS (Proteína de sinalização mitocondrial antiviral). Esse recrutamento proporciona uma cascata de sinalização com a fosforilação e translocação dos fatores de transcrição IRF-3 e de IRF-7 do citoplasma para o núcleo, induzindo a expressão de IFN do tipo I (YU *et al*., 2012; Chen *et al*., 2013; Zeng e Chen, 2008). A ativação desses sensores propicia a produção de citocinas proinflamatórias e quimiocinas, como IL-6, IL-8, TNF- α e CCL5. Esses mediadores induzem o recrutamento e a ativação de outros tipos celulares, amplificando a inflamação (Figura 5) (He *et al*., 2011; O' Leary *et al*., 2012; Lucas e Maes, 2013).

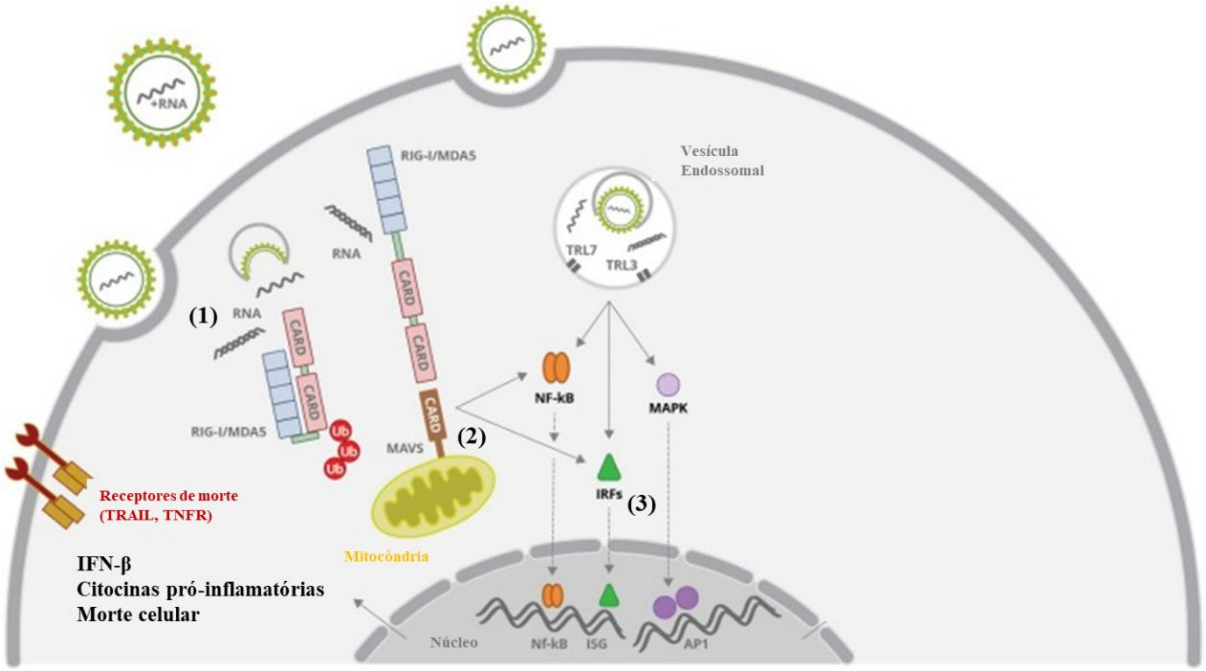

Figura 5: Reconhecimento dos vírus de RNA por sensores citoplasmáticos. (1) Sensores citoplasmáticos RIG-I e MDA5 reconhecem o intermediário RNAfd no citoplasma, (2) após este reconhecimento ocorre uma alteração conformacional, o que expõe o domínio CARD (Domínios de recrutamento e ativação de caspases) e consequentemente o recrutamento da proteína adaptadora MAVS. (3) Esse recrutamento, resulta em uma cascata de sinalização o que induz a translocação dos fatores de transcrição IRF-3 e de IRF-7 do citoplasma para o núcleo, induzindo a expressão de IFN do tipo I, citocinas proinflamatórias e quimiocinas como IL-6, IL-8, TNF- α e CCL5 (Adaptado. Valadão *et al*., 2016).

A ativação desses fatores também está associada com a indução de sinais de morte celular. A ativação de IRF-3 via RIG-I estimula uma série de genes relacionados com a apoptose (Chattopadhyay *et al*., 2010). A ativação de RIG-I em hepatócitos infectados com o vírus da Hepatite C (HCV) também induziu apoptose dependente de TRAIL (Ligante indutor de apoptose relacionado a TNF) (Yang *et al*., 2011). Estudos em linhagens de fibroblastos e em células endoteliais mostraram que a ativação via TLR3 induz morte celular de forma dependente de TRIF (Kaiser *et al*., 2013). E, a ativação de células dendríticas com poli I:C, mimetizando ativação por RNAfd, levou a morte celular por necroptose, de forma dependente de MAVS (Zou *et al*., 2013).

1.4. Morte celular em resposta as infecções virais

O processo de biossíntese viral altera diretamente o metabolismo celular; assim, uma infecção viral pode gerar respostas de estresse na célula hospedeira buscando recuperar a homeostase celular (Fernandez-Garcia *et al*., 2009). Para que ocorra essa recuperação, a célula induz respostas como inibição transitória da síntese de proteínas, estresse de retículo endoplasmático, alteração da função mitocondrial e produção de espécies reativas de oxigênio (ROS) (Valadão, 2016). Entretanto, a manutenção desses estímulos pode ocasionar a morte dessas células. Por outro lado, os vírus precisam de mecanismos de escape ou retardo da indução de morte celular, para permitir que ocorra a replicação viral.

As três vias de morte celular melhor caracterizadas são: apoptose, necrose e piroptose. Entretanto, nas últimas décadas, diferentes mecanismos de morte celular têm sido descritos, incluindo, necroptose, morte por abertura de poro de transição de permeabilidade mitocondrial (MPTP), NETose, pironecrose e piroptose (Kist e Vucic, 2021; D'Arcy, 2019; Nirmala e Lopus, 2020). Além dessas vias de morte celular, a autofagia, estratégia que normalmente é responsável pela garantia da sobrevivência da célula, também pode induzir a morte celular por mecanismos como a autose (Kist e Vucic, 2021; D'Arcy, 2019; Nirmala e Lopus, 2020). Os estudos vêm ressaltando que dificilmente essas vias funcionam sozinhas, pois as evidências experimentais apontam que muitas vias compartilham componentes e princípios de sinalização.

1.4.1. Apoptose

Apoptose morfologicamente é caracterizada pela compactação do núcleo e condensação da cromatina, seguidos de fragmentação do DNA. Assim, as células se dividem em pequenos corpos apoptóticos, que contém componentes nucleares e organelas citoplasmáticas. Durante o período inicial desse processo, observa-se a preservação da integridade estrutural e funcional da membrana plasmática e preservação dos lisossomos (Darzynkiewicz *et al*., 1997). Ainda durante essa fase inicial, ocorre mobilização de cálcio intracelular, desorganização de fosfolipídeos, diminuição de microtúbulos, em conjunto, esses fatores permitem a exposição da fosfatidilserina (PS) na superfície extracelular (Orzalli e Kagan, 2017; Barnaba, 2013; Elmore, 2007).

A indução de apoptose depende da ativação das caspases, que são proteases aspartato-específicas. Inicialmente, essas caspases são produzidas em uma forma inativa, chamada de

pró-caspases e se tornam ativas após sua clivagem (Orzalli e Kagan, 2017, Boathight e Salvesen, 2003). Atualmente, em mamíferos, já foram descritos 12 tipos de caspases, que são divididas em 2 grupos: caspases iniciadoras (caspases -1, -2, -4, -5, -8, -9, -10, -11, -12) e caspases efetoras (-3, -6, -7). A indução da apoptose pode estar associada à um mecanismo de defesa celular durante infecções virais, uma vez que a morte da célula infectada contribuiria para o controle da disseminação viral (Fan *et al*., 2014).

A apoptose extrínseca, ou também conhecida como "via do receptor de morte" é ativada por sinais externos a célula. Esses sinais contemplam radicais livres, agentes químicos, biológicos ou físicos, que são capazes de interagir e estimular receptores que estão presentes na superfície celular (Lavrik, Golks e Krammer, 2005). Os receptores celulares responsáveis pela indução da morte celular pertencem a família transmembrana do tipo I, podendo ser: fator de morte tumoral 1 (TNFR1), Fas (CD95), DR3, receptor relacionado ao ligante indutor de apoptose TNF 1 (TRAILR1), TRAILR2, DR6, receptor ectodisplasina A (EDAR) e receptor do fator de crescimento do nervo (Figura 6) (Lavrik, Golks e Krammer, 2005).

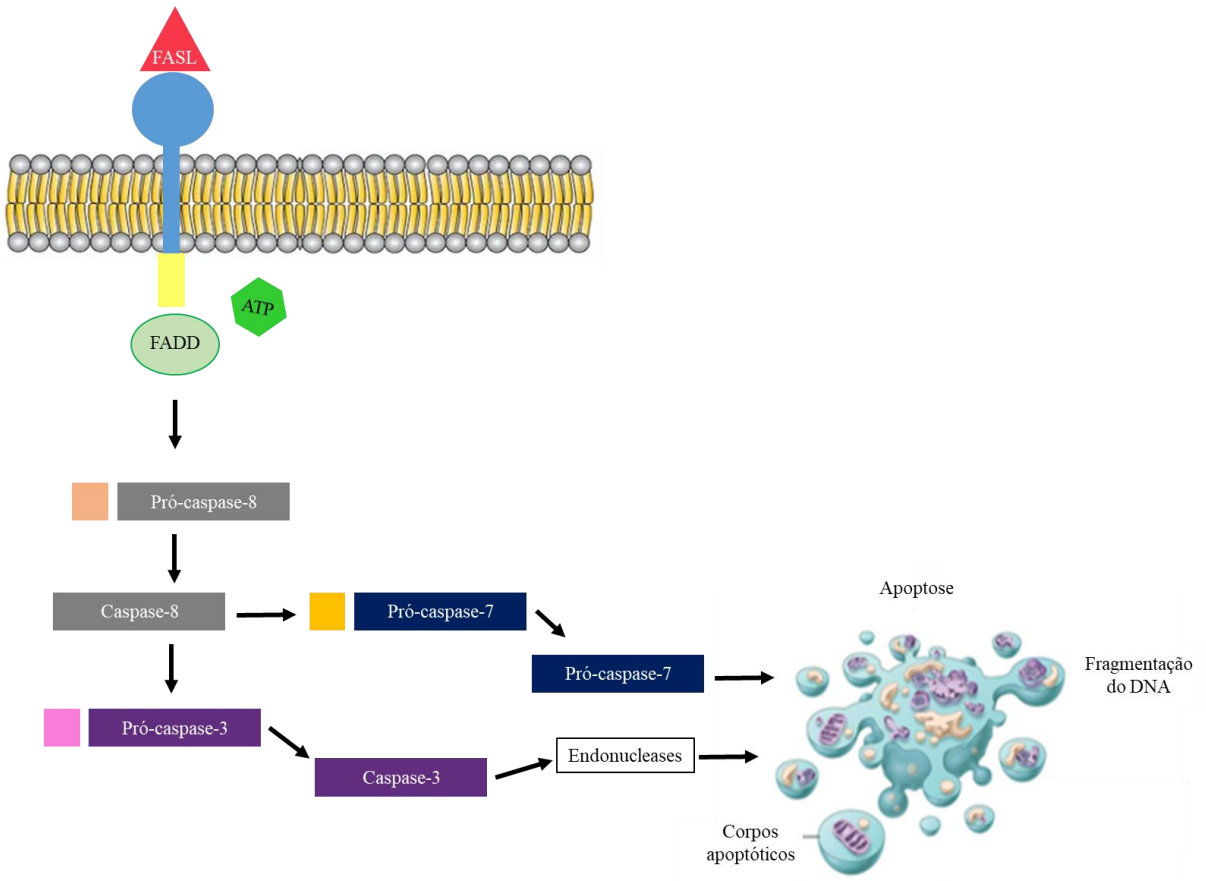

Figura 6: Representação esquemática da ativação da via apoptótica através da ligação de receptores transmembranar. O domínio de morte DD do receptor transmembrana Fas recruta a proteína FADD e ativa Caspase-8. A caspase 8 por ser iniciadora, ativa a caspase 3. Em seguida, a caspase 3 por ser efetora ativa as endonucleases e assim, é iniciado o processo de fragmentação do DNA (Fonte: Lana Meuren).

A ligação do ligante ao receptor de morte induz a clivagem da pró-caspase 8 em caspase 8, que é uma caspase iniciadora. Em seguida, a caspase 8, ativa a caspase efetora 3, cuja função é ativar endonucleases. Após a ativação dessas caspases, inicia-se o processo de clivagem do DNA (Figura 6) (Chang e Yang, 2000; Li e Yuan, 2008).

A via intrínseca de apoptose, também conhecida como via mitocondrial, é ativada em resposta a vários tipos de estresse intracelular, tais como: danos no DNA, estresse de retículo endoplasmático (ER), estresse por replicação, e até mesmo pelo aumento de ROS (Czabotar *et al.*, 2014; Pihán, Carreras-Sureda e Hetz, 2017; Roos, Thomas e Kaina, 2016; Vitale *et al.*, 2017; Nunez *et al.*, 1990; Brumatti, Salmanidis e Ekert, 2010). O estresse celular induz alterações morfofuncionais da mitocôndria, levando a liberação do citocromo C. O acoplamento do citocromo C à molécula adaptadora Apaf-1 (fator de ativação da apoptose) forma o

apoptossomo e culmina na ativação da pró-caspase 9, dando origem à caspase 9 ativa. Essa, por sua vez, leva a ativação da pró-caspase 3 (Figura 7) (Chang e Yang, 2000; Grutter, 2000).

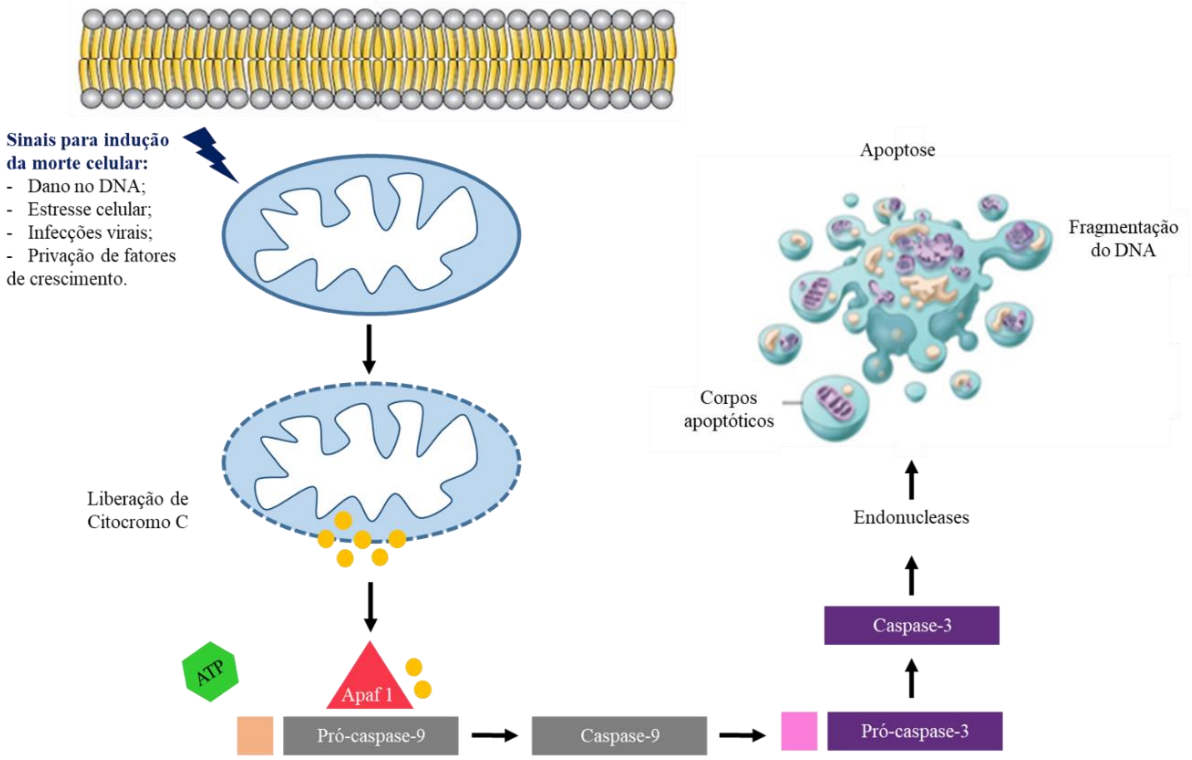

Figura 7: Indução de morte por apoptose através da ativação por capazes, via intrínseca. A ativação da via intrínseca ocorre em resposta a algum estresse intracelular. A presença do estresse celular estimula alterações na morfologia mitocondrial, culminando na liberação do citocromo C. O citocromo C após ser liberado, acopla à molécula adaptadora Apaf-1. Com isto, ocorre a ativação da pró-Caspase 9, formando o complexo apoptossomo. Esse complexo, por sua vez é responsável pela ativação da Caspase 9, que promove a ativação da pró-Caspase 3 (Fonte: Lana Meuren).

A apoptose é ainda regulada por proteínas da família Bcl-2. Essa família está dividida em 2 grupos: pró-apoptóticas (Bax, Bad, Bid, Bcl-xS, Bak, Box, Bik, Blk, Bim, Hrk, BNIP3), que estão localizadas, principalmente, nas mitocôndrias e na membrana externa; anti-apoptóticas (Bcl-2, Bcl-xl, A1, Mcl-1), presentes na membrana nuclear e no retículo endoplasmático (Jeong e Seol, 2008; Voss e Strasser, 2020). A regulação da apoptose a partir dessa família ocorre a partir do balanço entre as proteínas pró e anti-apoptóticas (Spanos *et al*., 2002).

1.4.2. Necroptose

A necrose é caracterizada pelo inchaço do citoplasma, das organelas e a ruptura da membrana plasmática, e em seguida a perda dos componentes citoplasmaticos (Kroemer *et al*., 2009). A necrose durante um tempo foi considerada como uma via de morte celular simples e sem um mecanismo que a regule (Vandenabeele *et al*., 2010). Contudo, nos últimos tempos foi descrito um mecanismo de morte celular também associado à perda de integridade de membrana e extravasamento de conteúdo citoplasmático, de forma independente de caspase (Orzalli e Kagan, 2017). Esse mecanismo, então, foi denominado como necrose programada ou necroptose (Vandenabeele *et al*., 2010). A indução da necroptose ocorre de forma RIPK1 ou RIPK3 dependente (Grootjans, Berghe e Vandenabeele, 2017; Cho *et al*., 2009; Vandenabeele *et al*., 2010; Mocarski, Upton e Kaiser, 2011). A indução dessa via de morte também pode ocorrer através da ativação de receptores de morte como, TNFR1, receptores de reconhecimento de patógenos, como por exemplo, TLR-3 e TLR-4 (Laster, Wood, Gooding, 1988; Vercammen *et al*., 1997; Chan *et al*., 2003; Vandenabeele *et al*., 2010). O engajamento desses receptores promove mudanças conformacionais, que induzem o recrutamento de RPIK1, RIPK3, TRADD, FAAD e caspase 8, formando um complexo. A caspase 8, é responsável por clivar RIPK1 e RIPK3, desta forma desencadear a morte celular via apoptose. Entretanto, quando há a inibição da caspase 8, ocorre a fosforilação de RIPK1 e RIPK3 (Grootjans, Berghe e Vandenabeele, 2017). A montagem do complexo pró-necrótico leva a ativação de NFκB, produção de ROS e a morte das células (Festjens *et al*., 2006).

Diferentes mecanismos de morte celular têm sido associados à infecção por DENV. Já foi demonstrado que a infecção por DENV induz a apoptose de células endoteliais *in vitro* (Avirutnan *et al*., 1998; Yen *et al*., 2008; Vásquez, *et al*., 2009; Liao, Xu, Huang, 2010). Corroborando esses dados, também foi visto que durante a infecção por DENV a produção de TNF-α potencializa à morte de células microvasculares de camundongos via apoptose celular (Barth *et al*., 2006; Chen *et al*., 2007). Além disso, estudos anteriores sugerem que a infecção por DENV em hepatócitos culmina na morte destas células via apoptose (Thepparit *et al*., 2013). Também já foi descrito que a própria resposta imune gerada durante a infecção viral, como a produção de TNF-α, IFN, ROS e de óxido nítrico (NO) podem estar associados à regulação da morte por apoptose (Orzalli e Kagan, 2017, Yen *et al*., 2008; Wu-hsieh, Yen e Chen, 2009; Limonta *et al*., 2014).

1.5. Espécies Reativas de Oxigênio (ROS)

As Espécies Reativas de oxigênio (ROS) compreendem uma gama de subprodutos derivados do oxigênio molecular (O_2), podendo ser em forma de radicais livres ou não (Halliwell e Gutterridge, 2015). Esses mediadores são produzidos durante a redução incompleta do oxigênio e incluem o ânion de superóxido (O_2), peróxido de hidrogênio (H_2O_2) e radicais hidroxilas (OH.) (Baud e Ardaillou, 1986). ROS são comumente produzidas durante o metabolismo aeróbio, estresse contínuo, exposição a luz UV, e infecção viral (Mittler *et al*., 2011; Reshi *et al*., 2014). O principal subproduto formado na redução de O_2 é o radical ânion superóxido (O2•-), pois ocorre após a transferência de um único elétron. Durante a fosforilação oxidativa, por volta de 1% a 2% do oxigênio utilizado é convertido em superóxido (Kowaltowski e Vercesi, 1999)

A produção de ROS pode ocorrer por diferentes enzimas presentes em sítios celulares, incluindo a NADPH oxidase (NOX), xantana oxigenase, ciclo-oxigenase e lipo-oxigenase, e através da fosforilação oxidativa na mitocôndria (Valadão, 2016; Pillai *et al*., 2019; Harijith *et al*., 2014).

As lipoxigenases (LOX) catalisam a hidroperoxidação de ácidos graxos poli-insaturados. Os produtos da via da LOX têm múltiplas funções, como reguladores de crescimento, compostos antimicrobianos, como moléculas de sinalização (Rosahl, 1996; Harijith *et al*., 2014). A Xantina oxidase catalisa a oxidação de vários substratos, incluindo purinas (xantina e hipoxantina), pteridinas, moléculas heterocíclicas, e aldeídos. Existe uma grande variedade de aceptores de elétrons existe para a xantina oxidase, como O_2, NAD1, metileno azul, quinonas, ferricianeto e nitrato. Tais reações levam à produção de radicais de superóxido e peróxido de hidrogênio (Lacy, Gough e Schmid-Schonbein, 1998).

As NADPH oxidases são um complexo enzimático transmembrana, cuja especialização é produzir ROS pela transferência de elétrons do doador NADPH para o oxigênio molecular (Bedard e Krause, 2007). O produto da transferência de elétrons é o superóxido. A NADPH oxidase é formada por seis subunidades: as proteínas transmembrana p22phox e gp91phox, que formam o sítio catalítico da enzima; três proteínas citosólicas, p47phox, p67phox, p40phox (phox- phagocyte oxidase); e uma GTPase (Rac1 ou Rac2). A separação desses componentes é o que garante o complexo NADPH oxidase permaneça inativo. Para que ocorra a ativação desse complexo é importante que haja a fosforilação de p47phox e RhoGDI, fenômeno que induz alterações estruturais, permitindo, assim, a migração dos demais componentes do complexo

localizados no citoplasma para a membrana (Figura 8) (Bedard e Krause, 2007). A fosforilação de p47phox pode ser ativada por proteínas, como a trombina; pelo fator de crescimento derivado de plaquetas (PDGF); LDL; e por citocinas como a IL-6, IL-1, TNF-α (O' Donnell, *et al*., 2003; Kaur, Dhaunsi e Turner, 2004; Kim *et al*., 2007; Behrens, Ali e Dugan, 2008; Filip-Ciubotaru *et al*., 2016).

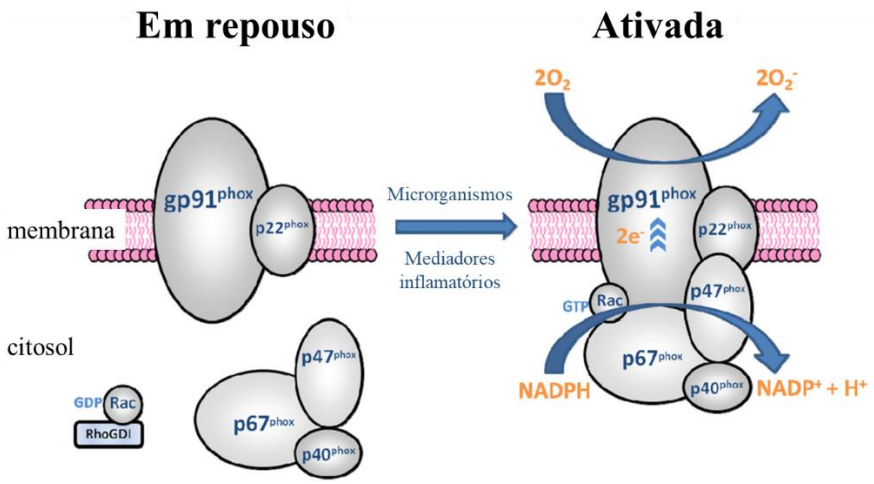

Figura 8: Ativação da NADPH oxidase. O complexo NADPH oxidase permanece em repouso quando as subunidades se encontram separadas. A ativação do complexo enzimático ocorre através da fosforilação da p47phox, o que resulta na migração de todos os componentes para a membrana (Adaptado. McCann e Roulston, 2013).

Outra fonte importante de geração de ROS é o processo de fosforilação oxidativa que ocorre nas mitocôndrias. ROS são gerados nos complexos I, II e III na cadeia respiratória, quando a fuga de elétrons do complexo I e III leva a redução parcial do oxigênio para formação de superóxido. Em seguida, a superóxido dismutase 2 (SOD2), que está presente na matriz mitocondrial, e a superóxido dismutase 1 (SOD1), localizada no espaço intermembrana mitocondrial, convertem o superóxido em H_2O_2 (Hamanaka e Chandel, 2010). Tanto o superóxido quanto o peróxido de hidrogênio, gerados durante esse processo são considerados ROS mitocondriais (mitROS) (Figura 9) (Hamanaka e Chandel, 2010).

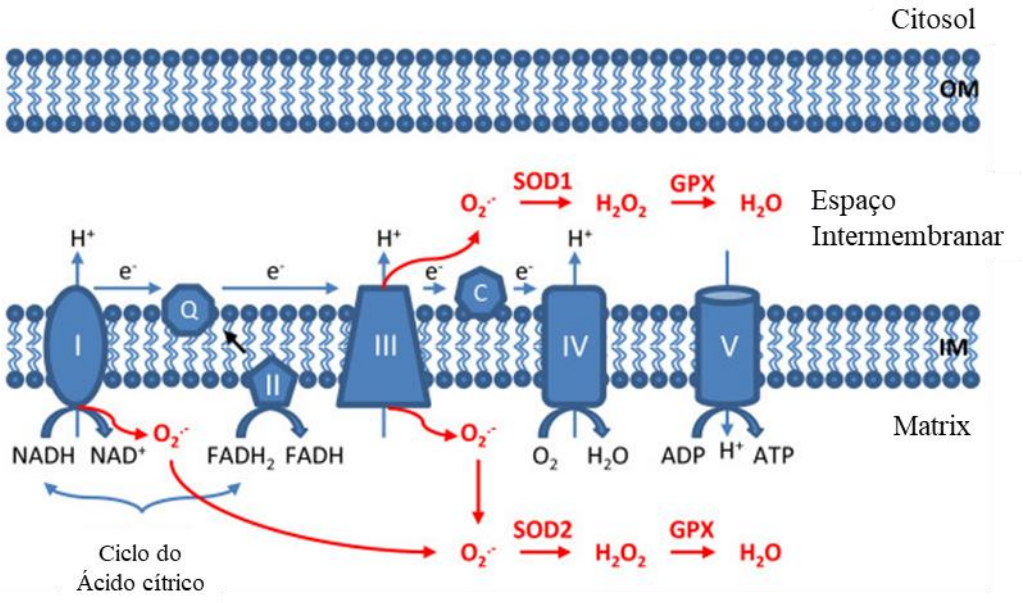

Figura 9: Sistema de transporte de elétrons (STE). Os ROS são produzidos na mitocôndria durante a respiração celular. Durante este processo, ocorre a fuga de elétrons do complexo I e III levando a redução parcial do oxigênio para formação de superóxido. (Li *et al*., 2013). Em seguida, a superóxido dismutase (SOD) transforma o superóxido em peróxido e a atividade da glutationa peroxidase (GPX) converte H_2O_2 em H_2O.

O aumento da produção de mitROS pode ocorrer por diversas alterações celulares, incluindo uma baixa de produção de ATP, falta de equilíbrio na relação NADH/ NAD+ e até mesmo através da despolarização da membrana interna. Esses fatores podem contribuir para o aumento na perda de elétrons nos complexos I e III da cadeia respiratória, gerando ROS (Turrens, 2003; Krylatov *et al*., 2018; Magnani *et al*., 2020). O acúmulo de ROS pode, então, induzir a despolarização da membrana mitocondrial, potencializando o dano mitocondrial (Zorov, Juhaszova e Sollott, 2014; Fukai e Fukai, 2020).

As espécies reativas de oxigênio podem atuar como moléculas sinalizadoras em uma série de eventos celulares e são essenciais para homeostasia celular. Entretanto, o desequilíbrio na produção das ROS com excesso de seus níveis intracelulares, levam a um estado conhecido como estresse oxidativo (Reshi, Su e Hong, 2014). Nesse cenário, o excesso de ROS pode causar danos importantes nas células, como por exemplo, danos às proteínas, aos lipídeos das membranas celulares, e até mesmo ao DNA e culminar em ativação de vias de morte celular (Halliwell e Cross, 1994).

Em contrapartida, mecanismos antioxidantes podem ser disparados para evitar o estresse oxidativo. Os antioxidantes podem ser compostos por sistemas enzimáticos e/ ou não enzimáticos. Os antioxidantes não enzimáticos são adquiridos pelos organismos de forma

dependente da alimentação, como o caso das vitaminas A e E, carotenoides, glutationa e os flavonóides (Costantini, 2019; Ratnam *et al*., 2006). O sistema antioxidante composto por componentes enzimáticos é formado por catalase (CAT), superóxido dismutase (SOD) e glutationa peroxidase (GPx) (Costantini, 2019; Reshi, Su e Hong, 2014). A SOD é uma metaloenzima que possui três isoformas: a citoplasmática (Cu/ZnSOD), mitocondrial (MnSOD) e extracelular (Cu/ZnSOD). A enzima é responsável por controlar o efeito oxidante do radical O2•-, através da dismutação do ânion superóxido e sua conversão em peróxido de oxigênio (Figura 10) (Perry *et al*., 2010). A CAT é uma proteína homotetramérica (240 kDa) responsável por reduzir o H_2O_2 em duas moléculas de água e uma de oxigênio. A enzima está presente, principalmente, nos peroxissomos, organela que mais produz H_2O_2 (Figura 10) (Valko *et al*., 2006). A glutationa é um tripeptídeo linear (γ–glutamil–cisteinilglicina) e cerca de 98% da glutationa presente na célula se encontra na forma reduzida (GSH), enquanto 2% estão na forma oxidada (GSSG). A enzima GPx é que catalisa GSH em GSSG (Meister e Anderson, 1983). Essa reação está acoplada à redução do H_2O_2 em água (Figura 10) (Halliwell, 2007).

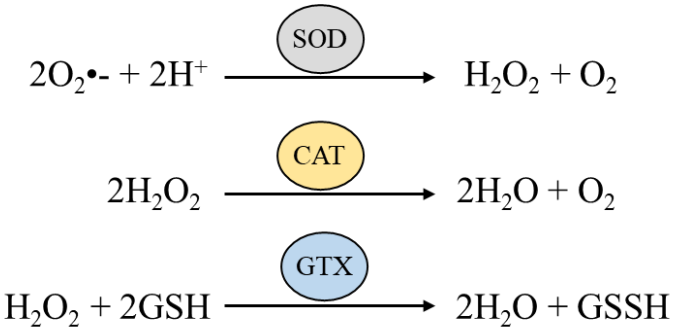

Figura 10: Reações catalisadas pelas enzimas Superoxido dismutase (SOD), catalase (CAT) e glutationa peroxidase (GPx), respectivamente. A enzima superóxido dismutase (SOD) converte o ânion superóxido (O2•-) em peróxido de hidrogênio (H_2O_2). As enzimas catalase (CAT) e a glutationa peroxidase (GPx) reduzem H_2O_2 em água e oxigênio molecular. Fonte: (Adaptado. Peng *et al*., 2014).

O fator de transcrição Nrf2 é um dos principais fatores que regulam genes desintoxicantes e antioxidantes de ROS (Deramaudt, Dill e Bonay, 2013). Em condições normais, esse fator se encontra presente no citosol associado à proteína 1 associada à ECH do tipo Kelch (Keap1). Essa associação facilita a ubiquitinação de Nrf2 e evita a translocação do fator para o núcleo (Cullinan *et al*., 2004). Quando ocorre uma situação e estresse, o que pode ser desencadeado por uma infecção viral, por exemplo, a Keap 1 se dissocia de Nfr2, promovendo a translocação deste fator para o núcleo. Com isso, ocorre a ativação de genes

relacionados com a homeostasia celular (Figura 11) (Ramezani, Nahad e Faghihloo, 2018; Zhang *et al*., 2019).

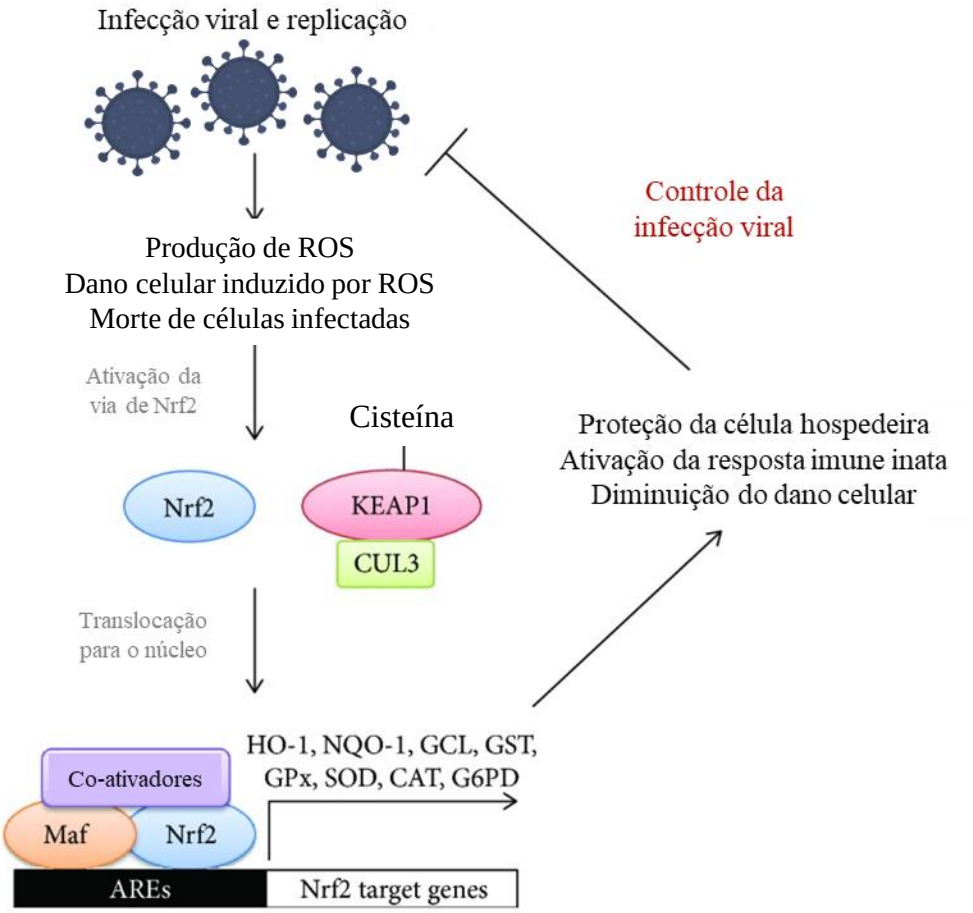

Figura 11: Ativação da via Nrf2 após indução do estresse oxidativo ocasionado por infecção viral. Após a indução do estado de estresse oxidativo ocasionado por uma infecção viral ou outro patógeno, o complexo Nrf2/Keap1 se dissocia e o Nrf2 transloca para o núcleo onde este fator de transcrição leva a ativação de vários genes envolvidos na homeostase redox. Este sistema de defesa antioxidante quando ativado protege a célula dos danos ocasionados pelo excesso de ROS. HO-1 (Heme oxigenase 1), NQO-1 (NADPH desidrogenase-1), GCL (γ-glutamilcisteína ligase), GST (Glutationa S-Transferase), GPx (glutationa peroxidase), SOD (Superóxido dismutase), CAT (Catalase), G6PD. (Adaptado. Lee, 2018).

1.6. Produção de ROS em resposta a infecção viral

O processo de replicação viral produtiva induz e depende de uma série de alterações no metabolismo celular, incluindo alterações de morfologia e função mitocondrial, estresse de retículo e reconhecimento viral que podem levar a produção de ROS e estresse oxidativo. De fato, as infecções virais comumente induzem um cenário de estresse oxidativo, resultando em

diferentes danos celulares, tais como mutações no DNA, indução de citocinas, alteração na transcrição, indução de morte celular, dentre outros (Pillai *et al*., 2019). Diversos estudos apontam que a produção de ROS pode ter efeitos anti- ou pró-replicação viral, dependendo da célula e vírus envolvidos (Olagnier *et al*., 2014; Shindo *et al*., 2013; Wu *et al*., 2017; Kim e Wong, 2013).

Dentre os flavivirus, o vírus da hepatite C (HCV) é um do que foi mais investigado no que diz respeito à indução e papel do estresse oxidativo na infecção. Níveis elevados de ROS e redução nos níveis de antioxidantes foram detectados em fígados de pacientes com infecções por HCV (Yadav *et al*., 2002). A infecção viral pode também levar a ativação da via NADPH oxidase. Foi demonstrado que a infecção de uma linhagem celular de hepatócitos humanos (Huh7) por HCV induziu a ativação de NOX 1 e 4, de forma dependente de TGFβ1 (Ivanov *et al*., 2015). Nesse trabalho caracterizou-se que uma região de 36 aminoácidos presente na porção N-terminal da proteína era responsável pela ativação de NOX. Outros estudos também demonstraram que a proteína do nucleocapsídeo de HCV induz aumento de produtos da peroxidação de lipídios e leva ao aumento de cálcio nas mitocôndrias em hepatócitos. Todos esses processos culminam no aumento da produção de ROS na mitocôndria, sendo NOX, então, considerada uma das principais contribuintes para o aumento do estresse oxidativo (Ivanov *et al*., 2011; Pal *et al*., 2010; Okuda *et al*., 2002).

As proteínas E1, E2 também já foram associadas ao aumento de ROS e alteração da homeostase do Ca^{2+} intracelular em hepatócitos (Ivanov *et al*., 2011; Ming-Ju *et al*., 2011). Além disso, em monócitos humanos, observou-se que as proteínas NS3 e NS5A também induziram o estresse oxidativo, através do aumento da absorção de cálcio, gerando oxidação da glutationa nas mitocôndrias e, por consequência, aumento na produção de ROS (Bureau *et al*., 2001; García-Mediavilla *et al*., 2005; Thorén *et al*., 2004). A infecção de linfócitos por HCV também acarreta na indução do estresse oxidativo, alterando a homeostasia mitocondrial e, por conseguinte, a permanência desse estresse desencadeia em danos ao DNA mitocondrial (Bhargava *et al*., 2011).

A infecção pelo vírus sincicial respiratório (VSR) em células A549 (Linhagem celular carcinoma de pulmão humano) induz alterações na bioenergética mitocondrial, através da diminuição do potencial de membrana mitocondrial, diminuição na taxa de consumo de oxigênio (OCR) máxima, do consumo basal e da OCR ligado ao ATP (Hu *et al*., 2019a; Hu *et al*., 2019). O aumento da produção de ROS foi demonstrado na infecção pelo VSR em células A549, e este aumento favorece a replicação viral. Além disso, foi demonstrado que ao tratar o

camundongo BALB/c com um inibidor de ROS mitocondrial, os animais apresentaram redução nos marcadores de inflamação (Hu *et al*., 2019a; Hu *et al*., 2019).

Em relação à infecção por DENV, o estresse oxidativo foi descrito em diferentes modelos, tendo sido relacionado com a gravidade da doença (Gil *et al*., 2004). Em pacientes com dengue grave não foi observado alterações nas taxas de glutationa (GSH) e de antioxidante total (TAS). Entretanto, foi visto aumento significativo no potencial de peroxidação (PP), na peroxidação lipídica e na quantificação da enzima superóxido dismutase (SOD) e níveis mais baixos na dosagem da glutationa peroxidase (GPx) (Gil *et al*., 2004). Além disso, foi demonstrado que DENV altera a homeostasia redox, induzindo o estresse oxidativo e este evento é responsável pelo aumento da replicação viral em monócitos obtidos de pacientes infectados (Al-alimi *et al*., 2014).

Em modelos de infecção por DENV *in vitro*, o aumento da produção de ROS foi demonstrado em células dendríticas derivadas de monócitos (Mo-DC), hepatócitos e células endoteliais (Lin *et al*., 2000; Yen *et al*., 2008; Wu-Hsieh *et al*., 2009; Olagnier *et al*., 2014). Em Mo-DC, o aumento da produção de ROS foi dependente da ativação de NOX, mostrando-se importante para replicação viral, ativação e morte celular (Olaigner *et al*., 2014). Em modelos de infecção de hepatócitos, a produção de ROS induziu ativação do fator nuclear de ativação para a sinalização da expressão de IL-6 (NF-IL-6), que culminou na secreção de CCL5, indicando o papel do estresse oxidativo também na ativação deste tipo celular (Lin *et al*., 2000).

Já no modelo de células endoteliais da veia umbilical humana (HUVEC), a infecção por DENV induziu o aumento da produção de ROS e RNS. Essas moléculas atuaram como sinalizadoras de morte celular, aumento a permeabilidade vascular e induziram as células à morte por apoptose (Yen *et al*., 2008). Dados desse trabalho ainda demonstraram que camundongos depletados de p47phox ou em tratamento com Apocinina, apresentaram redução de hemorragia, sugerindo que a produção de ROS derivado de NOX induz dano vascular e é importante para a indução de morte celular (Yen *et al*., 2008).

Além da ativação de NOX, outros modelos demonstraram que a infecção por DENV induz alteração na morfologia e na bioenergética mitocondrial, mas não há dados que demonstrem o papel do aumento de mitROS na replicação viral (El-Bacha *et al*., 2007; Chatel-Chaix *et al*., 2016).

No geral, em um cenário de infecção viral, os trabalhos demonstram que o aumento da produção de ROS está associado com o um papel antiviral (Olagnier *et al*., 2014; Wu *et al*., 2017; Kim *et al*., 2013). Inclusive, já foi descrito que a infecção por DENV induz o aumento na produção de ROS em células dendríticas associado a um efeito antiviral e de indução de morte celular (Olagnier *et al*., 2014; Shindo *et al*., 2013).

Por outro lado, o vírus pode se favorecer do aumento de ROS, através da indução de autofagia. Durante a evolução, os vírus adquiriam a capacidade de usufruir da indução da autofagia para o favorecimento da replicação viral (Choi *et al*., 2019). As espécies reativas derivadas da NADPH-Oxidase 2 são capazes de induzir a autofagia (Xiao *et al*., 2021; Jing *et al*., 2019). A infecção por diferentes flavivirus induziu autofagia em monócitos e este evento foi importante para proteger as células de outras respostas ao estresse e morte celular precoce (McLean *et al*., 2011). A infecção por DENV já demonstrou induzir a autofagia tanto em modelos de células HepG2. (Panyasrivanit *et al*., 2009a; Panyasrivanit *et al*., 2009). Datan e colaboradores (2016) descreveram que a infecção por DENV em células renais caninas (MDKC) induz o aumento de ROS de forma dependente de ER, cujo efeito está relacionado à indução de autofagia. Ainda, nesse modelo, a indução da autofagia foi importante para a replicação viral (Datan *et al*., 2016).

Diferentes mecanismos podem estar associados ao disparo da produção de ROS durante o processo de replicação viral. Estudos apontam que o acesso ao metabolismo glicolítico e mitocondrial durante a replicação viral é uma estratégia que os vírus utilizam para obter moléculas de alta energia ao seu favor, utilizando-as para replicação e montagem viral de forma mais eficiente (Widnell *et al*., 1990; Garry e Bostick, 1986; El-Bacha *et al*., 2004).

Finalmente, o *sensing* viral também pode induzir a produção de ROS via NOX ou mitocondrial. A ativação de receptores semelhantes a NOD (NLRs) foi associada ao aumento da produção de ROS dependente de NOX2 (Lipinski *et al*., 2009). Além disso, ativação via TLR4 em macrófagos e neutrófilos também induz estresse oxidativo (Asehnoune *et al*., 2004; Park *et al*., 2004). Também foi relatado que o *sensing* do vírus de RNA com TLR7 aumenta a ativação de NOX, com isso ocorre o estado de estresse oxidativo (Valadão *et al*., 2016). Além disso, o *sensing* de RNA pelo sensor citoplasmático RIG-I leva a ativação de MAVS, associado à mitocôndria. Essa ativação pode impactar a função mitocondrial e a geração de ROS por essa via (Buskiewicz *et al*., 2016).

2. Racional

Nosso grupo de pesquisa vem caracterizando os efeitos gerados pela infecção de células de endotélio microvascular humano (HBMEC) pelo DENV, incluindo o efeito da infecção na ativação celular, lesão endotelial e morte celular. Este modelo celular, é utilizado como modelo de célula endotelial no geral, mas também é considerado um modelo de barreira hematoencefálica. Dados do grupo mostram que DENV ativa as células endoteliais via RIG-I/MAVS, gerando a secreção de citocinas inflamatórias, normalmente, aumentadas durante a infecção. Além disso, nosso grupo também demonstrou que a infecção por DENV induz aumento da permeabilidade endotelial *in vitro* e morte celular, pelo menos em parte associada ao processo de necroptose (Papa, 2014). Dados preliminares gerados durante a dissertação de mestrado sugeriam que a infecção de HBMECs por DENV induzia produção de ROS (Meuren, 2016). Uma vez que foi demonstrado em diferentes modelos que ROS pode interferir em vias de replicação viral e levar a morte celular, na presente tese objetivamos avaliar se estes mediadores estariam envolvidos na replicação de DENV em células endoteliais, em mudanças na permeabilidade e na lesão endotelial na dengue. Bem como, avaliar se o reconhecimento viral por sensores de RNA estaria envolvido no disparo de produção de ROS, buscando compreender a inter-relação reconhecimento viral, estresse celular, replicação viral e lesão endotelial.

3. Objetivos

3.1. Objetivo Geral

Investigar os mecanismos moleculares envolvidos na produção de espécies reativas de oxigênio por células endoteliais infectadas por DENV, bem como avaliar seu papel na replicação viral, na ativação celular, permeabilidade e morte celular.

3.2. Objetivos Específicos

3.2.1. Confirmar se a infecção por DENV induz a produção de ROS em HBMECs;

3.2.2. Caracterizar a via envolvida na produção de ROS por HBMECs infectadas por DENV, particularmente, avaliando o papel da ativação de NADPH oxidase e da mitocôndria no processo;

3.2.3. Avaliar a função e bioenergética mitocondrial em HBMECs infectadas com DENV;

3.2.4. Avaliar o papel de ROS na morte de células endoteliais induzida por DENV;

3.2.5. Avaliar o papel de ROS na replicação viral;

3.2.6. Avaliar o papel da produção de ROS e os fenômenos associados na permeabilidade endotelial;

3.2.7. Avaliar o papel da produção de ROS no aumento da produção de citocinas pró-inflamatórias e Interferon-β;

3.2.8. Investigar o papel da ativação da via RIG-I/MAVS na indução da produção de ROS.

4. Material e Métodos

4.1. Cultura de células

Células C6/36 (linhagem celular da larva do mosquito *Aedes albopictus*) foram mantidas em meio Leibovitz (L-15 – *GIBCO*, Grand Island, NY, EUA) suplementado com 3% de triptose (*GIBCO*), 7,5% bicarbonato de sódio (*ISOFAR*, Duque de Caxias, RJ, Brasil), 2% L-glutamina (Glutamax – *GIBCO*), 0,2 mM aminoácidos não essenciais, 10 μg/ml gentamicina (*GIBCO*), e de 5% de Soro Fetal Bovino (SFB – *GIBCO*) a 28°C.

Células BHK-21 (linhagem celular de fibroblasto de *Mesocricetus auratus*) foram mantidas em meio α-MEM suplementado com 10μg/ml gentamicina (*GIBCO*), acrescido de 10% de SFB a 37ºC com 5% de CO_2.

Células HBMECs (linhagem celular do endotélio microvascular cerebral humano) foram, gentilmente, cedidas pelo Dr. Julio Scharfstein (IBCCF, UFRJ) e foram mantidas em meio 199 (M199 - *GIBCO*) acrescido de 10% de SFB a 37°C com 5% de CO_2.

Todas as culturas celulares descritas acima foram monitoradas, de forma mensal, para mycoplasma. A fim de, garantir que os experimentos seriam realizados em células livres de contaminaminações.

4.2. Vírus

As amostras de DENV sorotipo 2 da cepa 16681 foram doadas pela Professora Andréia Da Poian (IBqM, UFRJ, Rio de Janeiro). O vírus foi propagado em cultura de células C6/36 com o MOI (Multiplicidade de infecção) de 0,1. Após 9 dias de infecção, o sobrenadante da cultura foi coletado, centrifugado, filtrado em filtro de 0,22 μm e armazenado à -80ºC. A titulação dos estoques virais foi realizada por ensaio de plaque em células BHK-21, como descrito posteriormente. Para controle, foi utilizado o sobrenadante das células C6/36 não infectadas e que foram cultivadas pelos mesmos períodos de tempo e em mesmas condições. Esses sobrenadantes foram, então, chamados de “mock”. Em determinados experimentos foi utilizado o vírus inativado por radiação ultravioleta (UV). Para inativar o vírus por UV foi utilizada a placa de 24 poços (0,35 x 10 mm – *TPP*, Trasadingen, Suíça) contendo um volume total por poço de 200 μl de suspensão viral. As amostras foram expostas à luz UV (UV- 270 e 230 nm) a 30 cm da lâmpada por 2h. A inativação viral foi confirmada após ensaio de infecção

de células C6/36 por 48h, seguida de análise do genoma viral nas células e sobrenadantes das culturas por qPCR (descrito posteriormente).

4.3. Infecção de células endoteliais com DENV

As HBMECs foram incubadas em placas de 6 poços e plaqueadas na concentração de $3x10^5$ células por poço. As células foram infectadas com DENV 2, cepa 16681 com MOI de 1, referente a quantidade de células presentes no dia do plaqueamento ($3x10^5$). O vírus foi diluído em meio de cultura sem soro e adicionado à cultura por 90-120 minutos em ambiente úmido a 37°C com 5% de CO_2. Após a incubação, o inóculo foi removido, as células foram lavadas com PBS 1X e mantidas em meio de cultura com 10% SFB a 37°C a 5% de CO_2 por diferentes períodos de tempo (24h, 48h, 72h). Em alguns experimentos, após a adsorção, as células foram mantidas nas condições descritas acima, mas adicionamos no meio de cultura os inibidores de ROS ou de sua produção: Apocinina (Apo) a 1 mM (*Merck Millipore*, Darmstadt, Alemanha), N-Acetilcisteína (NAC) a 1 mM (*Merck Millipore*), MitoTEMPO (MitoT) a 50 µM (Arruda *et al*., 2006; Lu *et al*., 2008). A infecção foi avaliada por titulação, como descrito posteriormente.

4.4. Análise da replicação viral por ensaio de plaque e qRTPCR

Estoques virais ou sobrenadantes de HBMECs infectadas em diferentes ensaios foram avaliados quanto ao título de partículas infecciosas por ensaio de plaque. Para realizar a titulação viral, foi necessário fazer o plaqueamento da linhagem celular BHK-21 em placas de 24 poços (*TPP*). Foram plaqueadas $4x10^4$ células por poço foram incubadas por 24h para adesão. Em seguida, as células foram inoculadas com diluições decimais seriadas na base 10 das amostras virais. Após 2h para adsorção viral, as culturas foram lavadas com PBS (Tampão fosfato-salino) 1X, e o meio foi substituído por 1% de carboxi-metil-celulose (CMC) diluído em meio α-MEM com 1% de SFB. Após 5 dias de cultura, as células foram fixadas com 1 ml de formaldeído 10% por 1h. Posteriormente, as células foram lavadas com PBS 1X, coradas com solução Cristal Violeta 4%, cujo excesso foi retirado lavando a placa com água corrente. Em seguida, foi realizada a contagem das placas em cada poço.

Para análise da replicação viral por qRT PCR quantitativo, as HBMECs foram plaqueadas na placa de 24 poços numa concentração de $4x10^4$ por poço. As células foram infectadas com DENV, na presença ou ausência de inibidores de ROS, como descrito. Após 24

e 48h de infecção foram recolhidos os sobrenadantes das células e foi realizada a extração de RNA por Trizol (Invitrogen), seguindo as recomendações do fabricante.

Aproximadamente 2 µg do RNA total foram submetidos à síntese de cDNA, utilizando-se High-Capacity cDNA Archive Kit (Applied biosystems, Califórnia, EUA) seguindo o protocolo as recomendado pelo fabricante. Para a quantificação viral das amostras foi realizado um PCR quantitativo (qRT-PCR). O sistema utilizado foi TaqMan (Applied Biosystems), com os seguintes primers específicos DENV (F) 5'-CAGGTTATGGCACTGTCACGAT-3'; DENV (R) 5'-CCATCTGCAGCAACACCATCTC-3'; sonda (DENV) 5'-56FAM\CTCTCCGAGAACAGGCCTCG-3'; GAPDH (F) 5'-GTGGACCTGACCTGCCGTCT-3'; GAPDH (R) 5'-GGAGGAGTGGGTGTCGCTGT-3' e a reação foi realizada no equipamento Real Time PCR System 7300 (Applied Biosystems) com os seguintes ciclos: 95ºC por 10 min, 45 ciclos de 95°C por 15 segundos, 45ºC por 30 segundos e 72ºC por 1 minuto.

4.5. Avaliação da produção de ROS por citometria de fluxo e por imunofluorescência

HBMECs foram plaqueadas em placas de 6 poços numa concentração de $3x10^5$ células por poço. As células foram cultivadas com meio de cultura, mock, ou infectadas com DENV (cepa 16681) com MOI de 1, na sua forma nativa ou inativado por U.V., por diferentes periodos de tempo. Em alguns poços foram adicionados inibidores de ROS, como descrito anteriormente. Para a dosagem de ROS total as células foram incubadas com a sonda fluorescente CM-H2DCFDA (*Invitrogen*, Califórnia, EUA), adicionando-se 2 µM/10^6 células, por 30 minutos. Para dosagem de ROS mitocondrial (mitROS), foi utilizada a sonda MitoSOX (Dutra *et al*., 2014), a 5 µM, por 30 minutos. Em seguida, foi feita a lavagem das células com PBS 1X e as células foram retiradas da placa com o uso de tripsina (Gibco) a 0,05% por 10 min. As células foram analisadas por citometria de fluxo, utilizando o equipamento FACScalibur e programa CellQuest (BD *Biosciences*, Nova Jersey, EUA) ou o programa FlowJo (*LCC*, Ashland, EUA). Como controle de indução de ROS, as HBMECs foram tratadas com Heme a 30 µM por 30 min, a 37ºC. A mesma metodologia foi utilizada para medir as ROS por microscopia. Além disso, acrescentamos a marcação para DENV. Para isto, incubamos as HBMECS com o hibridoma 3H51 por 1h, em seguida utilizamos o anticorpo anti-mouse (diluição: 1:500) por

30min. e as células foram analisadas por imunofluorescência, utilizando microscopia OLYMPUS IX81.

4.6. Determinação do consumo de oxigênio e caracterização dos parâmetros respiratórios

Para esta avaliação foi utilizada a técnica de respirometria de alta resolução. Utilizamos o *Oroboros Oxygraph-2k*, pois permite que pequenas mudanças no fluxo de oxigênio das células fossem acompanhadas em tempo real. HBMECs foram cultivadas com meio de cultura, mock, ou infectadas com DENV2, nativo ou inativado, por diferentes periodos de tempo. Para o ensaio de respirometria foram utilizadas $2x10^6$ células em volume final 2 mL. As taxas de consumo de oxigênio e os parâmetros respiratórios foram avaliados nas HBMECs intactas mantidas no próprio meio de cultura. Em seguida, foi adicionado 200 µg/mL de Oligomicina (Oligo, Sigma-Aldrich, St. Louis, EUA). A oligomicina inibe o retorno dos prótons que ficam localizados no espaço intramembranar para a matriz mitocondrial, assim o consumo de oxigênio medido nesta etapa é considerado como o consumo de oxigênio não associado à síntese de ATP (Trifosfato de adenosina). Por último, foi adicionado 1 mM do FCCP (Carbonil cianeto-p-trifluorometoxifenilhidrazona, Sigma-Aldrich, St. Louis, EUA) para analisar o consumo máximo de oxigênio através do retorno dos prótons para a matriz mitocondrial, o que leva ao desacoplamento entre a síntese de ATP e o consumo de oxigênio.

4.7. Análise da expressão de SOD, LC3, P62, pAKT e AKT durante a replicação do DENV

Para avaliar a expressão de SOD, LC3, P62, pAKT e AKT durante a replicação, as HBMECs foram plaqueadas em placas de 6 poços numa concentração de $3x10^5$ células por poço. As células foram cultivadas com meio de cultura, mock, ou infectadas com DENV, (cepa 16681) com MOI de 1, na sua forma nativa ou inativado por U.V., por diferentes periodos de tempo. Em alguns poços foram adicionados inibidores de ROS, como descrito anteriormente (Item 4.3). Em seguida, as células foram recolhidas e lisadas com RIPA 0,1% triton X-100 (Sigma-Aldrich). Os lisados foram submetidas a SDS-PAGE no gel de poliacrilamida a 15%. Em seguida, foi efetuado a transferência das proteínas do gel de poliacrilamida para a membrana de PVDF. Por conseguinte, as membranas foram bloqueadas com 2% de soro de

burro por 30 minutos e posteriormente, foram incubadas com os anticorpos primários anti-SOD (diluição: 1:1.000, Cellsignaling), anti- LC3 (diluição: 1:10.000, Abcam), anti- P62 (diluição: 1:20.000, Abcam), anti- pAKT (diluição: 1:1.000, Cellsignaling) e anti- AKT (diluição: 1:1.000, Cellsignaling) e anticorpo secundário anti- rabbit (diluição: 1:2.000, Cellsignaling) a análise foi realizada blotting. O controle de carregamento foi realizado com a marcação da proteína β-actina. Para revelar os dados, foi adicionada na membrana o subestrado e, posteriormente, a solução de revelação e fixação (Kodak, Rochester, Nova York, EUA). A revelação foi realizada no filme de raio-x (Kodak). O filme foi escaneado (EPSON perfection V-19. Tóquio, Japão) e a análise da densidade densiométrica foi realizada através do programa ImageJ (National Institutes of Health) e expressas em unidades arbitrárias. Os resultados foram expressos pela razão dos valores da densiometria da proteína estudada pelo controle de carregamento.

4.8. Avaliação da secreção de citocinas por ELISA

HBMECs foram plaqueadas em placas de 6 poços numa concentração de $3x10^5$ células por poço. As células foram cultivadas com meio de cultura, mock, ou infectadas com DENV 2 (cepa 16681) com MOI de 1, na sua forma nativa ou inativado por UV. Em alguns poços foram adicionados inibidores da produção de ROS, como descrito anteriormente. Após 48h de infecção, os sobrenadantes foram recolhidos e a dosagem de IL-6, IL-8 e CCL5 foi realizada por ensaios de ELISA (Conceição *et al*., 2013). As concentrações foram determinadas usando ELISA Ready-SET-Go! (eBiosciences) e a concentração de RANTES foi determinada usando o kit de desenvolvimento ELISA (PeproTech), de acordo com as instruções do fabricante. A leitura foi realizada por Espectrofotômetro (*Bio-RAD*), com absorbância de 490 nm.

4.9. Avaliação da expressão de RNAm de IFN-β por qRT PCR

HBMECs foram plaqueadas em placas de 24 poços numa concentração de $4x10^4$ por poço. As células foram infectadas com DENV, na presença ou ausência de inibidores de ROS, como descrito. Após 48h de infecção as células foram recolhidas e foi realizada a extração de RNA por Trizol (I*nvitrogen*). Aproximadamente 2 µg do RNA total foram submetidos à síntese de cDNA, utilizando-se *High-Capacity cDNA Archive Kit* (*Applied biosystems,* Califórnia, EUA) segundo as recomendações do fabricante. Para a quantificação viral das amostras foi

realizado um PCR quantitativo (qRT-PCR). O sistema utilizado foi o *SYBR Green Real-Time PCR Master Mixes* (*Applied Biosystems*), com os primers IFN- β (F) 5'-TAGCACTGGCTGGAATGAGA-3'; IFN-β (R) 5'-TCCTTGGCCTTCAGGTAATG-3'; GAPDH (F) 5'-GTGGACCTGACCTGCCGTCT-3' e GAPDH (R) 5'-GGAGGAGTGGGTGTCGCTGT-3'. A reação foi realizada no Real Time PCR System 7300 (*Applied Biosystems*) com os seguintes ciclos: 50ºC por 2 min, 95ºC por 10min e 40 ciclos de 95°C por 15 segundos, 55ºC por 30 segundos e 60ºC por 1min, acrescido da curva de melt (95ºC por 15 segundos, 60ºC por 1min e 95ºC por 15 segundos).

4.10. Avaliação da viabilidade celular por ensaio de metabolização de XTT

HBMECs foram plaqueadas em placas de 96 poços na concentração de $4x10^4$ células por poço. As células foram cultivadas com mock ou infectadas com DENV2 (MOI-1), na sua forma nativa ou inativada, na presença ou ausência de inibidores de ROS, como descrito. Após diferentes períodos de tempo foi adicionado o composto XTT (2,3-Bis-(2-Methoxy-4-Nitro-5-Sulfophenyl)-2H-Tetrazolium-5-Carboxanilide) (Sigma-Aldrich, St. Louis, EUA). O XTT foi diluído em PBS e a solução foi aquecida à 56ºC. Em seguida, a solução foi resfriada e foi adicionado o PMS (N-methyl dibenzopyrazine methyl sulfate) (Sigma-Aldrich). As células foram incubadas com XTT por 2-4h e a leitura foi realizada no espectrofotômetro (Bio-RAD) no comprimento de onda de 450 nm. Como controle positivo as células foram incubadas com Triton X100 (10%) durante as 2h de incubação do XTT.

4.11. Avaliação da viabilidade celular por citometria de fluxo

HBMECs foram cultivadas como descrito em 4.3. Após diferentes períodos de tempo, as células foram recolhidas e incubadas com Iodeto de Propídeo (PI – 2,5 µg/ml) (BD *Biosciences*) durante 15 min. A incorporação de PI foi avaliada por citometria de fluxo, utilizando o equipamento FACScalibur® e o programa CellQuest (BD *Biosciences*) ou FlowJo (LCC).

4.12. Análise da viabilidade celular pela medida de atividade da enzima lactato desidrogenase (LDH)

HBMECs foram cultivadas como descrito em 4.3. Após 48h de infecção os sobrenadantes foram recolhidos e armazenados a -80ºC e foi realizada a mensuração da atividade da enzima desidrogenase láctica (LDH), através do Kit LDH (Doles, Cidade de Goiânia, Brasil). Basicamente, o ensaio é determinado por reações químicas que envolvem a mistura de reagentes que contém lactato (substrato), difosfopirido nucleótido (NAD), fenazina metosulfato (FMS), alúmen férrico e 1,10-fenantrolina. Então, ao adicionar o lactato e NAD ocorre a formação de NADH e piruvato. Posteriormente, adiciona-se o FMS, ocorrendo a redução a NAD e FMS reduzido. O FMS reduzido reage com o alúmen ferroso que gera o complexo corado. Então, a dosagem foi realizada em triplicata das amostras. A leitura foi realizada por Espectrofotômetro (Bio-RAD, Califórnia, EUA), com absorvância de 490 nm.

4.13. Avaliação do papel de ROS na permeabilidade de células endoteliais

As HBMECs foram plaqueadas numa concentração de $5x10^4$ células na parte superior do inserto do transwell (Corning Costar, ME, USA; membrana de 0,4 µM). As células foram cultivadas com mock ou infectadas com DENV2 (MOI-1), na sua forma nativa ou inativada, na presença ou ausência de inibidores de ROS, como descrito. Como controle positivo de permeabilidade, foi utilizado a Staurosporina a 10 µM (Sigma-Aldrich). A confluência foi monitorada durante toda cinética por medida de tensão elétrica trans-epitelial (TEER), usando o Voltohmmeter (Millicell ERS-2). O valor do TEER foi calculado usando o branco como controle, para considerar o valor da resistência da própria membrana. Além disso, após 72h de infecção, o sobrenadante foi retirado e, então foi adicionado uma solução de BSA conjugada por FITC por 30 min. O extravasamento de BSA para o inserto inferior, foi quantificado usando spectrofotometro SpectraMAX i3 (Molecular Devices, Lagerhausstrasse, Austria).

4.14. Análise da ativação da via RIG-I na indução da produção de ROS

HBMECs foram plaqueadas na placa de 6 poços numa concentração de $2x10^5$ células por poço. A expressão de RIG-I foi depletada através do uso de RNA de interferência específico (RNAi) (Santa Cruz, Biotechnology) (Conceição *et al*., 2013). Como controle negativo, as células foram transfectadas com RNAi *scramble*. Para tal, as células foram transfectadas

utilizando Lipofectamina e 30 pmol de RNAi, de acordo com as instruções do fabricante. Como controle, as HBMECs foram transfectadas com um RNAi codificada (Santa Cruz Biotechnology) na mesma concentração. Como controle de indução de RIG-I, as HBMECs foram infectadas com DENV 2 (cepa 16681) com MOI de 1 por 48 horas. A dosagem de ROS através da marcação com a sonda CM-H2DCFDA e MitoSOX. A expressão ROS foi avaliada por citometria de fluxo, utilizando o equipamento FACScalibur® e o programa CellQuest (BD *Biosciences*) ou FlowJo (LCC).

A fim de confirmar o silenciamento de RIG-I, as células foram tratadas como descrito anteriormente, e após 48h de cultura, as células foram a expressão foi avaliada por western blot. A mesma metodologia foi empregada para avaliar se a produção de ROS era importante para a expressão de RIG-I. Para isso, as HBMECs foram plaqueadas em placas de 6 poços numa concentração de $3x10^5$ células por poço. As células foram cultivadas com meio de cultura, mock, ou infectadas com DENV (cepa 16681) com MOI de 1, na sua forma nativa ou inativado por U.V., por diferentes periodos de tempo. Em alguns poços foram adicionados inibidores de ROS, como descrito anteriormente (Item 4.3) e lisadas com RIPA 0,1% triton. Os lisados foram submetidas a SDS-PAGE no gel de poliacrilamida a 15%. Em seguida, foi efetuado a transferência das proteínas do gel de poliacrilamida para a membrana de PVDF. Por conseguinte, as membranas foram bloqueadas com 2% de soro de burro por 30 minutos e posteriormente, foram incubadas com anticorpo anti-RIG-I (diluição, 1:500, Cellsignaling) e anticorpo secundário anti- rabbit (diluição: 1:2.000, Cellsignaling). O controle de carregamento foi realizado com a marcação da proteína β-actina. Para revelar os dados, foi adicionada na membrana o subestrado e, posteriormente, a solução de revelação e fixação (Kodak, Rochester, Nova York, EUA). A revelação foi realizada no filme de raio-x (Kodak). O filme foi escaneado (EPSON perfection V-19. Tóquio, Japão) e a análise da densidade densiométrica foi realizada através do programa ImageJ (National Institutes of Health) e expressas em unidades arbitrárias. Os resultados foram expressos pela razão dos valores da densiometria da proteína estudada pelo controle de carregamento.

4.15. Análise estatística

A média e o desvio padrão de cada grupo experimental foram calculados para cada situação experimental. A análise da diferença entre dois ou mais grupos foi realizada, respectivamente, pelo teste *t-student* e *One-way* ANOVA, seguida do pós-teste Newman-Keuls.

Para a análise de correlação foi utilizada a metodologia *r* de Pearson (*r*). As análises foram feitas usando a ferramenta de análise estatística do programa *GraphPad prisma*. A significância estatística foi estabelecida em $p<0,05$.

5. Resultados

5.1. Avaliação da produção de ROS durante a infecção por DENV em células HBMECs

Nosso grupo já havia demonstrado que as HBMECs eram permissivas ao vírus da DENV (Conceição *et al*., 2013) e dados preliminares, desenvolvidos durante o meu mestrado, sugeriram que a infecção induzia a produção de ROS de forma dependente da replicação viral (Meuren, 2014). Entretanto, observávamos uma variabilidade do nível basal ao longo do tempo, e a diferença da produção de ROS pelo vírus não era tão expressiva, mesmo sendo estatisticamente comprovada. Por isso, em um primeiro momento, precisamos ajustar o protocolo para confirmar os dados preliminares. Nós observamos que as células continuavam se multiplicando em tempos iniciais de infecção (dados não mostrados), e a quantidade de sonda adicionada para dosagem de ROS havia sido a mesma, independentemente do tempo de cultura. Então, avaliamos a concentração celular ao longo do tempo de cultura a fim de ajustar a concentração de sonda de ROS (CM-H2DCFDA) de acordo com quantidade de células em cada tempo de análise (2 µM para cada $1x10^6$ células).

HBMECs foram cultivadas com mock ou infectadas com DENV-2, na sua forma nativa ou inativado por U.V., incubadas com a sonda CM-H2DCFDA e analisadas por citometria de fluxo. Na figura 12 A-B, observamos a intensidade de fluorescência decorrente da marcação com a sonda, sem a normalização pela concentração celular. Nas figuras 12 C-E, encontramos as análises realizadas após a normalização. A infecção por DENV não afetou a produção de ROS após 24h de infecção (h p.i.). No entanto, foi observado aumento de ROS em 48h p.i., sustentado até 72h p.i. (Figura 12 C-E).

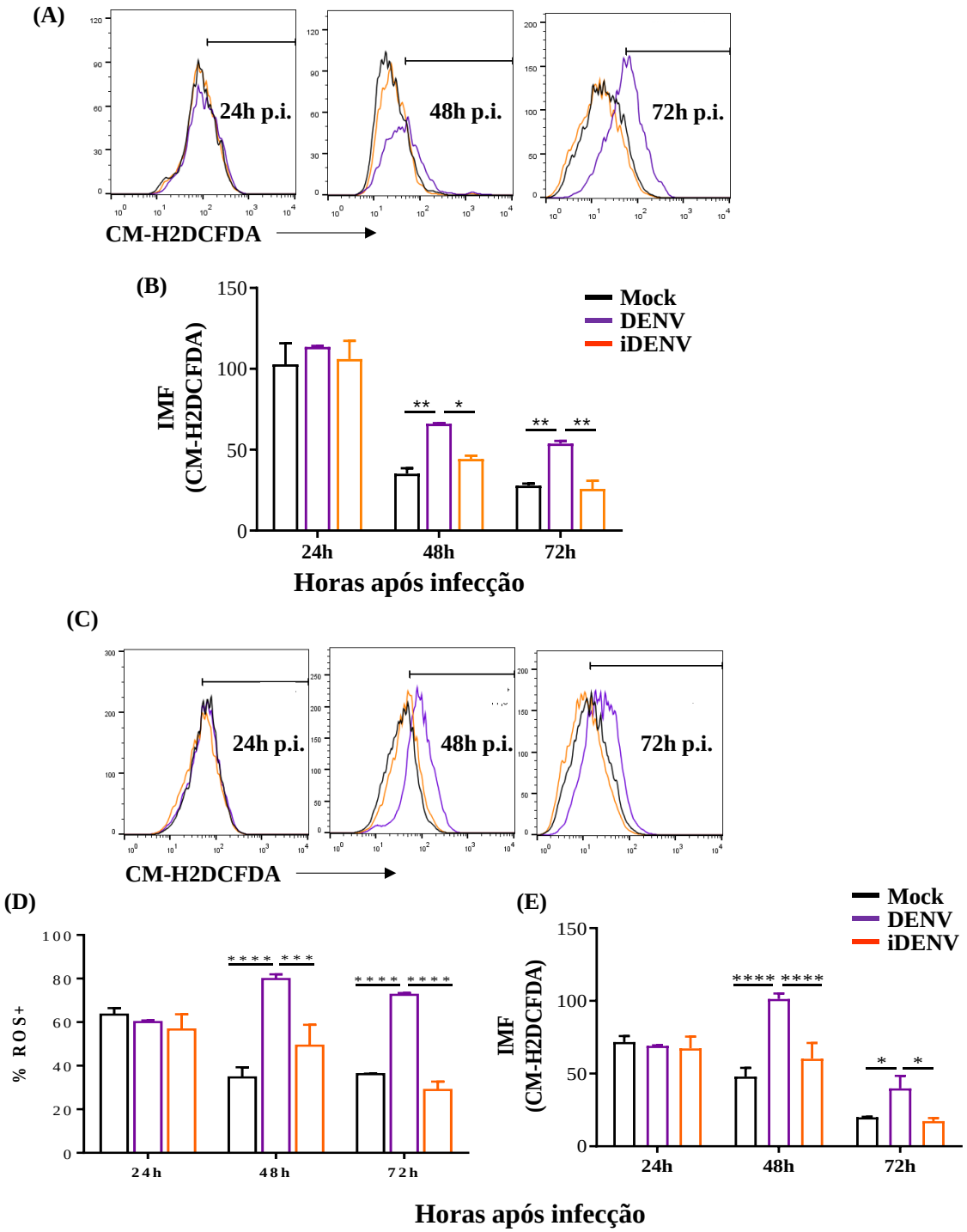

Figura 12: DENV induz aumento da produção de ROS em HBMECs. HBMECs foram cultivadas com mock, ou infectadas com DENV2 na sua forma ativa (DENV, cepa 16681) com MOI de 1 ou inativada por U.V. (iDENV UV). Após diferentes períodos de cultura, as células foram incubadas com a sonda CM-H2DCFDA e a medida da produção de ROS foi analisada por citometria de fluxo. **A)** Overlay. **B)** Gráfico de barras com os valores da intensidade média de fluorescência (MFI) com a sonda CM-H2DCFDA diluída 1:1000 (antes da padronização) e desvio padrão dos valores (DP) da MFI. **C)** Histogramas representativos contendo a sobreposição dos resultados obtidos em cada grupo experimental. **D)** Gráfico de barras com os valores que indicam o porcentual das células positivas e desvio padrão dos valores do porcentual das células positivas. **E)** Gráfico de barras com os valores da MFI com a sonda CM-H2DCFDA na concentração 2 µM para cada $1x10^6$ células (após a padronização) e desvio padrão dos valores da MFI. A média e o DP obtidos de três experimentos independentes. * representa $p \leq 0,05$; ** $p \leq 0,01$; *** $p \leq 0,001$; **** $p \leq 0,0001$.

Em seguida, avaliamos se havia aumento na produção de ROS nos períodos mais iniciais da infecção. Entre 0,5 a 8 h p.i. não observamos aumento na produção de ROS, sugerindo que ciclos de replicação viral sejam necessários para amplificar o sinal, ou que a produção ROS seja consequencia de outros efeitos celulares induzidos pela infecção (Figura 13).

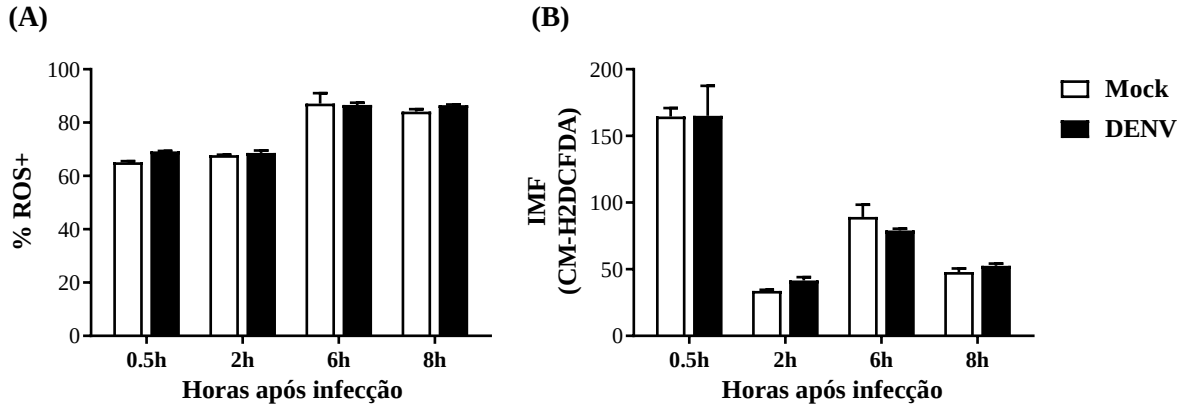

Figura 13: DENV não induz aumento da produção de ROS entre 0,5 a 8 h em HBMECs. HBMECs foram cultivadas com mock, ou infectadas com DENV2 na sua forma ativa (DENV, cepa 16681) com MOI de 1. Após diferentes períodos de cultura, as células foram incubadas com a sonda CM-H2DCFDA e a medida da produção de ROS foi analisada por citometria de fluxo. **A)** Gráfico de barras representando a média do valor do porcentual das células positivas e desvio padrão dos valores do porcentual. **B)** As barras a média do valor da MFI e desvio padrão dos valores da mesma. A média e o DP obtidos de três experimentos independentes. * representa $p \leq 0,05$; ** $p \leq 0,01$; *** $p \leq 0,001$; **** $p \leq 0,0001$.

Paralelamente, a medida da produção de ROS, acompanhamos a replicação viral e a permeabilidade celular ao longo do tempo de cultura, a fim de avaliar a correlação entre todos esses eventos. A anáise da replicação viral foi feita por ensaio de plaque e podemos observar um aumento da liberação de partículas infecciosas até o pico de 48h de infecção (Figura 14A). A análise da viabilidade celular por medida da liberação de LDH nos sobrenadantes demonstraram que a infecção por DENV induz a morte das células endoteliais de forma significativa a partir de 72h p.i., atingindo o pico após 96h p.i. (Figura 14B). A partir desses dados, determinamos que o aumento da quantidade de partículas infecciosas se correlaciona positivamente, de forma significativa, como aumento da produção de ROS (Figura 14C).

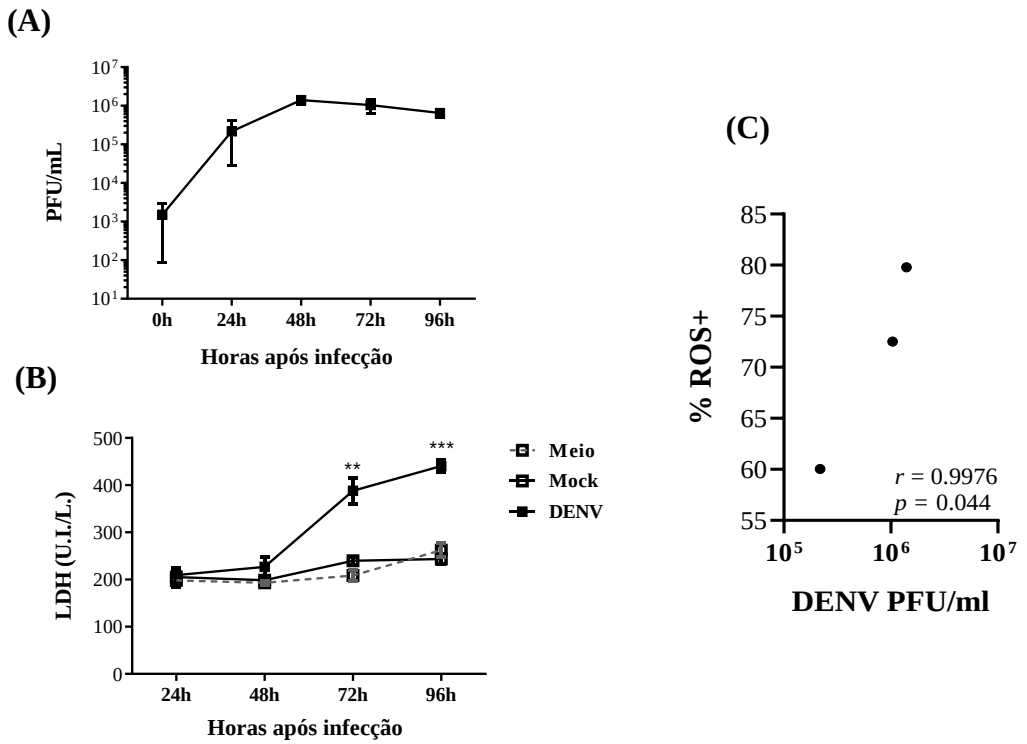

Figura 14: Relação de ROS com replicação e morte celular. HBMECs foram cultivadas com mock, ou infectadas com DENV2 na sua forma ativa (DENV, cepa 16681) com MOI de 1. Após diferentes períodos de tempo, os sobrenadantes celulares foram colhidos para a análise da morte celular e da replicação viral. **A)** Gráfico com cinética da replicação viral, análise por ensaio de *plaque*. **B)** Gráfico que indica a viabilidade celular valores indicam a medida da liberação de LDH nos sobrenadantes. **C)** Gráfico de correlação entre a quantidade de partículas infecciosas (PFU/mL) com a quantidade de células ROS+ após 48h de infecção. A média e o DP obtidos de três experimentos independentes. * representa $p \leq 0,05$; ** $p \leq 0,01$; *** $p \leq 0,001$; **** $p \leq 0,0001$.

Para confirmar esses dados, a infecção celular e produção de ROS foram avaliadas ainda, por imunofluorescência, através de marcação com hibridoma 3H51 (Figura 15), confirmando que a maior parte das células infectadas, de fato, produz ROS.

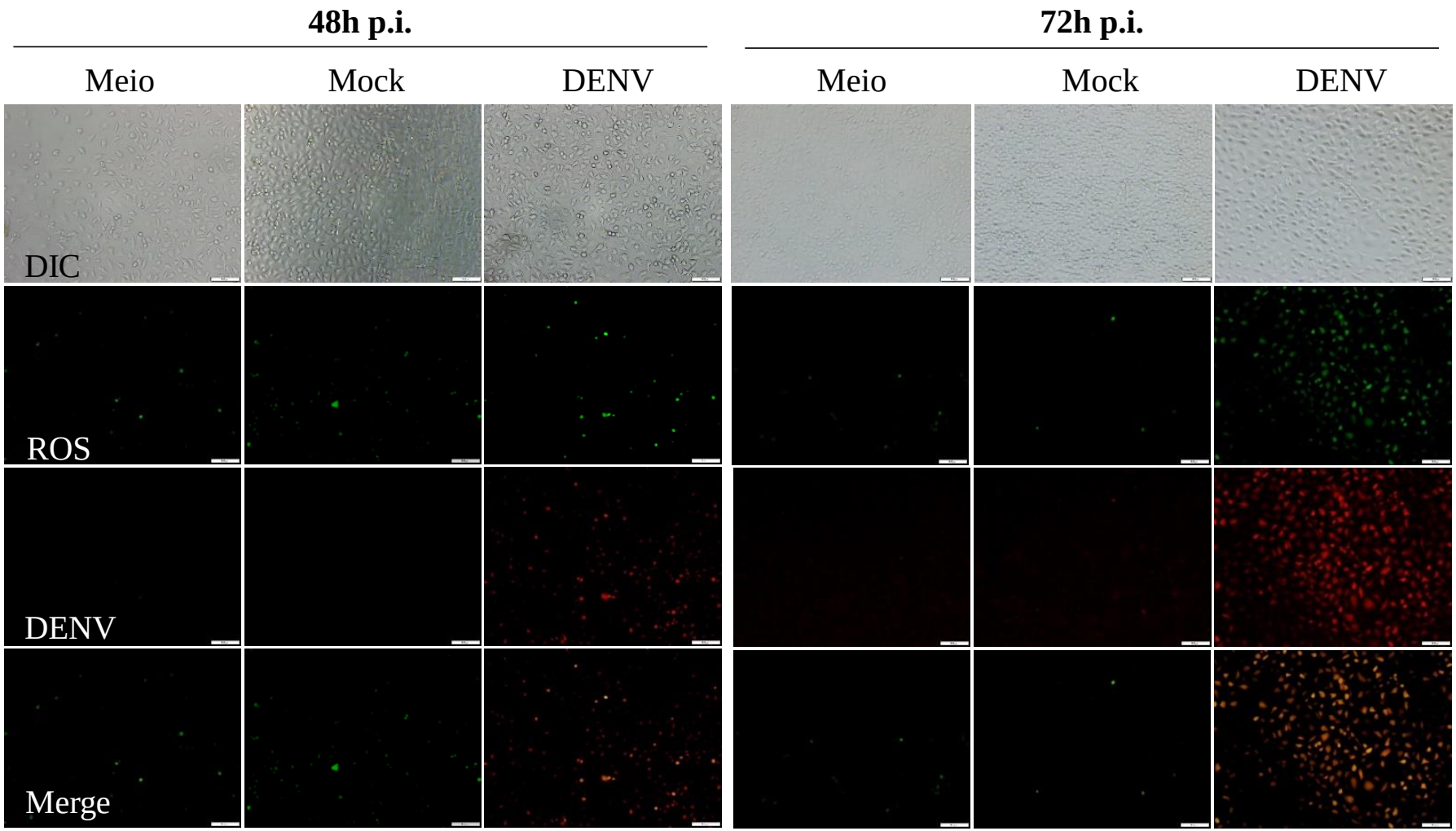

Figura 15: Avaliação da infecção viral e produção de ROS imunofluorência. HBMECs foram cultivadas com mock, ou infectadas com DENV2 na sua forma ativa (DENV, cepa 16681) com MOI de 1. Após diferentes períodos de cultura, as células foram incubadas com a sonda CM-H2DCFDA e marcadas com hibridoma 3h51, para analisar a produção de ROS e a infecção viral.

5.2. Avaliação da expressão de enzimas antioxidantes

Uma vez que nossos achados demonstraram que a infecção por DENV induz a produção de ROS de forma tardia, buscamos avaliar se havia alteração na expressão de SOD ao longo do tempo de infecção. Para isso, as HBMECs foram infectadas com o DENV e a expressão de SOD foi analisada por *western blotting*. O resultado sugere que a infecção por DENV não altera a expressão de SOD após 8h de infecção, entretanto o experimento foi realizado apenas 1 vez e precisa ser confirmado (Figura 16).

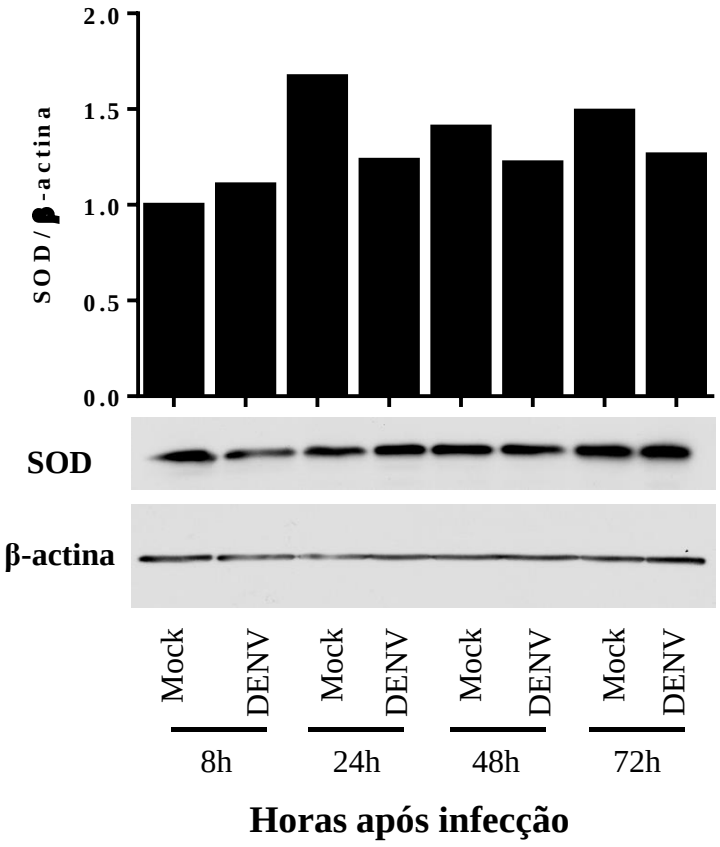

Figura 16: A expressão de SOD não sofre alteração nos tempos iniciais da infecção. As HBMECs foram infectadas com DENV 2 (cepa 16681) M.O.I de 1. Após uma cinética de infecção, as células foram recolhidas, lisadas com RIPA e submetidas a SDS-PAGE. A expressão de SOD foi realizada utilizando anticorpo anti-SOD e anticorpo anti-β-actina como controle de carregamento como descrito na metodologia. O gráfico de barras indica a razão da proteína SOD sobre a β-actina. Figura representativa de 1 experimento.

5.3. Caracterização da fonte de geração de ROS

Para investigar qual via era importante para o aumento da produção de ROS induzido pela infecção nas HBMECs, utilizamos os inibidores MitoTempo (MitoT) e a Apocinina (APO), inibidores da via mitocondrial e da NADH oxidase, respectivamente. Primeiramente, determinamos a concentração não tóxica dos inibidores através de ensaios de metabolização de XTT. A concentração não tóxica da Apocinina já havia sido avaliada durante o mestrado e determinada como 1 mM (Meuren, 2016). Para determinar a concentração de MitoTEMPO, as células foram cultivadas com doses entre 10 µM-500 µM, por 48h. Como podemos observar nenhuma das concentrações testadas foram tóxicas para célula (Figura 17).

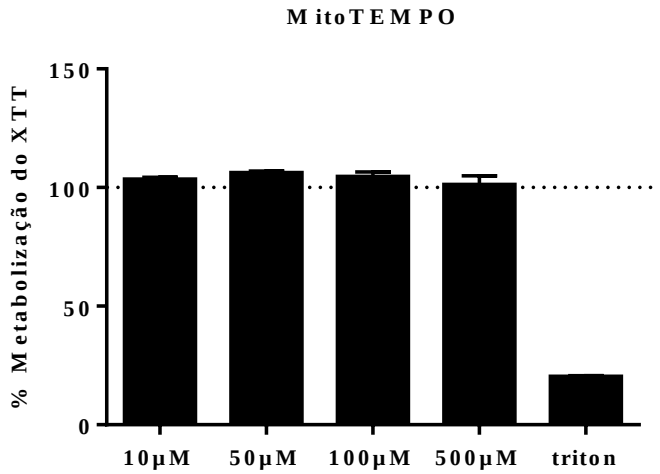

Figura 17: Curva de concentração de MitoTEMPO (MitoT) para determinar a concentração não tóxica em HBMECs. O triton foi utilizado como controle positivo para indução da morte celular. HBMECs foram mantidas com diferentes concentrações de MitoT e após 48h de contato com a cultura, o ensaio de viabilidade celular foi realizado por ensaio de XTT. A média e o DP obtidos de três experimentos independentes. * representa $p \leq 0,05$; ** $p \leq 0,01$; *** $p \leq 0,001$; **** $p \leq 0,0001$.

HBMECs foram então infectadas na presença ou ausência de Apocinina a 1 mM, N-acetilcisteína (NAC) a 1 mM ou de MitoTEMPO a 50 µM. Após 48h de infecção, foi observado uma diminuição na produção de ROS nas células tratadas com os 2 inibidores e com o antioxidante. Essa redução foi ainda maior após 72h de infecção (Figura 18A-C), sugerindo que a infecção por DENV induz aumento na produção de ROS tanto através da via NADPH-oxidase quanto da via mitocondrial.

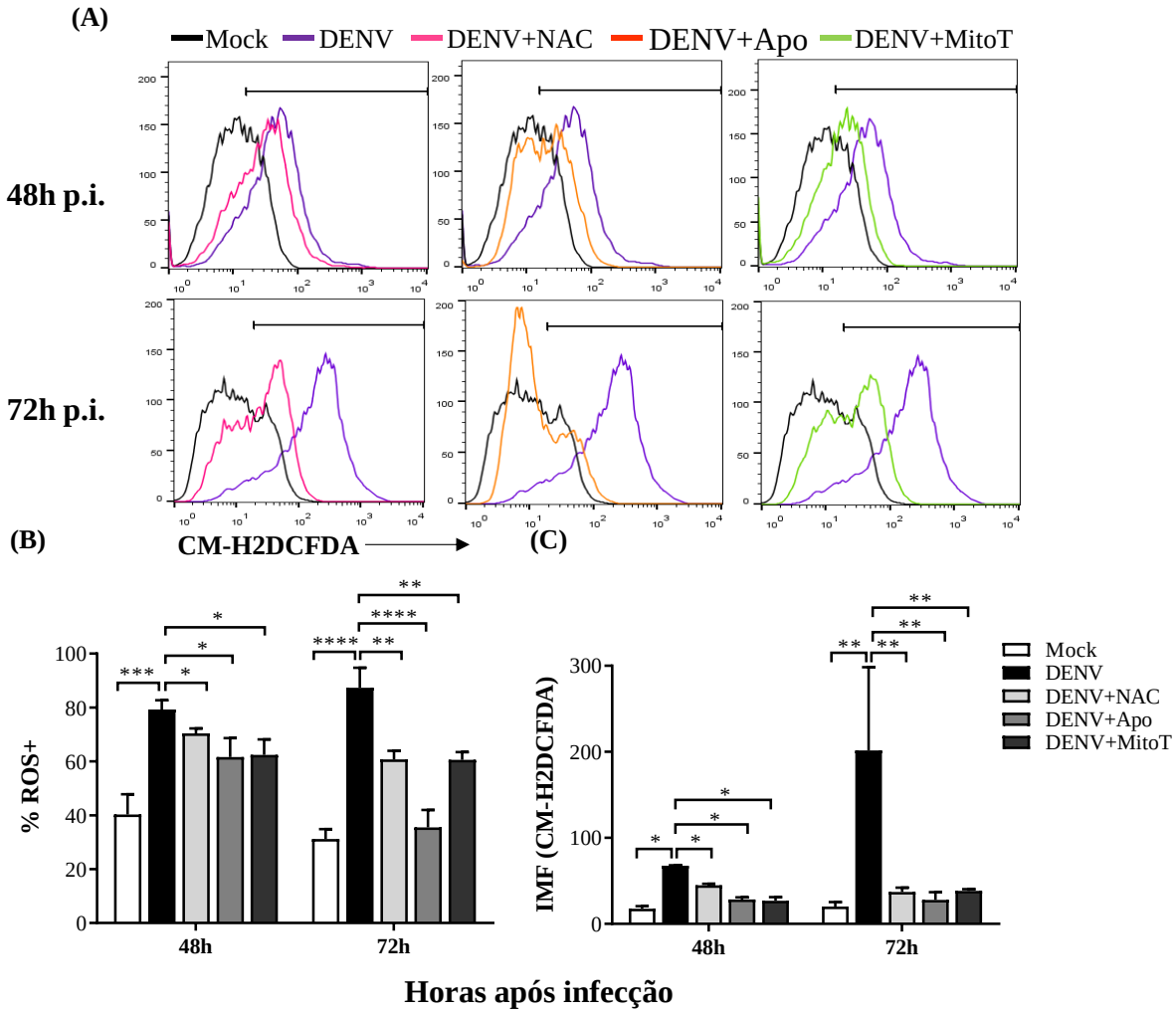

Figura 18: DENV induz aumento da produção de ROS em HBMECs via NADPH oxidase e via mitocôndria. As HBMECs foram infectadas com DENV 2 (cepa 16681) M.O.I de 1, na presença ou ausência de NAC a 1mM, Apocinina (Apo) a 1mM e MitoTEMPO (MitoT) a 50 µM. Após diferentes períodos de cultura, as células foram incubadas com a sonda CM-H2DCFDA e a medida da produção de ROS foi analisada por citometria de fluxo. **A)** Histogramas representativos contendo a sobreposição dos resultados obtidos em cada grupo experimental. **B)** Gráfico de barras com os valores que indicam o porcentual das células positivas e desvio padrão dos valores do porcentual das células positivas. **C)** Gráfico de barras com os valores da MFI e desvio padrão dos valores da mesma. A média e o DP obtidos de três experimentos independentes. * representa $p \leq 0,05$; ** $p \leq 0,01$; *** $p \leq 0,001$; **** $p \leq 0,0001$.

5.4. Confirmação que a infecção por DENV induz produção de ROS mitocondrial em HBMECs

Para confirmar que a infecção por DENV induz produção de mitROS, realizamos novo experimento utilizando a sonda MitoSOX, capaz de detectar especificamente a produção de mitROS. A adição de Heme, por 30 min, após os diferentes períodos de cultura foi realizada

como controle positivo (Fortes *et al*., 2012). Como podemos observar, a infecção induz um aumento na produção de mitROS após 48h de infecção e o pico de produção ocorre após 72h de infecção (Figura 19).

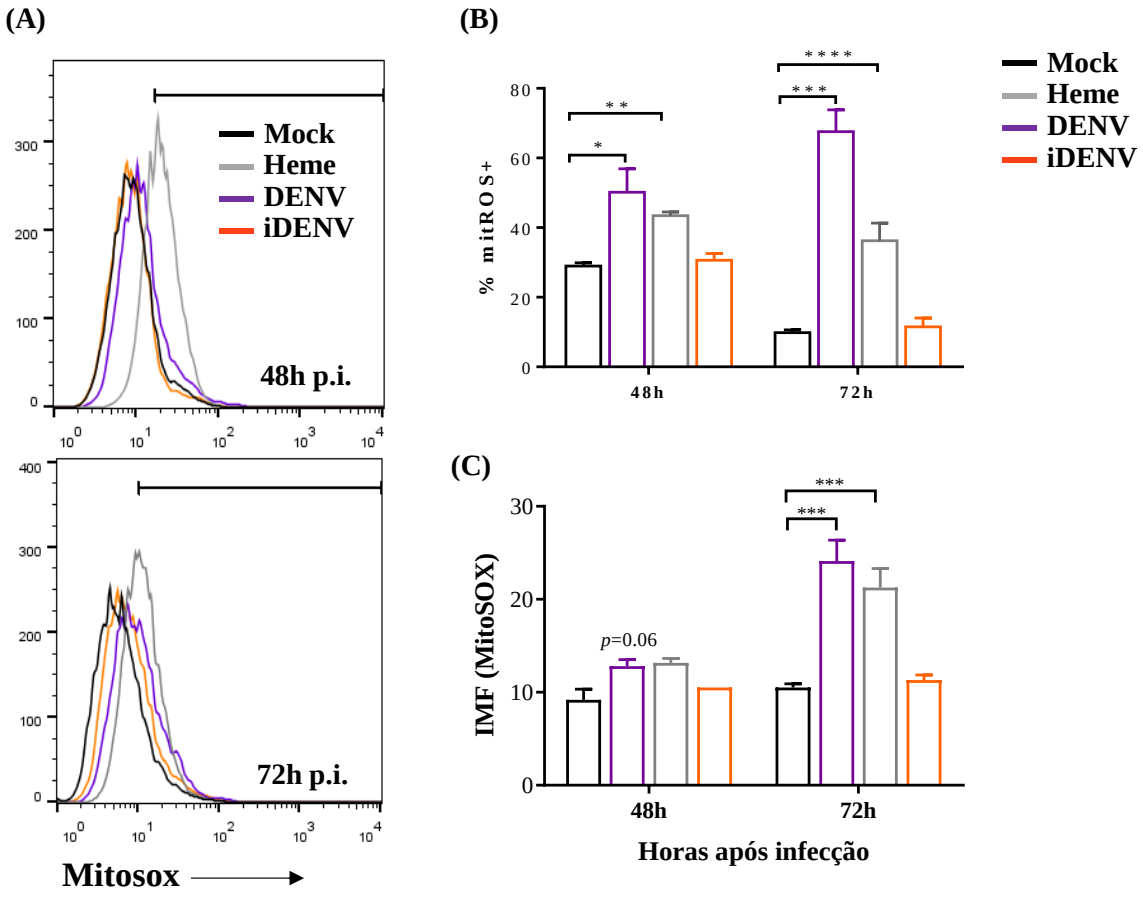

Figura 19: DENV induz aumento na produção de mitROS em HBMECs. Como controle positivo as HBMECs foram tratadas com Heme na concentração de 30 µM por 30min. As HBMECs foram infectadas com DENV 2 (cepa 16681) M.O.I de 1 por 48h a 72h. Em seguida, as células foram incubadas com a sonda MitoSOX e a medida da produção de ROS foi analisada por citometria de fluxo. **A)** Histogramas representativos contendo a sobreposição dos resultados obtidos em cada grupo experimental. **B)** Gráfico com os valores que indicam o valor do porcentual das células positivas. **C)** Gráfico com os valores que indicam a MFI em células com marcação positiva e desvio padrão dos valores da mesma. A média e o DP obtidos de três experimentos independentes. * representa $p \leq 0,05$; ** $p \leq 0,01$; *** $p \leq 0,001$; **** $p \leq 0,0001$.

5.5. Avaliação da bioenergética mitocondrial e do potencial da membrana

O envolvimento da via mitocondrial na produção de ROS induzida por DENV nos levou a avaliar a função mitocondrial por análise de respirometria de alta resolução. HBMECs foram cultivadas com mock ou infectadas com DENV por diferentes períodos de tempo entre 24 e 72 horas. Em seguida, avaliamos o consumo de oxigênio, utilizando agentes que interferem em diferentes parâmetros respiratórios. Inicialmente, foi avaliada a taxa de consumo de oxigenio (OCR) basal das células intactas no próprio meio de cultura. Em seguida, adicionamos Oligomicina, que inibe o retorno dos prótons localizados no espaço intermembranar para a matriz mitocondrial, por levar a inibição da subunidade F_o da F_oF_I-ATP-sintase. Assim, determinamos o OCR independente da síntese de ATP. Para avaliar a capacidade respiratória máxima, adicionamos FCCP, um ionóforo que carreia os prótons de volta à matriz mitocondrial, promovendo o desacoplamento entre o consumo do oxigênio e a síntese de ATP. Com esses parâmetros, foi possível avaliar a respiração basal (antes da adição de Oligomicina), a taxa de consumo independente de ATP ou desacoplada (*uncoupled OCR*, após a adição de Oligomicina), a taxa associada a ATP ou acoplada (*coupled OCR*, resultante da diferença entre respiração antes e após adição de Oligomicina), a capacidade máxima respiratória (após adição de FCCP), e a capacidade de reserva (resultante da diferença entre a respiração obtida após adição de FCCP e a respiração basal).

Após 24h de infecção não detectamos nenhuma diferença significativa nos parâmetros respiratórios das células infectadas com DENV em relação as células cultivadas com mock (Figuras 20A-B). Porém, em 48h p.i. as HBMECs infectadas com DENV apresentaram redução da respiração basal quando comparadas com as células controle (Figura 20 C-D). Como esperado, a inibição da ATP sintase pela adição de Oligomicina diminuiu, significativamente, a OCR das células controle (2,7 vezes, $p<0.001$). Por outro lado, a Oligomicina induziu uma diminuição sutil, não significativa, da OCR nas células infectadas (1,6 vezes, $p=0.082$). De fato, HBMECs infectadas com DENV apresentaram taxas semelhantes de consumo de oxigênio basal, acoplado ou desacoplado nesse período de tempo. Esse dado sugere que a respiração celular já estaria comprometida, possivelmente com perda de potencial de membrana mitocondrial. Além disso, as HBMECs infectadas com DENV apresentam redução do consumo máximo induzido por FCCP (Figura 20), o que reflete uma diminuição da capacidade máxima respiratória e da capacidade de reserva. Esses dados indicam que o DENV induz perturbações

na cadeia respiratória mitocondrial devido ao aumento do vazamento da membrana mitocondrial.

Em seguida, avaliamos o potencial de membrana mitocondrial, a partir de 48h p.i., através de marcação com a sonda JC-1. Este é um corante carbocianina catiônico, que emite fluorescência no espectro verde (Ex 514 nm/Em 529 nm), e que acumula na mitocôndria de forma dependente de potencial de membrana. Quando a membrana mitocondrial está polarizada, a sonda se acumula e forma agregados, passando a emitir fluorescência no espectro vermelho. A despolarização mitocondrial é indicada pela diminuição na razão de intensidade da fluorescência vermelho/verde. Como podemos observar, o DENV induz a perda do potencial de membrana em HBMECs (Figura 20 E-F). Em conjunto, esses achados sugerem que o DENV-2 prejudica a função mitocondrial e o potencial de membrana, o que pode contribuir para o aumento de mtROS, o qual foi detectado, principalmente, em momentos posteriores da infecção (72h p.i).

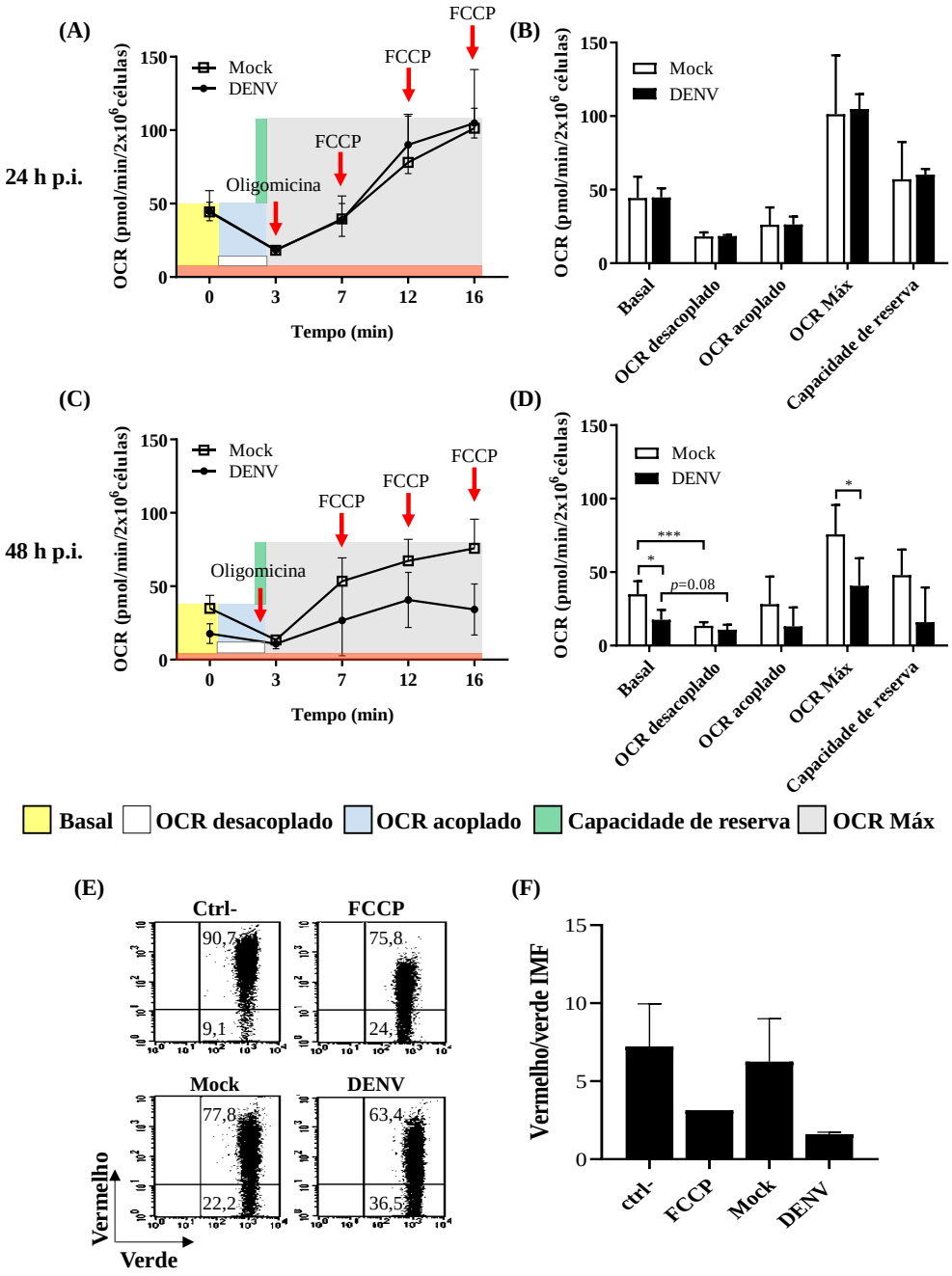

Figura 20: Análise da bioenergética mitocondrial em HBMECs infectadas com DENV. HBMECs foram infectadas com DENV2 MOI de 1 ou tratadas com Mock. **A e C)** Fluxograma da respiração do controle Mock e das células infectadas com DENV após 24h e 48h, respectivamente. **B e D)** Valores da respiração celular após 24h e 48h, respectivamente. Para essa análise foi adicionada a Oligomicina (200 µg/mL) e FCCP (1 mM). Basal é a respiração sem adição de nenhum inibidor ou indutor; OCR desacoplado valor da respiração após a adição da Oligomicina referindo ao OCR independente da ATP-sintase; OCR acoplado é o valor da Oligomicina menos o Basal o que representa o valor OCR ligado a ATP; OCR Máx é o valor após adição do FCCP e mede o OCR máximo; Capacidade de reserva é diferença entre o valor do FCCP com o Basal. **E) e F)** Análise do potencial de membrana mitocondrial com uso da sonda JC-1, CCCP utilizado como controle positivo. **E)** *Dot Plot* representativo com os valores que indicam porcentagem de células com marcação positiva JC-1. **F)** Razão do porcentual das células positivas para vermelho e porcentual das células positivas para verde obtido da média ± DP de 2 experimentos. * representa $p \leq 0,05$; ** $p \leq 0,01$; *** $p \leq 0,001$; **** $p \leq 0,0001$.

5.6. Avaliação entre a relação da produção de ROS total e de mitROS

Dados da literatura indicam que o próprio aumento de ROS intracelular pode levar a disfunção mitocondrial e geração subsequente de ROS por essa via, amplificando o processo (Zorov, Juhaszova e Sollott, 2014). Para investigar se a produção de mitROS ocorre de forma dependente do aumento de ROS via NOX, as células foram infectadas na presença ou ausência de Apocinina e marcadas com a sonda MitoSOX. Como controles, as células foram também marcadas com a sonda CM-H2DCFDA. Como esperado, a adição de Apocinina reduziu a frequência de produção de ROS total (Figura 21A-C). No entanto, a adição do inibidor não afetou os níveis de mitROS produzidos pelas células infectadas com DENV (Figura 21D-F), o que nos indica a produção de ROS via mitocôndria e via NADPH oxidase podem ocorrer de formas independentes.

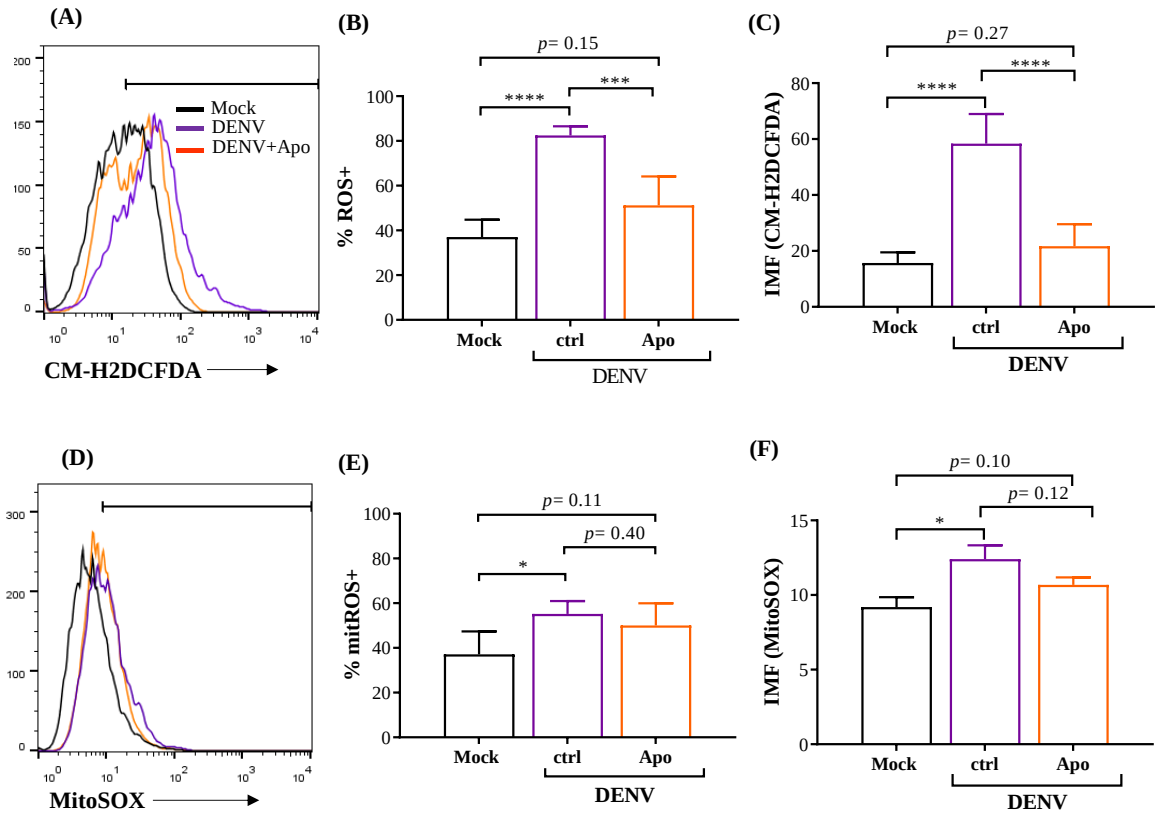

Figura 21: O aumento da produção de ROS dependente de NOX parece ocorrer de forma independente. As HBMECs foram infectadas com DENV 2 (cepa 16681) M.O.I de 1, na presença ou ausência do inibidor da NADPH oxidase (Apocinina, Apo a 1mM). Após diferentes períodos de cultura, as células foram incubadas com a sonda CM-H2DCFDA ou MitoSOX. A medida da produção de ROS foi analisada por citometria de fluxo. **A)** Histogramas representativos contendo a sobreposição dos resultados obtidos em cada grupo experimental. das HBMECs com marcação da sonda CM-H2DCFDA. **B)** Gráfico de barras com os valores que indicam o porcentual das células positivas para ROS total e desvio padrão dos valores do porcentual das células positivas. **C)** Gráfico de barras com os valores da MFI, sonda CM-H2DCFDA. **D)** Histogramas representativos contendo a sobreposição dos resultados obtidos em cada grupo experimental. das HBMECs com marcação da sonda MitoSOX. **E)** Gráfico de barras com os valores que indicam o porcentual das células positivas para ROS mitocondrial. **F)** Gráfico de barras com os valores da MFI, sonda MitoSOX. A média e o DP obtidos de três experimentos independentes. * representa $p \leq 0,05$; ** $p \leq 0,01$; *** $p \leq 0,001$; **** $p \leq 0,0001$.

5.7. A inibição das principais vias de produção de ROS reduzem a morte celular.

Dados anteriores do grupo demonstraram que a infecção de HBMECs por DENV induz morte celular, com expressão de fosfatidil serina e perda de integridade de membrana, de forma significativa, a partir de 72h pós infecção (PAPA, 2014). Para avaliar o papel da indução da produção de ROS na viabilidade das células endoteliais infectadas, as HBMECs foram infectadas com o DENV, na presença ou na ausência de Apocinina, ou mitoTEMPO ou N-acetilcisteína. A viabilidade celular foi avaliada por marcação com iodeto de propídeo (PI) e

análise por citometria de fluxo. Nós observamos que o tratamento com os inibidores de ROS da via NADPH-oxidase e da via mitocondrial, ou com antioxidante reduziram o porcentual de células positivas para PI a partir de 48h de infecção e esta diferença se manteve até 72h após infecção (Figura 22A, B), demonstrando que a geração de ROS por ambas as vias era importante na indução de morte celular nesse modelo de infecção.

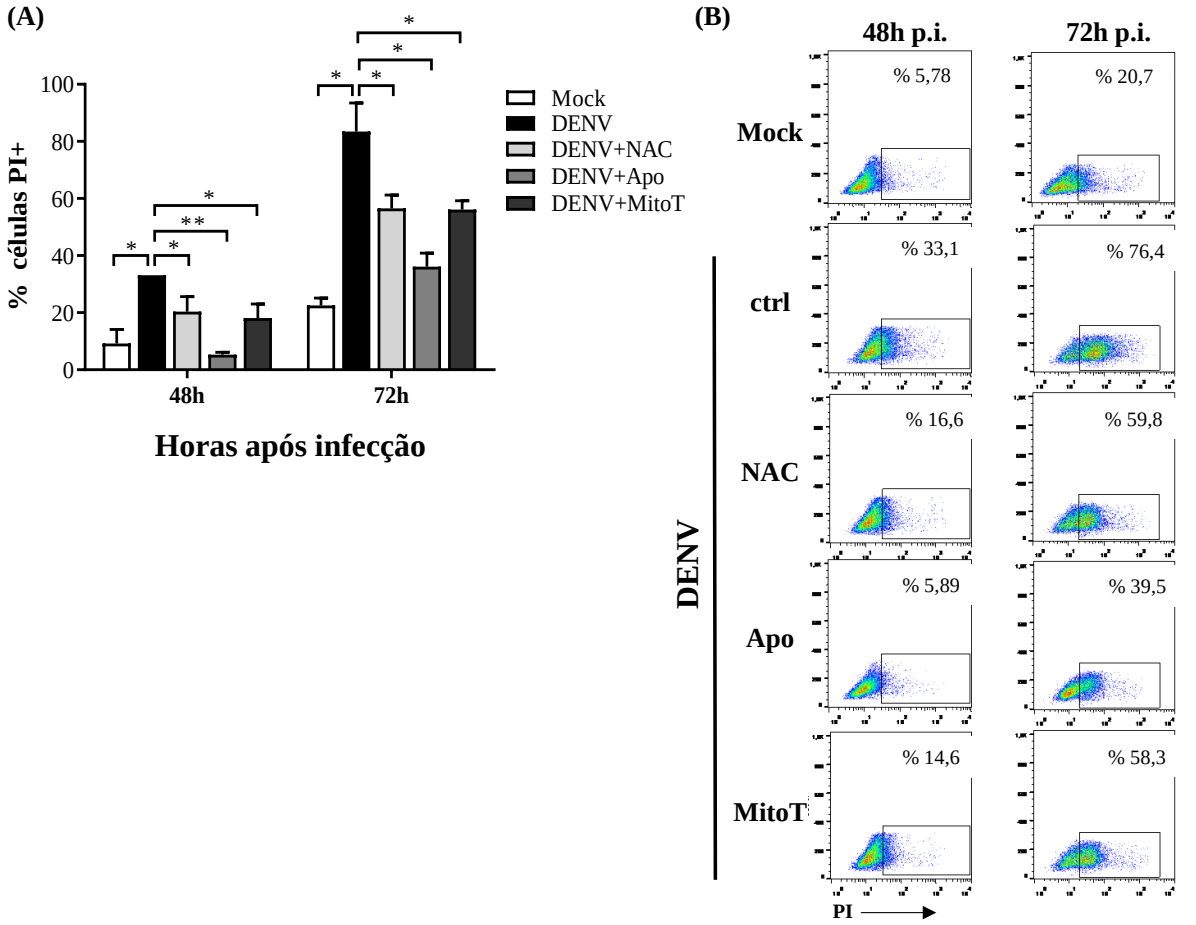

Figura 22: A inibição de ROS reduz a morte celular. As HBMECs foram infectadas com DENV 2 (cepa 16681) M.O.I de 1, na presença ou ausência de NAC a 1 mM, Apocinina (Apo) a 1 mM e MitoTEMPO (MitoT) a 50 µM. As células foram marcadas com Iodeto de Propídeo (PI). Em seguida, análise foi realizada por citometria de fluxo. **A)** As barras indicam a porcentagem de células PI+ para cada situação estudada. **B)** Dot Plot representativo com os valores que indicam porcentagem de células com marcação positiva para PI. A média e o DP obtidos de três experimentos independentes. * representa $p \leq 0,05$; ** $p \leq 0,01$; *** $p \leq 0,001$; **** $p \leq 0,0001$.

5.8. A inibição das principais vias de produção de ROS reduzem a replicação viral.

Em seguida, avaliamos se a produção de ROS afetava a replicação do DENV. Para tal, HBMECs foram infectadas na presença ou ausência de NAC a 1 mM. Na figura 23 observamos que a inibição de ROS diminui os níveis de RNA do sobrenadante após 48h de infecção. As HBMECs também foram infectadas na presença ou ausência de Apocinina e de MitoTEMPO, que promoveram a redução da quantidade de vírus após 48h de infecção. Entretanto, após 72h de infecção, apenas a Apocinina manteve a redução da quantidade de vírus produzida (Figura 23B).

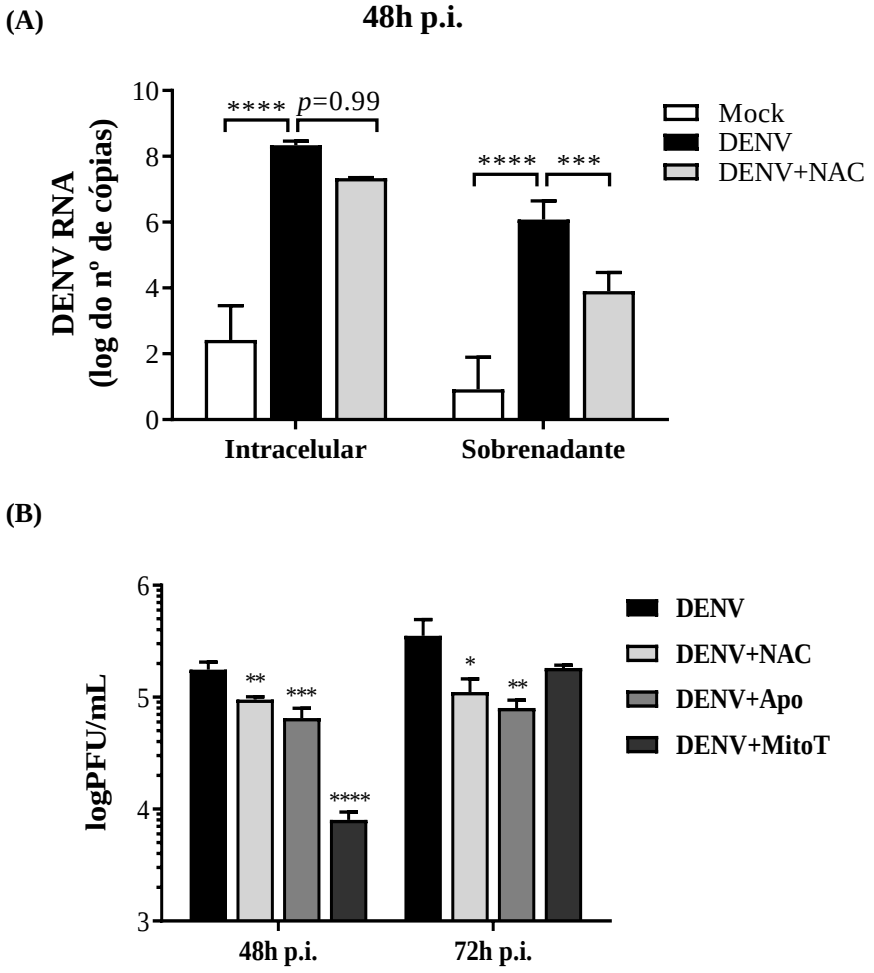

Figura 23: A inibição de ROS reduz a replicação viral. As HBMECs foram infectadas com DENV 2 (cepa 16681) M.O.I de 1, na presença ou ausência NAC a 1 mM, Apocinina (Apo) a 1mM e MitoTEMPO (MitoT) a 50 µM. **A)** Após 48h de infecção, as células e os sobrenadantes foram coletados, o RNA extraído, e após síntese do cDNA, a presença do genoma viral foi avaliada por PCR quantitativo em tempo real (qRT-PCR). **B)** A quantidade de partícula viral foi avaliada após 48h e 72h e a análise foi realizada por ensaio de plaque. A média e o DP obtidos de três experimentos independentes. * representa $p \leq 0,05$; ** $p \leq 0,01$; *** $p \leq 0,001$; **** $p \leq 0,0001$.

5.9. A infecção por DENV induz autofagia em HBMECs, que pode ser regulada por ROS

O estresse oxidativo é capaz de induzir a autofagia, e esta indução tem como objetivo contribuir com a redução dos danos oxidativos, através da degradação das substâncias oxidadas (Li *et al*., 2015). Estudos anteriores sugeriram o aumento da produção de ROS induzida por DENV em linhagem celular MDCK induz autofagia, e que este processo é importante para replicação viral (Datan *et al*., 2016). Portanto, a nossa hipótese é que a produção de ROS induza a autofagia, e esta maquinaria seria importante para a replicação de DENV em HBMECs. Inicialmente, avaliamos se DENV induz autofagia no nosso modelo, através da avaliação cinética da expressão de p62 e LC3 mensurada por *western blotting*.

Dados preliminares, nos demonstraram que a infecção por DENV parece induzir o acúmulo de p62 após 48h de infecção e aumento na conversão de LC3 para LC3b após 24h de infecção (Figura 24A-B). Em conjunto, esses dados nos indicam que o DENV induz autofagia em HBMECs e aparentemente, não pela via clássica, uma vez que observamos acúmulo, e não degradação de p62.

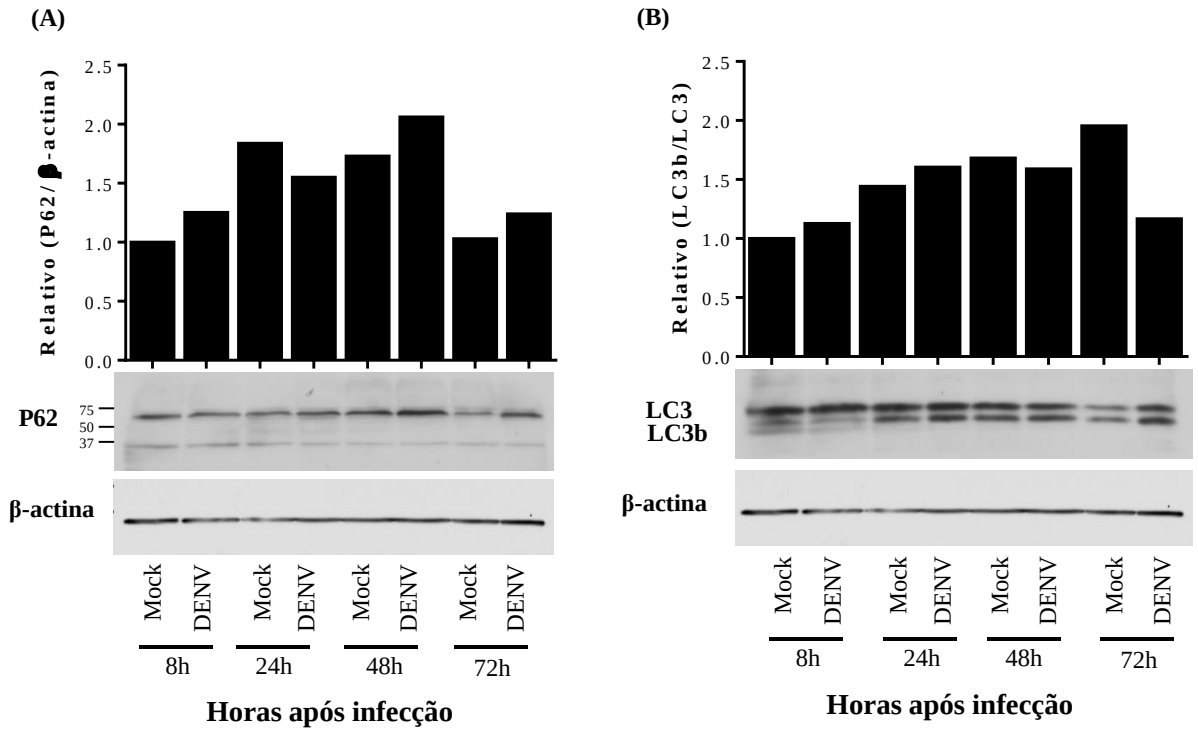

Figura 24: DENV induz a autofagia em HBMECs. As HBMECs foram tratadas com mock ou infectadas com DENV 2 (cepa 16681) M.O.I de 1. Após diferentes períodos de cultura, as células foram recolhidas, lisadas, e a expressão de p62 e LC3 foi avaliada por *western blotting*, utilizando anticorpos específicos. A expressão de β-actina foi utilizada como controle de carregamento, como descrito na metodologia. Os valores da densiometria foram determinados utilizando-se o programa ImageJ. A) Razão entre os níveis de expressão de p62 em relação a β-actina e normalização pelo Mock 8h p.i.; B) razão entre os níveis de expressão de LC3-II e LC3 e normalização pelo Mock 8h p.i.. Figura representativa de um único experimento realizado.

Em seguida, avaliamos se a produção de ROS era importante para a indução da autofagia. Para isso, as HBMECs foram infectadas com DENV, na presença ou ausência do antioxidante NAC; e a expressão de P62 foi dosada por *western blotting*. Como podemos observar, ainda que de forma preliminar, no tempo de 48h p.i. que é o pico de acúmulo de p62 induzido pelo a infecção, a adição de NAC reduziu o acúmulo de P62. (Figura 25). Esse dado preliminar, sugere o aumento da produção de ROS é importante para a indução da autofagia, o que pode favorecer a replicação viral.

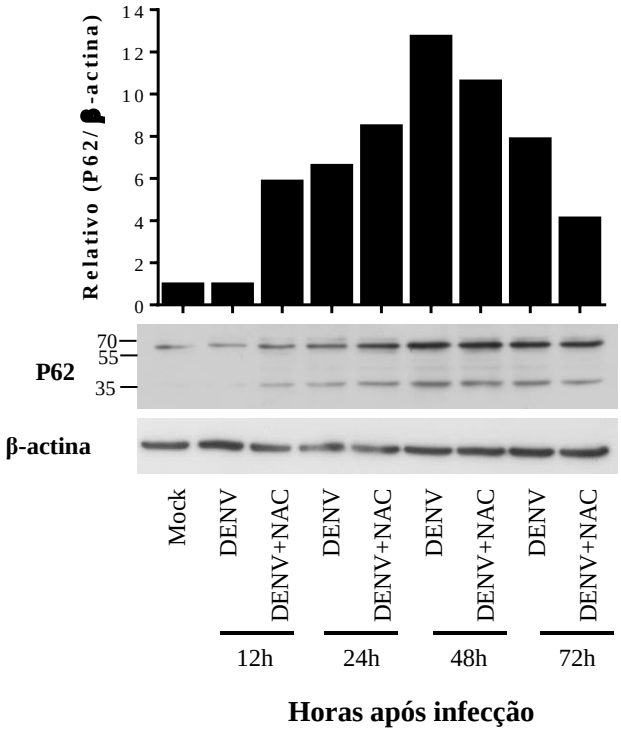

Figura 25: ROS parece ser importante na indução da autofagia. As HBMECs foram infectadas com DENV 2 (cepa 16681) M.O.I de 1. Após uma cinética de infecção, as células foram recolhidas, lisadas com RIPA e submetidas a SDS-PAGE como descrito na metodologia. A expressão de P62 foi realizada utilizando anticorpo anti-P62.O anticorpo anti-β-actina foi utilizado como controle de carregamento. O gráfico de barras indica a razão da proteína P62 sobre a β-actina e normalizado a partir do Mock. Figura representativa de um único experimento realizado.

5.10. Indução de ROS mitocondrial por DENV induz permeabilidade de HBMECs

Nosso próximo objetivo foi avaliar se a produção de ROS também estaria envolvida na perda de integridade da monocamada da HBMEC induzida por DENV. A células foram semeadas no lado superior do inserto (transwell) e infectadas com DENV-2, com ou sem NAC, apocinina ou mitoTEMPO. Após 48 e 72 h. p.i foi medida a resistência elétrica transendotelial (TEER) e a permeabilidade foi avaliada após 72 h.p.i. através do extravasamento de BSA conjugado com FITC. Mock e Estaurosporina (STS) foram usados como controles negativos e positivos, respectivamente. Como podemos observar, a infecção por DENV induz o aumento da permeabilidade celular (Figura 26A-B). O tratamento com NAC ou MitoTEMPO reverteram esse evento; entretanto, o tratamento com a Apocinina não foi capaz de proteger, significativamente, a monocamada (Figura 26A, B). Esses dados sugerem que a produção ROS

derivada da via mitocondrial está correlacionado com alteração na permeabilidade endotelial induzida por DENV.

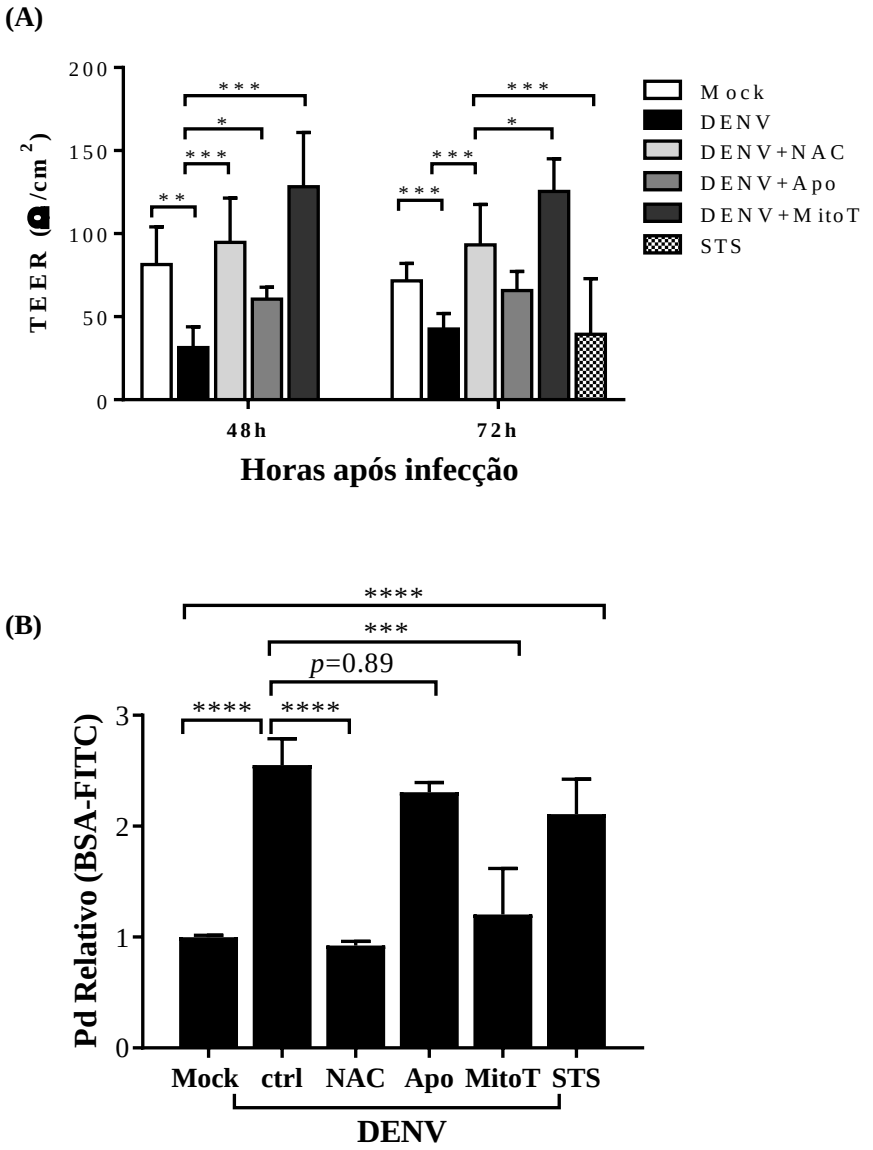

Figura 26: ROS mitocondrial está associado com o aumento da permeabilidade das HBMECs infectadas com DENV, mas o ROS produzido via NADPH-oxidase não está associada com este aumento. As HBMECs foram cultivadas na placa com inserto (transwell) e tratadas com Mock ou infectadas com DENV, na presença ou ausência de NAC a 1 mM, MitoT a 50 µM e Apo a 1 mM. **A)** TEER foi medido após 48h e 72h após infecção. Como controle as células foram tratadas com Estaurosporina (STS). **B)** Após 72h de infecção, as células foram incubadas com FITC-BSA por 1 hora, o extravasamento de BSA foi medido por espectrofotômetro, e o coeficiente de permeabilidade (Pd) foi calculado e normalizado em relação as células cultivadas apenas com meio. A média e o DP obtidos de três experimentos independentes. * representa $p \leq 0,05$; ** $p \leq 0,01$; *** $p \leq 0,001$; **** $p \leq 0,0001$.

5.11. ROS via NADPHox é essencial para a secreção de citocinas inflamatórias induzidas durante a infecção de HBMECs por DENV

Nosso grupo já havia demonstrado anteriormente que a infecção por DENV em HBMECs induz a produção de citocinas pró-inflamatórias, quimiocinas e interferon tipo I (Conceição *et al*, 2013). Uma vez que o aumento da produção de ROS intracelular já foi descrito como sinalizador de respostas imunes em outros tipos de células humanas (Olaigner *et al*., 2014), decidimos investigar se a produção de ROS em HBMECs também levava a ativação destas células. Para isso, as células foram infectadas, na presença ou ausência de moduladores de ROS. A expressão de IFN-β e os níveis de IL-6, IL-8 e CCL5 liberados nos sobrenadantes foram medidos por qRT-PCR e ELISA, respectivamente. A secreção de IL-6, IL-8 e CCL5 foi inibida por NAC e Apocinina, significativamente, mas não por mitoTEMPO (Figura 27A-C), indicando que apenas ROS derivados de NOX contribuem para a transdução de sinal associada à liberação destas citocinas. Curiosamente, a expressão aumentada de IFN-β induzida pela infecção por DENV não foi modulada por nenhum inibidor, ou foi recuperada neste momento (Figura 27D).

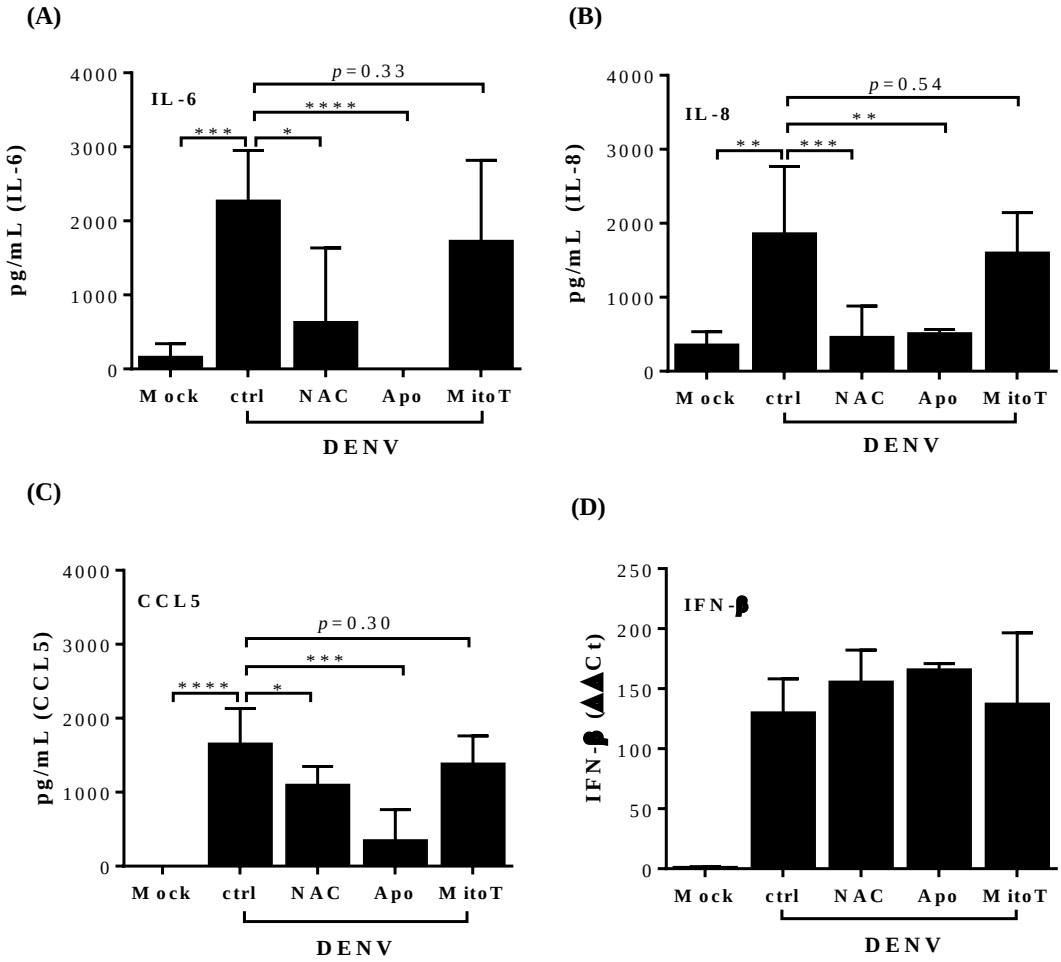

Figura 27: O aumento na produção de ROS via NADPHox é essencial para a secreção de citocinas inflamatórias induzidas pela infecção por DENV em HBMECs. As HBMECs foram infectadas com DENV 2 (cepa 16681) M.O.I de 1, na presença ou ausência de NAC a 1 mM, Apocinina (Apo) a 1 mM ou MitoTEMPO (MitoT) a 50 µM). Após 48h p.i., o sobrenadante foi colhido para avaliação da produção de citocinas. **A)** IL-6 **B)** IL-8 **C)** CCL5 foram quantificadas por ELISA. **D)** Os níveis de mRNA de IFN-β foi medido, após 48 h p.i., por PCR quantitativo em tempo real. A média e o DP obtidos de três experimentos independentes. * representa $p \leq 0,05$; ** $p \leq 0,01$; *** $p \leq 0,001$; **** $p \leq 0,0001$.

5.12. Ativação de RIG-I pode ser importante para induzir o aumento de ROS

Em seguida, investigamos se o reconhecimento viral e ativação de RIG-I era importante para induzir o aumento de ROS. Para isso, foi realizado o silenciamento gene que codifica RIG-I das HBMECs com auxílio de um RNA de interferência. Análise de *western blotting* demonstrou que, de fato o silenciamento é eficiente no período de 48h (Figura 28). As células silenciadas ou não para a expressão de RIG-I foram infectadas e marcadas com as sondas para avaliação da produção de ROS após 48h. No resultado preliminar foi possível observar uma

tendência na queda da produção de mitROS ao silenciar RIG-I (Figura 29A-C). Contudo precisamos confirmar esse resultado.

Também buscamos avaliar se a produção de ROS era importante para a expressão de RIG-I. Para isso, as HBMECs foram infectadas na presença ou ausência de Apocinina ou mitoTEMPO e, em seguida, avaliamos a expressão de RIG-I. Embora trate-se de experimento foi realizado apenas uma vez, podemos observar que ROS aparentemente é importante para a expressão de RIG-I (Figura 30). Esses dados em conjunto, sugerem que a ativação de RIG-I pode ser importante para o disparo para o aumento da produção de mitROS, podendo ser um efeito direto ou dependente da produção de outros mediadores. Além disso, o ROS produzido pode amplificar o processo inflamatório por via dependente de aumento da ativação de RIG-I.

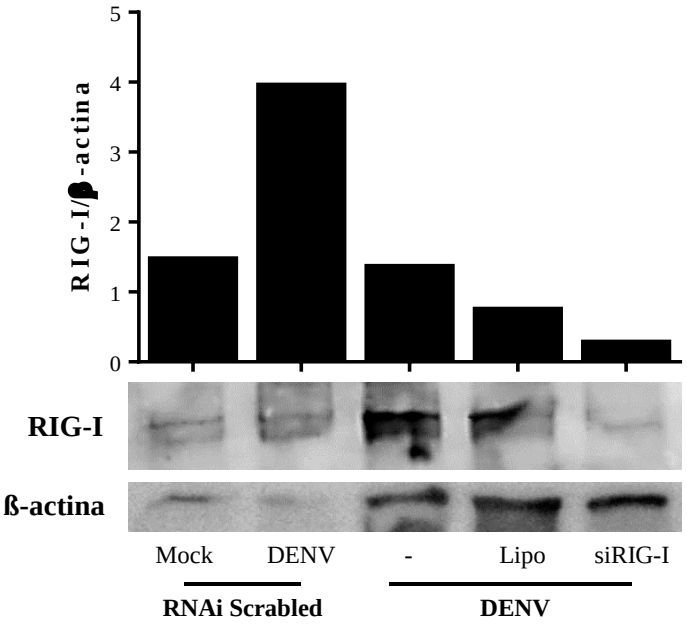

Figura 28: Confirmação do silenciamento de RIG-I. As HBMECs foram transfectadas com siRNA RIG-I e como controle positivo de indução de RIG-I, as células foram infectadas com DENV 2 (cepa 16681) M.O.I de 1. Após 48h de infecção, as células foram recolhidas, lisadas com RIPA e submetidas a SDS-PAGE. A expressão de RIG-I foi realizada utilizando anticorpo anti-RIG-I e anticorpo anti-β-actina como controle de carregamento como descrito na metodologia. O gráfico de barras indica a razão da proteína RIG-I sobre a β-actina. Figura representativa de um único experimento realizado.

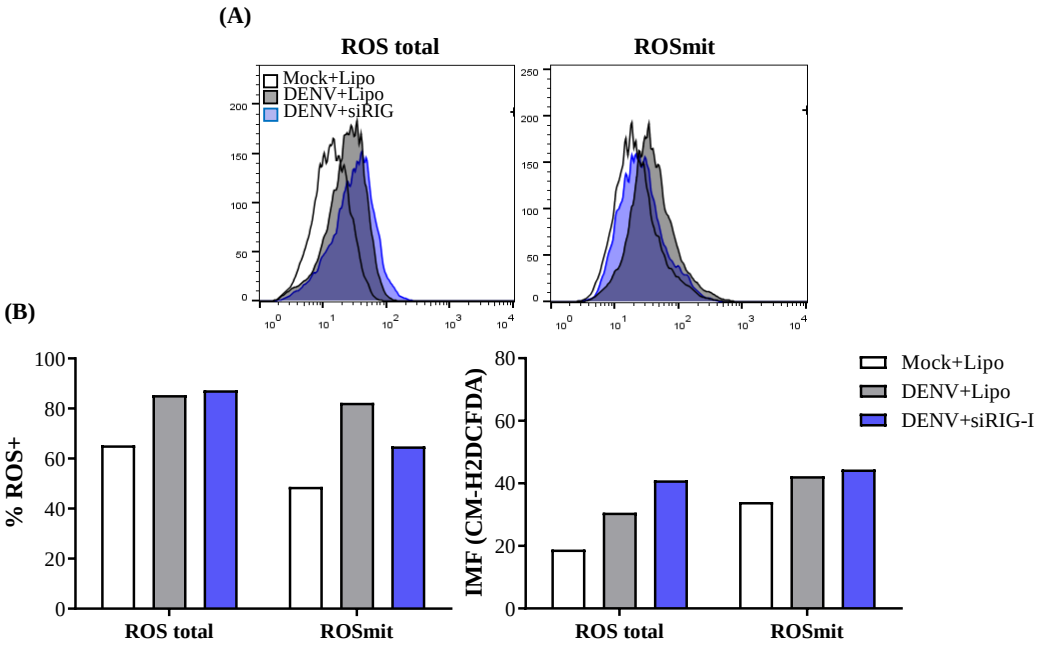

Figura 29: O aumento na produção de ROS via mitocondrial pode acontecer de forma dependente de ativação de RIG-I. As HBMECs foram infectadas com DENV 2 (cepa 16681, M.O.I) de 1. Após 48h de infecção, as células foram incubadas com a sonda CM-H2DCFDA ou MitoSOX, e a medida da produção de ROS foi analisada por citometria de fluxo. **A)** Histogramas representativos contendo a sobreposição dos resultados obtidos em cada grupo experimental. **B)** Gráfico de barras com os valores que indicam o porcentual das células positivas. **C)** Gráfico de barras com os valores da MFI. D) Imunofluorência. Figura representativa de um único experimento realizado.

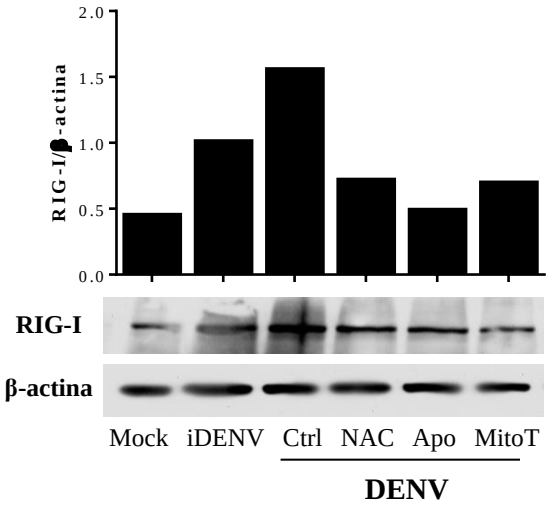

Figura 30: O aumento da produção de ROS pode ser importante para a ativação de RIG-I. As HBMECs foram infectadas com DENV 2 (cepa 16681) M.O.I de 1, na presença ou ausência de NAC a 1 mM, Apocinina (Apo) a 1mM e MitoTEMPO (MitoT) a 50 µM). Após 48h de infecção, as células foram recolhidas, lisadas com RIPA e submetidas a SDS-PAGE. A expressão de RIG-I foi realizada utilizando anticorpo anti-RIG-I e anticorpo anti-β-actina como controle de carregamento como descrito na metodologia. O gráfico de barras indica a razão da proteína RIG-I sobre a β-actina. Figura representativa de um único experimento realizado.

6. Discussão

A infecção por dengue está associada com a uma resposta inflamatória exacerbada, e alterações vasculares, como vasodilatação e aumento na permeabilidade vascular, indicando que as células endoteliais são um ponto chave na patogênese da doença. Nessa tese, demonstramos que a infecção das células endoteliais por dengue induz o aumento da produção ROS tanto mitocondrial quanto via NOX, que esse aumento depende parcialmente do reconhecimento viral por RIG-I, e está associado a modulação da replicação viral, ativação celular, morte celular e permeabilidade endotelial.

Como já mencionado, ROS são subprodutos derivados do oxigênio molecular e são produzidos durante a redução incompleta do oxigênio. E são normalmente produzidos em metabolismos aeróbicos durante a cadeia respiratória. Alguns fatores, como exposição UV, infecções virais são capazes de induzir a célula a um estado de estrese celular. Consta na literatura que as células endoteliais quando ativadas ou em situação de estresse, possuem a capacidade de aumentar os níveis de ROS e NO (Gorlach *et al*., 2000; Li e Shah, 2002). Também foi descrito que a infecção por DENV em células primárias HUVEC induz o aumento nos níveis de ROS, e que este aumento está relacionado com a indução de morte celular por apoptose (Yen *et al*., 2008).

Inicialmente, realizamos uma cinética para avaliar os níveis de ROS induzidos pela replicação de DENV em HBMECs e observamos que, em períodos iniciais de infecção, não houve indução de ROS. No entanto, detectamos um aumento na frequência de células produtoras de ROS e no nível de ROS produzido a partir de 48h p.i., que se sustentava por 72h p.i.. Além disso, a frequência de células produtoras de ROS se correlacionou positivamente com os títulos de partículas infecciosas produzidas, indicando que a produção de ROS dependente de replicação viral. O fato desse aumento de ROS acontecer somente nos tempos tardios de infecção, levantou algumas hipóteses. A primeira delas é que ciclos replicativos sucessivos seriam necessários para amplificar o sinal de indução de ROS, permitindo sua detecção, uma vez que dados anteriores do grupo demonstraram que apenas 20-30% de HBMECs apresentam antígeno viral após 48h de infecção com DENV2 (cepa 16681) MOI 1 (Conceição *et al*., 2013). Para avaliar essa hipótese precisaríamos utilizar MOIs mais altos para

infecção, no entanto, não obtivemos títulos suficientemente altos de estoques virais para realização desse experimento.

A segunda hipótese é que a infecção promova uma resposta antioxidante nos tempos iniciais, o que teria um papel no controle na produção de ROS durante o início do estabelecimento do estado de estresse celular. A geração tardia de ROS foi também demonstrada em modelos de infecção de células dendríticas derivadas de monócitos (Olagnier *et al*., 2014). Nesse modelo, foi observado que DENV induzia expressão de Nrf2 em períodos iniciais da infecção, antecedendo a produção de ROS (Ferrari *et al*., 2020). Subsequentemente, detectou-se a degradação de Nrf2, dependente das proteínas virais NS2B e NS3, o que permitia que ocorre o aumento na produção de ROS. Para investigar se mecanismos semelhantes ocorriam durante a infecção de HBMECs, iniciamos a investigação de dois antioxidantes-SOD e Nrf2. Ainda de forma preliminar, não observamos aumento na expressão de SOD, mas esses experimentos precisam ser repetidos para sua confirmação. Além disso, estamos padronizando a técnica para separação de núcleo e citoplasma celulares para investigar a expressão e translocação de Nrf2 para o núcleo.

Alternativamente, é possível que a produção de ROS seja um evento secundário, dependente da produção de outros mediadores induzidos pela infecção como IL-6, como descrito em outros modelos, incluindo o modelo de infecção por SARS-CoV-2 (Youn *et al*., 2021). De fato, nossos dados preliminares demonstraram que a depleção de RIG-I diminui a produção de ROS, mas ainda não sabemos se esse é um efeito direto, dependente de sinais disparados por RIG-I sobre a expressão de NOX ou lesão mitocondrial, ou se depende de outros mediadores induzidos por RIG-I, como a IL-6. Para avaliar essas hipóteses, precisamos neutralizar esses mediadores e avaliar a produção de ROS, posteriormente.

Em seguida, buscamos verificar qual a via ROS era a responsável por esse aumento durante a infecção das HBMECs por DENV. Inicialmente utilizamos inibidores específicos da via NOX e da via mitocondrial, bem como, utilizamos uma sonda específica para dosagem de mitROS. Tanto o inibidor de NOX, quanto o de mtROS reverteram o aumento de ROS induzido por DENV, indicando que ambas as vias devem ser disparadas durante a infecção. Embora a especificidade dos inibidores possa ser discutível, é importante notar que a adição Apocinina

nas culturas não inibiu a produção de mitROS, indicando que esse inibidor não agiu de forma inespecífica sobre essa via e que as duas fontes de ROS são induzidas de forma independente.

Cabe ressaltar que a infecção viral é capaz de modificar a função mitocondrial através da interação das suas proteínas virais com os componentes mitocondriais, foi descrito que proteínas do Core do HCV induz lesão mitocondrial (Okuda *et al*., 2002). Além disso, HCV é capaz de alterar níveis de proibitina, uma chaperona mitocondrial, cuja alteração induz uma superprodução de ROS (Dang *et al*., 2011). Durante este trabalho também observamos que a infecção por DENV em HBMECs alterou a bioenergética mitocondrial e despolarização mitocondrial. Dados da literatura, demonstram que a infecção por DENV em células HepG2, (Linhagem derivada de carcinoma hepatocelular humano) após 48h de infecção leva a diminuição da capacidade máxima respiratória e que induz o aumento no consumo de oxigênio não associado à síntese de ATP (Costa *et al*., 2012). Além disso, consta na literatura que a infecção por DENV induz o alongamento das mitocôndrias das células Huh7 (Linhagem celular de fígado humano). Segundo Chatel-Chaix *et al*. (2016) esse processo facilita o escape viral da resposta inata desencadeada via RIG-I. Com esse conjunto de dados, acreditamos que em nosso modelo, o DENV induz a perturbação mitocondrial e desde modo induza o aumento na produção de ROS. Caberia ainda investigar se a infecção por DENV induz alterações na morfologia das mitocôndrias das HBMECs e o impacto dessas alterações tanto para a viabilidade celular quanto para o estabelecimento da infecção viral.

Dentre várias funções, ROS podem atuar como moléculas sinalizadoras para indução de morte celular (Villalpando-Rodriguez e Gibson, 2021; Jang *et al*., 2015; Shindo *et al*., 2013). Nós observamos que a inibição de NOX e da via de mtROS reduziu a morte celular, por mecanismos ainda não elucidados. O aumento da produção de ROS pode contribuir para o disparo de diferentes vias de morte celular, incluindo apoptose, necroptose e modulação de autofagia. Em modelo de infecção por DENV, foi observado que as proteínas virais interagem com as membranas mitocondriais e essa interação leva a despolarização e alteração de permeabilidade das membranas mitocondriais, perda do potencial de membrana (Catteau *et al*.; 2003; El-Bacha *et al*., 2007; León-Juárez *et al*., 2016). Após essas alterações de permebilidade, que pode resultar em: inchamento osmótico mitocondrial, desacoplamento, perda da homeostase de cálcio e liberação de proteínas pró-apoptóticas, como por exemplo o citocromo

c. Assim, ocorre o escape do citocromo c para o citoplasma, onde ele atua como sinalizador para morte via apoptose (Everett e McFadden, 2001; Okuda *et al*., 2002; Piccoli *et al*., 2006). Além disso, o acúmulo de mitROS pode levar a um aumento da permeabilidade da membrana mitocondrial (MMP), o que contribui para a ativação de caspases e culmina na indução da apoptose (Fleury, Mignotte e Vayssière, 2002). O aumento da produção de ROS pode, ainda, modular a atividade de alguns reguladores chave apoptóticos, como proteínas da família Bcl-2 (Fleury, Mignotte e Vayssière, 2002). Além disso, ROS levam a ativação de como FASL e TNF-a (Fleury, Mignotte e Vayssière, 2002). Em um modelo de hemorragia induzida por DENV, *in vivo*, foi observado um aumento de iNOS e peroxinitrito e evidências de apoptose em células endoteliais no tecido hemorrágico, sugerindo que NO e ROS podem ser os mediadores responsáveis pela apoptose das células endoteliais e lesão vascular (Wu-Hsieh *et al*., 2009)

Em relação ao processo de necroptose, já foi demonstrado que ROS pode ativar a autofosforilação de RIP1 e estabilizar o complexo de necrosome (Fulda, 2016). O aumento da produção de ROS, seguido de indução de necroptose foi observado em outros modelos de infecção viral, como em modelos de infecção de neutrofilos e macrófagos por virus respiratório sincicial (RSV) (Muraro *et al*., 2018; Bedient *et al*., 2020); e de infecção de macrófagos por vírus da encefalite japonesa (JEV) (Wang *et al*., 2020). Dados anteriores do nosso grupo demonstraram que a infeção de HBMECs por DENV induz a morte por necroptose de células infectadas e *bystanders*. Esse efeito apresenta relação com a RIP1, pois a morte das células *bystanders* parcialmente foi retardada pela adição do inibidor de RIPK1, a nescrostatina (Papa, 2014). Além disso, o meio condicionado de células infectadas também induziu morte celular em cultura de HBMECs não infectadas. No entanto, a indução de morte era inibida quando as células eram infectadas na presença de antioxidante (Slongo, 2016). Esses dados indicam que a produção de ROS induzida por DENV induz a secreção de mediadores que levam a morte de células *bystander*. Com este conjunto de dados, acreditamos que a infecção induza o aumento de ROS e esta molécula esteja envolvida na autofosforilação de RIP1 e morte por necroptose. Ainda seria interessante, infectar as HBMECs na presença ou na ausência dos inibidores de ROS (Apocinina e MitoTEMPO) e investigar a fosforilação de RIP1 e formação do necrossomo, com o intuito de correlacionar o aumento de ROS com a morte por necroptose.

Nós observamos que a produção de ROS por ambas as vias era importante também para replicação viral. Diferente dos nossos dados, a maioria dos estudos anteriores associava a produção de ROS ao controle da replicação viral. Ranger-Zisman e colaboradores (1982) demonstraram que a infecção de uma linhagem celular de monócitos por VSV induzia aumento na produção de ROS, o que teria um papel protetor como antiviral (Ranger-Zisman *et al*., 1982). Em seguida, outros trabalhos demonstraram que o aumento de ROS ocasionado por DENV em células dendríticas, também estava associado com um efeito antiviral (Olagnier *et al*., 2014; Shindo *et al*., 2013). Por outro lado, Anticoli e colaboradores (2019) demonstraram que na fase aguda da infecção por HCV em Huh7, ocorre o aumento da produção de ROS e este aumento favorece a replicação viral (Anticoli *et al*., 2019). Além disso, sabemos que o estado de estresse oxidativo induz a autofagia, e que a indução desse evento favorece a replicação de diferentes vírus em diferentes modelos celulares (Li *et al*., 2015; Lee *et al*., 2008; Datan *et al*., 2016). A indução de autofagia durante a infecção pelo vírus Chikungunya (CHIKV) foi muito bem caracterizada e é essencial para replicação viral (Echavarria-Consuegra, Smit e Reggiori, 2019; Krejbich-Trotot *et al*., 2011). De forma semelhante, foi observado que a infecção por DENV em células deficientes em Atg5 (proteína relacionada à autofagia 5) resulta redução da concentração de partículas infecciosas liberadas, indicando que a autofagia é importante para o aumento da replicação viral (Lee *et al*., 2008). Datan e colaboradores (2016), observaram que a infecção por DENV em células renais canina (MDKC) induz o aumento de ROS, com disparo de autofagia e que ambos os eventos eram essenciais para a replicação viral (Datan *el al*., 2016). Em nossos resultados preliminares, observamos um acúmulo de P62 e aumento na conversão de LC3b, indicando que o DENV induz a autofagia em HBMECs. Além disso, a adição de antioxidantes as culturas de células infectadas diminuiu o acúmulo de P62. Nossa hipótese é que o DENV induz o aumento da produção de ROS e esta seja responsável pela indução da autofagia, a qual é importante para o processo de replicação viral.

Outro aspecto relevante para a patogênese da dengue que investigamos em nosso modelo foi a integridade da monocamada de células endoteliais. Estudos anteriores haviam descrito que infecção das células endoteliais da veia umbilical humana (HUVECs) com DENV induzia o aumento na produção de ROS e RNS e que esses mediadores induziram apoptose dessas células, contribuindo para o aumento na permeabilidade (Yen *et al*., 2008). Curiosamente, no nosso modelo, embora tanto Apocinina quanto mitoTEMPO tenham inibido

a morte celular, apenas o tratamento com mitoTEMPO reduziu a permeabilidade da monocamada de HBMECs induzida por DENV de forma significativa.

O aumento da produção de ROS pode alterar a permeabilidade endotelial por diferentes mecanismos. Os lipídeos formam um importante constituinte da BBB e o acúmulo de ROS pode promover a peroxidação lipídica, liberando 4-hydroxy-2-nonenal (4-HNE) e culminando no aumento da BBB (Jong *et al*., 2008). O acúmulo de ROS causam a hipermetilação da região promotora da caderina-E, resultando em uma regulação negativa da mesma e culminando na perda da integridade da BBB (He, Talukder e Gao, 2020; Song *et al*., 2020; Redzic, 2011). Além disso, ROS também podem alterar a permeabilidade BBB ao influenciar a distribuição da *Tight junction* (TJ) ZO-1 (Lee *et al*., 2004). É possível, portanto, que os níveis de morte celular detectados na cultura nesse período de tempo não sejam o principal responsável pelo aumento de permeabilidade observado. Esse fenômeno seria resultado de alterações nas junções intercelulares. Assim, a produção de mtROS e não de ROS derivado de NOX, poderia estar envolvida nas alterações de permeabilidade endotelial nesse momento. Por outro lado, a inibição de NOX deve resultar também em resgate significativos da integridade das monocamadas por inibição da morte célula em períodos de tempo subsequentes.

Esse conjunto de dados sugere, ainda, que o aumento produção de mitROS poderia contribuir para a disseminação do vírus para o SNC através da ruptura da BBB. A presença da infecção viral ao SNC já foi detectada pela presenta de antígenos virais e RNA viral em tecido cerebral e em líquido cefalorraquidiano (LCR) (Balsitis *et al*., 2009; Povoa *et al*., 2014). Embora alterações neurológicas por DENV não sejam comuns, já foram descritas, de forma mais frequente, em crianças e a manifestação clínica é similiar a outras meningites virais (Soares *et al*., 2010).

Finalmente, investigamos o papel de ROS como sinalizador na secreção dessas citocinas pró-inflamatórias. Interessantemente, apenas o tratamento com o inibidor de ROS derivado de NOX que foi capaz de diminuir a liberação de IL-6, IL-8 e CCL5, indicando que apenas ROS derivados de NOX contribuem para a transdução de sinal associada à liberação dessas citocinas. Além disso, nosso trabalho não observou nenhuma modulação em IFN-β, indicando um possível papel de ROS na ativação via NF-KB, mas não via IRF-3.

Semelhante aos nossos achados, a infecção por DENV em Mo-DC resulta no aumento da produção de ROS dependente de NOX e este é responsável pela ativação de sinais inflamatórios, como a produção de IFN-β, IL-1β, IL-6 e CCL5 (Olaigner *et al*., 2014). Além disso, Soucy-Faulkner e colaboradores (2010) descreveram que a infecção por Sendai vírus (SeV) em células epiteliais de adenocarcinoma alveolar de células basais de pulmão humano (A549) induzia o aumento da produção de ROS de forma dependente de NOX2 (Soucy-Faulkner *et al*., 2010). O grupo ainda observou que o aumento da produção de ROS mediava uma resposta antiviral que era mediada por RIG-I, de forma dependente da regulação da expressão de MAVS (Soucy-Faulkner *et al*., 2010).

Nosso grupo já demonstrou que a infecção por DENV em HBMECs induz o aumento na expressão de receptores do tipo RIG-I e que esse sensor era essencial para a expressão e secreção de IL-6, IL-8 e CCL5 (Conceição, 2013). Investigamos, então, se o aumento da produção de ROS impactava também a expressão de RIG-I. De fato, o tratamento de HBMECs infectadas com os inibidores específicos de cada via de ROS resultou na diminuição da expressão de RIG-I, o que nos sugere que ROS pode atuar como uma molécula sinalizadora para a expressão de RIG-I. Cabe ressaltar que o experimento foi realizado apenas 1 vez e precisaria de replicatas para a confirmação do dado.

Em outro *set* de experimentos, avaliamos se, por outro lado, o próprio *sensing* viral poderia levar ao aumento da produção de ROS. Avaliamos se a ativação de RIG-I era necessária para induzir o aumento da produção de ROS, ou seja, o papel da ativação da via RIG-I/MAVS na indução de estresse oxidativo. Para isso, silenciamos RIG-I e dosamos tanto o ROS total quanto o mitROS. O experimento foi realizado apenas 1 vez, mas podemos observar uma tendência na queda do porcentual de células positivas expressando mitROS, com isso, acreditamos na possibilidade da produção de ROS derivado de NOX seja disparada por outra via. Dados da literatura mostram que há interação entre a via PI3K/AKT com a NADPH oxidase em diferentes modelos de estudos (De Oliveira *et al*., 2018; Nakanish *et al*., 2014; Koundouros e Poulogiannis, 2018, Kinoshita *et al*., 2008). Por isso, pretendemos investigar se DENV induz ativação da via PI3K/AKT e se esta via é responsável pela ativação de NOX, o que culminaria no aumento da produção de ROS e estabelecimento do estado de estresse celular.

Tomados em conjunto, nossos dados indicam que a infecção por DENV induz o aumento de ROS tanto pela via mitocondrial quanto derivado da NOX. Além disso, ROS é importante para a replicação viral, a ativação celular, permeabilidade e indução da morte das células endoteliais (Figura 31). Acreditamos que esses achados auxiliarão nos entendimentos das alterações que ocorrem no endotélio durante a infecção por DENV. Além disso, possibilita novos estudos a adotar o uso de antioxidante como um possível alvo terapêutico.

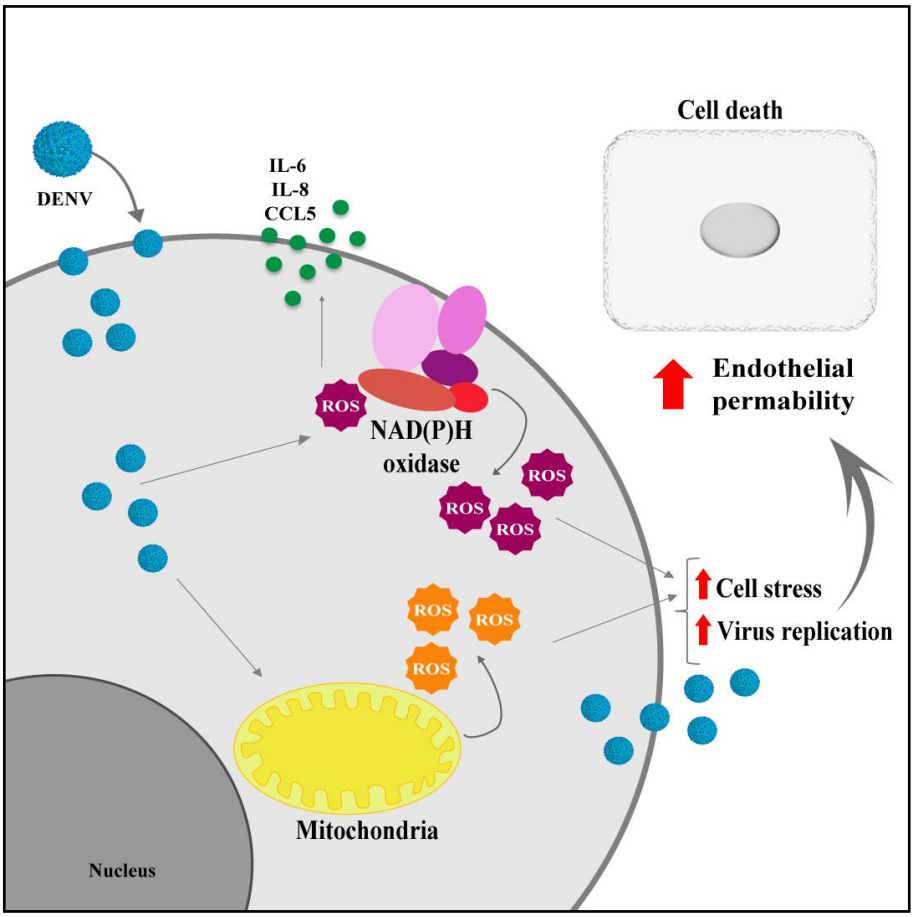

Figura 31: A infecção por DENV em células endoteliais induz aumento na produção de ROS. A replicação viral induz o aumento da produção de ROS mitocondrial e ROS dependente de NOX. Em seguida, o esse acúmulo de ROS é responsável por induzir replicação viral, ativação celular, aumento da permeabilidade e morte celular.

7. Conclusões

- A infecção por DENV em HBMECs induz aumento na produção de ROS nos tempos mais tardios;
- O aumento na produção de ROS em HBMECs induzido pela infecção por DENV ocorre por forma dependente de NAPH-oxidase e da via mitocondrial;
- A infecção por DENV induz alterações na bioenergética mitocondrial e perda no potencial de membrana mitocondrial das HBMECs;
- O aumento na produção de ROS via NAPH-oxidase e da via mitocondrial durante a infecção com DENV induz a morte de HBMECs;
- A produção de ROS favorece a replicação viral;
- mitROS está associado com o aumento da permeabilidade das HBMECs infectadas com DENV;
- O aumento na produção de ROS via NADPHox é essencial para a secreção de citocinas inflamatórias induzidas pela infecção por DENV em HBMECs;

8. Referências Bibliográficas

ACOSTA, E. G.; CASTILLA, V.; DAMONTE, E. B. Functional Entry of Dengue Virus Into Aedes Albopictus Mosquito Cells is Dependent On Clathrin-mediated Endocytosis. **J Gen Virol**. Buenos Aires, V. 89, n. 2, p. 474-484, fev. 2008.

AL-ALIMI, A. A.; ALI, S. A.; AL-HASSAN, F. M.; IDRIS, F. M.; TEOW, SIN-YEANG.; YUSOFF, N. M. Dengue virus type 2 (DENV2)-induced oxidative responses in monocytes from glucose-6-phosphate dehydrogenase (G6PD)-deficient and G6PD normal subjects. **PloS Negl Trop Dis**. V. 8. 2014.

ANDERSON, R.; WANG, S.; OSIOWY, C.; ISSEKUTZ, A. C. Activation of endothelial cells via antibody-enhanced dengue virus infection of peripheral blood monocytes. **J Virol**. Halifax, V. 71, n. 6, p.4226-4232, jun. 1997.

ANTICOLI, S.; AMATORE, D.; MATARRESE, P.; DE ANGELIS, M.; PALAMARA, A. T.; NENCIONI, L.; RUGGIERI, A. Counteraction of HCV-Induced Oxidative Stress Concurs to Establish Chronic Infection in Liver Cell Cultures. **Oxid Med Cell Longev**. 2019.

ARÉVALO, M. T.; SIMPSON-HAIDARIS, P. J.; KOU, Z.; SCHLESINGER, J. J.; JIN, X. Primary human endothelial cells support direct but not antibody-dependent enhancement of dengue viral infection. **J Med Virol**. P. 519-528. 2009.

ASEHNOUNE, K.; STRASSHEIM, D.; MITRA, S.; KIM, J. Y.; ABRAHAM, E. Involvement of reactive oxygen species in Toll-like receptor 4-dependent activation of NF-kappa B. **J Immunol**. V. 172. P. 2522-2529. 2004.

AVIRUTNAN, P.; MALASIT, P.; SELIGER, B.; BHAKDI, S.; HUSMANN, M. Dengue virus infection of human endothelial cells leads to chemokine production, complement activation, and apoptosis. **Journal of Immunology**. V. 161, n. 11, p. 6338–6346, dez. 1998.

AZEREDO, E. L.; ZAGNE, S. M.; SANTIAGO, M. A.; GOUVEA, A. S.; SANTANA, A. A.; NEVES-SOUZA, P. C.; NOGUEIRA, R. M.; MIAGOSTOVICH, M. P.; KUBELKA, C. F. Characterisation of lymphocyte response and cytokine patterns in patients with dengue fever. **Immunobiology**. P. 494-507. 2001.

BALDWIN, A. L.; THURSTON, G. Mechanics of endothelial cell architecture and vascular permeability. **Crit Rev Biomed Eng**. P. 247-78. 2001.

BALSITIS, S. J.; COLOMA, J.; CASTRO, G.; ALAVA, A.; FLORES, D.; MCKERROW, J. H.; BEATTY, P. R.; HARRIS, E. Tropism of dengue virus in mice and humans defined by viral nonstructural protein 3-specific immunostaining. **Am J Trop Med Hyg**. V. 80. P. 416-424. 2009.

BARNABA V. Tuning cross-presentation of apoptotic T cells in immunopathology. **Adv Exp Med Biol**. V. 785. P. 27-35. 2013.

BARTH, O. M.; BARRETO, D. F.; PAES, M. V.; TAKIYA, C. M.; PINHÃO, A. T.; SCHATZMAYR, H. G. Morphological studies in a model for dengue-2 virus infection in mice. **Mem Inst Oswaldo Cruz**. Rio de Janeiro, V. 101, n. 8, p. 905-915, dez. 2006.

BASU, A.; JAIN, P.; SARKAR, P.; GANGODKAR, S.; DESHPANDE, D.; GANTI, K.; SHETTY.; GHOSH, K. Dengue virus infection of SK Hep1 cells: inhibition of in vitro angiogenesis and altered cytomorphology by expressed viral envelope glycoprotein. **FEMS Immunol Med Microbiol**. P.140-147. 2011.

BAUD, L.; ARDAILLOU, R. Reactive oxygen species: production and role in the kidney. **Am J Physiol.** V. 251, n.5, p.765-776. 1986.

BEATTY, P. R.; PUERTA-GUARDO, H.; KILLINGBECK, S. S.; GLASNER, D. R.; HOPKINS, K.; HARRIS, E. Dengue virus NS1 triggers endothelial permeability and vascular leak that is prevented by NS1 vaccination. **Sci Transl Med**. V.304. sep. 2015.

BEDARD, K.; KRAUSE, K. H. The NOX family of ROS-generating NADPH oxidases: physiology and pathophysiology. **Physiol Rev**. p. 245-313. 2007.

BEDIENT, L.; POKHAREL, S. M.; CHIOK, K. R.; MOHANTY, I.; BEACH, S. S.; MIURA, T. A.; BOSE, S. Lytic Cell Death Mechanisms in Human Respiratory Syncytial Virus-Infected Macrophages: Roles of Pyroptosis and Necroptosis. **Viruses**. 2020.

BEHRENS, M. M.; ALI, S. S.; DUGAN, L. L. Interleukin-6 mediates the increase in NADPH-oxidase in the ketamine model of schizophrenia. **J Neurosci**. V. 28. P. 13957-13966. 2008.

BHARGAVA, A.; RAGHURAM, G. V.; PATHAK, N.; VARSHNEY, S.; JATAWA, S. K.; JAIN, D.; MISHRA, P. K. Occult hepatitis C virus elicits mitochondrial oxidative stress in lymphocytes and triggers PI3-kinase-mediated DNA damage response. **Free Radic Biol Med**. V. 51. P. 1806-1814. 2011.

BOATRIGHT, K. M.; SALVESEN, S. E. Mechanisms of caspase activation. **Curr Opin Cell Biol**. V.15. p.725-731. 2003.

BOO, K. H.; YANG, J. S. Intrinsic cellular defenses against virus infection by antiviral type Iinterferon. **Yonsei Med**.J. V. 51, p.9–17. 2010.

BORISH, L.; STEINKE, J. Cytokines and chemokines. **Journal of Allergy and Clinical Immunology**. Virgínia, V. 111, n. 2, p. 460–475, fev. 2003.

BRUMATTI, G.; SALMANIDIS, M.; EKERT, P. G. Crossing paths: interactions between the cell death machinery and growth factor survival signals**. Cell Mol Life Sci**. V. 67. P. 1619–1630. 2010.

BUNYARATVEJ, A.; BUTTHEP, P.; YOKSAN, S.; BHAMARAPRAVATI, N. Dengue viruses induce cell proliferation and morphological changes of endothelial cells. **Southeast Asian J Trop Med Public Health**. P. 32-37. 1997

BUREAU, C.; BERNAD, J.; CHAOUCHE, N.; ORFILA, C.; BÉRAUD, M.; GONINDARD, C.; ALRIC, L.; VINEL, J. P.; PIPY, B. Nonstructural 3 protein of hepatitis C virus triggers an oxidative burst in human monocytes via activation of NADPH oxidase. **J Biol Chem**. V. 276. P.23077-23083. 2001.

BUSKIEWICZ, I. A.; MONTGOMERY, T.; YASEWICZ, E. C.; HUBER, S. A.; MURPHY, M. P.; HARTLEY, R. C.; KELLY, R.; CROW, M. K.; PERL, A.; BUDD, R. C.; KOENIG, A. Reactive oxygen species induce virus-independent MAVS oligomerization in systemic lupus erythematosus. **Sci Signal**. 2016.

CARDIER, J. E; MARIÑO, E.; ROMANO, E.; TAYLOR, P.; LIPRANDI, F.; BOSCH, N.; ROTHMAN, A. L. Proinflammatory factors present in sera from patients with acute dengue infection induce activation and apoptosis of human microvascular endothelial cells: possible role of TNF-alpha in endothelial cell damage in dengue. **Cytokine**. V. 30, n. 6, p. 359-365, jun. 2005.

CARR, J. M.; HOCKING, H.; BUNTING, K.; WRIGHT, P. J.; DAVIDSON, A.; GAMBLE, J.; BURRELL, C. J. Supernatants from dengue virus type-2 infected macrophages induce permeability changes in endothelial cell monolayers. **J Med Virol**. P. 521-528. 2003.

CARVALHO, F. D.; MOREIRA, L. A. Why is Aedes aegypti Linnaeus so Successful as a Species? **Neotrop Entomol**. P. 243-255. 2017.

CATTEAU, A.; ROUE, G.; YUSTE, V.J.; SUSIN, S. A.; DESPRES P. Expression of dengue ApoptoM sequence results in disruption of mitochondrial potential and caspase activation. **Biochimie**. V. 85. P. 789–793. 2003.

CHAN, F. K.; SHISLER, J.; BIXBY, J. G.; FELICES, M.; ZHENG, L.; APPEL, M.; ORENSTEIN, J.; MOSS, B.; LENARDO, M. J. A role for tumor necrosis factor receptor-2 and receptor-interacting protein in programmed necrosis and antiviral responses. **J Biol Chem**. P. 51613-21. 2003.

CHANG, H. Y.; YANG, X. Proteases for cell suicide: functions and regulation of caspases. **Microbiol Mol Biol Rev**. V. 64. P. 821-846. 2000.

CHANG, T. H.; LIAO, C. L; LIN, Y. L. Flavivirus induces interferon- beta gene expression through a pathway involving RIG-I-dependent IRF-3 and PI3K-dependent NF-kappaB activation. **MicrobesInfect**. V. 8, p.157–171. 2006.

CHATEL-CHAIX, L.; CORTESE, M.; ROMERO-BREY, I.; BENDER, S.; NEUFELDT, C. J.; FISCHL, W.; SCATURRO, P.; SCHIEBER, N.; SCHWAB, Y.; FISCHER, B.; RUGGIERI, A.; BARTENSCHLAGER, R. Dengue Virus Perturbs Mitochondrial Morphodynamics to Dampen Innate Immune Responses. **Cell Host Microbe**. V. 20. P. 342-356. 2016.

CHATTOPADHYAY, S.; MARQUES, J. T.; YAMASHITA, M.; PETERS, K. L.; SMITH, K.; DESAI, A.; WILLIAMS, B. R.; SEN, G. C. Viral apoptosis is induced by IRF-3-mediated activation of Bax. **EMBO J**. Victoria, 29(10):1762-73, mai. 2010.

CHEN, H. C.; HOFMAN, F. M.; KUNG, J. T.; LIN, Y. D.; WU-HSIEH, B. A. Both virus and tumor necrosis factor alpha are critical for endothelium damage in a mouse model of dengue virus-induced hemorrhage. **J Virol**. V. 8, n. 11, p. 5518-5526, jun. 2007.

CHEN, H. W.; KING, K. TU, J.; SANCHEZ, M.; LUSTER, A. D.; SHRESTA S. The roles of IRF-3 and IRF-7 in innate antiviral immunity against dengue virus. **J Immunol**. 2013.

CHEN, J. P, LU, H. L.; LAI, S. L.; CAMPANELLA, G. S.; SUNG, J. M.; LU, M. Y.; WU-HSIEH, B. A.; LIN, Y. L.; LANE, T. E.; LUSTER, A. D.; LIAO, F. Dengue virus induces expression of CXC chemokine ligand 10/IFN-gamma-inducible protein 10, which competitively inhibits viral binding to cell surface 70eporto sulfate. **J Immunol**. P. 3185-92. 2006.

CHMALJOHN, A. L.; MCCLAIN, D. Alphaviruses (Togaviridae) and Flaviviruses (Flaviviridae). **Medical Microbiology**. Texas, Cap. 54, 1996.

CHO, Y. S.; CHALLA, S.; MOQUIN, D.; GENGA, R.; RAY, T. D.; GUILDFORD, M.; CHAN, F. K. Phosphorylation-driven assembly of the RIP1-RIP3 complex regulates programmed necrosis and virus-induced inflammation. P. 1112-1123. 2009.

CHOI, JANG-GI.; LEE, H.; KIM, Y. S.; HWANG, YOUN-HWAN.; OH, YOU-CHANG.; LEE, B.; MOON, K. M.; CHO, WON-KYUNG.; MA, J. Y. Aloe vera and its Components Inhibit Influenza A Virus-Induced Autophagy and Replication. **Am J Chin Med**. V. 47. P. 1307-1324. 2019.

CLYDE, K.; JENNIFER, L.; HARRIS, E. Recent advances in deciphering viral and host determinants of dengue virus replication and pathogenesis. **Journal of virology**. Berkeley, V. 80, n. 23, p. 11418– 11431, ago. 2006.

COMMINS, P.; BORISH L.; STEINKE, J. Immunologic messenger molecules: cytokines, interferons, and chemokines. **The journal of allergy and clinical immunology**. V. 125, n. 2, p. 53–72, Virgínia, fev. 2010.

CONCEIÇÃO, T. M.; RUST, N. M.; BERBEL, A. C.; MARTINS, N. B.; DO NASCIMENTO, C. A.; DA POIAN, A. T.; ARRUDA, L. B. Essential role of RIG-I in the activation of endothelial cells by dengue virus. **Virology**. P. 281-292. 2013.

COSTANTINI, D.; BLÉVIN, P.; HERZKE, D.; MOE, B.; GABRIELSEN, G. W.; BUSTNES, J. O.; OLIVIER CHASTEL, O. Higher plasma oxidative damage and lower plasma antioxidant defences in an Arctic seabird exposed to longer perfluoroalkyl acids. **Environ Res. V**. 168 p. 278-285. 2019.

CULLINAN, S. B.; GORDAN, J. D.; JIN, J.; HARPER, J. W.; DIEHL, J. A. The Keap1-BTB protein is an adaptor that bridges Nrf2 to a Cul3-based E3 ligase: oxidative stress sensing by a Cul3-Keap1 ligase. **Mol Cell Biol. V. 24**. P. 8477-8486. 2004.

CZABOTAR, P. E.; LESSENE, G.; STRASSER, A.; ADAMS, J. M. Control of apoptosis by the BCL-2 protein family: implications for physiology and therapy. **Nat Em Mol Cell Biol**. V. 15. P. 49-63. 2014.

D'ARCY M. S. Cell death: a review of the major forms of apoptosis, necrosis and autophagy. **Cell Biol Int**. V. 43, n. 6. P. 582-592. 2019.

DA COSTA, L. S.; DA SILVA, A. P. P.; DA POIAN, A. T.; EL-BACHA, T. **PloS One**. 2012. Mitochondrial 71eporto f71ics alterations in mouse neuroblastoma cells infected with Sindbis virus: implications to viral replication and neuronal death. 2012.

DALRYMPLE, N.; MACKOW, E. Productive Dengue Virus Infection of Human Endothelial Cells Is Directed by Heparan Sulfate-Containing Proteoglycan Receptors. **J Virol**. P. 9478–9485. 2011.

DANG, SHUANG-SUO.; SUN, MING-ZHU.; YANG, E.; XUN, M.; MA, L.; JIA, ZHAN-SHENG.; WANG, WEN-JUN.; JIA, XIAO-LI. Prohibitin is overexpressed in Huh-7-HCV and Huh-7.5-HCV cells harboring in vitro transcribed full-length hepatitis C virus RNA. **Virol. J**. 2011.

DARZYNKIEWICZ, Z.; JUAN, G.; LI, X.; GORCZYCA, W.; MURAKAMI, T.; TRAGANDS, F. Cytometry in cell necrobiology: Analysis of apoptosis and accidental cell death (necrosis). **Cytometry**. V. 27. P. 1-20. 1997.

DATAN, E.; ROY, S. G.; GERMAIN, G.; ZALI, N.; MCLEAN, J. E.; GOLSHAN, G.; HARBAJAN, S.; LOCKSHIN, R. A.; ZAKERI, Z. Dengue-induced autophagy, virus replication and protection from cell death require ER stress (PERK) pathway activation. **Cell Death Dis**. 2016.

DE OLIVEIRA, J. S. S.; SANTOS, G. S.; MORAES, J. A.; SALIBA, A. M.; BARJA-FIDALGO, T. C.; MATTOS-GUARALDI, A. L.; NAGAO, E. M. Reactive oxygen species generation mediated by NADPH oxidase and PI3K/Akt pathways contribute to invasion of Streptococcus agalactiae in human endothelial cells. **Mem Inst Oswaldo Cruz**. 2018.

DERAMAUDT, T. B.; DILL, C.; BONAY, M. Regulation of oxidative stress by Nrf2 in the pathophysiology of infectious diseases. **Med Mal Infect**. V. 43. P. 100-107. 2013.

ECHAVARRIA-CONSUEGRA, L.; SMIT, J. M.; REGGIORI, F. Role of autophagy during the replication and pathogenesis of common mosquito-borne flavi- and alphaviruses. **Open Biol**. 2019

EL-BACHA, T.; MENEZES, M. M. T.; SILVA, M. C. A.; SOLA-PENNA, M.; DA POIAN, A. T. Mayaro virus infection alters glucose metabolism in cultured cells through activation of the enzyme 6-phosphofructo 1-kinase. **Mol Cell Biochem**. V. 266. P. 191-198. 2004.

EL-BACHA, T.; MIDLEJ, V.; DA SILVA, A. P. P.; DA COSTA, L. S.; BENCHIMOL, M.; GALINA, A.; DA POIAN, A. T. Mitochondrial and 71eporto f71ics dysfunction in human hepatic cells infected with dengue 2 virus. **Biochim Biophys Acta**. V. 1772. P. 1158-1166. 2007.

ELMORE, S. Apoptosis: a review of programmed cell death. **Toxicol Pathol**. V. 35. P. 495-516. 2007.

ESPINA, L. M.; VALERO, N. J.; HERNÁNDEZ, J. M.; MOSQUERA, J. A. Increased apoptosis and expression of tumor necrosis factor-alpha caused by infection of cultured human monocytes with dengue virus. **Am J Trop Med Hyg**. P.48-53. 2003.

EVERETT, H.; MCFADDEN, G. Viruses and apoptosis: meddling with mitochondria. **Virology**. V. 288. P. 1-7. 2001.

FAN, R.; DONG, Y.; HUANG, G.; TAKEUCHI, YASUHIRO. Apoptosis in virus infection dynamics models. **J Biol Dyn**. V. 8. p. 20-41. 2014.

FÉLÉTOU, M. The Endothelium: Part 1: Multiple Functions of the Endothelial Cells—Focus on Endothelium-Derived Vasoactive Mediators. Integrated Systems Physiology: from Molecule to Function to Disease. **Morgan & Claypool Life Sciences**. 2011.

FERNANDEZ-GARCIA, M. D.; MAZZON, M.; JACOBS, M.; AMARA, A. Pathogenesis of flavivirus infections: using and abusing the host cell. **Cell Host Microbe**. P. 318-328. 2009.

FERNANDO, S.; WIJEWICKRAMA, A.; GOMES, L.; PUNCHIHEWA, C. T.; MADUSANKA, S. D.; DISSANAYAKE, H.; JEEWANDARA, C.; PEIRIS, H.; OGG, G. S.; MALAVIGE, G. N. B. M. C. Patterns and causes of liver involvement in acute dengue infection. **Infect Dis**. 2016 p.316-319.

FERRARI, M.; ZEVINI, A.; PALERMO, E.; MUSCOLINI, M.; ALEXANDRIDI, M.; ETNA, M. P.; COCCIA, E. M.; FERNANDEZ-SESMA, A.; COYNE, C.; ZHANG, D. D.; MARQUES, E. T. A.; OLAGNIER, D.; HISCOTT, J. Dengue Virus Targets Nrf2 for NS2B3-Mediated Degradation Leading to Enhanced Oxidative Stress and Viral Replication. **J Virol**. 2020.

FERREIRA-DE-LIMA, V. H.; LIMA-CAMARA, T. N. Natural vertical transmission of dengue virus in Aedes aegypti and Aedes albopictus: a systematic review. **Parasit Vectors**. V. 11. 2018.

FESTJENS, N.; VANDEN BERGHE, T.; VANDENABEELE, P. Necrosis, a well-orchestrated form of cell demise: 72eporto f cascades, important mediators and concomitant immune response. Biochim Biophys Acta. P.1371-87. 2006.

FILIP-CIUBOTARU, F.; MANCIUC, C.; STOLERIU, G.; FOIA, LILIANA. Nadph oxidase: structure and activation mechanisms. **Rev Med Chir Soc Med Nat Iasi**. V. 120. P. 29-33. 2016.

FILOMATORI, C. V.; IGLESIAS, N. G.; VILLORDO, S. M.; ALVAREZ, D. E.; GAMARNIK, A. V. RNA Sequences And Structures Required For The Recruitment And Activity Of The Dengue Virus Polymerase. **J Biol Chem**. V. 286, n. 9, p. 6929-6939. Mar. 2011.

FLEURY, C.; MIGNOTTE, B.; VAYSSIÈRE, JEAN-LUC. Mitochondrial reactive oxygen species in cell death signaling. **Biochimie**. V. 84. P. 131-141. 2002.

FORTES, G. B.; ALVES, L. S.; DE OLIVEIRA, R.; DUTRA, F. F.; RODRIGUES, D.; FERNANDEZ, P. L.; SOUTO-PADRON,T.; DE ROSA, M. J.; KELLIHER, M.; GOLENBOCK, D.; CHAN, F. K. M.; BOZZA, M. T. Heme induces programmed necrosis on macrophages through autocrine TNF and ROS production. **Blood**. V. 119. P. 2368-2375. 2012.

FRIEBE, P.; HARRIS, E. Interplay of RNA elements in the dengue virus 5” and 3” ends required for viral RNA replication. **J Virol**. Berkeley, V. 84, n.12, p. 6103-6118, jun. 2010.

FUKAI, T.; FUKAI, M. U. Cross-Talk between NADPH Oxidase and Mitochondria: Role in ROS Signaling and Angiogenesis. **Cells**. V. 9. P. 2-17. 2020.

FULDA, S. Regulation of necroptosis signaling and cell death by reactive oxygen species. **Biol Chem**. V. 397. P. 657-660. 2016.

GARCÍA-MEDIAVILLA, M. V.; SÁNCHEZ-CAMPOS, S.; GONZÁLEZ-PÉREZ, P.; GÓMEZ-GONZALO, M.; MAJANO, P. L.; LÓPEZ-CABRERA, M.; CLEMENTE, G.; GARCÍA-MONZÓN, C.; GONZÁLEZ-GALLEGO, J. Differential contribution of hepatitis C virus NS5A and core proteins to the induction of oxidative and nitrosative stress in human hepatocyte-derived cells. **J Hepatol**. V. 43. P. 606-613. 2005.

GARRY, R. F.; BOSTICK, D. A. Induction of the stress response: alterations in membrane-associated transport systems and protein modification in heat shocked or Sindbis virus-infected cells. **Virus Res**. V. 8. P. 245-259. 1987.

GIL, L.; MARTÍNEZ, G.; TÁPANES, R.; CASTRO, O.; GONZÁLEZ, D.; BERNARDO, L.; VÁZQUEZ, S.; KOURÍ, G.; GUZMÁN, M. G. Oxidative stress in adult dengue patients. **Am J Trop Med Hyg**. V. 71. P. 652-657. 2004.

GÖRLACH, A.; BRANDES, R. P.; BASSUS, S.; KRONEMANN, N.; KIRCHMAIER, C. M.; BUSSE, R.; SCHINI-KERTH, V. B. Oxidative stress and expression of p22phox are involved in the up-regulation of tissue factor in vascular smooth muscle cells in response to activated platelets. **FASEB J**. 2000 V. 14. P. 1518-1528.

GROOTJANS, S.; BERGHE, V. VANDENABEELE, P. Initiation and execution mechanisms of necroptosis: an overview. **Cell Death Differ**. P.1184-1195. 2017.

GRÜTTER, M. G. Caspases: key players in programmed cell death. **Curr Opin Struct Biol**. V. 10. P. 649-655. 2000.

GUZMAN, M. G.; HALSTEAD, S. B.; ARTSOB, H.; BUCHY, P.; FARRAR, J.; GUBLER, D. J.; HUNSPERGER, E.; KROEGER, A.; MARGOLIS, H. S.; MARTÍNEZ, E.; NATHAN, M. B.; PELEGRINO, J. L.; SIMMONS, C.; YOKSAN, S.; PEELING, R. W. Dengue: a Continuing Global Threat. **Nat Rev Microbiol**. Habana. V. 8, n. 12, p. 7-16, dez. 2010.

GUZMAN, M.G.; GLUBLER, D. J.; IZQUIERDO, A.; MARTINEZ, E.; HALSTEAD, S. B. Dengue infection. **Nat Rev Dis Primers**. V. 2, p. 1, ago. 2016.

HALLIWELL B. Biochemistry of oxidative stress. **Biochem Soc Trans**. V. 35. P. 1147-1150. 2007.

HALLIWELL, B.; CROSS, C. E. Oxygen-derived species: their relation to human disease and environmental stress. **Environ Health Perspect**. 1994.

HALLIWELL, B.; GUTTERIDGE, J. M. C. Free Radicals in Biology and Medicine. **Oxford University Press**. 22015.

HALSTEAD, S.; CASALS, J.; SHOTWELL, H.; PALUMBO, N. Studies on the immunization of monkeys against dengue. I. Protection derived from single and sequential virus infections. **American Journal of Tropical Medicine and Hygiene**. V. 22, n. 3, p. 365-374, mai. 1970.

HALSTEAD, S.; O" ROURKE; E. Dengue viruses and mononuclear phagocytes. I. Infection enhancement by non-neutralizingantibody. **J Exp Med**, Hawai, V. 146, n. 1, p. 201-217, jul. 1976.

HAMANAKA, R. B.; CHANDEL, N. S. Mitochondrial reactive oxygen species regulate cellular signaling and dictate biological outcomes. **Trends Biochem** Sci. V.35, p. 505-13. Sep. 2010.

HARIJITH, A.; EBENEZER, D. L.; NATARAJAN, V. Reactive oxygen species at the crossroads of inflammasome and inflammation. Chicago, Front Physiol. V. 29, n. 5, p. 352. 2014.

HARRIS, E.; HOLDEN, K. L.; EDGIL, D.; POLACEK, C.; CLYDE, K. Molecular biology of flaviviruses. **Novartis Found Symp.** Berkeley, V. 40, p. 71-251. 2006.

HE, S.; LIANG, Y.; SHAO, F.; WANG, X. Toll-like receptors activate programmed necrosis in macrophages through a receptor-interacting kinase-3-mediated pathway. **Proc Natl Acad Sci U S A**. 2011.

HENCHAL, A. PUTNAK, J. R. The dengue viruses. **Clin Microbiol**. Washington, V. 3, n. 4, p. 376-396, out. 1990.

HENCHAL, E.; HENCHAL, L.; SCHLESINGER, J. Synergistic Interactions of Anti-NS1 Monoclonal Antibodies Protect Passively Immunized Mice from Lethal Challenge with Dengue 2 Virus. **The Journal of general virology**. Washington, V. 69, n. 8, p. 2101–2107, ago. 1988.

HER, Z.; KAM, Y. W.; GAN, V. C.; LEE, B.; THEIN, T. L.; TAN, J. J.; LEE, L. K.; FINK, K.; LYE, D. C.; RÉNIA, L.; LEO, Y. S. Severity of Plasma Leakage Is Associated With High Levels of Interferon γ-Inducible Protein 10, Hepatocyte Growth Factor, Matrix Metalloproteinase 2 (MMP-2), and MMP-9 During Dengue Virus Infection. **J Infect Dis**. P.42-51. 2017.

HIDARI, KI.; SUZUKI, T. Dengue 74epor receptor. **Trop Med Health**. Shizuoka, V. 39, n. 4, p. 37-43, ago. 2011.

HU M, BOGOYEVITCH MA, JANS DA. Subversion of Host Cell Mitochondria by RSV to Favor Virus Production is Dependent on Inhibition of Mitochondrial Complex I and ROS Generation. **Cells**. 2019.

HU M, SCHULZE KE, GHILDYAL R, HENSTRIDGE DC, KOLANOWSKI JL, NEW EJ, HONG Y, HSU AC, HANSBRO PM, WARK PA, BOGOYEVITCH MA, JANS DA. Respiratory syncytial virus co-opts host mitochondrial function to favour infectious virus production. **Elife**. 2019.

HUANG, Y. H.; LEI, H. Y.; LIU, H. S.; LIN, Y. S.; LIU, C. C.; YEH, T. M. Dengue virus infects human endothelial cells and induces IL-6 and IL-8 production. **Am J Trop Med Hyg**. P.71-75. 2000.

IVANOV, A. V.; SMIRNOVA, O. A.; IVANOVA, O. N.; MASALOVA, O. V.; KOCHETKOV, S. N.; ISAGULIANTS, M. G. Hepatitis C virus proteins activate NRF2/ARE pathway by distinct ROS-dependent and independent mechanisms in HUH7 cells. **PloS One**. 2011.

IVANOV, A. V.; SMIRNOVA, O. A.; PETRUSHANKO, I. Y.; IVANOVA, O. N.; KARPENKO, I. L.; ALEKSEEVA, E.; SOMINSKAYA, I.; MAKAROV, A. A.; BARTOSCH, B.; KOCHETKOV, S. N. ISAGULIANTS, M. G. HCV core protein uses multiple mechanisms to induce oxidative stress in human hepatoma Huh7 cells. **Viruses**. V. 7. P. 2745-2770. 2015.

JANG, Y. J.; WON, J. H.; BACK, M. J.; FU, Z.; JANG, J. M.; HA, H. C.; HONG, S.; CHANG, M.; KIM, D. K. Paraquat Induces Apoptosis through a Mitochondria-Dependent Pathway in RAW264.7 Cells. **Biomol Ther (Seoul)**. V. 23. P. 407-413. 2015.

JEONG, JAE-YEON.; KWON, HYOUK-BUM.; AHN, JONG-CHAN.; KANG, D.; KWON, SEUNG-HAE.; PARK, J. A.; KIM, KYU-WON. Functional and developmental analysis of the blood-brain barrier in zebrafish. **Brain Res Bull**. 2008.

JEONG, SEON-YONG.; SEOL, DAI-WU. The role of mitochondria in apoptosis. **BMB Rep**. V.41. p.11-22. 2008.

JESSIE, K.; FONG, M. Y.; DEVI, S.; LAM, S. K.; WONG, K. T. Localization of dengue virus in naturally infected human tissues, by immunohistochemistry and in situ hybridization. **J Infect Dis**. P. 1411-8. 2004.

JING, H.; WANG, Z.; ZHANG, L.; ZHOU, G.; GU, Z.; SHAN, Y.; ZHOU, Y.; YANG, Z.; KONG, Z. Reactive oxygen species derived from NADPH oxidase regulate autophagy. **Biologia plantarum**. V. 64. P. 87-94. 2020.

JULIO F TURRENS, J. F. Mitochondrial formation of reactive oxygen species. **J Physiol**. V. 552. P. 335-344. 2003.

KAISER WJ, SRIDHARAN H, HUANG C, MANDAL P, UPTON JW, GOUGH PJ, SEHON CA, MARQUIS RW, BERTIN J, MOCARSKI ES. Toll-like receptor 3-mediated necrosis via TRIF, RIP3, and MLKL. **J Biol Chem**. V. 288, n. 43, p. 31268-31279. 2013.

KATO, H.; TAKEUCHI, O.; SATO, S.; YONEYAMA, M.; YAMAMOTO, M.; MATSUI, K. Differential roles of MDA5 and RIG-I helicases in there cognition of RNA viruses. **Nature**. V. 441, p.101–105. 2006.

KAUR, J.; DHAUNSI, G. S.; TURNER, R. B. Interleukin-1 and nitric oxide increase NADPH oxidase activity in human coronary artery smooth muscle cells. **Med Princ Pract**. V. 13. P. 26-29. 2004.

KIM, S. J.; WONG, P. K. Y. ROS upregulation during the early phase of retroviral infection plays an important role in viral establishment in the host cell. **J Gen Virol**. V. 94. P. 2309-2317. 2013.

KIM, YOU-SUN.; MORGAN, M. J.; CHOKSI, S.; LIU, ZHENG-GANG. TNF-induced activation of the Nox1 NADPH oxidase and its role in the induction of necrotic cell death. **Mol Cell**. V. 26. P. 675-687. 2007.

KINOSHITA, H.; MATSUDA, N.; KABA, H.; HATAKEYAMA, N.; AZMA, T.; NAKAHATA, K.; KURODA, Y.; TANGE, K.; IRANAMI, H.; HATANO, Y. Roles of phosphatidylinositol 3-kinase-Akt and NADPH oxidase in adenosine 5'-triphosphate-sensitive K+ channel function impaired by high glucose in the human artery. **Hypertension**. V. 52. P. 507-513. 2008.

KOUNDOUROS, N.; POULOGIANNIS, G. Phosphoinositide 3-Kinase/Akt Signaling and Redox Metabolism in Cancer. **Front Oncol**. 2018.

KOWALTOWSKI, A. J.; VERCESI, A. E. Mitochondrial damage induced by conditions of oxidative stress. **Free Radic Biol Med**. V. 26. P. 463-471. 1999.

KREJBICH-TROTOT, P.; GAY, B.; LI-PAT-YUEN, G.; HOARAU, JEAN-JACQUES.; JAFFAR-BANDJEE, MARIE-CHRISTINE.; BRIANT, LAURENCE.; GASQUE, P.; DENIZOT, M. Chikungunya triggers an autophagic process which promotes viral replication. **Virol J**. 2011.

KROEMER, G.; GALLUZZI, L.; VANDENABEELE, P.; ABRAMS, J.; ALNEMRI, E. S.; BAEHRECKE, E. H.; BLAGOSKLONNY, M. V.; EL-DEIRY, W. S.; GOLSTEIN, P.; GREEN, D. R.; HENGARTNER, M.; KNIGHT, R. A.; KUMAR, S.; LIPTON, S. A.; MALORNI, W.; NUÑEZ, G.; PETER, M. E.; TSCHOPP, J.; YUAN, J.; PIACENTINI, M.; ZHIVOTOVSKY, B.; MELINO, G. Classification of cell death: recommendations of the Nomenclature Committee on Cell Death. **Cell Death Differ**. V. 16. P. 3-11. 2009.

KRYLATOV, A. V.; MASLOV, L. N.; VORONKOV, N. S.; BOSHCHENKO A. A.; POPOV, S. V.; GOMEZ, L.; WANG H.; JAGGI, A. S.; DOWNEY, J. M. Reactive Oxygen Species as Intracellular Signaling Molecules in the Cardiovascular System. **Curr Cardiol Rev**. V. 14. P. 290-300. 2018.

KUHN, R. J.; ZHANG, W.; ROSSMANN, M. G.; PLETNEV, S. V.; CORVER, J. C.; LENCHES, E.; JONES, C. T.; MUKHOPADHYAY, S.; CHIPMAN, P. R.; STRAUSS, E. G.; BAKER, T. S.; STRAUSS, J. H. Structure of dengue virus: implications for flavivirus organization, maturation, and fusion. **Cell**. V. 5, p. 717-725, mar. 2002.

KYLE, J. L.; BALSITIS, S. J.; ZHANG, L.; P. BEATTY, P. R.; HARRIS, E. Antibodies play a greater role than immune cells in heterologous protection against secondary dengue virus infection in a mouse model. **Virology**. P. 296–303. 2008.

LACY, F.; GOUGH, D. A.; SCHMID-SCHÖNBEIN, G. W. Role of xanthine oxidase in hydrogen peroxide production. **Free Radic Biol Med**. V.25, p.720-7. Oct. 1998.

LASTER, S. M.; WOOD, J. G.; GOODING, L. R. Tumor necrosis factor can induce both apoptic and necrotic forms of cell lysis. **J Immunol**. P. 2629-34. 1988.

LAVRIK, I.; GOLKS, A.; KRAMMER, P. H. Death receptor signaling. **J Cell Sci**. V 118. P. 265-267. 2005.

LEE, C. Therapeutic Modulation of Virus-Induced Oxidative Stress via the Nrf2-Dependent Antioxidative Pathway. **Oxid Med Cell Longev**. 2018.

LEE, HEE-SANG.; NAMKOONG, K.; KIM, DONG-HWA.; KIM, KI-JEONG.; CHEONG, YOON-HEE.; KIM, SUNG-SU.; LEE, WON-BOK.; KIM, KYUNG-YONG. Hydrogen peroxide-induced alterations of tight junction proteins in bovine brain microvascular endothelial cells. **Microvasc Res**. 2004.

LEE, Y. H.; LEONG, W. Y.; WILDER-SMITH, A. Markers of dengue severity: a systematic review of cytokines and chemokines. **J Gen Virol**. P. 3103-3119. 2016.

LEE, YING-RAY.; LEI, HUAN-YAO.; LIU, MING-TAO.; WANG, JEN-REN.; CHEN, SHUN-HUA.; JIANG-SHIEH, YA-FEN.; LIN, YEE-SHIN.; YEH, TRAI-MING.; LIU, CHING-CHUAN.; LIU, HSIAO-SHENG. Autophagic machinery activated by dengue virus enhances virus replication. **Virology**. V. 374, p. 240-248. 2008.

LEI, H.; YEH, T., LIU, H., LIN, Y., CHEN, S., LIU, C. Immunopathogenesis of Dengue Virus. **J Biomed Sci**. V. 8, n. 5, p. 377-388, sep. 2001.

LEÓN-JUÁREZ, M.; MARTÍNEZ-CASTILLO, M.; SHRIVASTAVA, G.; GARCÍA-CORDERO, J.; VILLEGAS-SEPULVEDA, N.; MONDRAGÓN-CASTELÁN, M.; MONDRAGÓN-FLORES, R.; CEDILLO-BARRÓN, L. Recombinant Dengue virus protein NS2B alters membrane permeability in different membrane models. **Virol J**. 2016.

LI, J.; SHAH, A. M. Intracellular localization and preassembly of the NADPH oxidase complex in cultured endothelial cells. **J Biol Chem**. V. 277. P. 19952-19960. 2002.

LI, J.; YUAN, J. Caspases in apoptosis and beyond. **Oncogene**. V. 27. P. 6194-6206. 2008.

LI, L.; TAN, J.; MIAO, Y.; LEI, P.; ZHANG, Q. ROS and Autophagy: Interactions and Molecular Regulatory Mechanisms. **Cell Mol Neurobiol**. V. 35. P. 615-621. 2015.

LI, X.; FANG, P.; MAI, J.; CHOI, E. T.; WANG, H.; YANG, X. F. Targeting mitochondrial reactive oxygen species as novel therapy for inflammatory diseases and cancers. **J Hematol Oncol**. 2013.

LIAO, H.; XU, J.; HUANG, J. FasL/Fas pathway is involved in dengue virus induced apoptosis of the vascular endothelial cells. **J Med Virol**. P. 1392-1399. 2010.

LIMONTA, D.; TORRENTES-CARVALHO, A.; MARINHO, C.F.; DE AZEREDO, E. L.; DE SOUZA, L. J.; MOTTA-CASTRO, A. R.; DA CUNHA, R. V.; KUBELKA, C. F.; NOGUEIRA, R. M.; DE-OLIVEIRA-PINTO, L. M. Apoptotic mediators in patients with severe and non-severe dengue from Brazil. **J Med Virol**. P. 1437-47. 2014.

LIMONTA; D.; CAPÓ, V.; TORRES, G.; PÉREZ, A. B.; GUZMÁN, M. G. Apoptosis in tissues from fatal dengue shock syndrome. Havana. **J Clin Virol**. V. 40, n. 1, p. 50-54, set. 2007.

LIN, Y. L.; LIU, C. C.; CHUANG, J. I.; LEI, H. Y.; YEH, T. M.; LIN, Y. S.; HUANG, Y. H.; LIU, H. S. Involvement of oxidative stress, NF-IL-6, and RANTES expression in dengue-2-virus-infected human liver cells. **Virology**. 2000.

LIPINSKI, S.; TILL, A.; SINA, C.; ARLT, A.; GRASBERGER, H.; SCHREIBER, S.; ROSENSTIEL, P. DUOX2-derived reactive oxygen species are effectors of NOD2-mediated antibacterial responses. **J Cell Sci**. V. 122. P. 3522-3230. 2009.

LOO, Y. M.; FORNEK, J.; CROCHET, N.; BAJWA, G.; PERWITASARI, O.; MARTINEZ-SOBRIDO, L.; AKIRA, S.; GILL, M. A.; GARCÍA-SASTRE, A.; KATZE, M. G.; GALE, M, JR. Distinct RIG-I and MDA5 signaling by RNA viruses in innate immunity. **J Virol**. P. 335-345. 2008.

LUCAS, K.; MAES, M. Role of the Toll Like receptor (TLR) radical cycle in chronic inflammation: possible treatments targeting the TLR4 pathway. **Mol Neurobiol**. 2013.

MAGNANI, N. D.; MARCHINI, T.; CALABRÓ, V.; ALVAREZ, S.; EVELSON, P. Role of Mitochondria in the Redox Signaling Network and Its Outcomes in High Impact Inflammatory Syndromes. **Front Endocrinol**. 2020.

MALAVIGE, G. N.; OGG, G. S. Pathogenesis of vascular leak in dengue virus infection. **Immunology**. V. 151, p. 261-269. Jul. 2017.

MATTHIAS KIST, M.; VUCIC D. Cell death pathways: intricate connections and disease implications. **EMBO J**. V. 40. 2021.

MCCANN, S. K.; ROULSTON, C. L. NADPH Oxidase as a Therapeutic Target for Neuroprotection against Ischaemic Stroke: Future Perspectives. **Brain Sci**. V. 3. P. 561-598. 2013.

MCLEAN, J. E.; WUDZINSKA, A.; DATAN, E.; QUAGLINO, D.; ZAKERI, Z. Flavivirus NS4A-induced autophagy protects cells against death and enhances virus replication. **J Biol Chem**. V. 286. P. 22147-22159. 2011.

MEDIN, C.; FITZGERALD, K.; ROTHMAN, A. Dengue Virus Nonstructural Protein NS5 Induces Interleukin-8 Transcription and Secretion Dengue Virus Nonstructural Protein NS5 Induces Interleukin-8 Transcription and Secretion. **Journal of Virology**. Massachusetts, V. 79, n. 17, p. 11053-11061, set. 2005.

MEISTER, A.; ANDERSON, M. E. Glutathione. **Annu Rev Biochem**. V. 52. P. 711-760. 1983.

Meuren, 2016. " Indução de Espécies Reativas de Oxigênio (ROS) pelo vírus da Dengue em células endoteliais afeta a replicação viral e a ativação celular". Dissertação (Mestrado de Microbiologia). Centro de Ciências da Saúde, Universidade Federal do Rio de Janeiro, Rio de Janeiro, 2016.

MING-JU, H.; YIH-SHOU, H.; TZY-YEN, C.; HUI-LING, C. Hepatitis C virus E2 protein induce reactive oxygen species (ROS)-related fibrogenesis in the HSC-T6 hepatic stellate cell line. **J Cell Biochem**. V. 112. P. 233-243. 2011.

MINISTÉRIO DA SAÚDE. Boletim epidemiológico, semana 36. Disponível em: https://www.gov.br/saude/pt-br/media/pdf/2021/outubro/11/boletim_epidemiologico_svs_36.pdf. Acesso em: 08 de nov. 2021.

MITTLER, R.; VANDERAUWERA, S.; SUZUKI, N.; MILLER, G.; TOGNETTI, V. B.; VANDEPOELE, K.; GOLLERY, M.; SHULAEV, V.; BREUSEGEM, F. V. ROS signaling: the new wave?. **Trends Plant Sci**. V. 16. P. 300-309. 2011.

MOCARSKI, E. S.; UPTON, J. W.; KAISER, W. J. Viral infection and the evolution of caspase 8-regulated apoptotic and necrotic death pathways. **Nat Rev Immunol**. P. 79-88. 2011.

MODHIRAN, N.; WATTERSON, D.; BLUMENTHAL, A.; BAXTER, A. G.; YOUNG, P. R.; STACEY, K. J. Dengue virus NS1 protein activates immune cells via TLR4 but not TLR2 or TLR6. **Immunol Cell Biol**. P. 491-495. 2017.

MODHIRAN, N.; WATTERSON, D.; MULLER, D. A.; PANETTA, A. K.; SESTER, D. P.; LIU, L.; HUME, D. A.; STACEY, K. J.; YOUNG, P. R. Dengue virus NS1 protein activates cells via Toll-like receptor 4 and disrupts endothelial cell monolayer integrity. **Sci Transl Med**. Queensland, V. 7, n. 304, set. 2015.

MONGKOLSAPAYA, J.; DUANGCHINDA, T.; DEJNIRATTISAI, W.; VASANAWATHANA, S.; AVIRUTNAN, P.; JAIRUNGSRI, A.; KHEMNU, N.; TANGTHAWORNCHAIKUL, N.; CHOTIYARNWONG, P.; SAE-JANG, K.; KOCH, M.; JONES, Y.; MCMICHAEL, A.; XU, X.; MALASIT, P.; SCREATON, G. T cell responses in dengue hemorrhagic fever: are cross-reactive T cells suboptimal? **J. Immunol**. P.3821-3829. 2006.

MUKHOPADHYAY, S.; KUHN, R.; ROSSMANN, M. A Structural Perspective of the Flavivirus Life Cycle. **Nature Microbiology**. Indiana, V. 3, n. 1, p. 13–22. 2005.

MUKHOPADHYAY, S.; KUHN, R.; ROSSMANN, M. A Structural Perspective of the Flavivirus Life Cycle. **Nature Microbiology**. Indiana, V. 3, n. 1, p. 13–22. 2005.

MUÑOZ-JORDÁN, J. L.; FREDERICKSEN, B. L. How flaviviruses activate and suppress the interferon response. **Viruses**. V.2, p. 676–691. 2010.

MURARO, S. P.; DE SOUZA, F. G.; GALLO, S. W.; DA SILVA, B. K.; DE OLIVEIRA, S. D.; VINOLO, M. A. R.; SARAIVA, E. M.; PORTO, B. N. Respiratory Syncytial Virus induces the classical ROS-dependent NETosis through PAD-4 and necroptosis pathways activation. **Sci Rep**. 2018.

MURRAY, C. L.; JONES, C. T.; RICE, C. M. Architects of Assembly: Roles of Flaviviridae Nonstructural Proteins in Virion Morphogenesis. **Nat Rev Microbiol**. New York, V. 6, n. 9, p. 699-708, set. 2008.

NAKANISHI, A.; WADA, Y.; KITAGISHI, Y.; MATSUDA, S. Link between PI3K/AKT/PTEN Pathway and NOX Proteinin Diseases. Aging Dis. V. 5. P. 203-211. 2014.

NASIRUDEEN, A. M.; WONG, H. H.; THIEN, P.; XU, S., LAM, K. P.; LIU, D. X. RIG-I, MDA5 and TLR3 synergistically play an important role in restriction of dengue virus infection. **PloS Negl Trop Dis**. Singapore. V. 5, n. 1, p. e926, jan. 2011.

NIRMALA, J. G.; LOPUS, M. Cell death mechanisms in eukaryotes. **Cell Biol Toxicol**. V. 36, n. 2. P. 145-164. 2020.

NUÑEZ, G.; LONDON, L.; HOCKENBERY, D.; ALEXANDER, M.; MCKEARN, J. P.; KORSMEYER, S. J. Deregulated Bcl-2 gene expression selectively prolongs survival of growth factor-deprived hemopoietic cell. **J Immunol**. V. 144. P. 3602–3610. 1990.

O'DONNELL, R. W.; JOHNSON, D. K.; ZIEGLER, L. M.; DIMATTINA, A. J.; STONE, R. I.; HOLLAND, J. A. Endothelial NADPH oxidase: mechanism of activation by low-density lipoprotein. **Endothelium**. V. 10. P. 201-297. 2003.

O'LEARY, D. P.; BHATT, L.; WOOLLEY, J. F.; GOUGH, D. R.; WANG, J. H.; COTTER, T. G.; REDMOND, H. P. TLR-4 signalling accelerates colon cancer cell adhesion via NF-κB mediated transcriptional up-regulation of Nox-1. **PloS One**. 2012.

OKUDA, M.; LI, K.; BEARD, M. R.; SHOWALTER, L. A.; SCHOLLE, F.; LEMON, S. M.; WEINMAN, S. A. Mitochondrial injury, oxidative stress, and antioxidant gene expression are induced by hepatitis C virus core protein. **Gastroenterology**. V. 122. P. 366-375. 2002.

OLAGNIER, D.; PERI, S.; STEEL, C.; VAN MONTFOORT, N.; CHIANG, C.; BELJANSKI, V.; SLIFKER, M.; HE, Z.; NICHOLS, C. N.; LIN, R.; BALACHANDRAN, S.; HISCOTT, J. Cellular oxidative stress response controls the antiviral and apoptotic programs in dengue virus-infected dendritic cells. **PloS Pathog**. 2014.

ONG, S. P.; NG, M. L.; CHU, J. J. H. Differential regulation of angiopoietin 1 and angiopoietin 2 during dengue virus infection of human umbilical vein endothelial cells: implications for endothelial hyperpermeability. Med **Microbiol Immunol**. p. 437-452. 2013.

ORGANIZAÇÃO MUNDIAL DA SAÚDE. A statistical update – latest data available. **Neglected Tropical Diseases**, jan. 2015.

ORGANIZAÇÃO MUNDIAL DA SAÚDE. **Dengue and severe dengue**. Disponível em: https://apps.who.int/mediacentre/factsheets/fs117/en/index.html. Acesso em: 08 de nov. 2021.

ORGANIZAÇÃO MUNDIAL DA SAÚDE. **Dengue: Guiderlines for diagnosis, treatment, prevention and control.** Geneva: World Health Organization, 2009.

ORGANIZAÇÃO MUNDIAL DA SAÚDE. Integrated Management Strategy for Dengue Prevention and Control in the Region of the Americas.Geneva: World Health Organization, 2017.

ORZALLI, M. H.; KAGAN, J. C. Apoptosis and Necroptosis as Host Defense Strategies to Prevent Viral Infection. **Trends Cell Biol**. V. 27. P. 800-809. 2017.

PAL, S.; POLYAK, S. J.; BANO, N.; QIU, W. C.; CARITHERS, R. L.; SHUHART, M.; GRETCH, D. R.; DAS, A. Hepatitis C virus induces oxidative stress, DNA damage and modulates the DNA repair enzyme NEIL1. **J Gastroenterol Hepatol**. V. 25. P. 627-634. 2010.

PANYASRIVANIT, M.; KHAKPOOR, A.; WIKAN, N.; SMITH, D. R. Co-localization of constituents of the dengue virus translation and replication machinery with amphisomes (a). **J. Gen. Virol**. V. 90, 448– 456. 2009.

PANYASRIVANIT, M.; KHAKPOOR, A.; WIKAN, N.; SMITH, D. R. Linking dengue virus entry and translation/ replication through amphisomes. **Autophagy**. V. 5, 434–435. 2009.

PAPA, 2014. "Mecanismos de morte celular induzidos pelo vírus da dengue em células do endotélio microsvacular humano". Dissertação (Mestrado de Microbiologia). Centro de Ciências da Saúde, Universidade Federal do Rio de Janeiro, Rio de Janeiro, 2014.

PARK, H. S.; JUNG, H. Y.; PARK, E. Y.; KIM, J.; LEE, W. J.; BAE, Y. S. Cutting edge: direct interaction of TLR4 with NAD(P)H oxidase 4 isozyme is essential for lipopolysaccharide-induced production of reactive oxygen species and activation of NF-kappa B. **J Immunol**. V. 173. 3589-3593. 2004.

PENG, C.; WANG, X.; CHEN, J.; JIAO, R.; WANG, L.; LI, Y. M.; ZUO, Y.; LIU, Y.; LEI, L.; MA, K. Y.; HUANG, Y.; CHEN, ZHEN-YU. Biology of ageing and role of dietary antioxidants. **Biomed Res Int**. 2014.

PENG, T.; WANG, J. L.; CHEN, W.; ZHANG, J. L.; GAO, N.; CHEN, Z. T.; XU, X. F.; FAN, D. Y.; ANJ. Entry of Dengue Virus Serotype 2 Into ECV304 Cells Depends on Clathrin-Dependent Endocytosis, But Not on Caveolae-dependent Endocytosis. **Can J Microbiol**. V. 55, n. 2, p. 139-145, fev. 2009.

PERERA, R.; KUHN, R. Structural proteomics of dengue virus. **Curr Opin Microbiol**. West Lafayette, V. 11, n. 4, p. 369-377, ago. 2008.

PERRY, J. J. P.; SHIN, D. S.; GETZOFF, E. D.; TAINER, J. A. The structural biochemistry of the superoxide dismutases. **Biochim Biophys Acta**. V. 1804. P. 245-262. 2010.

PEYREFITTE, C. N.; PASTORINO, B.; GRAU, G. E.; LOU, J.; TOLOU, H.; COUISSINIER-PARIS, P. Dengue virus infection of human microvascular endothelial cells from different vascular beds promotes both common and specific functional changes. **J Med Virol**. V.78, p. 229-42. Feb. 2006.

PHANTHANAWIBOON, S.; LIMKITTIKUL, K.; SAKAI, Y.; TAKAKURA, N.; SAIJO, M.; KUROSU, T. Acute Systemic Infection with Dengue Virus Leads to Vascular Leakage and Death through Tumor Necrosis Factor-α and Tie2/Angiopoietin Signaling in Mice Lacking Type I and II Interferon Receptors. **Plos One**. 2016.

PICCOLI, C.; SCRIMA, R.; D'APRILE, A.; RIPOLI, M.; LECCE, L.; BOFFOLI, D.; CAPITANIO, D. Mitochondrial dysfunction in hepatitis C virus infection. **Biochim Biophys Acta**. V 1757. P. 1429-1437. 2006.

PIHÁN, P.; CARRERAS-SUREDA, A.; HETZ, C. BCL-2 family: integrating stress responses at the ER to control cell demise. **Cell Death Differ**. V. 24. P. 1478-1487. 2017.

PILLAI, A. B.; MUTHURAMAN, K. R.; MARIAPPAN, V.; BELUR, S. S.; LOKESH, S.; RAJENDIRAN, S. Oxidative stress response in the pathogenesis of dengue virus virulence, disease prognosis and therapeutics: an update. Arch Virol. V.164. p. 2895-2906. 2019.

PINGNIAN HE, P.; TALUKDER, M. A. H.; GAO, F. Oxidative Stress and Microvessel Barrier Dysfunction. **Front Physiol**. 2020.

PÓVOA, T. F.; ALVES, A. M.; OLIVEIRA, C. A.; NUOVO, G. J.; CHAGAS, V. L.; PAES, M. V. The pathology of severe dengue in multiple organs of human fatal cases: histopathology, ultrastructure and virus replication. **PloS One**. 2014.

PÓVOA, T. F.; OLIVEIRA, E. R.; BASÍLIO-DE-OLIVEIRA, C. A.; NUOVO, G. J.; CHAGAS, V. L.; SALOMÃO, N. G.; MOTA, E. M.; PAES, M. V. Peripheral Organs of Dengue Fatal Cases Present Strong Pro-Inflammatory Response with Participation of IFN-Gamma-, TNF-Alpha- and RANTES-Producing Cells. **PloS One**. 2016.

RAGER-ZISMAN, B.; KUNKEL, M.; TANAKA, Y.; BLOOM, B. R. Role of macrophage oxidative metabolism in resistance to vesicular stomatitis virus infection. **Infect Immun**. V. 36. P. 1229–1237. 1982.

RAMEZANI, A.; NAHAD, M. P.; FAGHIHLOO, E. F. The role of Nrf2 transcription factor in viral infection. **J Cell Biochem**. V.119. p. 6366-6382. 2018.

RAMOS, C.; SÁNCHEZ, G.; PANDO, R. H.; BAQUERA, J.; HERNÁNDEZ, D.; MOTA, J.; RAMOS, J.; FLORES, A.; LLAUSÁS, E. Dengue virus in the brain of a fatal case of hemorrhagic dengue fever. **J Neurovirol**. P. 465-468. 1998.

RATNAM, D. V.; ANKOLA, D. D.; BHARDWAJ, V.; SAHANA, D. K.; KUMAR, M. N. V. R. Role of antioxidants in prophylaxis and therapy: A pharmaceutical perspective. **J Control Release**. V. 113. P. 189-207. 2006

REDZIC, Z. Molecular biology of the blood-brain and the blood-cerebrospinal fluid barriers: similarities and differences. **Fluids Barriers CNS**. 2011.

RESHI, M. L.; SU, YI-CHE.; HONG, JIANN-RUEY. RNA Viruses: ROS-Mediated Cell Death. **Int J Cell Biol**. 2014.

ROOS, W. P.; THOMAS, A. D.; KAINA, B. DNA damage and the balance between survival and death in cancer biology. **Nat Rev Cancer**. V. 16. P. 20–33. 2016.

ROSAHL S. Lipoxygenases in plants-their role in development and stress response. **Z Naturforsch C**. v.51, p.123-38 Apr. 1996.

SAMPATH, A., PADMANABHAN, R. Molecular targets for flavivirus drug discovery. **Antiviral Res**. Washington, V. 81, n. 1, p. 6-15, jan. 2009.

SHAH, M.; WADOOD, A.; RAHMAN, Z.; HUSNAIN, T. Interaction and Inhibition of Dengue Envelope Glycoprotein With Mammalian Receptor DC-sign, an In-silico Approach. **PloS One**. Mardan, V. 8, n. 3, p. 59211. Mar. 2013.

SHINDO, R.; KAKEHASHI, H.; OKUMURA, K.; KUMAGAI, Y.; NAKANO, H. Contribution of oxidative stress to TNFα-induced necroptosis downstream of RIPK1 activation. **Biochem Biophys Res Commun**. Tokyo, V. 436, n. 2, p. 212-216, jun. 2013.

SHIRYAEV, S. A.; KOZLOV, I. A.; RATNIKOV, B. I.; SMITH, J. W.; LEBL, M.; STRONGIN, A. Y. Cleavage Preference Distinguishes The Two-component NS2B-NS3 Serine Proteinases of Dengue And West Nile Viruses. Califórnia, **Biochem J**. V. 401, n. 3, p. 743-752. Fev. 2007.

SINGH S.; ANUPRIYA M. G.; MODAK A.; SREEKUMAR, E. Dengue virus or NS1 protein induces trans-endothelial cell permeability associated with VE-Cadherin and RhoA phosphorylation in HMEC-1 cells preventable by Angiopoietin-1. **J Gen Virol**. p. 1658-1670. 2018.

Slongo, 2016. " Avaliação dos efeitos de mediadores secretados por células endoteliais infectadas pelo vírus da dengue sobre a viabilidade de células adjacentes". Dissertação (Mestrado de Microbiologia). Centro de Ciências da Saúde, Universidade Federal do Rio de Janeiro, Rio de Janeiro, 2016.

SOARES, C. N.; CABRAL-CASTRO, M. J.; PERALTA, J. M.; FREITAS, M. R. G.; PUCCIONI-SOHLER, M. Meningitis determined by oligosymptomatic dengue 80epor type 3 infection: 80eporto f a case. **Int J Infect Dis**. 2010.

SOE, H. J.; KHAN, A. M.; MANIKAM, R.; SAMUDI, R. C.; VANHOUTTE, P.; SEKARAN, S. D. High dengue virus load differentially modulates human microvascular endothelial barrier function during early infection. **J Gen Virol**. P. 2993-3007. 2017.

SONG, K.; LI, Y.; ZHANG, H.; AN, N.; WEI, Y.; WANG, L.; TIAN, C.; YUAN, M.; SUN, Y.; XING, Y.; GAO, Y. Oxidative Stress-Mediated Blood-Brain Barrier (BBB) Disruption in Neurological Diseases. **Oxidative Medicine and Cellular Longevity**. 2020.

SOUCY-FAULKNER, A.; MUKAWERA, E.; FINK, K.; MARTEL, A.; JOUAN, L.; NZENGUE, Y.; LAMARRE, D.; VELDE, C. V.; GRANDVAUX, N. Requirement of NOX2 and reactive oxygen species for efficient RIG-I-mediated antiviral response through regulation of MAVS expression. **PloS Pathog**. 2010.

SPANOS, S.; RICE, S.; KARAGIANNIS, P.; TAYLOR, D.; BECKER, D. L.; WINSTON, R. M. L.; HARDY, K. Caspase activity and expression of cell death genes during development of human preimplantation embryos. **Reproduction**. V. 124. P. 353-363. 2002

SUHARTI, C.; VAN E. C.; DOLMANS, W. M.; SETIATI, T. E.; HACK, C. E.; DJOKOMOELJANTO, R.; VAN DER MEER, J. W. Cytokine patterns during dengue shock syndrome. **Eur Cytokine Netw**. P. 172-177. 2003.

TAN, T. Y.; CHU, J. J. Dengue virus-infected human monocytes trigger late activation of caspase-1, which mediates pro-inflammatory IL-1β secretion and pyroptosis. **J Gen Virol**. P2215-2220. 2013.

TEIXEIRA, M. G.; SIQUEIRA, J. B.; GERMANO L. C.; BRICKS, L.; JOINT, G. Epidemiological Trends of Dengue Disease in Brazil (2000–2010): A Systematic Literature Search and Analysis. **Plos neglected tropical diseases**. V. 7, p. 2520.

THEPPARIT, C.; KHAKPOOR, A.; KHONGWICHIT, S.; WIKAN, N.; FONGSARAN, C.; CHINGSUWANROTE, P.; PANRAKSA, P.; SMITH, D. R. Dengue 2 infection of HepG2 liver cells results in endoplasmic reticulum stress and induction of multiple pathways of cell death. **BMC Res Notes**. V. 6. P. 372. 2013.

THORÉN, F.; ROMERO, A.; LINDH, M.; DAHLGREN, C.; HELLSTRAND, K. A. hepatitis C virus-encoded, nonstructural protein (NS3) triggers dysfunction and apoptosis in lymphocytes: role of NADPH oxidase-derived oxygen radicals. **J Leukoc Biol**. V. 76. P. 1180-1186. 2004.

VALADÃO, A. L.; AGUIAR, R. S.; DE ARRUDA, L. B. Interplay between Inflammation and Cellular Stress Triggered by Flaviviridae Viruses. **Front Microbiol**. 2016.

VALKO, M.; RHODES, C. J.; MONCOL, J.; IZAKOVIC, M.; MAZUR, M. Free radicals, metals and antioxidants in oxidative stress-induced cancer. **Chem Biol Interact**. V. 160. P. 1-40. 2006.

VANDENABEELE, P.; GALLUZZI, L.; VANDEN BERGHE, T.; KROEMER, G. Molecular mechanisms of necroptosis: an ordered cellular explosion. **Nat Rev Mol Cell Biol**. P.700-714. 2010.

VÁSQUEZ, O. M.; GARCÍA, C. J.; GUTIÉRREZ, C. B.; SANTOS, A. L.; VILLEGAS, S. N.; CEDILLO, B. L. A clinical isolate of dengue virus and its proteins induce apoptosis in HMEC-1 cells: a possible implication in pathogenesis. **Arch Virol**. V. 154. P.919-28. May. 2009.

VERCAMMEN, D.; VANDENABEELE, P.; BEYAERT, R.; DECLERCQ, W.; FIERS, W. Tumour necrosis factor-induced necrosis versus anti-Fas-induced apoptosis in L929 cells. **Cytokine**. P. 801-808. 1997.

VILLALPANDO-RODRIGUEZ, G. E.; GIBSON, S. B. Reactive Oxygen Species (ROS) Regulates Different Types of Cell Death by Acting as a Rheostat. **Oxid Med Cell Longev**. 2021.

VITALE, I.; MANIC, G.; DE MARIA, R.; KROEMER, G.; Galluzzi, L. DNA damage in stem cells. **Mol Cell**. V. 66. P. 306-319. 2017.

VOSS, A. K.; STRASSER, A. The essentials of developmental apoptosis. **F1000Res**. p. 1-12. 2020.

WANG, Z. Y.; ZHEN, Z. D.; FAN, D. Y.; WANG, P. G.; AN J. Transcriptomic Analysis Suggests the M1 Polarization and Launch of Diverse Programmed Cell Death Pathways in Japanese Encephalitis Virus-Infected Macrophages. **Viruses**. 2020.

WENGLER, G.; WENGLER, G. Cell-associated West Nile flavivirus is covered with E+pre-M protein heterodimers, which are destroyed and reorganized by proteolytic cleavage during virus release. **J Virol**. Giessen, V. 63, n. 6, p. 2521-2526, jun.1989.

WIDNELL, C. C.; BALDWIN, S. A.; DAVIES, A.; MARTIN, S.; PASTERNAK, C. A. Cellular stress induces a redistribution of the glucose transporter. FASEB J. V. 4. P. 1634-1637. 1990.

WU, J.; YANG, R.; YANG, Z.; YAO, S.; ZHAO, S.; WANG, Y.; LI, P.; SONG, X.; JIN L.; ZHOU, T.; LAN, Y.; XIE, L.; ZHOU, X.; CHU, C.; QI, Y.; CAO, X.; LI, Y. ROS accumulation and antiviral defence control by microRNA528 in rice. **Nat Plants**. 2017.

WU-HSIEH, B. A.; YEN, Y. T.; CHEN, H. C. Dengue hemorrhage in a mouse model. **Ann N Y Acad Sci**. 2009.

XIAO, X.; BU, H.; LI, Z.; LI, Z.; BA, Q.; WANG, Z.; YAN, L.; LIU, D.; PENG, X.; JIA, X.; GAO, F. NADPH-Oxidase 2 Promotes Autophagy in Spinal Neurons During the Development of Morphine Tolerance. **Neurochem Res**. V. 46. P. 2089-2096. 2021.

YADAV, D.; HERTAN, H. I.; SCHWEITZER, P.; NORKUS, E. P.; PITCHUMONI, C. S. Serum and liver micronutrient antioxidants and serum oxidative stress in patients with chronic hepatitis C. **Am J Gastroenterol**. V. 97. P. 2634–2639. 2002.

YANG, D.; LIU,N.; ZUO, C.; LEI, S.; WU, X.; ZHOU, F. Innate host response in primary human hepatocytes with hepatitis C virus infection. **PloS ONE**. 2011.

YEN, Y. T.; CHEN, H. C.; LIN, Y. D.; SHIEH, C. C.; WU-HSIEH, B. A. Enhancement by tumor necrosis factor alpha of dengue virus-induced endothelial cell production of reactive nitrogen and oxygen species is key to hemorrhage development. **J Virol**. Tainan, V. 82, n. 24, p. 12312-12324, out. 2008.

YOUN, J. Y.; ZHANG, Y.; WU, Y.; CANNESSON, M.; CAI, H. Therapeutic application of estrogen for COVID-19: Attenuation of SARS-CoV-2 spike protein and IL-6 stimulated, ACE2-dependent NOX2 activation, ROS production and MCP-1 upregulation in endothelial cells. **Redox Biol**. 2021.

YU, C.Y.; CHANG, T. H.; LIANG, J. J.; CHIANG, R. L.; LEE, Y. L.; LIAO, C. L.; LIN, Y. L. Dengue virus targets the adaptor protein MITA to subvert host innate immunity. **PloS Pathog**. Taipe, V. 8, n. 6, p. e1002780, jun. 2012.

YUAN, S. Y.; RIGOR, R. R. Regulation of Endothelial Barrier Function. San Rafael (CA): Morgan & Claypool Life Sciences; 2010. Disponível em: https://www.ncbi.nlm.nih.gov/pubmed/21634066. Acesso em: jan de 2018.

ZELLWEGER, R. M.; PRESTWOOD, T. R.; SHRESTA, S. Antibodies enhance infection of LSECs in a model of ADE-induced severe dengue disease. **Cell Host Microbe**. P. 128-139. 2010.

ZENG, W.; CHEN, Z. J. MITAgating viral infection. **Immunity**. Dallas, V. 29, n. 4, p. 513–515, out. 2008.

ZHANG, Y.; WANG G.; WANG, T.; CAO, W.; ZHANG, L.; CHEN, X. Nrf2-Keap1 pathway-mediated effects of resveratrol on oxidative stress and apoptosis in hydrogen peroxide-treated rheumatoid arthritis fibroblast-like synoviocytes. **Ann N Y Acad Scin**. V. 1457. P. 166-178. 2019.

ZHAO, L.; HUANG, X.; HONG, W.; QIU, S.; WANG, J.; YU, L.; ZENG, Y.; TAN, X.; ZHANG, F. Slow resolution of inflammation in severe adult dengue patients. **BMC Infect Dis**. 2016.

ZHENG, A.; UMASHANKAR, M.; KIELIAN, M. *In vitro* And *In vivo* Studies Identify Important Features of Dengue Virus pr-E Protein Interactions. **PloS Pathog**. New York. V. 6, n. 10, p. 1001-157, out. 2010.

ZOROV, D. B.; JUHASZOVA, M.; SOLLOTT, S. J. Mitochondrial reactive oxygen species (ROS) and ROS-induced ROS release. **Physiol Rev**. V. 94, p. 909-950. 2014.

ZOU, J.; KAWAI, T.; TSUCHIDA, T.; KOZAKI, T.; TANAKA, H.; SHIN.; K. S.; KUMAR, H., AKIRA, S. Poly IC triggers a cathepsin D- and IPS-1-dependent pathway to enhance cytokine production and mediate dendritic cell necroptosis. **Immunity**. V. 38, n. 4, p. 717-728. 2013.

9. Anexos

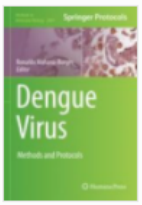

Dengue Virus pp 207-222 | Cite as

Evaluation of DENV-Induced Endothelial Cell Permeability by Measurements of Transendothelial Electrical Resistance (TEER) and Extravasation of Proteins and Virus

Authors | Authors and affiliations

Lana Monteiro Meuren, Sharton Vinicius Antunes Coelho, Luciana Barros de Arruda

Protocol
First Online: 29 October 2021

Part of the Methods in Molecular Biology book series (MIMB, volume 2409)

frontiers in Immunology

ORIGINAL RESEARCH
published: 02 February 2022
doi: 10.3389/fimmu.2022.810376

Infection of Endothelial Cells by Dengue Virus Induces ROS Production by Different Sources Affecting Virus Replication, Cellular Activation, Death and Vascular Permeability

*Lana Monteiro Meuren[1], Elisa Beatriz Prestes[2], Michelle Premazzi Papa[1,3], Luiza Rachel Pinheiro de Carvalho[4], Yasmin Mucunã Mustafá[1], Leandro Silva da Costa[4], Andrea T. Da Poian[4], Marcelo Torres Bozza[2] and Luciana Barros Arruda[1]**

[1] Departamento de Virologia, Instituto de Microbiologia Paulo de Góes, Universidade Federal do Rio de Janeiro, Rio de Janeiro, Brazil, [2] Laboratório de Inflamação e Imunidade, Departamento de Imunologia, Instituto de Microbiologia Paulo de Góes, Universidade Federal do Rio de Janeiro, Rio de Janeiro, Brazil, [3] Department of Microbiology, Immunology and Tropical Medicine, The George Washington University, Washington, DC, United States, [4] Instituto de Bioquímica Médica Leopoldo de Meis, Universidade Federal do Rio de Janeiro, Rio de Janeiro, Brazil

OPEN ACCESS

Edited by:
Francesca Chiodi,
Karolinska Institutet (KI), Sweden

Reviewed by:
Maria Issagouliantis,
Riga Stradiņš University, Latvia
Alexander V. Ivanov,
Engelhardt Institute of Molecular Biology (RAS), Russia

***Correspondence:**
Luciana Barros Arruda
arruda@micro.ufrj.br

Specialty section:
This article was submitted to Viral Immunology, a section of the journal Frontiers in Immunology

Received: 06 November 2021
Accepted: 11 January 2022
Published: 02 February 2022

Citation:
Meuren LM, Prestes EB, Papa MP, de Carvalho LRP, Mustafá YM, da Costa LS, Da Poian AT, Bozza MT and Arruda LB (2022) Infection of Endothelial Cells by Dengue Virus Induces ROS Production by Different Sources Affecting Virus Replication, Cellular Activation, Death and Vascular Permeability. Front. Immunol. 13:810376. doi: 10.3389/fimmu.2022.810376

Exacerbated inflammatory response and altered vascular function are hallmarks of dengue disease. Reactive oxygen species (ROS) production has been associated to endothelial barrier disturbance and microvascular alteration in distinct pathological conditions. Increased ROS has been reported in *in vitro* models of dengue virus (DENV) infection, but its impact for endothelial cell physiology had not been fully investigated. Our group had previously demonstrated that infection of human brain microvascular endothelial cells (HBMEC) with DENV results in the activation of RNA sensors and production of proinflammatory cytokines, which culminate in cell death and endothelial permeability. Here, we evaluated the role of mitochondrial function and NADPH oxidase (NOX) activation for ROS generation in HBMEC infected by DENV and investigated whether altered cellular physiology could be a consequence of virus-induced oxidative stress. DENV-infected HBMECs showed a decrease in the maximal respiratory capacity and altered membrane potential, indicating functional mitochondrial alteration, what might be related to mtROS production. Indeed, mtROS was detected at later time points after infection. Specific inhibition of mtROS diminished virus replication, cell death, and endothelial permeability, but did not affect cytokine production. On the other hand, inhibition of NOX-associated ROS production decreased virus replication and cell death, as well as the secretion of inflammatory cytokines, including IL-6, IL-8, and CCL5. These results demonstrated that DENV replication in endothelial cells induces ROS production by different pathways, which impacts biological functions that might be

relevant for dengue pathogenesis. Those data also indicate oxidative stress events as relevant therapeutical targets to avoid vascular permeability, inflammation, and neuroinvasion during DENV infection.

Keywords: dengue, human brain microvascular endothelial cells (HBMEC), reactive oxygen species, mitochondria, NADPH oxidase, cytokines, cell death

INTRODUCTION

Dengue virus (DENV) infection is a major public health problem worldwide, mostly in tropical and subtropical countries, affecting about 400 million people every year (1). Infection by any of the four described serotypes can induce a range of clinical manifestations, from mild to severe hemorrhagic forms, that can be fatal (2). Vascular alterations, including vasodilation and increased permeability, are major consequences of DENV infection, contributing to plasma extravasation to the tissues, hemorrhagic manifestations, and hypotension, which are hallmarks of severe disease, but may also happen at lower levels in mild and moderate disease (3, 4). Previous studies indicated that vascular disturbances result from systemic inflammation and endothelial lesion (4–7). In addition, direct infection of endothelial cells was demonstrated in histopathological analysis of different tissues from fatal cases, as well as in primary cells and different cell lines (7–11).

We have previously demonstrated that human brain microvascular endothelial cells (HBMECs) are permissive to DENV, and virus replication triggers the activation of RNA sensors, inducing the production of inflammatory cytokines, chemokines and type I interferon (9). Evidence of virus-induced cell death was also detected, but the involved mechanisms had not been addressed (9, 12). A number of studies have been unraveling the complex connections between virus sensing, cellular stress response and cell death [rev in (13)]. Some of those signals converge to the production of nitrogen and oxygen reactive species, which accumulation stimulate the secretion of inflammatory mediators, and trigger autophagy, apoptosis and necroptosis in different models of viral infections (14–18). Oxidative stress may be particularly deleterious in the vascular context, since ROS-mediated endothelial cell activation and death will contribute to vascular permeability and barrier disruption, as demonstrated under several pathological conditions (19–21). Although it has been largely demonstrated that excessive ROS impair microvessel integrity and that leukocyte-derived ROS might be an important contributor to endothelial barrier damage [rev in (21)], the role of endogenous endothelial cell-derived ROS has been poorly addressed, especially in the context of virus infections.

Increased ROS production was evidenced in *in vitro* and *in vivo* models of dengue infection. *In vitro* infection of human monocyte derived dendritic cells (Mo-DC) induced the activation of NADPH oxidases (NOX) and accumulation of intracellular ROS, which contribute to enhanced production of inflammatory cytokines and chemokines (14). NOX-derived ROS was also associated to vascular damage in a mouse experimental model, in which depletion of p47phox significantly reduced DENV-induced systemic hemorrhage, in comparison to control mice (22).

Mitochondrial oxidative phosphorylation metabolism is another major source of intracellular ROS (23, 24). However, despite previous observations of altered mitochondrial bioenergetics and morphology in *in vitro* experimental models of DENV infection, the impact of virus replication in the generation of mitochondrial-derived ROS (mtROS) had not been clearly addressed (25, 26). In fact, cellular ROS may be generated by different enzymes present in distinct intracellular sites, also including xanthan oxygenase, cyclooxygenase and lipooxygenase, further contributing to overall oxidative stress (13, 19, 27).

Here, we evaluated whether infection of HBMEC with DENV resulted in enhanced cellular ROS by NOX and mitochondrial-derived pathways and assessed the relative role of each ROS source for viral replication, endothelial activation, cell death and endothelium permeability. We observed that DENV replication triggered mitochondrial and NOX-mediated ROS production, which were essential for viral replication and cell death. Mitochondrial-derived ROS was a major inducer of HBMEC permeability, whereas NOX-derived ROS played a relevant role for endothelial activation and production of inflammatory mediators. This study reveals new information about the impact of oxidative stress caused by DENV during infection of endothelial cells and provides a new perspective for the use of antioxidants for dengue treatment.

MATERIAL AND METHODS

Cells and Virus

Human brain microvascular endothelial cell line (HBMEC) (28) was kindly given by Dr. Dennis J. Grab (The Johns Hopkins University, MD, USA). The cells were cultivated in medium M199 (M199), supplemented with 10% fetal bovine serum (FBS) (Thermo Fisher Scientific Inc), at 37°C. *Aedes albopictus* clone C6/36 cell line (ATCC® CRL-1660™) was cultured in Leibovitz (L-15) medium (Invitrogen), supplemented with 10% FCS, tryptose phosphate (2.95 g/L), 0.75% sodium bicarbonate, and 0.2% of L-glutamine (Sigma-Aldrich), at 28°C. Baby hamster kidney cells [BHK-21 (C-13]) ATCC® CCL-10™] were cultured in Minimum Essential Medium Eagle - Alpha Modification (α-MEM) (Thermo Fisher Scientific Inc) supplemented with 5% of FBS, at 37°C.

DENV serotype 2 strain 16681 was propagated in C6/36 cells. The supernatants of infected cells were harvested, filtered, and

stored at -80°C, and virus stock was titrated by plaque assay using BHK cells, as described below. Supernatants obtained from noninfected C6/36 cells cultured under the same conditions were used as mock control. Virus inactivation was performed by 2 hours UV exposure and confirmed by qRT-PCR in HBMECs.

Ethical Statements and Obtention of Human Primary Macrophages

Blood samples (buffy coat) were obtained from the Hemotherapy Service at the Hospital Universitário Clementino Fraga Filho (HUCFF) of Universidade Federal do Rio de Janeiro (UFRJ). The study protocol was approved by the Experimental Ethics Committee of UFRJ (Permit Number: CAAE 27600314.7.0000.5275). Fresh peripheral blood mononuclear cells (PBMCs) were obtained by Ficoll-Hypaque density gradient centrifugation and cultured for 7-10 days with RPMI medium, supplemented with L-glutamine, and 2% human serum (Thermo Fisher Scientific Inc). Macrophage differentiation was confirmed by CD68 staining and flow cytometry analysis.

Infection of HBMECs and Macrophages

HBMECs were incubated with DENV-2 virus, with a MOI of 1, for 1h at 37°C in 5% CO_2 atmosphere. As a control, cells were mock-treated or incubated with UV-inactivated DENV-2 (iDENV). After the adsorption, the inoculum was removed, the cells were washed with phosphate buffer saline (PBS 1x) and maintained in culture medium with 10% FBS at 37°C at 5% de CO_2 for different periods of time (24hpi-72hpi). Primary macrophages were infected, under the same conditions, using a MOI of 2. In some experiments, the following ROS inhibitors/scavengers were added to the cultures: N-Acetylcysteine (NAC; 1mM; Merck Millipore; Darmstadt, Germany), Apocynin (Apo; 1mM; Merck Millipore); mitoTEMPO (MitoT; 50μM; Enzo Life Sciences). The culture supernatants were harvested, and the titer of infectious particles released was evaluated by plaque assay.

Virus Titration by Plaque Assay

Titration of virus stocks and measurement of infectious particles released in the supernatants of experimental cultures were performed by plaque assay using BHK cells, as described (29). Briefly, the cells were inoculated with serial dilutions of the infected samples for 2h, at 37^0C for virus adsorption. Then, medium was replaced with 1% carboxymethylcellulose (CMC) diluted in α-MEM medium with 1% FBS. After 5 days of culture, the cells were fixed with 1ml of 10% formaldehyde for 1h and stained with 4% crystal violet solution. Virus titers were indicated as PFU/ml.

Analysis of Virus Replication by RT-qPCR

HBMECs and macrophages were infected with DENV-2, in the presence or absence of N-acetylcysteine. After 48hpi, cell lysates and supernatants were harvested and RNA was isolated using TRIZOL reagent (Life Technologies), according to the manufacturer's instructions. First strand cDNA was synthesized using 2 μg RNA using High-Capacity cDNA Archive Kit (Life Technologies), according to the manufacturer's instructions. Quantitative real-time PCR was performed using a StepOnePlus Real-time PCR system (Life Technologies) and Taqman Master Mix Reagents (Life Technologies), as described before (9).

ROS Quantification by Flow Cytometry and Immunofluorescence

To measure total or mtROS, the cells were incubated with the probes CM-H2DCFDA (1μM/1x10^6 cells; Thermo Fisher Scientific Inc) or MitoSOX (1μM; Thermo Fisher Scientific Inc), respectively, at different time points post infection. The cells were analyzed by flow cytometry using the FACScalibur and FlowJo software (LCC, Ashland, USA). The same methodology was used to measure ROS by fluorescence microscopy and the cells were analyzed using OLYMPUS IX81 microscopy.

Analysis of Oxygen Consumption and Assessment of Mitochondrial Bioenergetics

Oxygen consumption rate (OCR) by control or DENV-2-infected cells was evaluated by high resolution respirometry. HBMECs (2 x 10^6 cells) were mock-treated or infected with DENV-2 for different periods of time. Respirometry was monitored in real time using Oroboros equipment (Oxygraph-2K, Instruments, Innsbruck, Austria) and sequentially adding pharmacological inhibitors of the oxidative phosphorylation. Oligomycin (200μg/mL) was used to determine oxygen consumption not associated with ATP synthase, and the mitochondrial oxidative phosphorylation uncoupler carbonyl cyanide p-trifluoromethoxyphenylhydrazone (FCCP) (1mM) was used to allow maximum electron flow in the electron transport chain. These parameters allowed the evaluation of basal respiration (before oligomycin addition), OCR due to proton leak (uncoupled OCR; after oligomycin addition), OCR associated to ATP synthase (coupled OCR - difference between basal and oligomycin OCR), maximum respiratory capacity (after addition of FCCP), and reserve capacity (difference between FCCP and basal OCR).

Evaluation of Mitochondrial Membrane Potential ($\Delta\psi_m$)

Mitochondrial membrane potential in mock-treated or DENV-2-infected HBMEC was evaluated using JC-1 dye (5,5′,6,6′-tetrachloro-1,1′,3,3′-tetraethylbenzimidazolyl-carbocya-nine iodide; Molecular Probes). Cells were incubated with 5μg/mL JC-1 at 37°C for 1 h. Culture medium and 10 minutes incubation with FCCP were used as negative and positive control, respectively. The cells were analyzed by flow cytometry using the FACScalibur equipment and FlowJo software (LCC, Ashland, USA), and the ratio red/green fluorescence was used to measure the membrane potential.

Cell Viability Assays

HBMECs and macrophages were mock-treated or infected with DENV-2, in the presence or absence of ROS inhibitors. After 48hpi, macrophage metabolic activity was addressed by MTT assay, according to the manufacturers protocol (Thermo Fisher

Scientific Inc). In addition, after 48-72hpi, the integrity of the plasma membrane and cell viability was carried out using propidium iodide (PI) staining (2,5μg/ml per well) for 15 min. The cells were analyzed by flow cytometry using the FACScalibur and FlowJo software.

Endothelial Permeability Assay

HBMECs were cultured onto transwell insert (Corning Costar, ME, USA; 0,4 μM membrane), at a concentration of $5x10^4$ cells. The cells were mock treated or infected with DENV-2 (MOI of 1), in the presence or absence of ROS inhibitors, as described. Staurosporine (10 μM; Sigma-Aldrich) was used as a positive control. Cell confluence was monitored before infection and during all the experiment by measuring the transendothelial electrical resistance (TEER), using a Voltohmmeter (Millicell ERS-2), as previously described (30). To calculate the TEER (reported as 'Ω/cm2'), the membrane resistance itself (without cells) was considered as blank, and the obtained TEER value was subtracted from the resistance value obtained in each experimental conditions; also, the resistance was considered inversely proportional to the area of the membrane. All the experiments were started when a high resistance (> 80 Ω/cm^2) was reached (31, 32). Endothelial permeability was further evaluated by measuring extravasation of FITC-conjugated BSA through the culture. After 72 hpi, the culture supernatant was removed and a solution of BSA-FITC was added for 30 minutes. BSA extravasation to the lower transwell chamber was quantified using spectrophotometer SpectraMAX i3 (Molecular Devices, Lagerhausstrasse, Austria). The Permeability Coefficient (Pd) of albumin was calculated as described previously (30).

Analysis of Cytokine Production by ELISA and qRT-PCR

HBMECs were mock-treated or infected with DENV-2, in the presence or absence of NAC, apocynin or mitoTEMPO, and cytokine production was evaluated at 48 hpi, as determined elsewhere (9). The supernatants were harvested and the concentration of secreted CCL5 was determined using the ELISA Development Kit (PeproTech), whereas IL-6 and IL-8 levels were determined using ELISA Ready-SET-Go! (eBiosciences), according to manufacturer's instructions. The expression of IFN-β mRNA was evaluated in the cell lysates by qRT-PCR. Briefly, RNA was isolated using TRIZOL reagent, and cDNA synthesis was performed using the High-Capacity cDNA Archive Kit (Life Technologies), following the manufacturer's recommendations. The cDNA was subjected to real-time PCR using Power SYBR Green PCR master mix reagent (Thermo Fisher Scientific Inc.), with the following primers: IFN-β sense: 5'-TAG CAC TGG CTG GAA TGA GA-3′; IFN-b antisense: 5′-TCC TTG GCC TTC AGG TAA TG-3'. GAPDH expression was measured as control gene, using the primers: GAPDH sense 5′-GTG GAC CTG ACC TGC CGT CT-3′, and GAPDH antisense 5′-GGA GGA GTG GGT GTC GCT GT-3′. The reactions were carried out in a StepOnePlus real-time PCR system (Thermo Fisher Scientific Inc.). The comparative CT method (ΔΔCt) (33) was used to quantify gene expression levels.

Statistical Analysis

Data were analyzed using the GraphPad Prism software (GraphPad Software, San Diego, CA, USA). Comparisons among every two groups were performed by t-test, and two way ANOVA followed by Dunnett's multiple comparison test were used when different time points were considered; $p < 0.05$ were considered statistically significant.

RESULTS

Infection of HBMEC With DENV-2 Induces ROS Production Through Different Pathways, Which Modulate Virus Replication

Our group demonstrated that infection of HBMEC with DENV-2 induced RIG-I expression, cytokine production, and cell death (9, 12). Since NOX-mediated ROS production has been associated to cellular activation and death upon DENV infection in other cell models (14), here we investigated whether altered HBMEC biology could also be a consequence of DENV-induced oxidative stress.

HBMECs were infected with DENV-2, at a MOI of 1, and stained with CM-H2DCFDA probe at different time points until 72 hours post infection (hpi). DENV infection stimulated ROS production at 48 and 72 hpi, in comparison to mock-treated cells, which was evidenced by a significant increase in the frequency of cells producing higher ROS levels (% ROShi cells) and in the overall level of intracellular ROS in the culture (MFI) (**Figures 1A–C**). UV-inactivated virus (iDENV) did not affect ROS levels. Also, ROS production was not observed at earlier time points (**Figures S1A, B**), probably reflecting the need for virus replication cycles to amplify the stimulatory signal. As a control, HBMECs were cultured with heme (34), which resulted in increased ROS production after 24h, indicating that there was no intrinsic impairment of the cultures at this time point (**Figures S1C, D**). We evaluated the concentration of released infectious particles in the cultures (PFU) (**Figure 1D**) and observed that ROS levels positively correlated with virus titer overtime (**Figure 1E**). This data was corroborated by immunofluorescence analyses, showing that the majority of DENV-2-infected cells were generating ROS (**Figure 1F**).

In another set of experiments, HBMECs were stained with MitoSox probe to specifically investigate mitochondrial-derived ROS. Increased mtROS were also detected in DENV-infected cells from 48hpi, with a significant enhancement at 72hpi (**Figures 1G–I**).

To identify the ROS-inducing pathway, HBMECs were infected in the presence or absence of apocynin or mitoTEMPO, to respectively inhibit NOX or scavenge mtROS. The antioxidant N-acetyl-L-cystein (NAC) was used as a control. Decreased ROS levels were observed when HBMECs were cultured with either apocynin or mitoTEMPO, indicating that cytoplasmic and mitochondrial sources are important for ROS generation induced upon DENV-2 infection (**Figures 2A–C**). Viability assays using the drugs alone confirmed that none of the

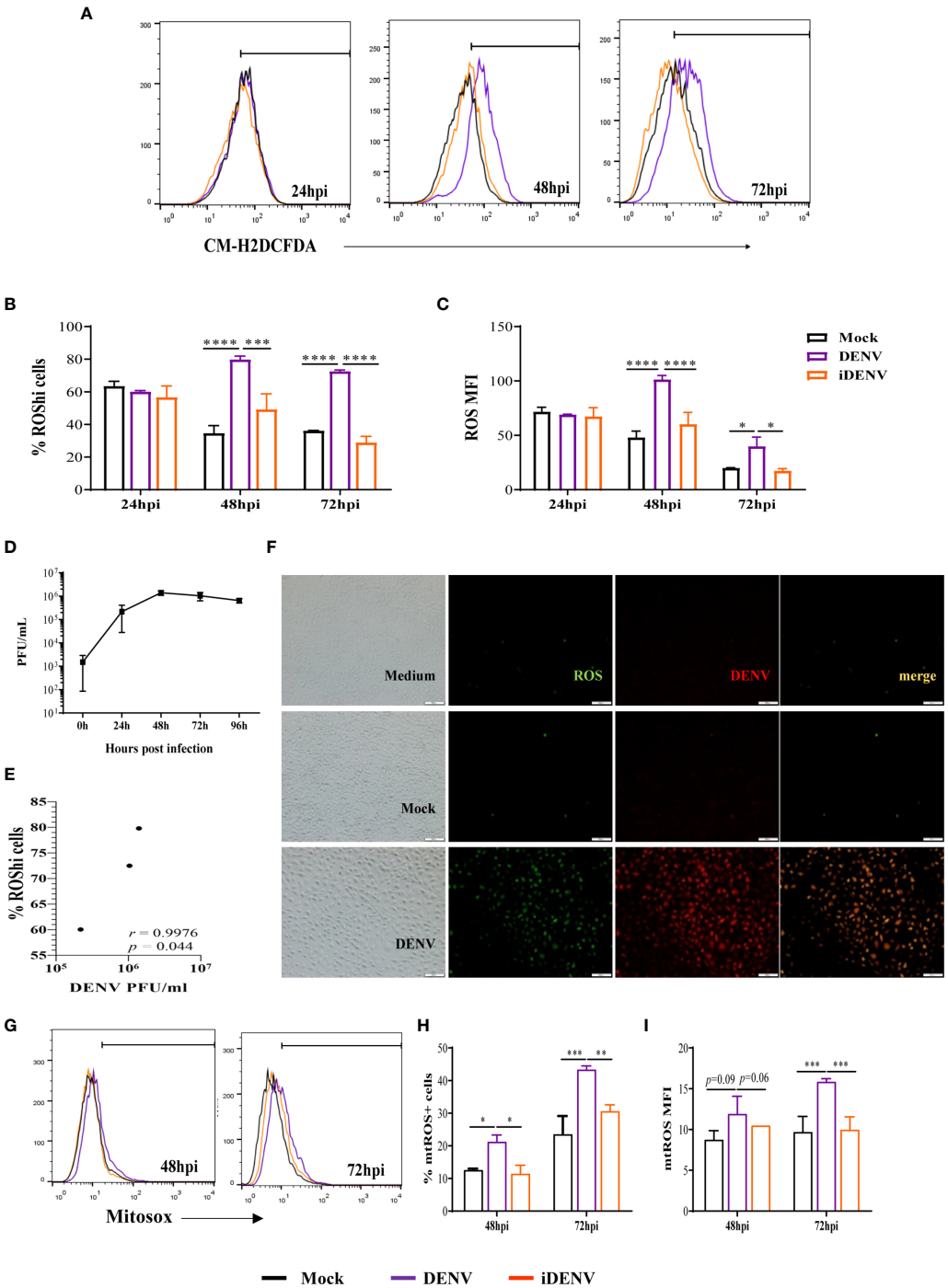

FIGURE 1 | Infection of human brain endothelial cells (HBMEC) with DENV-2 induces ROS production. HBMECs were mock-treated or inoculated with infectious (DENV) or UV-inactivated DENV-2 (iDENV), at an MOI of 1, for the indicated time points. **(A–C)** After 24, 48 and 72hpi, the cells were incubated with CM-H2DCFDA and ROS production was analyzed flow cytometry. A representative histogram overlay is depicted in **(A)** the medians of the frequency of cells producing increased ROS (%ROShi), and the level of ROS production (MFI) obtained from five independent experiments are showed in **(B, C)**. **(D)** The concentration of released infectious particles was measured at the same time points by plaque assay and **(E)** the correlation between DENV-2 titer (PFU/ml) and the frequency of ROS producing cells was analyzed. **(F)** At 72hpi the cells were incubated with anti-DENV antibody and with CM-H2DCFDA probe and analyzed by immunofluorescence. **(G–I)** After 48 and 72hpi, the cells were incubated with MitoSox probe and mtROS production was analyzed flow cytometry. Representative histograms are depicted in **(G)** and the medians of the frequency of cells producing mtROS (%mtROS+ cells), and the level of mtROS production (MFI) obtained from four independent experiments are showed in **(H, I)** *Represents $p \leq 0.05$; **$p \leq 0.01$; ***$p \leq 0.001$; ****$p \leq 0.0001$.

inhibitors were cytotoxic at the concentrations and time points evaluated, supporting their use in the system (**Figure S2**). In addition, since apocynin may function as a ROS scavenger and not as a specific NOX inhibitor in some systems (35), we evaluated whether it could be in fact inhibiting mtROS. The addition of apocynin did not affect MitoSox staining, corroborating with the hypothesis that DENV infection induces ROS generation by different sources in HBMECs (**Figures 2D–F**).

Importantly, ROS scavenging by NAC resulted in diminished intracellular and released virus RNA (**Figure 2G**). Furthermore, addition of NAC, apocynin or mitoTEMPO to the cultures decreased the concentration of released DENV-2 infectious particles, indicating that DENV infection induces the production of ROS, which further contribute to virus replication (**Figure 2H**). Interestingly, inhibition of released virus RNA and infectious particles were more pronounced, in comparison to intracellular RNA reduction, suggesting that ROS may affect later steps of DENV biosynthetic cycle, delaying virus replication.

DENV-2 Infection of HBMEC Affects Mitochondrial Bioenergetics and Membrane Potential

Virus infection and intracellular virus biosynthesis relies on enhanced energy spent, what may trigger increased respiration. Abnormal respiration may then result in increased electron leakage and generation of mtROS. Indeed, we had demonstrated that infection of hepatic cell lines with DENV resulted in altered mitochondrial bioenergetics and morphology and cell death (25). To evaluate mitochondrial function in DENV-2-infected HBMECs, bioenergetic and membrane potential analyses were performed by high-resolution respirometry and flow cytometry assays. HBMECs were mock-treated or infected with DENV-2 for different periods, and oxygen consumption rate (OCR) was measured after sequentially adding pharmacological modulators of the oxidative phosphorylation. We did not detect any alterations in mitochondrial bioenergetics at 24hpi (**Figures 3A, B**). However, at 48hpi, we observed a significant decrease in the basal OCR in DENV-infected cells, in comparison to the mock treated ones (**Figures 3C, D**). As expected, inhibition of ATP synthase through the addition of oligomycin strongly diminished the OCR in the mock-treated cells (2.7 times, $p<0.001$). In contrast, oligomycin did not significantly affected the OCRs of the infected cells (1.6 times, $p=0.082$), which showed similar basal, coupled, and uncoupled values at this time point. In addition, DENV-2-infected cells presented a reduced maximum respiratory capacity evidenced by the lower OCR detected after addition of the proton ionophore FCCP (**Figures 3C, D**). These data indicate that DENV induced mitochondrial membrane leak, detected by diminished basal OCR, which could not be further affected by the modulators of oxidative phosphorylation. In addition, cellular staining with JC1 dye indicated mitochondrial depolarization after 48hpi (**Figures 3E, F**). Taken together, these findings suggest that DENV-2 impairs mitochondrial function and affects membrane potential, resulting in the increased mtROS, which was mostly detected at later time points upon infection.

DENV-2-Induced ROS Production Promotes Cell Death and Endothelial Permeability

Since DENV infection impacted HBMEC survival (9), and given that endothelial cell death would affect the endothelium permeability, we investigated whether ROS generation was also involved in these events. Analysis of propidium iodide staining at 48 and 72hpi demonstrated that NAC, apocynin and mitoTEMPO partially reduced HBMECs death induced by DENV-2 infection (**Figures 4A, B**).

We then evaluated whether endothelial permeability induced by DENV-2 would also be restored by reducing ROS accumulation. HBMECs were seed onto transwell inserts and infected with DENV-2, with or without NAC, apocynin or mitoTEMPO, and transendothelial electrical resistance (TEER) was measured at 48 and 72hpi. At 72hpi, culture permeability was also accessed by measuring the extravasation FITC-conjugated BSA through the transwell membrane. Mock and staurosporin (STS) were used as negative and positive controls, respectively. As expected, DENV-2 infection promoted a decrease in the TEER, associated to increased extravasation of BSA-FITC to the lower transwell compartment (**Figures 4C, D**), demonstrating that DENV-2 induces permeability in this cell model. HBMEC permeability was completely rescued when the cells were treated with NAC or mitoTEMPO. Addition of apocynin resulted in increased TEER but did not significantly protect the monolayer from BSA extravasation, suggesting that mtROS might be a major mediator in DENV-2-induced endothelial permeability.

To investigate whether these events were specific to endothelial cells, we evaluated ROS production, virus replication, and cell viability after infection of primary human macrophages with DENV-2. DENV-infected macrophages also showed increased total and mtROS production as evidenced by staining with CM-H2DCFDA or MitoSox probes (**Figures S3A, B**). As observed for HBMEC, macrophage treatment with NAC resulted in diminished virus replication and cellular survival (**Figures S3C, D**), indicating that oxidative stress induced by DENV-2 infection might be essential for fueling virus replication, resulting in cell death.

Apocynin-Modulated ROS, But Not mtROS, Is Essential for the Secretion of Inflammatory Cytokines Induced by DENV-2 Infection of HBMECs

Given that HBMEC infection with DENV-2 promoted cellular activation (9) and since accumulation of intracellular ROS had been previously proposed to stimulate immune responses in other human cell types (14), we investigated whether this stress response could also contribute to HBMEC activation. HBMECs were infected, in the presence or absence of ROS inhibitors, and IFN-β expression and IL-6, IL-8 and CCL5 secretion were measured by qRT-PCR and ELISA, respectively. Cytokine secretion was significantly inhibited by NAC and apocynin, but not by mitoTEMPO (**Figures 5A–C**), indicating that other ROS sources, but not mtROS, contributes to signal transduction associated to IL-6 and chemokine release. Surprisingly, increased IFN-β expression induced by DENV-2 infection was not modulated by any inhibitors (**Figure 5D**).

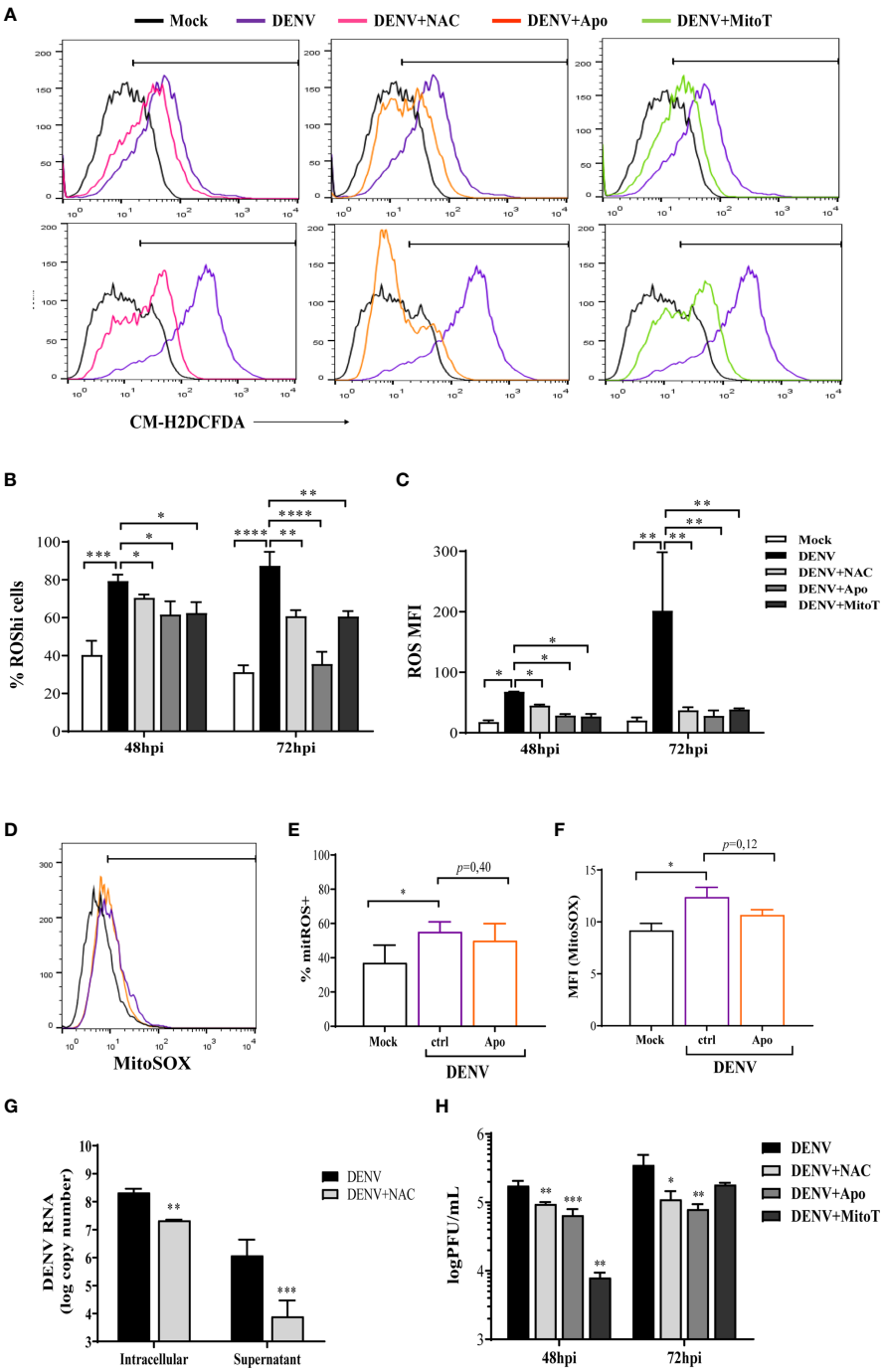

FIGURE 2 | DENV-induced ROS by different intracellular sources modulate virus replication. HBMECs were mock treated or infected with DENV-2, in the presence or absence of N-acetyl-L-cysteine (NAC), apocynin (Apo), or mitoTEMPO (MitoT). **(A–C)** At the indicated time points, the cells were incubated with CM-H2DCFDA probe and the analysis of ROS production was performed by flow cytometry. A representative histogram overlay is shown in **(A)**, the medians of the frequency of cells producing increased ROS (%ROShi), and the level of ROS production (MFI) obtained from four independent experiments are showed in **(B, C)**. **(D–F)** Mock-treated or DENV-infected HBMECs were cultured in the presence or absence of apocynin (Apo) and mtROS production was evaluated by MitoSOX staining and flow cytometry analysis. A representative histogram overlay is shown in **(D)**, the medians of the frequency of cells producing ROS (%ROS), and the level of ROS production (MFI) obtained from two independent experiments are showed in **(E, F)**. **(G–H)** Mock-treated or DENV-infected HBMECs were cultured in the presence or absence of the indicated ROS inhibitors. The concentration of intracellular and released virus RNA were measured by qRT-PCR **(G)** and concentration of released virus particles was evaluated by plaque assay **(H)** data is representative of three independent experiments. *Represents $p \leq 0.05$; **$p \leq 0.01$; ***$p \leq 0.001$; ****$p \leq 0.0001$.

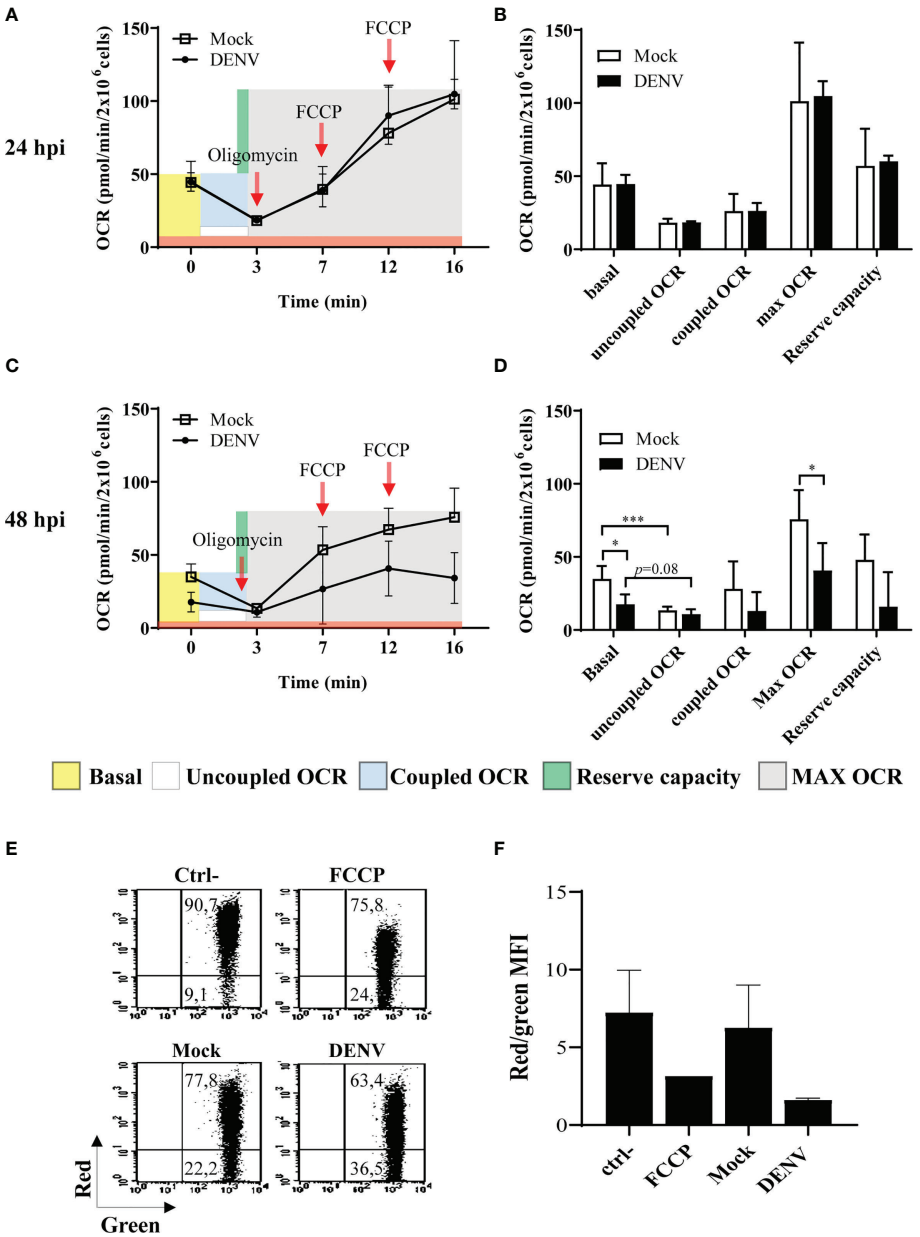

FIGURE 3 | DENV infection impacts mitochondrial function in HBMECs. HBMECs were mock-treated or infected with DENV-2, at a MOI of 1. **(A–D)** At 24 and 48 hpi the oxygen consumption ratio (OCR) was analyzed by high resolution respirometry. OCR in intact cells and after addition of oligomycin and FCCP were sequentially measured **(A, C)** and the obtained values used to calculate the basal respiration, uncoupled OCR (ATP-independent oxygen consumption); coupled OCR (consumption of oxygen dependent on ATP synthase); Max OCR (maximum respiration independent of ATP transport); and the reserve capacity (consumption capacity available during ATP increase) **(B, D)**. Data are represented as mean ± SD of seven independent experiments. *Represents $p \leq 0.05$; ***$p \leq 0.001$. **(E, F)** Cells were incubated with JC-1 probe and membrane potential was evaluated as the ration red/green fluorescence by flow cytometry. A representative dot plot is shown in **(E)** and the average of the ratio values obtained from three independent experiments are demonstrated in **(F)**.

DISCUSSION

Dengue severity correlates with exacerbated inflammation, cytokine storm, vascular hyperpermeability, and plasma leakage (2, 3, 36). Enhanced circulation of inflammatory cytokines has been assumed to be the major cause of vascular lesion (4–6). However, virus replication in endothelial cells may directly affect endothelium integrity or synergize with the inflammatory mediators, further contributing to dengue-mediated vascular dysfunction. In the present study we demonstrated that infection of HBMEC by DENV results in increased generation of ROS, which in turn modulates virus replication, cell death and cellular activation.

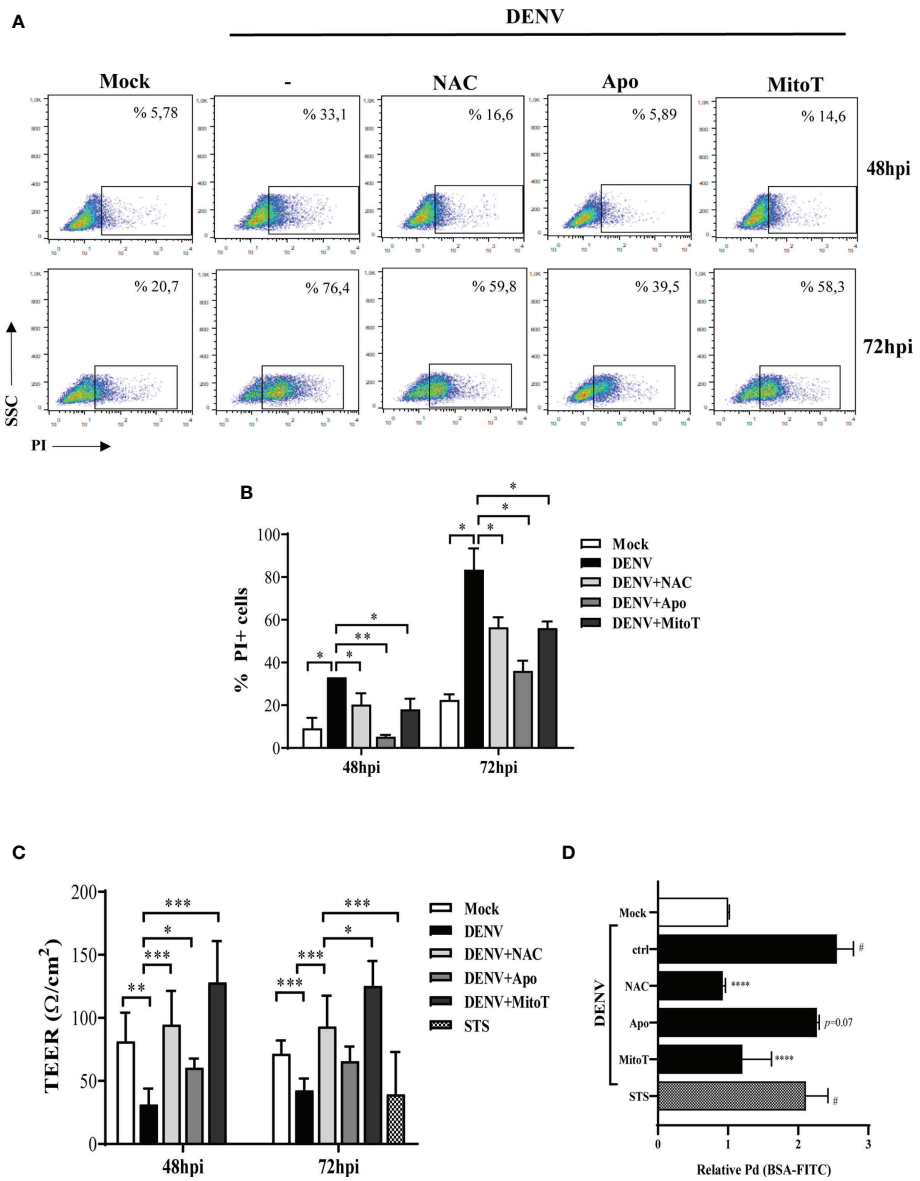

FIGURE 4 | ROS inhibition reduced DENV-induces HBMEC death and partially recover endothelial permeability *in vitro*. HBMECs were mock-treated or infected with DENV-2 for 48 or 72h, in the presence or absence of NAC, apocynin (Apo) or MitoTEMPO (MitoT). **(A, B)** The cells were incubated with propidium iodide (PI) and cell death was evaluated by flow cytometry. A representative dot blot is shown in **(A)** and the bar graph **(B)** demonstrates the average and SD of the frequency of PI^+ cells (%PI+ cells) obtained from three independent experiments. **(C, D)** HBMECs were cultured onto transwell insert plates and infected with DENV-2, in the presence or absence of NAC, apocynin (Apo) or MitoTEMPO (MitoT). Mock and staurosporin (STS) were used as negative and positive controls, respectively. **(C)** At 48 and 72hpi, transendothelial electrical resistance (TEER) was measured using a volthmeter. **(D)** After 72hpi, the cells were incubated with FITC-conjugated BSA for 1 hour, and the amount of extravasated albumin was measured by spectrophotometry. The permeability coefficient (Pd) was calculated and normalized in relation to cells cultured in medium only. Data represent the mean and SD obtained from four independent experiments. *$p \leq 0.05$; **$p \leq 0.01$; ***$p \leq 0.001$; ****$p \leq 0.0001$ in relation to ctrl; $^{\#}p \leq 0.0001$ in relation to mock.

Evidence of oxidative stress has been reported in patients and *in vivo* experimental models. Plasma obtained from dengue patients showed higher levels of lipid oxidation and increased ratio of protein carbonylation (PCOs) in relation to protein-bound sulphydryl (PBSH) group, which are indicatives of protein oxidation and decreased plasma antioxidants (37). Importantly, protein and lipid alterations were detected early after the symptoms onset and positively correlated with dengue severity and cytokine storm (38).

Using a mouse model of dengue infection, Yen and collaborators showed that iNOS- and 47phox-deficient mice were partially protected from hemorrhage development (22). In this model, DENV antigens were detected in hemorrhagic tissues in association with CD31+ endothelial cells, which also

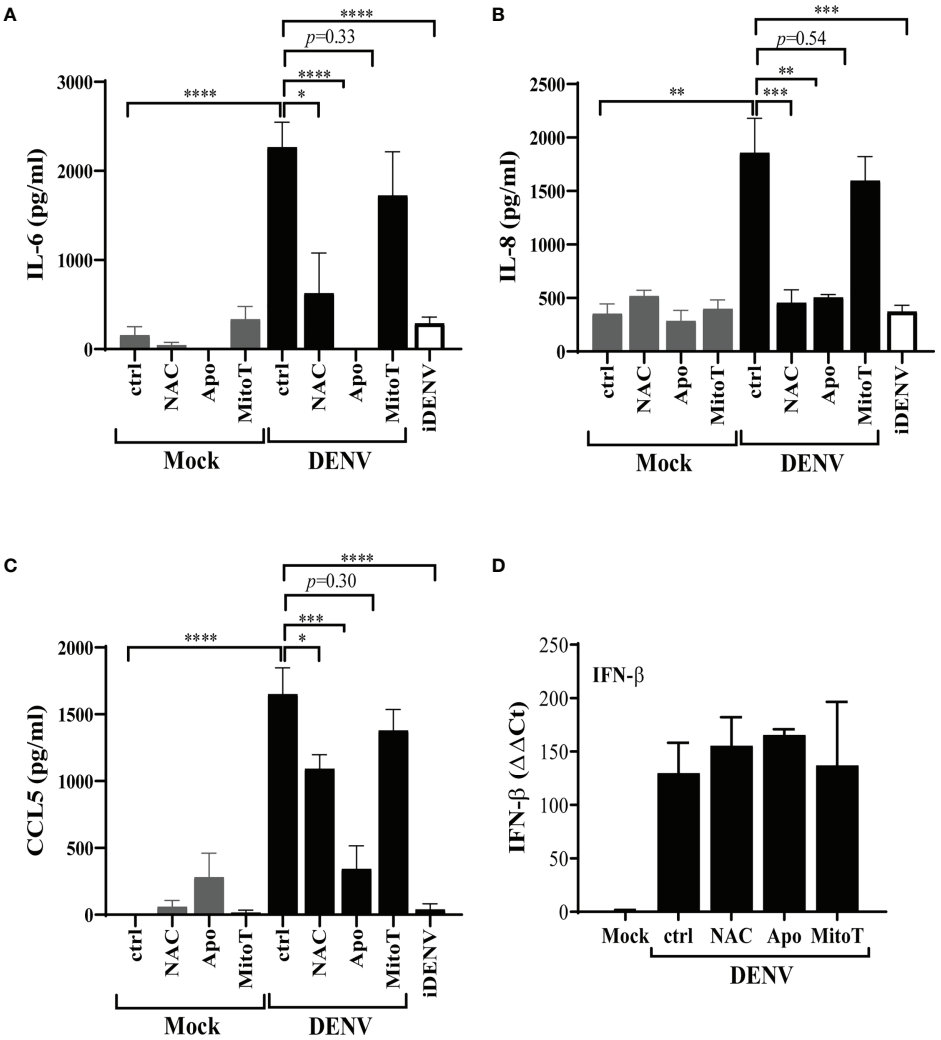

FIGURE 5 | Apocynin-inhibited ROS is essential for the secretion of inflammatory cytokines induced by DENV infection of HBMECs. HBMECs were mock treated or infected with DENV-2 for 48h, in the presence or absence of NAC, apocynin (Apo) or mitoTEMPO (MitoT). **(A–C)** The supernatants were harvested and the concentration of IL-6 **(A)**, IL-8 **(B)**, and CCL5 **(C)** were measured by ELISA. **(D)** The expression of IFN-β mRNA was measured in the cell lysates by quantitative real time PCR. Data represent the mean and SD obtained from three independent experiments. *p ≤ 0.05; **p ≤ 0.01; ***p ≤ 0.001; ****p ≤ 0.0001.

showed an apoptotic phenotype, potentiated by TNFα. In addition, *in vitro* infection of HUVEC with DENV-2 resulted in increased iNOS and NOX activity, which appeared to be related to DENV-induced apoptosis. We have previously demonstrated that HBMECs are productively infected by DENV, resulting in prompt cellular activation and late cell death (9), what might be associated to the increased vascular permeability. In this HBMEC model, we have now showed that DENV replication stimulated ROS generation, which depended on virus replication. It is important to notice, however, that most of the probes available to measure ROS may eventually react with other species such reactive nitrogen species (RNS) (39). Although we cannot discard that DENV also increased nitric oxide production, DCF staining was reduced by apocynin and mitoTEMPO inhibitors, supporting ROS production by DENV-infected HBMEC. Also, ROS inhibition reduced cell death, corroborating the previous reported data regarding HUVEC infection.

Infection of HBMECs, however, also induced mtROS, probably as a consequence of mitochondrial dysfunction. Altered mitochondrial bioenergetics and depolarization of mitochondrial membrane were clearly observed after 48hpi, when increased mtROS was detected with additional increase afterwards. Inhibition of mtROS also reduced cell death, suggesting that DENV-induced mitochondrial stress further contribute to HBMEC death.

Several pathological conditions have been associated to abnormal mtROS generation, due to inefficient production of ATP, altered NADH/NAD+ ratio in the matrix, or inner membrane depolarization, promoting an unbalanced escape of

electrons from complex I and III (24, 40, 41). Increased ROS may then act in a feedback loop, inducing the depolarization of membrane potential, and impairment of oxidative metabolism, potentiating mitochondrial damage (42, 43). Interaction of viral proteins with mitochondrial membranes, leading to depolarization and increased permeability, has been largely described, and leakage of mitochondrial content was associated to apoptosis (44–46). Additionally, recruitment and activation of mitochondrial antiviral-signaling protein (MAVS) triggered by cytoplasmic sensing of virus RNA was also associated to cell death in *in vitro* infection models (47).

We had demonstrated that infection of hepatocytes with DENV as well as of neuroblastoma cells with Sindbis virus induced altered mitochondrial bionenergetics (25, 48). These events probably reflect additional energy demands during virus replication with disruption of the energetic mitochondrial flux. Increased ATP flux might be necessary for efficient virus replication, whereas sustained stress resulted in cell death (48).

Despite possible antiviral effects of oxidative stress responses (49, 50), we observed that ROS inhibition reduced DENV replication in HBMEC. Different mechanisms might explain this phenomenon. Like our model, infection of A549 cells with Respiratory Syncytial Virus (RSV) altered mitochondrial bioenergetics, evidenced by lower basal OCR and decreased maximal respiratory capacity. Enhanced ROS production was also detected and inhibition of ROS dampened virus replication (51, 52). Taken together with other morphological and functional alterations detected in the mitochondria, one can suggest that mitochondrial components might be coopted by viruses favoring their replication. Accordingly, HBMEC treatment with mitoTEMPO decreased the production of DENV infectious particles, indicating that mitochondrial dysfunction is also associated with viral replication in this system. Decreased effect of mitoTEMPO at later time points may indicate that mtROS scavenging is hindering, but not preventing virus replication. Supplementation of the cell culture with ROS inhibitors overtime could foster their effect. Still, more than 50% inhibition in the virus titers were detected at 72hpi, even by adding mitoTEMPO only at the beginning of the culture.

Increased ROS may also trigger autophagy, and subversion of autophagy machinery has been demonstrated to benefit viral replication in different infection models, including dengue (53, 54). Infection of monocytes with different flaviviruses induced autophagy and this event was important to protect the cells from other stress responses and early cell death. Early inhibition of cellular stress contributed to virus replication (55). Accordingly, increased LC3/LC3II conversion and accumulation of p62 was observed in HBMECs infected with at 24hpi, but not at later time points (data not shown), suggesting that autophagy may be an earlier event conferring cell protection. These events will be further investigated. On the other hand, ROS-mediated cell death phenotype started to be detected at 48hpi, being significantly increased at 72hpi, suggesting that apoptotic or necroptic events are later triggered probably as a resulted of sustained ROS production.

We could only detect significant ROS enhancement after 48hpi, what indicates that sequential virus replication cycles might be necessary to amplify the response. In fact, we previously observed that HBMEC infection with a MOI of 1 resulted in about 30% of infected cells at early time points (9). Alternatively, earlier oxidative stress could be impaired by stimulation of antioxidant responses. DENV infection of monocytes derived dendritic cells (mo-DC) induced NOX-mediated late ROS response, which was also associated to cell death in that model (14). It was also showed that Nrf2 antioxidant was increased at earlier time points, but it was later degraded due to action of NS2BNS3 viral proteins, allowing ROS accumulation (16). Nrf2 depletion resulted in increased frequency of DENV infected cells, indicating that ROS was also important for virus replication in those cells.

Besides fueling virus replication, NOX-dependent ROS production in Mo-DC resulted in activation of inflammatory signals, with the production of IFN-β, IL-1β and CCL5 (14, 16). In our model, treatment of DENV-infected HBMEC with apocynin inhibited CCL5, IL-6, and IL-8 secretion, suggesting that NOX-derived ROS may also take part in vascular inflammation induced by the virus. It is important to notice, however, that apocynin may not function as a *bona fide* NOX inhibitor in endothelial cells. Heumuller and colleagues described that porcine aortic endothelial cells (PAEC) might not express myeloperoxidase and failed to form apocynin dimers, which would be essential to its activation and NOX inhibition (35). In these cells, apocynin mostly functioned as a peroxidase scavenger. In another set of studies, using a HUVEC-derived cell free system, it was demonstrated that addition of peroxidase to the system was indeed important to form apocynin dimer and that those dimers induced a prompt and almost complete inhibition of O2- production. Still, apocynin monomers also resulted in decreased O2- production, although after a lagtime (56). It is important to point that previous studies addressing multiple effects of oxidative stress specifically in HBMECs have reported that apocynin reduced the activation of NADPH oxidases or, at least, NOX-dependent cellular dysfunction (57–59), highlighting the complexity and diversity of vascular endothelial models. Importantly, in DENV-infected HBMEC model it was clearly demonstrated that apocynin-inhibited ROS, but not mtROS, was a major contributor to the secretion of inflammatory cytokines and chemokines. Therefore, although we had not fully elucidated the source of non mtROS, it is worth to mention that inhibition of ROS by apocynin might be a potential strategy to control DENV-induced inflammation. It was previously demonstrated that cytoplasmic ROS may induce MAVS oligomerization, potentiating RIG-I-MAVS signaling pathway, independent of virus RNA sensing (60). Interestingly, IFN-β expression was not affected by ROS inhibition, suggesting that ROS may differentially impact NF-κB and IRF signaling pathways, what should be further investigated.

Cell death and NF-kB inflammatory signaling pathways were also detected after infection of neuroblastoma cells with DENV (61). Given that the endothelial cells used in this study are a representative model of *in vitro* blood brain barrier (BBB), we

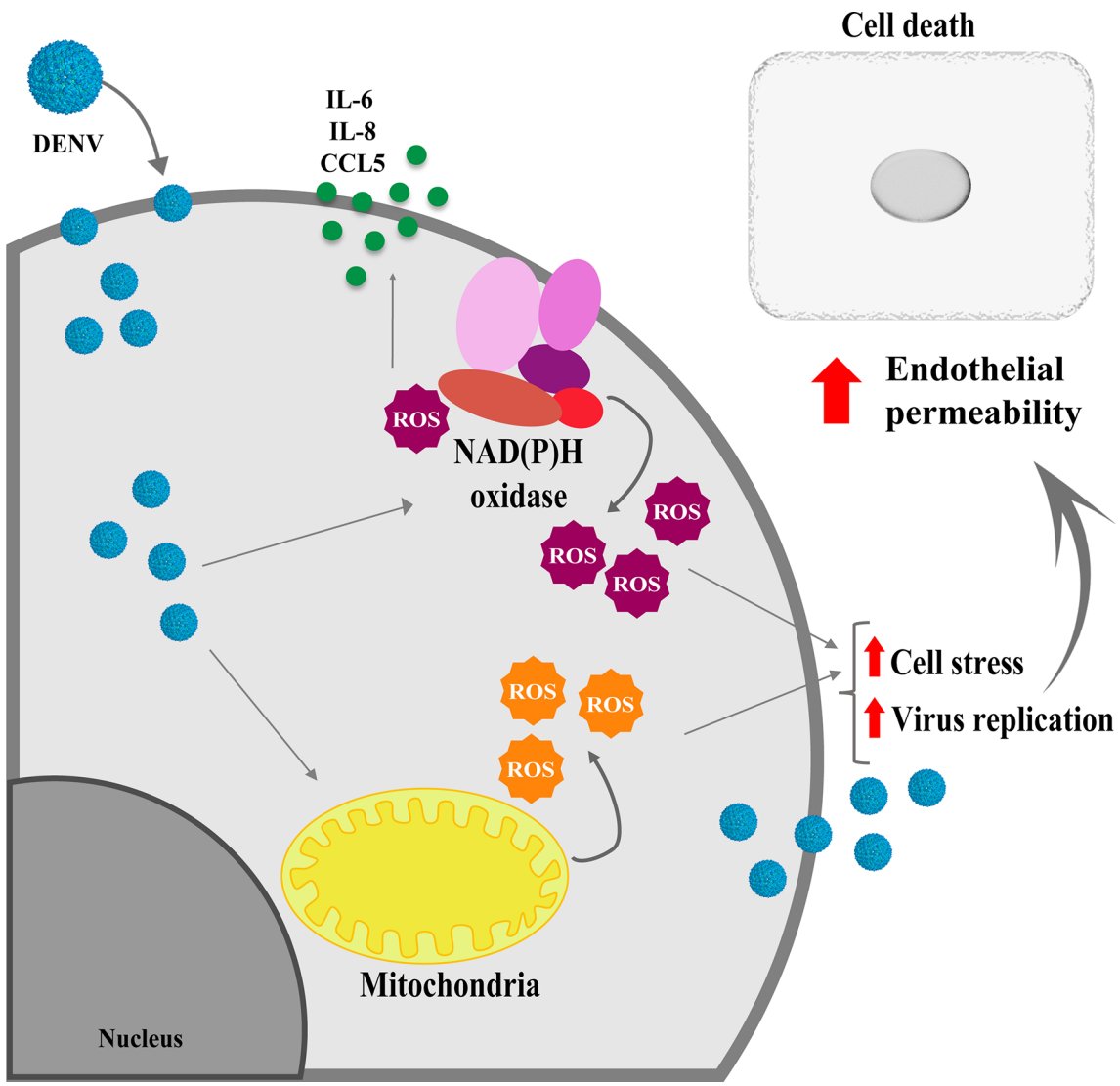

FIGURE 6 | Schematical representation showing the effects of ROS induced by DENV infection in HBMECs. Infection of endothelial cells by DENV-2 impact the mitochondrial physiology, leading to ROS production, which will fuel virus replication and induce cell death, contributing to endothelial permeability. In addition, activation of other intracellular sources, such as NOX enzymes further enhance ROS production, which will be essential to increase secretion of chemokine and inflammatory cytokines.

can speculate that when DENV achieves the BBB and the central nervous system, ROS production might contribute to virus invasion and neuroinflammation. Finally, DENV-induced ROS was important for increased endothelial permeability and mtROS appeared to be the major pathway, although inhibition of NOX activation also increased the TEER.

Taken together our data indicate that altered metabolism triggered by DENV replication results in ROS production from different cell sources, which is important for virus replication, endothelial activation, and increased permeability (**Figure 6**). Further studies addressing the effect of antioxidants *in vivo* may contribute to avoid vascular permeability, inflammation and neuroinvasion upon DENV infection.

DATA AVAILABILITY STATEMENT

The raw data supporting the conclusions of this article will be made available by the authors, without undue reservation.

ETHICS STATEMENT

The studies involving human participants were reviewed and approved by Experimental Ethics Committee of Universidade Federal do Rio de Janeiro. Written informed consent for participation was not required for this study in accordance with the national legislation and the institutional requirements.

AUTHOR CONTRIBUTIONS

Conceptualization, LA. Data curation, LM and EP. Formal analysis, AP, MB, and LA. Funding acquisition, AP, MB, and LA. Investigation, LM, EP, MP, YM, AP, MB, and LA. Methodology, LM, LRPC, LSC, AP, MB, and LA. Project administration, LA. Resources, LRPC, AP, MB, and LA. Supervision, LA. Writing – original draft, LM, EP, and LA. Writing – review & editing, AP, MB, and LA.

FUNDING

This work was supported by Coordination for the Improvement of Higher Education Personnel (CAPES); Brazilian National Council for Scientific and Technological Development (CNPq; #405323/2016-6; #310867/2018-5); Carlos Chagas Filho Research Support Foundation (FAPERJ; #E-26/201.324/2016; #E-26/210.371/2019, #E-26/201.206/2021; #E-26/010/002999/2014; #E-26/202.877/2018; #E-26/010.02425/2019); Funding Authority for Studies and Projects (FINEP). LM, AP, MB, and LA were recipients of a CNPq fellowship.

ACKNOWLEDGMENTS

The authors wish to thank Dr. Dennis J. Grab (The Johns Hopkins University School of Medicine, MD, US) for kindly providing us with HBMEC. The authors also wish to thank Ronaldo Rocha (UFRJ) for technical support.

SUPPLEMENTARY MATERIAL

The Supplementary Material for this article can be found online at: https://www.frontiersin.org/articles/10.3389/fimmu.2022.810376/full#supplementary-material

REFERENCES

1. Pierson TC, Diamond MS. The Continued Threat of Emerging Flaviviruses. *Nat Microbiol* (2020) 5(6):796–812. doi: 10.1038/s41564-020-0714-0
2. Martina BE, Koraka P, Osterhaus AD. Dengue Virus Pathogenesis: An Integrated View. *Clin Microbiol Rev* (2009) 22(4):564–81. doi: 10.1128/CMR.00035-09
3. Malavige GN, Ogg GS. Pathogenesis of Vascular Leak in Dengue Virus Infection. *Immunology* (2017) 151(3):261–9. doi: 10.1111/imm.12748
4. Yacoub S, Lam PK, Huynh TT, Nguyen Ho HH, Dong Thi HT, Van NT, et al. Endothelial Nitric Oxide Pathways in the Pathophysiology of Dengue: A Prospective Observational Study. *Clin Infect Dis* (2017) 65(9):1453–61. doi: 10.1093/cid/cix567
5. Basu A, Chaturvedi UC. Vascular Endothelium: The Battlefield of Dengue Viruses. *FEMS Immunol Med Microbiol* (2008) 53(3):287–99. doi: 10.1111/j.1574-695X.2008.00420.x
6. Wu-Hsieh BA, Yen YT, Chen HC. Dengue Hemorrhage in a Mouse Model. *Ann N Y Acad Sci* (2009) 1171 Suppl 1:E42–7. doi: 10.1111/j.1749-6632.2009.05053.x
7. Póvoa TF, Alves AM, Oliveira CA, Nuovo GJ, Chagas VL, Paes MV. The Pathology of Severe Dengue in Multiple Organs of Human Fatal Cases: Histopathology, Ultrastructure and Virus Replication. *PLoS One* (2014) 9(4):e83386. doi: 10.1371/journal.pone.0083386
8. Zellweger RM, Prestwood TR, Shresta S. Enhanced Infection of Liver Sinusoidal Endothelial Cells in a Mouse Model of Antibody-Induced Severe Dengue Disease. *Cell Host Microbe* (2010) 7(2):128–39. doi: 10.1016/j.chom.2010.01.004
9. Conceição TM, Rust NM, Berbel AC, Martins NB, do Nascimento Santos CA, Da Poian AT, et al. Essential Role of RIG-I in the Activation of Endothelial Cells by Dengue Virus. *Virology* (2013) 435(2):281–92. doi: 10.1016/j.virol.2012.09.038
10. Vervaeke P, Alen M, Noppen S, Schols D, Oreste P, Liekens S. Sulfated Escherichia Coli K5 Polysaccharide Derivatives Inhibit Dengue Virus Infection of Human Microvascular Endothelial Cells by Interacting With the Viral Envelope Protein E Domain III. *PLoS One* (2013) 8(8):e74035. doi: 10.1371/journal.pone.0074035
11. Kong W, Mao J, Yang Y, Yuan J, Chen J, Luo Y, et al. Mechanisms of mTOR and Autophagy in Human Endothelial Cell Infected With Dengue Virus-2. *Viral Immunol* (2020) 33(1):61–70. doi: 10.1089/vim.2019.0009
12. Coelho SVA, Rust NM, Vellasco L, Papa MP, Pereira ASG, Silva Palazzo MFD, et al. Contact System Activation in Plasma From Dengue Patients Might Harness Endothelial Virus Replication Through the Signaling of Bradykinin Receptors. *Pharmaceut (Basel)* (2021) 14(1):56. doi: 10.3390/ph14010056
13. Valadão AL, Aguiar RS, de Arruda LB. Interplay Between Inflammation and Cellular Stress Triggered by Flaviviridae Viruses. *Front Microbiol* (2016) 7:1233. doi: 10.3389/fmicb.2016.01233
14. Olagnier D, Peri S, Steel C, van Montfoort N, Chiang C, Beljanski V, et al. Cellular Oxidative Stress Response Controls the Antiviral and Apoptotic Programs in Dengue Virus-Infected Dendritic Cells. *PLoS Pathog* (2014) 10(12):e1004566. doi: 10.1371/journal.ppat.1004566
15. Reshi ML, Su YC, Hong JR. RNA Viruses: ROS-Mediated Cell Death. *Int J Cell Biol* (2014) 2014:467452. doi: 10.1155/2014/467452
16. Ferrari M, Zevini A, Palermo E, Muscolini M, Alexandridi M, Etna MP, et al. Dengue Virus Targets Nrf2 for NS2B3-Mediated Degradation Leading to Enhanced Oxidative Stress and Viral Replication. *J Virol* (2020) 94(24):e01551–20. doi: 10.1128/JVI.01551-20
17. Wang ZY, Zhen ZD, Fan DY, Wang PG, An J. Transcriptomic Analysis Suggests the M1 Polarization and Launch of Diverse Programmed Cell Death Pathways in Japanese Encephalitis Virus-Infected Macrophages. *Viruses* (2020) 12(3):356. doi: 10.3390/v12030356
18. Bedient L, Pokharel SM, Chiok KR, Mohanty I, Beach SS, Miura TA, et al. Lytic Cell Death Mechanisms in Human Respiratory Syncytial Virus-Infected Macrophages: Roles of Pyroptosis and Necroptosis. *Viruses* (2020) 12(9):932. doi: 10.3390/v12090932
19. Madamanchi NR, Vendrov A, Runge MS. Oxidative Stress and Vascular Disease. *Arterioscler Thromb Vasc Biol* (2005) 25(1):29–38. doi: 10.1161/01.ATV.0000150649.39934.13
20. Mittal M, Siddiqui MR, Tran K, Reddy SP, Malik AB. Reactive Oxygen Species in Inflammation and Tissue Injury. *Antioxid Redox Signal* (2014) 20(7):1126–67. doi: 10.1089/ars.2012.5149
21. He P, Talukder MAH, Gao F. Oxidative Stress and Microvessel Barrier Dysfunction. *Front Physiol* (2020) 11:472. doi: 10.3389/fphys.2020.00472
22. Yen YT, Chen HC, Lin YD, Shieh CC, Wu-Hsieh BA. Enhancement by Tumor Necrosis Factor Alpha of Dengue Virus-Induced Endothelial Cell Production of Reactive Nitrogen and Oxygen Species is Key to Hemorrhage Development. *J Virol* (2008) 82(24):12312–24. doi: 10.1128/JVI.00968-08
23. Topf U, Uszczynska-Ratajczak B, Chacinska A. Mitochondrial Stress-Dependent Regulation of Cellular Protein Synthesis. *J Cell Sci* (2019) 132(8):jcs226258. doi: 10.1242/jcs.226258
24. Magnani ND, Marchini T, Calabró V, Alvarez S, Evelson P. Role of Mitochondria in the Redox Signaling Network and Its Outcomes in High Impact Inflammatory Syndromes. *Front Endocrinol (Lausanne)* (2020) 11:568305. doi: 10.3389/fendo.2020.568305
25. El-Bacha T, Midlej V, Pereira da Silva AP, Silva da Costa L, Benchimol M, Galina A, et al. Mitochondrial and Bioenergetic Dysfunction in Human Hepatic Cells Infected With Dengue 2 Virus. *Biochim Biophys Acta* (2007) 1772(10):1158–66. doi: 10.1016/j.bbadis.2007.08.003

26. Chatel-Chaix L, Cortese M, Romero-Brey I, Bender S, Neufeldt CJ, Fischl W, et al. Dengue Virus Perturbs Mitochondrial Morphodynamics to Dampen Innate Immune Responses. *Cell Host Microbe* (2016) 20(3):342–56. doi: 10.1016/j.chom.2016.07.008
27. Pillai AB, Muthuraman KR, Mariappan V, Belur SS, Lokesh S, Rajendiran S. Oxidative Stress Response in the Pathogenesis of Dengue Virus Virulence, Disease Prognosis and Therapeutics: An Update. *Arch Virol* (2019) 164 (12):2895–908. doi: 10.1007/s00705-019-04406-7
28. Nikolskaia OV, de Alima AP, Kim YV, Lonsdale-Eccle JD, Fukuma T, Scharfstein J, et al. Blood-Brain Barrier Traversal by African Trypanosomes Requires Calcium Signaling Induced by Parasite Cysteine Protease. *J Clin Invest* (2006) 116(10):2739–47. doi: 10.1172/JCI27798
29. Conceição TM, Da Poian AT, Sorgine MH. A Real-Time PCR Procedure for Detection of Dengue Virus Serotypes 1, 2, and 3, and Their Quantitation in Clinical and Laboratory Samples. *J Virol Methods* (2010) 163(1):1–9. doi: 10.1016/j.jviromet.2009.10.001
30. Papa MP, Meuren LM, Coelho SVA, Lucas CGO, Mustafá YM, Lemos Matassoli F, et al. Zika Virus Infects, Activates, and Crosses Brain Microvascular Endothelial Cells, Without Barrier Disruption. *Front Microbiol* (2017) 8:2557. doi: 10.3389/fmicb.2017.02557
31. Srinivasan B, Kolli AR, Esch MB, Abaci HE, Shuler ML, Hickman JJ. TEER Measurement Techniques for In Vitro Barrier Model Systems. *J Lab Autom* (2015) 20(2):107–26. doi: 10.1177/2211068214561025
32. Mahad D, Callahan MK, Williams KA, Ubogu EE, Kivisäkk P, Tucky B, et al. Modulating CCR2 and CCL2 at the Blood-Brain Barrier: Relevance for Multiple Sclerosis Pathogenesis. *Brain* (2006) 129(Pt 1):212–23. doi: 10.1093/brain/awh655
33. Livak KJ, Schmittgen TD. Analysis of Relative Gene Expression Data Using Real-Time Quantitative PCR and the 2(-Delta Delta C(T)) Method. *Methods* (2001) 25(4):402–8. doi: 10.1006/meth.2001.1262
34. Fortes GB, Alves LS, de Oliveira R, Dutra FF, Rodrigues D, Fernandez PL, et al. Heme Induces Programmed Necrosis on Macrophages Through Autocrine TNF and ROS Production. *Blood* (2012) 119(10):2368–75. doi: 10.1182/blood-2011-08-375303
35. Heumüller S, Wind S, Barbosa-Sicard E, Schmidt HH, Busse R, Schröder K, et al. Apocynin is Not an Inhibitor of Vascular NADPH Oxidases But an Antioxidant. *Hypertension* (2008) 51(2):211–7. doi: 10.1161/HYPERTENSIONAHA.107.100214
36. Paessler S, Walker DH. Pathogenesis of the Viral Hemorrhagic Fevers. *Annu Rev Pathol* (2013) 8:411–40. doi: 10.1146/annurev-pathol-020712-164041
37. Soundravally R, Sankar P, Hoti SL, Selvaraj N, Bobby Z, Sridhar MG. Oxidative Stress Induced Changes in Plasma Protein can be a Predictor of Imminent Severe Dengue Infection. *Acta Trop* (2008) 106(3):156–61. doi: 10.1016/j.actatropica.2008.03.001
38. Soundravally R, Hoti SL, Patil SA, Cleetus CC, Zachariah B, Kadhiravan T, et al. Association Between Proinflammatory Cytokines and Lipid Peroxidation in Patients With Severe Dengue Disease Around Defervescence. *Int J Infect Dis* (2014) 18:68–72. doi: 10.1016/j.ijid.2013.09.022
39. Kalyanaraman B, Darley-Usmar V, Davies KJ, Dennery PA, Forman HJ, Grisham MB, et al. Measuring Reactive Oxygen and Nitrogen Species With Fluorescent Probes: Challenges and Limitations. *Free Radic Biol Med* (2012) 52(1):1–6. doi: 10.1016/j.freeradbiomed.2011.09.030
40. Krylatov AV, Maslov LN, Voronkov NS, Boshchenko AA, Popov SV, Gomez L, et al. Reactive Oxygen Species as Intracellular Signaling Molecules in the Cardiovascular System. *Curr Cardiol Rev* (2018) 14(4):290–300. doi: 10.2174/1573403X14666180702152436
41. Turrens JF. Mitochondrial Formation of Reactive Oxygen Species. *J Physiol* (2003) 552:335–44. doi: 10.1111/j.1469-7793.2003.00335.x
42. Zorov DB, Juhaszova M, Sollott SJ. Mitochondrial Reactive Oxygen Species (ROS) and ROS-Induced ROS Release. *Physiol Rev* (2014) 94(3):909–50. doi: 10.1152/physrev.00026.2013
43. Fukai T, Ushio-Fukai M. Cross-Talk Between NADPH Oxidase and Mitochondria: Role in ROS Signaling and Angiogenesis. *Cells* (2020) 9 (8):1849. doi: 10.3390/cells9081849
44. Everett H, McFadden G. Viruses and Apoptosis: Meddling With Mitochondria. *Virology* (2001) 288(1):1–7. doi: 10.1006/viro.2001.1081
45. Okuda M, Li K, Beard MR, Showalter LA, Scholle F, Lemon SM, et al. Mitochondrial Injury, Oxidative Stress, and Antioxidant Gene Expression Are Induced by Hepatitis C Virus Core Protein. *Gastroenterology* (2002) 122:366–75. doi: 10.1053/gast.2002.30983
46. Piccoli C, Scrima R, D'Aprile A, Ripoli M, Lecce L, Boffoli D, et al. Mitochondrial Dysfunction in Hepatitis C Virus Infection. *Biochim Biophys Acta* (2006) 1757(9-10):1429–37. doi: 10.1016/j.bbabio.2006.05.018
47. Yu CY, Chiang RL, Chang TH, Liao CL, Lin YL. The Interferon Stimulator Mitochondrial Antiviral Signaling Protein Facilitates Cell Death by Disrupting the Mitochondrial Membrane Potential and by Activating Caspases. *J Virol* (2010) 84(5):2421–31. doi: 10.1128/JVI.02174-09
48. Silva da Costa L, Pereira da Silva AP, Da Poian AT, El-Bacha T. Mitochondrial Bioenergetic Alterations in Mouse Neuroblastoma Cells Infected With Sindbis Virus: Implications to Viral Replication and Neuronal Death. *PLoS One* (2012) 7(4):e33871. doi: 10.1371/journal.pone.0033871
49. Marino-Merlo F, Papaianni E, Frezza C, Pedatella S, De Nisco M, Macchi B, et al. NF-κb-Dependent Production of ROS and Restriction of HSV-1 Infection in U937 Monocytic Cells. *Viruses* (2019) 11(5):428. doi: 10.3390/v11050428
50. Khan NA, Kar M, Panwar A, Wangchuk J, Kumar S, Das A, et al. Oxidative Stress Specifically Inhibits Replication of Dengue Virus. *J Gen Virol* (2021) 102 (4):10.1099/jgv.0.001596. doi: 10.1099/jgv.0.001596
51. Hu M, Schulze KE, Ghildyal R, Henstridge DC, Kolanowski JL, New EJ, et al. Respiratory Syncytial Virus Co-Opts Host Mitochondrial Function to Favour Infectious Virus Production. *Elife* (2019) 8:e42448. doi: 10.7554/eLife.42448
52. Hu M, Bogoyevitch MA, Jans DA. Subversion of Host Cell Mitochondria by RSV to Favor Virus Production is Dependent on Inhibition of Mitochondrial Complex I and ROS Generation. *Cells* (2019) 8(11):1417. doi: 10.3390/cells8111417
53. Datan E, Roy SG, Germain G, Zali N, McLean JE, Golshan G, et al. Dengue-Induced Autophagy, Virus Replication and Protection From Cell Death Require ER Stress (PERK) Pathway Activation. *Cell Death Dis* (2016) 7(3): e2127. doi: 10.1038/cddis.2015.409
54. Echavarria-Consuegra L, Smit JM, Reggiori F. Role of Autophagy During the Replication and Pathogenesis of Common Mosquito-Borne Flavi- and Alphaviruses. *Open Biol* (2019) 9(3):190009. doi: 10.1098/rsob.190009
55. McLean JE, Wudzinska A, Datan E, Quaglino D, Zakeri Z. Flavivirus NS4A-Induced Autophagy Protects Cells Against Death and Enhances Virus Replication. *J Biol Chem* (2011) 286(25):22147–59. doi: 10.1074/jbc.M110.192500
56. Johnson DK, Schillinger KJ, Kwait DM, Hughes CV, McNamara EJ, Ishmael F, et al. Inhibition of NADPH Oxidase Activation in Endothelial Cells by Ortho-Methoxy-Substituted Catechols. *Endothelium* (2002) 9(3):191–203. doi: 10.1080/10623320213638
57. Liu C, Wu J, Zou MH. Activation of AMP-Activated Protein Kinase Alleviates High-Glucose-Induced Dysfunction of Brain Microvascular Endothelial Cell Tight-Junction Dynamics. *Free Radic Biol Med* (2012) 53(6):1213–21. doi: 10.1016/j.freeradbiomed.2012.07.003
58. Abdullah Z, Bayraktutan U. NADPH Oxidase Mediates TNF-α-Evoked *In Vitro* Brain Barrier Dysfunction: Roles of Apoptosis and Time. *Mol Cell Neurosci* (2014) 61:72–84. doi: 10.1016/j.mcn.2014.06.002
59. Zhao Z, Hu J, Gao X, Liang H, Liu Z. Activation of AMPK Attenuates Lipopolysaccharide-Impaired Integrity and Function of Blood-Brain Barrier in Human Brain Microvascular Endothelial Cells. *Exp Mol Pathol* (2014) 97 (3):386–92. doi: 10.1016/j.yexmp.2014.09.006
60. Buskiewicz IA, Montgomery T, Yasewicz EC, Huber SA, Murphy MP, Hartley RC, et al. Reactive Oxygen Species Induce Virus-Independent MAVS Oligomerization in Systemic Lupus Erythematosus. *Sci Signal* (2016) 9(456): ra115. doi: 10.1126/scisignal.aaf1933
61. Jan JT, Chen BH, Ma SH, Liu CI, Tsai HP, Wu HC, et al. Potential Dengue Virus-Triggered Apoptotic Pathway in Human Neuroblastoma Cells: Arachidonic Acid, Superoxide Anion, and NF-kappaB Are Sequentially Involved. *J Virol* (2000) 74(18):8680–91. doi: 10.1128/jvi.74.18.8680-8691.2000

Conflict of Interest: The authors declare that the research was conducted in the absence of any commercial or financial relationships that could be construed as a potential conflict of interest.

this article, or claim that may be made by its manufacturer, is not guaranteed or endorsed by the publisher.

frontiers in Microbiology

ORIGINAL RESEARCH
published: 22 December 2017
doi: 10.3389/fmicb.2017.02557

Zika Virus Infects, Activates, and Crosses Brain Microvascular Endothelial Cells, without Barrier Disruption

*Michelle P. Papa[1†], Lana M. Meuren[1†], Sharton V. A. Coelho[1], Carolina G. de Oliveira Lucas[1,2], Yasmin M. Mustafá[1], Flavio Lemos Matassoli[1], Paola P. Silveira[3], Paula S. Frost[4], Paula Pezzuto[3], Milene R. Ribeiro[5], Amilcar Tanuri[3], Mauricio L. Nogueira[5], Loraine Campanati[6], Marcelo T. Bozza[2], Heitor A. Paula Neto[7], Pedro M. Pimentel-Coelho[8], Claudia P. Figueiredo[4], Renato S. de Aguiar[3] and Luciana B. de Arruda[1]**

[1] Departamento de Virologia, Instituto de Microbiologia Paulo de Góes, Universidade Federal do Rio de Janeiro, Rio de Janeiro, Brazil, [2] Departamento de Imunologia, Instituto de Microbiologia Paulo de Góes, Universidade Federal do Rio de Janeiro, Rio de Janeiro, Brazil, [3] Departamento de Genética, Instituto de Biologia, Universidade Federal do Rio de Janeiro, Rio de Janeiro, Brazil, [4] Núcleo de Neurociências da Faculdade de Farmácia, Universidade Federal do Rio de Janeiro, Rio de Janeiro, Brazil, [5] Laboratório de Pesquisas em Virologia, Faculdade de Medicina de São José do Rio Preto, São José do Rio Preto, Brazil, [6] Instituto de Ciências Biomédicas, Universidade Federal do Rio de Janeiro, Rio de Janeiro, Brazil, [7] Laboratório de Alvos Moleculares, Departamento de Biotecnologia Farmacêutica, Faculdade de Farmácia, Universidade Federal do Rio de Janeiro, Rio de Janeiro, Brazil, [8] Instituto de Biofísica Carlos Chagas Filho, Universidade Federal do Rio de Janeiro, Rio de Janeiro, Brazil

Zika virus (ZIKV) has been associated to central nervous system (CNS) harm, and virus was detected in the brain and cerebrospinal fluids of microcephaly and meningoencephalitis cases. However, the mechanism by which the virus reaches the CNS is unclear. Here, we addressed the effects of ZIKV replication in human brain microvascular endothelial cells (HBMECs), as an *in vitro* model of blood brain barrier (BBB), and evaluated virus extravasation and BBB integrity in an *in vivo* mouse experimental model. HBMECs were productively infected by African and Brazilian ZIKV strains ($ZIKV_{MR766}$ and $ZIKV_{PE243}$), which induce increased production of type I and type III IFN, inflammatory cytokines and chemokines. Infection with $ZIKV_{MR766}$ promoted earlier cellular death, in comparison to $ZIKV_{PE243}$, but infection with either strain did not result in enhanced endothelial permeability. Despite the maintenance of endothelial integrity, infectious virus particles crossed the monolayer by endocytosis/exocytosis-dependent replication pathway or by transcytosis. Remarkably, both viruses' strains infected IFNAR deficient mice, with high viral load being detected in the brains, without BBB disruption, which was only detected at later time points after infection. These data suggest that ZIKV infects and activates endothelial cells, and might reach the CNS through basolateral release, transcytosis or transinfection processes. These findings further improve the current knowledge regarding ZIKV dissemination pathways.

Keywords: Zika virus, endothelial cells, blood brain barrier, transcytosis, mouse experimental model

OPEN ACCESS

Edited by:
Francois Villinger, University of Louisiana at Lafayette, United States

Reviewed by:
Eduardo L. V. Silveira, University of São Paulo, Brazil
Karen M. Smith, University of Louisiana at Lafayette, United States

****Correspondence:***
Luciana B. de Arruda
arruda@micro.ufrj.br

[†] These authors have contributed equally to this work.

Specialty section:
This article was submitted to Virology, a section of the journal Frontiers in Microbiology

Received: *16 July 2017*
Accepted: *08 December 2017*
Published: *22 December 2017*

Citation:
Papa MP, Meuren LM, Coelho SVA, Lucas CGdO, Mustafá YM, Lemos Matassoli F, Silveira PP, Frost PS, Pezzuto P, Ribeiro MR, Tanuri A, Nogueira ML, Campanati L, Bozza MT, Paula Neto HA, Pimentel-Coelho PM, Figueiredo CP, Aguiar RS and Arruda LB (2017) Zika Virus Infects, Activates, and Crosses Brain Microvascular Endothelial Cells, without Barrier Disruption. Front. Microbiol. 8:2557. doi: 10.3389/fmicb.2017.02557

INTRODUCTION

Zika virus (ZIKV) is an arthropod-borne virus (arbovirus), from *Flaviviridae* family, genus Flavivirus, which is now associated with a large spectrum of clinical manifestations and different forms of transmission, being a unique Arbovirus (WHO, 2016). ZIKV was first isolated in 1947, in Uganda, during a surveillance study in mosquitoes and primates (Dick et al., 1952). Until 2007, few sporadic human cases had been reported in African and Southeast Asiatic countries, and were associated to mild clinical manifestations. After human-associated ZIKV outbreaks in Micronesia and Pacific Islands in 2007 and 2013, the virus spread to the Americas, and has now been reported in more than 60 countries around the world (Lanciotti et al., 2008; Cao-Lormeau et al., 2014; Faria et al., 2016; WHO, 2016).

ZIKV circulation positively correlated with enormous increase in the number of cases of microcephaly, suggesting a causal association between ZIKV infection during pregnancy and neonatal microcephaly (Calvet et al., 2016; Oliveira Melo et al., 2016; Rasmussen et al., 2016; Schuler-Faccini et al., 2016). This was further supported by virus detection in the brains and in amniotic fluid of fetuses with microcephaly by qRT-PCR, immunohistochemistry and electron microscopy (Calvet et al., 2016; Martines et al., 2016; Mlakar et al., 2016). Later on, ZIKV congenital transmission was associated to further fetal malformations, including several neurological manifestations, which are now described as congenital Zika syndrome (CZS) (Miranda-Filho et al., 2016; Lucey et al., 2017). Meningoencephalitis was also reported in ZIKV-infected adult patients and during experimental infection of rhesus monkeys, and the viral RNA was detected in their cerebrospinal fluid (Carteaux et al., 2016; Dudley et al., 2016). These lines of evidence suggest that virus replication may be, eventually, associated to invasion of central nervous system (CNS).

In spite of multiple sources of evidence indicating that ZIKV penetrates CNS, the mechanism associated to this infiltration is unknown. Neurotropic viruses may access the brain by either neural or hematogenic pathways; in the latter case, viruses or virus-infected cells must cross the blood brain barrier (BBB) (Salinas et al., 2010; Luethy et al., 2016). BBB is a dynamic structure of specialized cells that limits the passage of circulating molecules and cells to the brain, and restricts the entry of pathogens, including viruses or virus-infected cells to the CNS. Brain microvascular endothelial cells are the most prominent cell type, responsible for this control, acting in concert with astrocytes, microglia, pericytes, and neurons (Ballabh et al., 2004; Miner and Diamond, 2016). Disruption of the BBB, commonly due to increased endothelial cell permeability, is a hallmark of CNS infections and can be induced by virus replication or neuroinflammation (Daniels and Klein, 2015). Alternatively, it was suggested that increased BBB permeability might not be essential for lethal disease induced by another flavivirus infection model (Morrey et al., 2008). Infection and activation of endothelial cells in the retina and placenta of ZIKA experimental models have been previously observed (Noronha et al., 2016; Singh et al., 2017; Vermillion et al., 2017); however, the role of the virus replication in endothelial cell for virus dissemination or extravasation to other tissues has not been addressed.

Two different ZIKV lineages have been epidemiologically characterized, named African and Asian, the latter being associated to the epidemic outbreak in Brazil (Calvet et al., 2016; Weaver et al., 2016; Zhu et al., 2016). It was recently demonstrated that ZIKV infects human brain microvascular endothelial cells, which is a model of BBB tissue (Bayer et al., 2016; Mladinich et al., 2017). HBMECs infection by ZIKV was associated to a persistent infection with no evidences of increased permeability *in vitro* (Mladinich et al., 2017). Nevertheless, the effect of different ZIKV strains, obtained from mosquitoes and mammal cells, in HBMECs survival, activation and permeability worth to be further addressed and compared. Importantly, it is still not established whether a systemic infection with ZIKV *in vivo* may promote virus extravasation and infection of CNS. Here, we described that different strains of ZIKV productively infect HBMECs and induce cell activation, with increased production of type I and type III IFN, IL-6, and CCL5, confirming previous data obtained with a different strain (Mladinich et al., 2017). HBMEC infection with either virus did not result in significant disruption of the monolayer permeability. Still, infectious virus crossed the endothelial monolayer through replication and transcytosis dependent pathways. Remarkably, infection of A129 mice with either virus strain did not result in BBB permeability at early time points after infection, although high viral load had been detected in the brain. Subtle BBB alteration was detected at later time points post infection, which might be a result of a virus-induced inflammatory response. These data suggest that ZIKV virus cross BBB through transcytosis or transinfection after endothelial cell infection and activation.

MATERIALS AND METHODS

Ethical Statements

Blood samples (buffy coats) from healthy donors were obtained anonymously from the Hemotherapy Service from the Hospital Universitário Clementino Fraga Filho (HUCFF) of Universidade Federal do Rio de Janeiro (UFRJ). The study protocol was approved by the Experimental Ethics Committee of UFRJ (Permit Number: 105/07) and the review board waived the need for informed patient consent.

A129 (deficient of IFNARI) mice were obtained from the mice facility of the Instituto de Microbiologia, Universidade Federal do Rio de Janeiro (IMPPG, UFRJ), Brazil. The animals were bred and housed according to institutional policies for animal care and usage and the protocol was approved by The Ethics Committee of Animal Care and Use (Comite de Etica no Uso de Animais-CEUA) from Centro de Ciencias da Saude, UFRJ (Permit Number: no104/16).

Virus and Cells

Vero cells were cultured in DMEM supplemented with L-glutamine and 5% fetal bovine serum (Life Technologies, Grand Island, NY) and maintained at 37°C with 5% CO_2. C6/36

mosquito cell line were cultured at 28°C in Leibovitz (L-15) medium (Life Technologies) supplemented with 10% of tryptose phosphate broth, 0.75% sodium bicarbonate, 0.2% of L-glutamine (Sigma-Aldrich, St Louis, MO), and 10% FBS (Life Technologies). Human brain microvascular endothelial cells (HBMEC) have been previously described (Nikolskaia et al., 2006) and were kindly given by Dr. Julio Scharfstein (Instituto de Biofísica Carlos Chagas Filho, UFRJ). The cells were cultured in M199, supplemented with L-glutamine, non-essential aminoacids, and 10% FBS (Life Technologies). Peripheral blood mononuclear cells (PBMC) were obtained after centrifugation of buffy coats samples over ficoll-hypaque gradients and cultured with RPMI supplemented with L-glutamine, and 10% FBS.

ZIKV strain MR766 ($ZIKV_{MR766;}$ ATCC VR1838) was propagated in Vero or C6/36 cells, as indicated in each experiment. $ZIKV_{PE243}$ (gene bank ref. number KX197192) was isolated from a febrile case in the state of Pernambuco, Brazil, and was kindly given by Dr. Ernesto T.A. Marques Jr. (Centro de Pesquisas Aggeu Magalhães, FIOCRUZ, PE, Brazil; and Center for Vaccine Research, University of Pittsburgh, PA). Viruses were propagated in C6/36 cells and sequence analysis was performed after six passages. In some experiments, viruses were also propagated in Vero cells, as indicated in each experiment. $ZIKV_{BR-SP}$ (gene bank ref. number KU497555; kindly given by Pedro Vasconcelos, Instituto Evandro Chagas, FIOCRUZ, PA, Brazil) was isolated from a mild ZIKV case, in the state of Paraíba, Brazil, and it was distributed as part of ZIKA FAPESP NETWORK after four passages in C6/36 cells (Faria et al., 2016). Viral titers were determined by plaque assay in Vero cells, as previously described (Coelho et al., 2017) and are indicated as PFU/ml. Supernatants of non-infected C6/36 or Vero cells cultured in the same conditions were used as mock controls. Inactivated virus (iZIKV) was obtained after U.V. exposition for 2 h and the inactivation was confirmed by qRT-PCR in Vero cells.

HBMECs and PBMCs Infection

HBMECs were infected with $ZIKV_{MR766}$ or $ZIKV_{PE243}$ with a MOI of 1 for 2 h, at 37°C in 5% CO_2 atmosphere, for virus adsorption. As a control, the cells were incubated with supernatant of non-infected Vero or C6/36 cells (mock-infected). Cells were, then, washed with PBS and cultured with complete medium. After different time points, cells and supernatants were harvested and virus infection, cell survival, and cytokine secretion were evaluated as described below.

PBMCs were infected at the same conditions and, after 48 h, supernatants were harvested, and stored at −80°C. Supernatants from PBMC treated with mock, or infected with $ZIKV_{PE243}$ or $ZIKV_{MR766}$ were inactivated by U.V. radiation for 2 h and used as conditioned medium (iCM-PBMC). Virus inactivation was confirmed by qRT-PCR and plaque assay after 48 h infection of Vero cells.

Analysis of HBMECs Infection by Immunofluorescence, qRT-PCR, and Plaque Assay

HBMECs were mock-treated or infected with $ZIKV_{PE243}$ or $ZIKV_{MR766}$ at different MOIs. After 48 hpi, cells were blocked, permeabilized, and stained with anti-flavivirus 4G2 antibody (ATCC HB112), followed by AlexaFluor488-conjugated anti-mouse IgG (Life Technologies). HBMEC infection was then analyzed by immunofluorescence, using OLYMPUS IX81 microscopy.

Viral replication was also analyzed by qRT-PCR. Cells were treated as described and, after different time points, cells, and supernatants were harvested and RNA was isolated using TRIZOL reagent (Life Technologies), according to the manufacturer's instructions. Treatment with DNAse I (Ambion, Thermo Fischer) was performed to prevent genomic DNA contamination and first strand cDNA was synthesized using High-Capacity cDNA Archive Kit (Applied Biosystems), according to the manufacturer's instructions. cDNAs were subjected to quantitative real-time PCR for detection of viral RNA using a StepOnePlus Real-time PCR system and Taqman Master Mix Reagents (Applied Biosystems), using primers and probe specific for protein E sequence, as previously described (Lanciotti et al., 2008). cDNA obtained from virus samples ranging from 75,000 to 0.75 PFU/ml were used to construct a standard curve for estimating the genome copy number of ZIKV (RNA equivalent).

To evaluate secretion of infectious viral particles by HBMECs, cells were infected as described and, after different time points, the supernatants were harvested and titrated by plaque assay, using Vero cell line.

Cell Viability Assays

HBMECs were infected with ZIK_{PE243} or $ZIKV_{MR766}$ propagated in C6/36 cells and determination of cell viability after different time points was carried out using XTT 2,3-Bis-(2-Methoxy-4-Nitro-5-Sulfophenyl)-2H-Tetrazolium-5-Carboxanilide (XTT) (Sigma-Aldrich, St. Louis, MO). Cells were incubated with XTT solution for 2–4 h and metabolization was evaluated by spectrophotometry at 450 nm OD. One percent Triton X100 was used as a positive control.

Annexin V and propidium iodide (AnnV/PI) staining was also performed in HBMECs-infected cells. Briefly, HBMECs were mock treated or infected with $ZIKV_{PE243}$ or $ZIKV_{MR766}$ at a MOI of 1. After different time points, cells were stained with FITC-AnnexinV and 2.5 μg/ml of PI and analyzed by flow cytometry. Alternatively, cells were incubated with Muse Annexin V and Dead cell kit (Millipore) and were also analyzed by flow cytometry. Samples acquisition and analysis were performed using FACSCanto equipment (BD Biosciences) and Flow Jo software. In addition, supernatants were harvested and release of lactate dehydrogenase was measured by LDH assay, according to manufacturer's protocol (Bioclin, RJ, Brazil).

Plasma membrane integrity and apoptosis induction were also evaluated by PI and TUNEL staining, respectively, and fluorescence microscopy analysis. HBMECs were seeded on transwell inserts (Costar—Corning®) and infected with $ZIKV_{PE243}$ or $ZIKV_{MR766,}$ as described. After 72 hpi, we performed TUNEL staining (*In Situ* Cell Death Kit—Roche), following manufacturer's instructions, or the cells were incubated with Propidium Iodide (BD Biosciences). The fluorescence was evaluated using OLYMPUS IX81 microscopy. Staurosporin (50 μM; Sigma- Aldrich) and Triton X-100 (0.1%; J.T. Baker)

were used as positive controls for TUNEL and PI staining, respectively.

Evaluation of Cytokine Production

HBMECs were infected as described and, the indicated time points, supernatants were harvested and cytokine concentrations were measured using a human cytokine 27-plex multiplex assay (Bio-Plex kit) and Bio-Plex® MAGPIX™ Multiplex equipment (Bio-Rad). The secretion of IL-6, IL-8, CCL5, and CXCL10 were confirmed by ELISA, according to manufacturer's protocol (Peprotech).

IFN-β, IFN-λ1, and IFN-λ4 expression in the cell lysates were measured at different time points post infection by qRT-PCR, and GAPDH expression was measured as a housekeeping control gene. RNA was extracted using TRIZOL reagent (Life Technologies), and first strand cDNA was synthesized using High-Capacity cDNA Archive Kit (Applied Biosystems), according to the manufacturer's instructions. Expression of type I and type III IFN mRNAs were measured using SYBR Green (Applied Biosystems), using the following primers: IFN-β sense: 5′-TAG CAC TGG CTG GAA TGA GA-3′, IFN-β antisense 5′-TCC TTG GCC TTC AGG TAA TG-3′; IFN-λ1 sense: 5′-GGG AAG CAG TTG CGA TTT AG-3′ and IFN-λ1 antisense 5′-GAT TTG AAC CTG CCA ATG TG-3′; IFN-λ4 sense: 5′-AGG GTC CTT AAC CGA CTG TG-3′ and IFN-λ4 antisense 5′-AAA CAA CCA ATG CGA TCA AA-3′; GAPDH sense 5′-GTG GAC CTG ACC TGC CGT CT-3′ and GAPDH antisense 5′-GGA GGA GTG GGT GTC GCT GT-3′. All qRT-PCR were performed with a standard PCR: the samples were subjected to 50°C for 2 min, 95°C for 10 min and 40 cycles of denaturation (95°C, 15 s), primer annealing (55°C, 30 s), and primer extension (60°C, 1 min). Next, the samples were subjected to a melt curve to eliminate primer dimers: 95°C, 15 s; 60°C, 1 min and 95°C, 15 s. Comparative CT method (ΔΔ Ct) was used to quantify gene expression levels with GAPDH used for normalization. Results are expressed as Mean ± *SD*. Kruskal–Wallis test One-way ANOVA was employed to compare differences between expressions of target genes with a significance level of 0.05.

Endothelial Permeability Assay

HBMECs (5×10^4 cells/well) were seed onto transwell inserts (Corning Costar, ME, USA; 0.4 μm membrane) and confluence was monitored everyday by measuring transendothelial electrical resistance (TEER) across cell monolayers using a Voltohmmeter (Millicell ERS-2). TEER was calculated after subtracting the resistance value in each experimental situation by the blank resistance of the membrane (without cells), and considering that resistance is inversely proportional to the area of the membrane. Resistance values were reported as "Ω/cm^2" and the experiments were performed when a high resistance (>80 Ω/cm^2) was reached (Mahad et al., 2006; Srinivasan et al., 2015). Cells were infected, from the apical side, with $ZIKV_{PE243}$ or $ZIKV_{MR766}$ (propagated in C6/36 cells) with a MOI of 1. As negative controls, cells were cultured with mock supernatants obtained from C6/36 cells. Staurosporin (STS; 10 μM; Sigma-Aldrich) was used as positive control. In some experiments, after virus adsorption, the cells were treated with Chloroquine diphosphate (50 μM; kindly supplied by FarManguinhos, Fiocruz, Rio de Janeiro, Brazil), or Nystatin (10 μM; Sigma-Aldrich), or Brefeldin A (BFA; 2 μg/ml; eBiosciences, San Diego, CA). After 72 h, supernatants were harvested and cells were incubated with FITC-conjugated BSA for 30 min. BSA extravasation was evaluated by measuring fluorescence intensity in the lower chamber, using spectrofotometer SpectraMax i3 (Molecular Devices, Lagerhausstrasse, Austria). The Permeability Coefficient (Pd) of albumin was calculated as: $Pd = [A]/t \times 1/A \times V/[L]$, where [A] is the albumin concentration in lower chamber, t refers to time in seconds, A indicates the area of the membrane (in cm^2), V is the volume of the bottom chamber, [L] is the albumin concentration in upper chamber. Data was normalized in relation to cells culture in culture medium only.

Virus RNA was measured in the upper and lower chamber of the transwell by qRT-PCR, as previously described. Also, the medium harvested from the lower chamber was inoculated into a Vero cell culture and virus RNA in the cell lysates and supernatants were measured by qRT-PCR. To confirm the presence of infectious virus in the abluminal chamber, Vero cells (8×10^4 cells/well) were seeded in the lower chamber and, at 48 hpi, a real time PCR targeting viral negative strand was performed with the cell lysates. Briefly, intracellular viral RNA was extracted as described, and reverse transcription was performed using 835 forward primer instead of random primers (Lanciotti et al., 2008). Real time PCR was performed using TaqMan Universal Master Mix, as described.

In some experiments, HBMECs were also cultured with 50% conditioned medium obtained from PBMCs mock-treated or infected with $ZIKV_{PE243}$ or $ZIKV_{MR766}$ (iCM-PBMC) and cell permeability was evaluated as described.

Analysis of Endothelial Cell Adhesion Protein by Immunofluorescence

HBMECs were cultured onto coverslips and cells were mock treated or infected as described. After 72 hpi, cells were fixed with 4% paraformaldehyde in PBS for 20 min, washed in PBS twice and permeabilized with 0.1% Triton X-100 (Sigma Aldrich) plus 3% bovine serum albumine (BSA—Sigma Aldrich) for 25 min. Cells were incubated with both an anti-flavivirus 4G2 antibody (ATCC HB112) and anti-ß-catenin (Sigma Aldrich) antibodies diluted in PBS−3% BSA overnight at 4°C. After washing in PBS, cells were incubated with the AlexaFluor488-conjugated anti-mouse IgG (4G2 staining), or with AlexaFluor594-conjugated goat anti-rabbit IgG (β-catenin staining) (Life technologies) for 40 min. The cells were then washed three times in PBS and incubated with DAPI for 5 min. Following thorough washing with PBS, the coverslips were mounted with prolong gold antifade reagent (Life technologies) and imaged on a Zeiss LSM 710 confocal.

Mouse Infection

A129 mice (4 weeks age) were infected with 2×10^5 PFU of $ZIKV_{PE243}$ or $ZIKV_{MR766}$ by i.v route. Mock supernatants were used as negative control. To evaluate virus replication, mice brains were removed at 2 or 5 days p.i. and macerated. RNA

isolation, cDNA, and qRT-PCR were performed as described previously.

Analysis of Blood Brain Barrier Integrity *in Vivo* by Evans Blue Staining

A129 mice were infected with $ZIKV_{PE243}$ or $ZIKV_{MR766}$, as described. Two or five days post infection, mice were i.v. injected with 0.5% Evans blue solution (EB, 200 μL per mouse) (Vetec, Rio de Janeiro, BR). After 1 h, mice were perfused with PBS and their brains were carefully removed. Brains were weighted, placed in 1 mL formamide (Vetec) and kept at room temperature for 3 days for stain extraction. As a positive control for BBB permeabilization, we used C57BL/6 mice infected with Plasmodium berguei ANKA, an experimental model of cerebral malaria (Reis et al., 2012). Mice were intraperitoneally inoculated with 10^5 infected erythrocytes and BBB permeability was assayed 7 days after infection. The amount of Evans blue in solution was measured by optical spectroscopy using SpectraMax i3 (Molecular Devices), and calculated using a standard curve. Blood brain barrier permeability was estimated as μg Evans Blue/mg tissue.

Immunoglobulin G Staining

A129 mice were infected with $ZIKV_{PE243}$ or $ZIKV_{MR766}$, as described. Two or five days post infection, mice were deeply anesthetized and then transcardially perfused with ice-cold 0.9% saline, followed by 4% paraformaldehyde (PFA) in 0.1 M sodium phosphate buffer, pH 7.4. Brains were rapidly removed from skulls, postfixed in PFA for 1 d at 4°C, and cryoprotected in a PFA solution containing 20% (w/v) sucrose overnight. The frozen brains were then sectioned into 20 μm-thick coronal sections using a sliding microtome (Leica). Slices were collected in a cold cryoprotectant solution (0.05 M sodium phosphate buffer, pH 7.4, 30% ethylene glycol, 20% glycerol) and stored at −20°C. Free-floating sections were washed with 0.4% Triton X-100 in PBS (3 × 10 min) and then incubated for 30 min in a blocking solution containing 4% normal goat serum (Thermo Fisher Scientific) in PBS. Sections were washed with PBS (3 × 10 min), followed by an overnight incubation with a biotinylated goat anti-mouse IgG (H+L) antibody (1:500, Vector Laboratories). Binding was visualized using the peroxidase-based Vectastain ABC kit and 3,3′-diaminobenzidine (Vector Laboratories). Tissues were thereafter dehydrated through graded concentrations of alcohol, cleared in HistoChoice® Clearing agent (Sigma-Aldrich) and coverslipped with Organo/Limonene Mount™ (Sigma-Aldrich). Slides were scanned with a Pannoramic MIDI II scanner (3DHISTECH).

Immunohistochemistry Analysis of Mice Brain Tissues

A129 mice were infected with $ZIKV_{PE243}$, as described. Five days post infection, mice were transcardially perfused with cold phosphate-buffered saline (PBS) solution followed by fresh ice-cold 4% formaldehyde (PFA). The brain samples were fixed in 4% PFA, and cryoprotected with sucrose 30%. Slides with coronal frozen brain sections (30 μm-thick) were fixed in acetone for 30 min, washed twice with PBS and slides were blocked with PBS supplemented with 10% FBS and 1% NDS (normal donkey serum) (blocking buffer), for 1 h. The tissues were then incubated with mouse antibodies anti-4G2 antibody, or anti-VE-cadherin (2 μg/ml; Santa Cruz Biotechnology), or anti-occludin (2.5 μg/ml; Invitrogen), all diluted in blocking buffer. Primary antibodies were incubated overnight, at 4°C, in humid chamber. After washing in PBS, cells were incubated with Alexa Fluor 488-conjugated anti-mouse IgG diluted in blocking buffer (2.5 μg/ml; Invitrogen), for 1 h, at 4°C, in humid chamber. Then, the slides were mounted in Prolong Gold Antifade with DAPI (Invitrogen) and imaged on a Zeiss Axio Observer Z1 microscope equipped with an Apotome module.

Statistical Analysis

Data were analyzed using the GraphPad Prism software (GraphPad Software, San Diego, CA, USA). Comparisons among groups were performed by two way ANOVA; $p < 0.05$ were considered statistically significant.

RESULTS

HBMECs Are Productively Infected by ZIKV

Human brain microvascular cells were previously shown to be susceptible to ZIKV (Bayer et al., 2016); however, a productive infection was not fully addressed. We further investigated HBMEC infection by different strategies. Initially, cells were infected with different MOIs of $ZIKV_{PE243}$ or $ZIKV_{MR766}$ and, after 48 h, ZIKV antigen expression was analyzed by immunofluorescence, using anti-flavivirus 4G2 antibody. We observed that virus antigen was clearly detected after infection with either ZIKV strain, with 10 or 1 MOI (**Figure 1A**). The replication efficiency of $ZIKV_{PE243}$ and $ZIKV_{MR766}$, obtained from C6/36 or Vero cell lines, were then compared by performing kinetic measurements of virus RNA and infectious particles release. We observed that infection with both strains resulted in similar level of virus RNA release, independent of the virus source (**Figures 1B,C**). Analysis of the production of infectious particles by plaque assay confirmed that HBMEC were permissive to infection with both ZIKV strains (**Figures 1D,E**). Infection with viruses produced in Vero cells resulted in slightly increased replication of $ZIKV_{MR766}$; in addition, a significant drop in viral secretion was observed at 96 hpi (**Figure 1E**), which was not observed when cells were infected with viruses obtained from C6/36 cells (**Figure 1D**). Therefore, further investigation of the effects of ZIKV infection on HBMEC physiology was performed using C6/36-derived virus stocks.

$ZIKV_{MR766}$ Induces Higher Cytotoxicity in HBMECs than $ZIKV_{PE243}$

We then evaluated whether infection with ZIKV would affect HBMEC physiology and survival. Initial analyses were performed by XTT metabolization assay at different time points post infection, normalized according to cell cultures with culture medium only. Infection with $ZIKV_{MR766}$ resulted in decreased XTT metabolization levels in comparison to mock-treated cells, from 48 hpi and thereafter, suggesting that HBMEC infection with this strain induced cell death. On the other hand, alteration

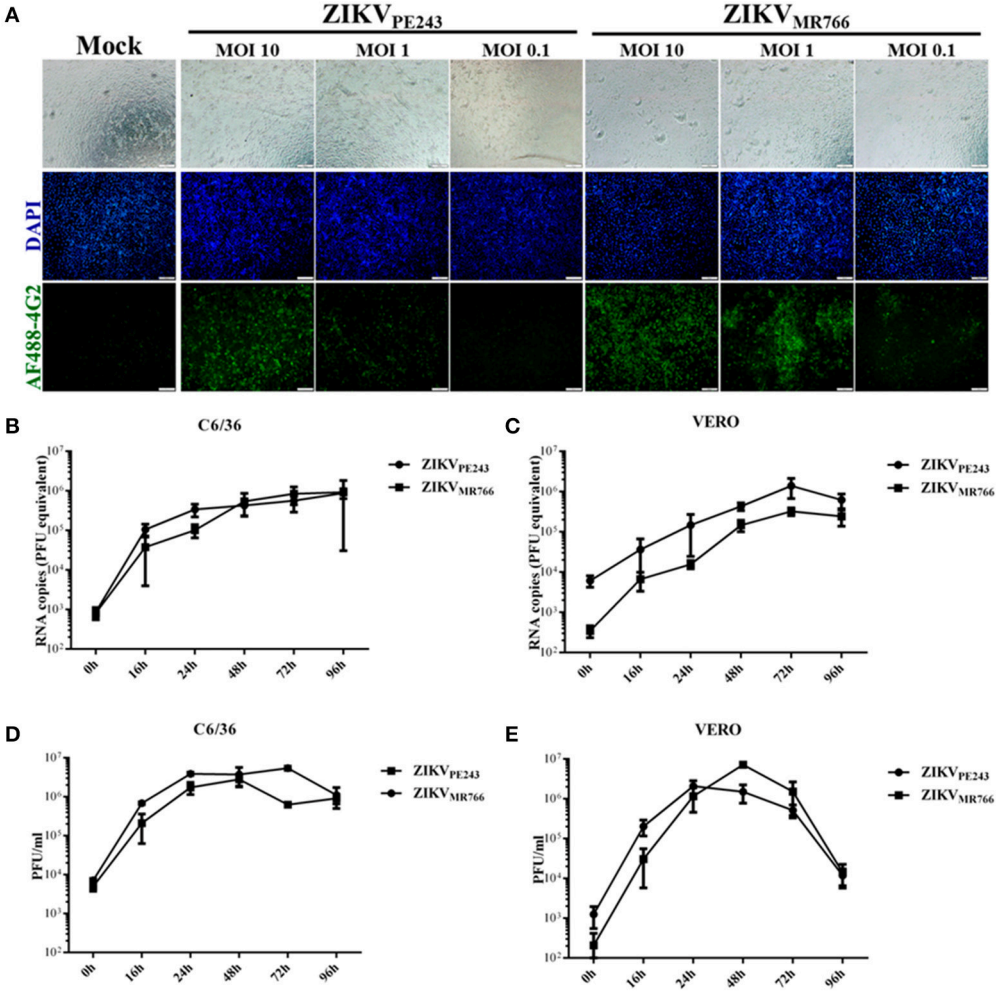

FIGURE 1 | HBMECs are productively infected by ZIKV. **(A)** HBMECs were mock treated or infected with ZIKV$_{PE243}$ or ZIKV$_{MR766}$, at the indicated MOI. After 48 h, cells were stained with 4G2 antibody and analyzed by immunofluorescence. **(B,C)** HBMECs were infected with ZIKV$_{PE243}$ or ZIKV$_{MR766}$ (MOI 1), produced in C6/36 cells **(B)** or produced in Vero cells **(C)**. After different time points, supernatants were harvested and viral RNA was measured by qRT-PCR. **(D,E)** HBMECs were infected with ZIKV$_{PE243}$ or ZIKV$_{MR766}$ (MOI 1), produced in C6/36 cells **(D)** or produced in Vero cells **(E)**. After different time points, supernatants were harvested and infectious particles were titrated by plaque assay. Data are represented as mean ± *SD* of two independent experiments.

in XTT metabolization by infection with ZIKV$_{PE243}$ was not detected until 72 hpi, indicating that the Brazilian strain was not associated to a severe cytophatic effect in these cells (**Figure 2A**). ZIKV-induced altered cell metabolism or viability depended on virus replication, since HBMEC culture with inactivated viruses did not result in any alteration of XTT metabolization. HBMECs cell death was also evaluated after infection with another Brazilian virus isolated (ZIKV$_{BR-SP}$), and the results obtained were very similar to the ones obtained with ZIKV$_{PE243}$ (**Figure 2B**).

Cell viability was also accessed by Annexin V/PI staining and LDH release. Flow cytometry analysis demonstrated that around 35% of cells infected with ZIKV$_{MR766}$ were AnnV/PI-positive after 72 hpi, in contrast to 20% of the cells infected with the Brazilian strain. About 70% of HBMECs were still alive even at 96 h after ZIKV$_{PE243}$ infection, when almost 60% of the cells infected with ZIKV$_{MR766}$ were dead (**Figures 2C,D**). This kinetic was consistent with the detection of LDH release, which was observed from 48 hpi; and peaked at 96 hpi (**Figure 2E**). Similarly, infection with ZIKV$_{MR766}$ resulted in higher levels of LDH activity detected in the supernatants, in comparison to infection with ZIKV$_{PE243}$.

To confirm that infection with ZIKV$_{PE243}$ was not associated to a remarkable cytopathic effect, HBMEC viability was also evaluated by different techniques, including flow cytometry analysis, based on 7AAD staining; fluorescence microscopy analysis, after PI and TUNEL staining; and cell counting with Trypan blue exclusion dye. Flow cytometry analysis demonstrated that dead cells could only be detected after 72 hpi with ZIKV$_{MR766}$, but not in mock-treated or ZIKV$_{PE243}$-infected cells (**Supplementary Figure 1A**). Fluorescence analysis did not indicate a significant TUNEL staining in any

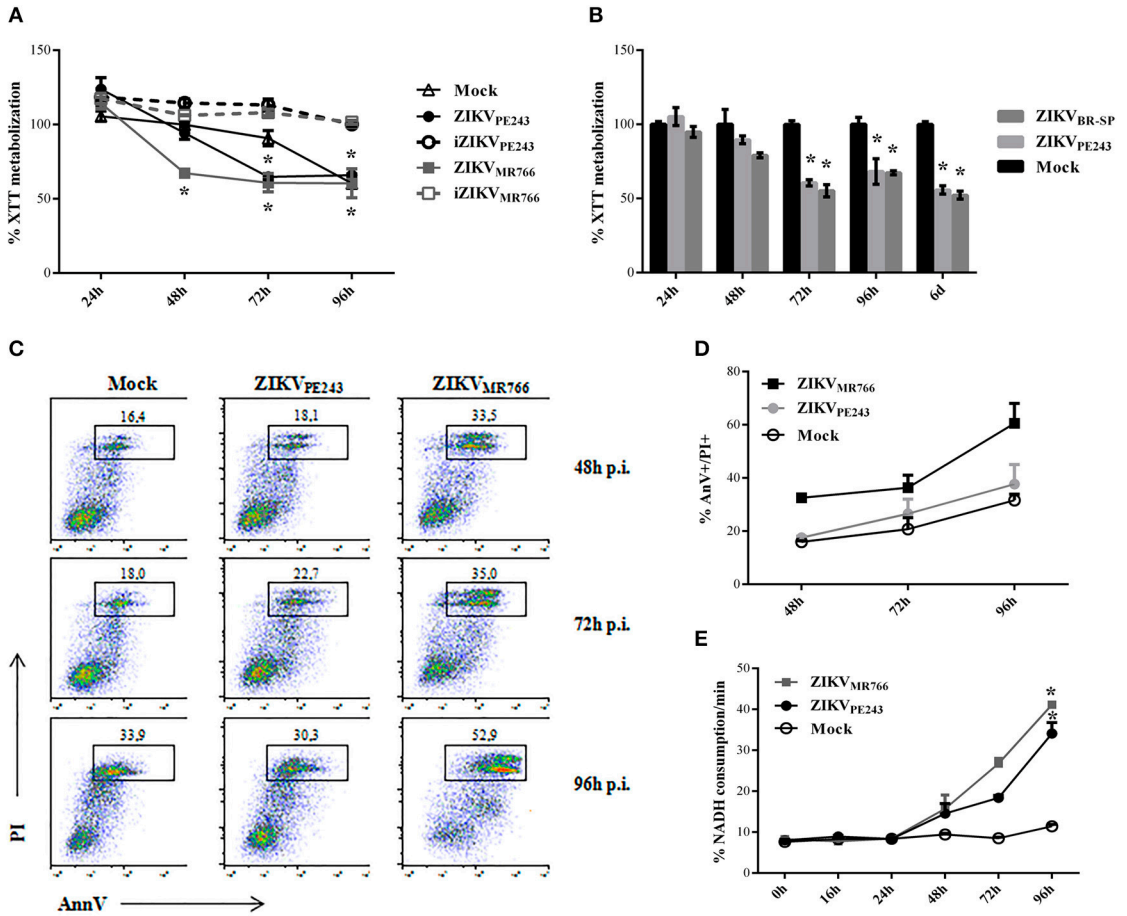

FIGURE 2 | Cell viability of HBMECs infected with ZIKV. **(A)** HBMECs were mock-treated or cultured with ZIKV$_{PE243}$ or ZIKV$_{MR766}$, produced in C6/36 cells, in their native and inactivated forms (iZIKV). XTT metabolization was assayed at the indicated time points, and normalized according to the values obtained in cell cultures maintained in culture medium only. Data are represented as mean ± *SD* of six independent experiments. *$p < 0.05$ in relation to mock. **(B)** HBMECs were mock-treated or infected with ZIKV$_{PE243}$ or ZIKV$_{BR-SP}$ and XTT assay was performed as in **(A)**. **(C,D)** HBMECs were infected with ZIKV$_{PE243}$ or ZIKV$_{MR766}$. Cells were stained with AlexaFluor488-Annexin V (AnnV) and propidium iodide (PI) and were evaluated by flow cytometry, at the indicated time points. **(C)** Dot plot indicating the percentage of AnV$^+$PI$^+$ cells at each time point, in a representative experiment. **(D)** Average percentage of AnnV$^+$PI$^+$cells at each time point from three independent experiments. **(E)** Culture supernatants were harvested and LDH release was evaluated by measurement of NADH consumption/min in a LDH activity assay. Data are represented as mean ± *SD* of three independent experiments. *$p < 0.05$ in relation to mock.

experimental situation, although PI staining could be detected in ZIKV infected cells (**Supplementary Figure 1B**). Finally, cell proliferation and viability was accessed by following the absolute cell numbers recovered after tripsinization of HBMECs infected with ZIKV$_{PE243}$ or ZIKV$_{MR766}$, in comparison to Vero cells. We observed that HBMECs infected with ZIKV$_{PE243}$ were still able to replicate during 48 h culture, although the absolute number of cells recovered after 48 h was a little lower (about 7–12%) than the mock-treated cells (**Supplementary Figure 1C**). HBMECs infected with ZIKV$_{MR766}$ also replicated, but at much lower efficiency. In contrast, the proportion of ZIKV-infected Vero cells recovered after 48 hpi was much lower (40–50%), in comparison to mock-treated cells (**Supplementary Figure 1D**). Taken together, these data corroborates with previous observation that HBMEC is more resistant to ZIKV-induced CPE than other cell types, such as Vero cells.

ZIKV Stimulates the Secretion of Proinflammatory Cytokines by HBMECs

We have previously demonstrated that dengue virus stimulated HBMEC to produce increased levels of chemokines and proinflammatory cytokines, which might contribute to the inflammatory response observed during the disease (da Conceição et al., 2013). Here, we evaluated whether ZIKV was able to induce the same activation pattern. Supernatants of HBMECs infected with ZIKV$_{PE243}$ were harvested at different time points and levels of IL-6, IL-8, and CCL5 were measured by ELISA. We observed a significant increase in secretion of IL-6 and CCL5, but not IL-8, at 72 hpi, in comparison to mock treated cells (**Figure 3A**). To investigate whether HBMECs activation would be a unique feature of the Brazilian strains, we compared cytokine secretion induced by ZIKV$_{PE243}$ or ZIKV$_{MR766}$ by 27-plex multiplex analysis (**Table 1**). The cytokines that

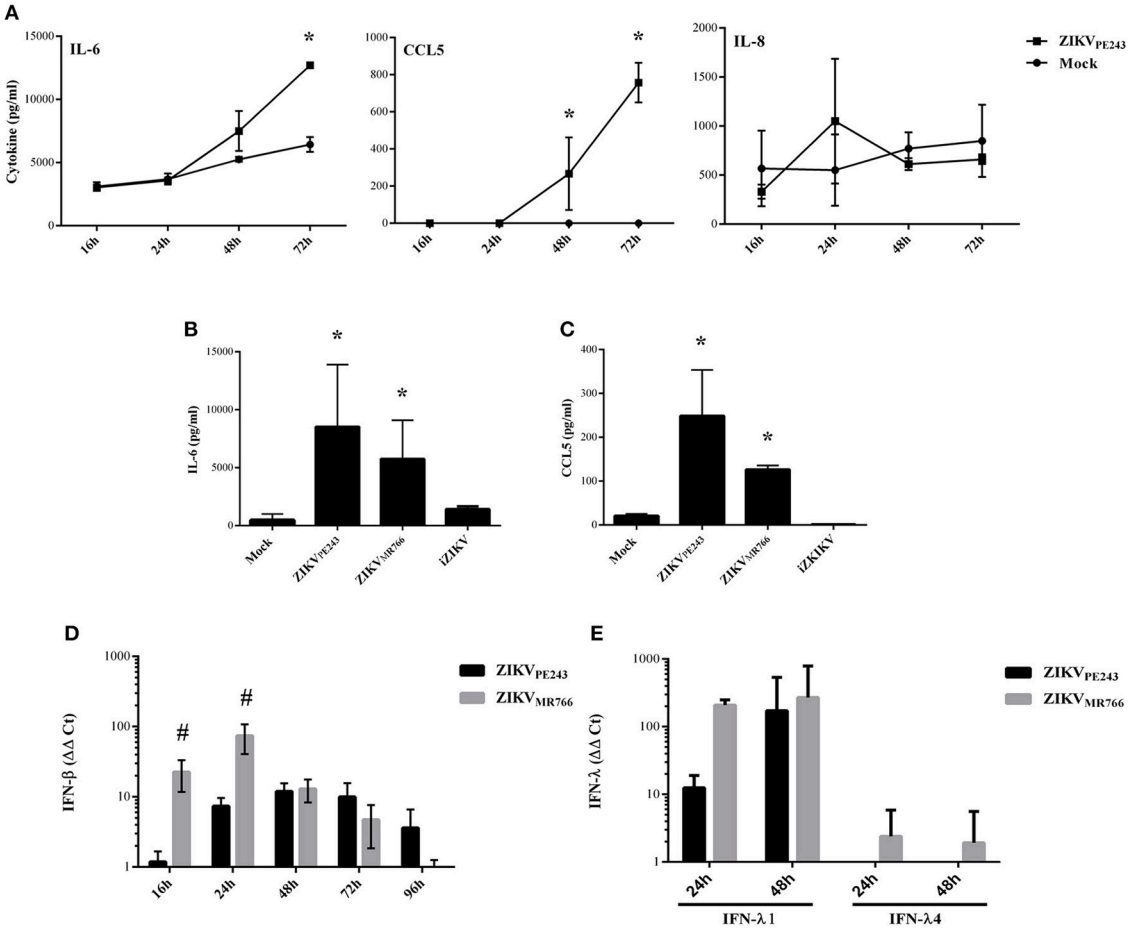

FIGURE 3 | ZIKV induces the secretion of inflammatory cytokines and chemokines by HBMECs. **(A)** HBMECs were mock-treated or infected with $ZIKV_{PE243}$, with a MOI of 1. After different time points, supernatants were harvested and IL-6, IL-8, and CCL5 were measured by ELISA. Data are represented as mean ± *SD* of two independent experiments and $^*p < 0.05$ in relation to mock. **(B,C)** HBMECs were mock-treated or infected with $ZIKV_{PE243}$ or $ZIKV_{MR766}$, with a MOI of 1. After 48 hpi, supernatants were harvested and IL-6 **(B)** and CCL5 **(C)** were measured by ELISA. Data are represented as mean ± *SD* of eight independent experiments and $^*p < 0.05$ in relation to mock. **(D,E)** HBMECs were treated as in **(B)** and cell lysates were obtained at the indicated time points. Expression of IFN-β mRNA **(D)** or IFN-λ1 and IFN-λ4 mRNA **(E)** were measured by qRT-PCR; GAPDH expression was measured as a housepkeeping control. Bars indicate ΔΔCt values, normalized according to *gapdh* values and mock results. Data are represented as mean ± *SD* of three independent experiments. $\#p < 0.05$ in relation to $ZIKV_{PE243}$.

showed significant increased levels were confirmed by ELISA in additional experiments. $ZIKV_{PE243}$ and $ZIKV_{MR766}$ stimulated the secretion of IL-6 and CCL5 (**Figures 3B,C**), whereas CXCL10 secretion was not detected in any situation (data not shown). These data suggest that both viruses activated HBMECs, what may equally contribute to attraction of leukocytes, especially lymphocytes to BBB.

Expression of type I and type III interferons were also evaluated in infected cells by qRT-PCR. We observed that both virus strains stimulated IFN-β and IFN-λ1 production; however, $ZIKV_{MR766}$ promoted earlier and higher levels of IFN expression (**Figures 3D,E**). In addition, only $ZIKV_{MR766}$ produced IFN-λ4, although at low levels (**Figure 3E**). These data suggest that although $ZIKV_{MR766}$ induces increased CPE, virus replication was also associated to enhanced type I and III IFNs, what might contribute to the control of virus dissemination and endothelial lesion *in vivo*.

ZIKV Infection Does Not Induce Enhanced Permeability of the Endothelial Cell Monolayer

We finally analyzed whether ZIKV would alter BBB permeability. Cells were seed onto transwell inserts and infected with $ZIKV_{MR766}$ or $ZIKV_{PE243}$, with a MOI of 1. Mock supernatants and staurosporin (STS) were used as negative and positive controls, respectively. Transendothelial electrical resistance (TEER) was measured for 48 h and no significant differences were observed between ZIKV-infected and mock-treated cells (**Figure 4A**). After 72 hpi, the supernatants were harvested, cells were incubated with FITC-conjugated albumin for 30 min, and the fluorescence intensity was measured in the abluminal chamber. The permeability coefficient (Pd) was calculated and normalized in relation to cells cultures in culture medium only. We did not observe any significant difference in the levels of

TABLE 1 | Comparison of Inflammatory cytokines, chemokines, and growth factors levels in supernatant from human brain microvascular endothelial cell line (HBMEC) after infection with Brazilian and African ZIKV strains ($ZIKV_{PE243}$ and $ZIKV_{MR766}$).

	Control	$ZIKV_{PE243}$ (MOI 0.1)		$ZIKV_{MR766}$ (MOI 0.1)	
	pg/mL	pg/mL	Fold change	pg/mL	Fold change
IMFLAMMATORY CYTOKINES					
IL1β	1.11	1.56	1.41	0.76	0.68
IL1ra	28.13	52.9	1.88	52.9	1.88
IL2	–	–	–	–	–
IL4	5.35	10.74	2.01	7.77	1.45
IL5	–	–	–	0.52	–
IL6	356.83	929.23	2.60	469.71	1.32
IL9	–	2.09	–	4.76	–
IL10	12.93	13.33	1.03	37.04	2.86
IL12	62.97	68.49	1.09	197.02	3.13
IL13	1.04	1.15	1.11	2.91	2.80
IL15	–	1.49	–	0.37	–
IL17a	94.98	113.23	1.19	11.4	0.12
IFNγ	46.27	72.54	1.57	90.71	1.96
TNFα	7.04	13.27	1.88	10.16	1.44
CHEMOKINES					
Eotaxin	36.45	64.74	1.78	50.08	1.37
IL8	225.15	674.93	3.00	583.62	2.59
CXCL10	54.27	71.46	1.32	71.46	1.32
CCL2	539.54	736.19	1.36	640.37	1.19
CCL3	1.71	1.95	1.14	0.83	0.49
CCL4	0.56	0.91	1.63	0.31	0.55
CCL5	6.50	16.03	2.47	27.63	4.25
GROWTH FACTORS					
Basic FGF	97.97	116.48	1.19	21.2	0.22
G-CSF	3.29	13.04	3.96	6.53	1.98
GM-CSF	–	–	–	–	–
IL7	10.43	11.35	1.09	21.36	2.05
PDGF-BB	137.21	364.5	2.66	149.3	1.09
VEGF	1111.64	1236.97	1.11	5505.51	4.95

albumin extravasation at this time point, in comparison to mock-treated cells (**Figure 4B**).

Interestingly, in spite of the maintenance of endothelial monolayer integrity, virus RNA could be detected in the lower chamber of the transwell system, suggesting that ZIKV may cross BBB through basolateral virus release, transcytosis or paracytosis (**Figure 4C**). Conditioned medium obtained from the lower chamber of the transwell system was inoculated in ZIKV-susceptible Vero cells and, after 48 hpi, ZIKV RNA was measured in Vero cell lysates and supernatants. Intracellular and supernatant RNA virus were detected in the cultures, indicating that extravasated ZIKV was able to productively infect other cells (**Figure 4D**). To confirm the infectivity of the viruses crossing the monolayer, Vero cells were seeded in the lower chamber of the transwell system and the presence of virus negative strand RNA was accessed by qRT-PCR. As a negative and positive control, Vero cells were mock treated or directly infected with ZIKV. Virus negative strand RNA was detected in the Vero cell lysates, confirming that the virus crossed the HBMEC barrier, and replicated into the cells in the lower chamber (**Figure 4E**). These results confirm that ZIKV may cross endothelial cell monolayer without increasing permeability. To further evaluate endothelial monolayer integrity in the cultures, cells were stained with anti-flavivirus 4G2 antibody and anti-β-catenin. Immunofluorescence analysis did not indicate any cell junction disorganization in ZIKV-infected cultures, in comparison to mock-treated cells (**Figure 4F**).

We then asked whether inflammatory mediators produced by blood cells would be able to affect the permeability of ZIKV-infected HBMECs. PBMC were infected with either $ZIKV_{PE243}$ or $ZIKV_{MR766}$ for 72 h. Then, supernatants were harvested, and virus infectious particles were inactivated by U.V. radiation and used as PBMC conditioned medium (iCM-PBMC). HBMECs were mock treated or infected with $ZIKV_{PE243}$ or $ZIKV_{MR766}$, in the presence of absence of 50% the indicated iCM-PBMC. After 72 hpi, albumin extravasation was measured, as described before. Surprisingly, neither the supernatant obtained from $ZIKV_{MR766}$ nor $ZIKV_{PE243}$-infected cells were able to induce HBMECs permeability in any tested situation (**Figure 5**). These data indicate that rupture of BBB integrity is not the main pathway stimulated by ZIKV to invade the CNS.

ZIKV Extravasation through BBB May Occur through Endocytosis/Exocytosis Replication Pathway Or through Transcytosis

Since virus extravasation was not related to cell death-mediated monolayer disruption, we investigated whether it was dependent on virus replication or transcytosis, by treating ZIKV-infected HBMECs with different pharmacological inhibitors of these pathways. Chloroquine is a weak base able to raise the pH of acidic compartments, which was previously shown to inhibit ZIKV-replication (Delvecchio et al., 2016); nystatin was reported to inhibit virus-induced transcytosis through caveola-mediated pathways (Harmon et al., 2012; Tugizov et al., 2013; Chanthick et al., 2016); brefeldin A (BFA) modulates vesicle traffic from endoplasmic reticulum to Golgi, leading to exocytosis inhibition (Fujiwara et al., 1988). Initially, we analyzed if the drugs would affect cell survival themselves, and none of them were cytotoxic at the concentrations used (**Figure 6A**). To investigate whether this drugs would affect virus extravasation, cells were cultured onto transwell plates, infected, and treated with them. HBMEC TEER was not altered by any drug during 48 h culture, confirming our previous data that ZIKV does not disturb cell resistance and demonstrating that the drugs did not induce cell permeability themselves (**Figure 6B**).

Finally, we investigated the effect of each drug in ZIKV replication and extravasation through HBMECs monolayers. Cells were infected with $ZIKV_{PE243}$, from the apical side, and treated with chloroquine, nystatin or brefelding A. The medium obtained from the luminal (upper) and abluminal (lower) chambers were harvested after 48 hpi, and virus RNA in each

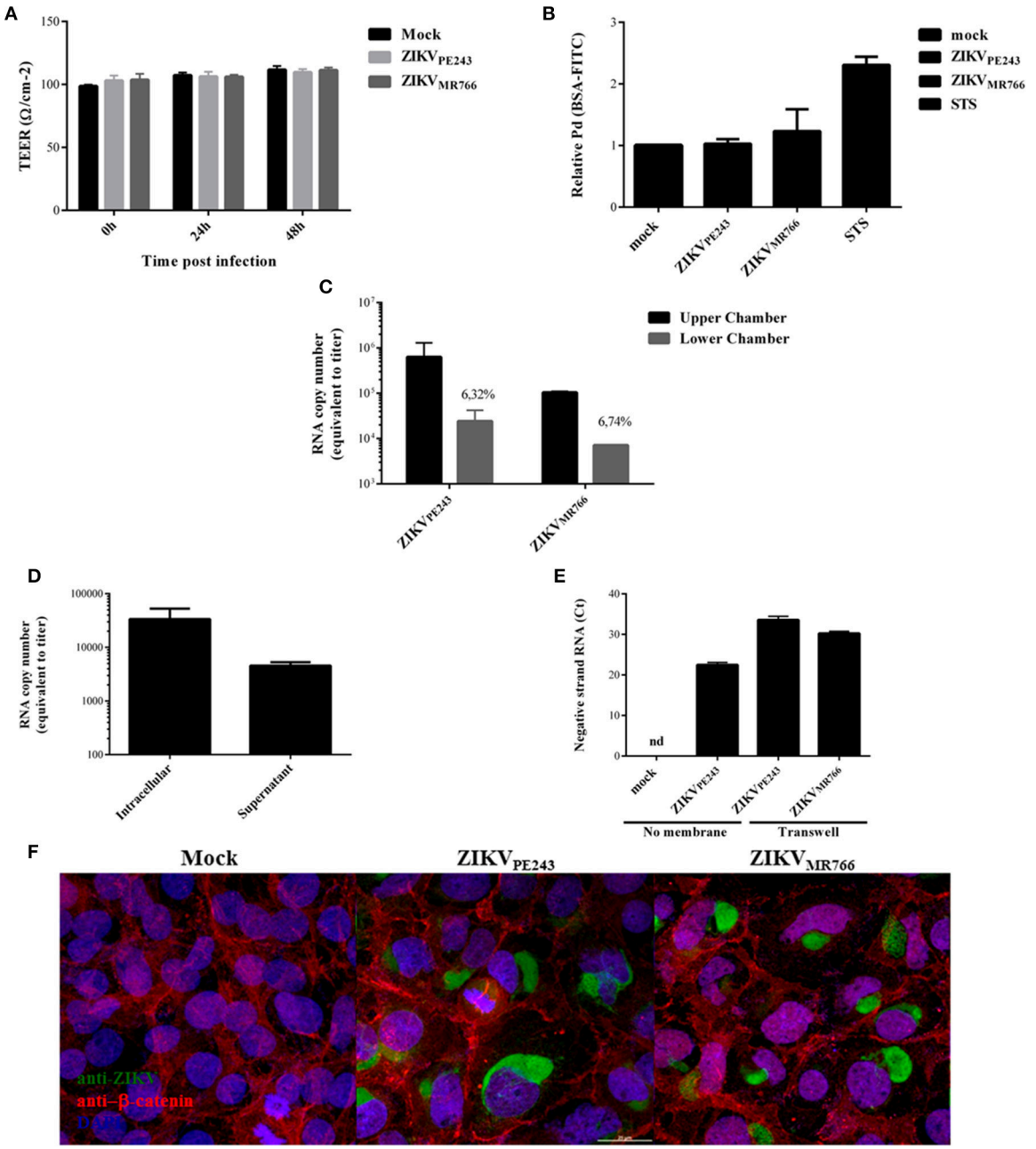

FIGURE 4 | ZIKV crosses endothelial cell monolayer, without increasing permeability. **(A)** HBMECs were cultured onto transwell plates and the cells were mock-treated or infected with $ZIKV_{PE243}$ or $ZIKV_{MR766}$. TEER was measured at 24 and 48 h post infection. **(B)** HBMECs were infected as in **(A)**; as controls, the cells were cultured with staurosporin (STS). After 72 hpi, cells were incubated with FITC-BSA for 30 min, the amount of extravasated albumin was measured by spectrophotometry, and the permeability coefficient (Pd) was calculated and normalized in relation to cells cultured in medium only. **(C)** Virus RNA was measured in the luminal (upper) and abluminal (lower) chambers of the transwell plates by qRT-PCR. Insert numbers indicate the percentage of RNA copies in relation to the corresponding upper chamber. **(D)** Conditioned media harvested from the lower transwell chamber of $ZIKV_{PE243}$ infected cells were inoculated into Vero cells. After 48 h, virus RNA present in the cell lysates and supernatant from Vero cells were measured by qRT-PCR. **(E)** HBMECs and Vero cells were cultured in the upper and lower chamber of a transwell plates, respectively. HBMECs were infected from the apical side, as described. After 72 hpi, Vero cells were harvested, and ZIKV negative strand RNA was measured by qRT-PCR. As positive and negative controls, Vero cells were mock-treated or directly infected with $ZIKV_{PE243}$ (no membrane); nd, not detected. **(F)** HBMECs were cultured as in **(A).** After 48 hpi, the cells were stained with anti-Flavivirus (4G2 antibody), followed with anti-mouse IgG-AlexaFluor488; and with anti-β-catenin, followed by anti-rabbit IgG-AlexaFluor 594; and with DAPI. ZIKV infection and β-catenin expression were then analyzed by immunofluorescence. Data are represented as mean ± *SD* of four independent experiments.

compartment was measured by qRT-PCR (**Figures 6C,D**). As expected, analysis of apical release of virus RNA demonstrated that chloroquine and BFA inhibited around 50% ZIKV infection.

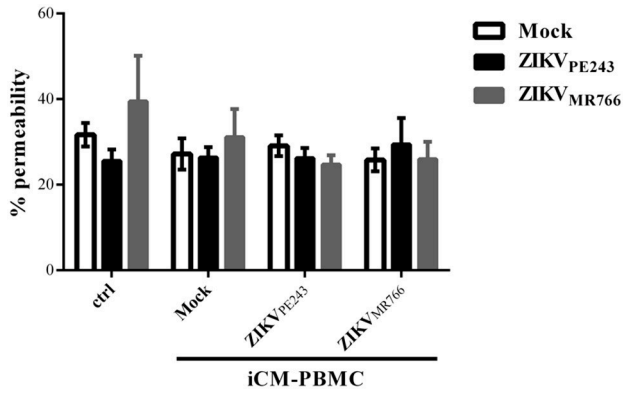

FIGURE 5 | Supernatants from ZIKV-infected PBMC did not induce permeability of ZIKV-infected HBMEC. HBMECs were mock treated or infected with ZIKV$_{PE243}$ or ZIKV$_{MR766}$, in the presence of absence of 50% conditioned inactivated medium obtained from PBMC cultured with mock or infected with ZIKV$_{PE243}$ or ZIKV$_{MR766}$ (iCM-PBMC). Data are represented as mean ± *SD* of five independent experiments.

On the other hand, addition of nystatin did not decrease virus RNA release (**Figure 6C**). Treatment of ZIKV-infected HBMEC with chloroquine or BFA also resulted in around 50 and 65% decrease of virus RNA in the abluminal transwell chamber, respectively, indicating that virus replication and exocytosis or basolateral release were necessary for extravasation (**Figure 6D**). Interestingly, despite having no effect in virus replication and apical release, addition of nystatin to the cultures also decreased virus extravasation by around 50% (**Figure 6D**), suggesting that caveola-mediated transcytosis and/or basolateral release is an important pathway for ZIKV extravasation through brain endothelial cells.

ZIKV Reaches the Central Nervous System without Disrupting the Blood Brain Barrier *in Vivo*

To confirm that ZIKV was able to reach the brain without disrupting BBB, we evaluated BBB integrity in a mouse experimental model. For this purpose, we infected IFNAR-deficient A129 mice, which was previously demonstrated to be susceptible to ZIKV infection (Dowall et al., 2016; Lazear et al., 2016; Rossi et al., 2016). Mice were intravenously inoculated with ZIKV$_{PE243}$ or ZIKV$_{MR766}$ (2×10^5 PFU). After 2 and 5 days p.i., virus RNA was quantified in the mice brains by qRT-PCR and

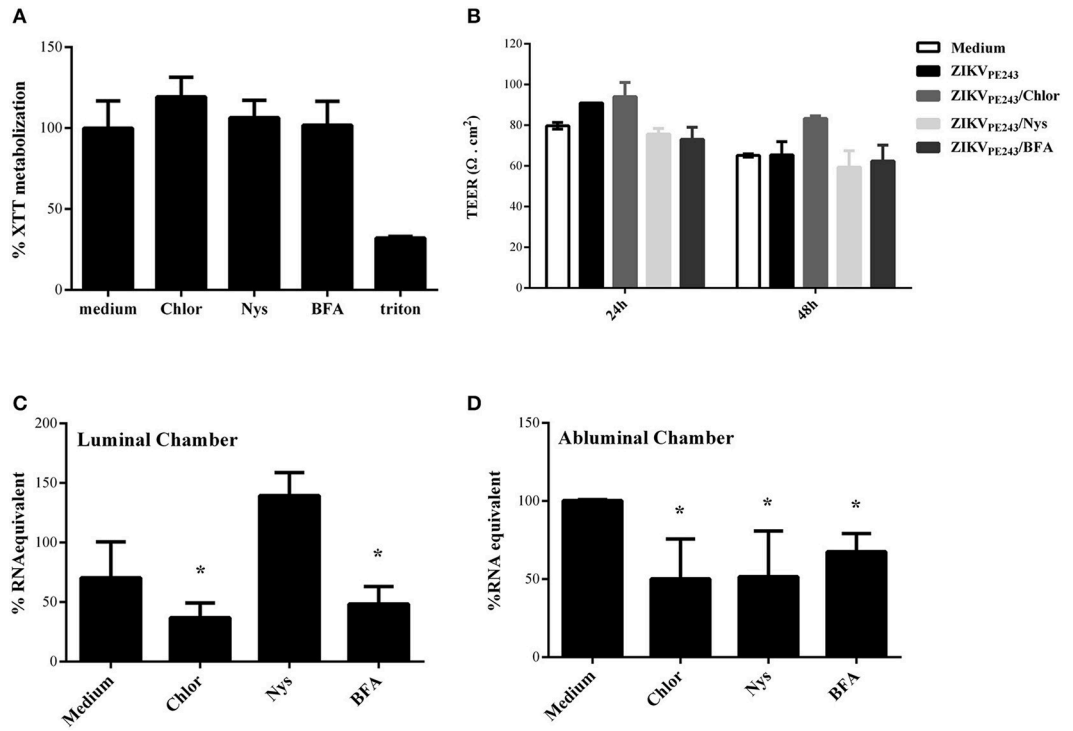

FIGURE 6 | ZIKV extravasation depends on viral replication and basolateral release or transcytosis. **(A)** HBMECs were cultured with chloroquine (Chlor), nystatin (Nys), or brefeldin a (BFA) for 48 h, except for BFA, which was added in the last 10 h culture. Then, cell viability was analyzed by XTT assay. Cells were also cultured with culture medium only or with triton, as negative and positive controls, respectively. **(B–D)** HBMECs were cultured onto transwell systems and then infected with ZIKV$_{PE243}$, from the apical side. The infected cells were treated or not with Chlor, Nys, or BFA and cultured for 48 h. **(B)** TEER was measured at 24 and 48 hpi, **(C,D)** After 48 hpi, the supernatants from the upper (luminal) **(C)** and lower (abluminal) **(D)** chambers were harvested and virus RNA was measured by qRT-PCR. The data indicate the percentage of virus RNA in relation to cells infected in the absence of inhibitors. Data represents the average of three independent experiments; *$p < 0.05$.

BBB integrity was accessed by Evans Blue extravasation assay and measurement of endogenous IgG in the brains. ZIKV genome was highly detected in all the brains investigated, from mice infected with either $ZIKV_{PE243}$ or $ZIKV_{MR766}$, at 2 and 5 dpi (**Figure 7A**). BBB integrity was initially analyzed by inoculating Evans blue dye (EB), i.v., after 2 and 5 dpi. After 1 h, the brains were harvested and the amount of EB per mg tissue was measured. We could not detect a significant amount of EB in the brains obtained from ZIKV-infected mice, in comparison to mock-treated ones (**Supplementary Figure 2**). Since recent studies have questioned the sensibility of this method (Saunders et al., 2015), we performed another set of experiments, in which the presence of endogenous IgG was histologically evaluated in the brain sections. Corroborating with the previous data, no staining could be detected at 2 dpi in any of the experimental groups (**Figure 7B**). At 5 dpi, however, a diffuse staining pattern was observed in 1 out of 3 animals infected with $ZIKV_{MR766}$ (**Figure 7B**). In addition, small, focal areas of immunoglobulin G staining were detected in another animal infected with $ZIKV_{MR766}$ and in 3 out of 4 animals infected with $ZIKV_{PE243}$. No staining for immunoglobulin G was seen in the brain of control mice. These data supports the hypothesis that ZIKV is able to reach the CNS, without disrupting the BBB; however, blood brain barrier disruption may be a delayed event following ZIKV infection in young A129 mice.

Immunostaining for ZIKV envelope protein in the brain sections revealed robust staining in blood vessels (**Figure 7C**) and in the cells of plexus choroid of subventricular zone (SVZ) (**Figure 7D**), indicating that brain endothelial cells are actually infected by ZIKV. We also performed immunostaining of VE-cadherin and occludin proteins and we found no changes in the expression profile of these adherens and tight junctions markers in the brains of ZIKV-infected mice (**Figures 7E,F**), further suggesting that BBB was not remarkably affected.

Taken together, our data indicate that ZIKV productively infects HBMECs, and induces cellular activation. However, infection did not induce BBB permeability, *in vitro* nor *in vivo*, suggesting that ZIKV is able to reach the CNS without disrupting the BBB and that the invasion of CNS by ZIKV might be associated to transinfection or transcytosis from the endothelial cells of the BBB. However, the persistent CPE caused by the presence of $ZIKV_{MR766}$ and/or the subsequent inflammation triggered by the replication either virus strain in the brains may induce a slight disruption of BBB at later time points.

DISCUSSION

In the present work, we demonstrated that ZIKV infection of brain endothelial cells result in cellular activation and release of infectious virus particles, with no increase of endothelial monolayer permeability *in vitro* and no significant disruption of BBB *in vivo*.

ZIKV infection has been associated to alteration of CNS, including microcephaly and other neurological abnormalities after congenital infection, and meningoencephalitis in adults (Calvet et al., 2016; Carteaux et al., 2016; Cugola et al., 2016; Driggers et al., 2016; Martines et al., 2016; Miranda-Filho et al., 2016; Mlakar et al., 2016). Virus was detected in the brains from microcephaly and meningoencephalitis cases, indicating that ZIKV might cross the BBB and infect CNS cells (Cugola et al., 2016; Driggers et al., 2016; Martines et al., 2016; Mlakar et al., 2016). However, the mechanism by which the virus reaches the brain has not been addressed yet.

Our results demonstrated that both Brazilian and African ZIKV strains efficiently infected HBMECs and induced the secretion of type I and III IFNs and inflammatory cytokines. Infection of HBMECs by a Puerto Rican ZIKV strain (from Asian lineage) was recently demonstrated and the secretion of chemokines and interferons were also observed (Mladinich et al., 2017). Also, that article described that HBMECs became resistant to IFN effects and to virus-induced cell death, and that ZIKV infection did not result in increased permeability of HBMECs (Mladinich et al., 2017). The Brazilian lineages used in this study were isolated from patients with mild disease and both isolates were phylogenetically related to the Asian lineage of ZIKV. Brazilian ZIKV lineages behaved quite similar regarding the infection rate and cell death induction, showing less CPE than $ZIKV_{MR766,}$ in accordance with the previous data. These data suggest that the differences in the sequences of ZIKV lineages might affect virus-induced cytotoxicity, although we cannot discard that $ZIKV_{MR766}$ fitness might be related to higher passage numbers of this reference strain, in comparison to the Brazilian strains used in this study, which were under eight passages in culture. Other studies suggested that ZIKV-BR induced a higher cytopathogenic effect than ZIKV-AFR, but those were conducted in human neuron derived from pluripotent cells (NPC) and in human neurospheres (Cugola et al., 2016). Still, these findings need further investigation and may indicate that a higher CPE induction on brain endothelial cells might not be related to increased cases of microcephaly and other CNS alterations observed during infection with Brazilian ZIKV. In fact, the increased cell death induced by $ZIKV_{MR766}$ might contribute to limit virus dissemination and benefit immune control. Interestingly, we observed that, although both $ZIKV_{PE243}$ and $ZIKV_{MR766}$ induced IFN-β and IFN–λ expression, the African strain induced a higher and earlier IFN production. Similar findings have been described in an immunodeficient mouse experimental models, in which infection with African strains were more aggressive than with Asian ZIKV strains (Tripathi et al., 2017). These findings suggest that despite the supposed higher virulence of African ZIKV isolates, the earlier and increased production of type I IFN may contribute to controlling of virus dissemination *in vivo*. However, virus control is not apparent in mouse models, which does not respond to IFN, such as IFNAR or Stat2 deficient mice.

We also observed that both virus strains induced HBMEC activation, with production of IL-6 and CCL5 at similar levels, which might contribute to the recruitment and activation of inflammatory cells. These data support the previous results showing increased expression of inflammatory mediators, particularly CCL5, in HBMECs infected by ZIKV (PRVABC59 strain) (Mladinich et al., 2017). Analysis of inflammatory mediators in the cerebrospinal fluid (CSF) of stillborns and in

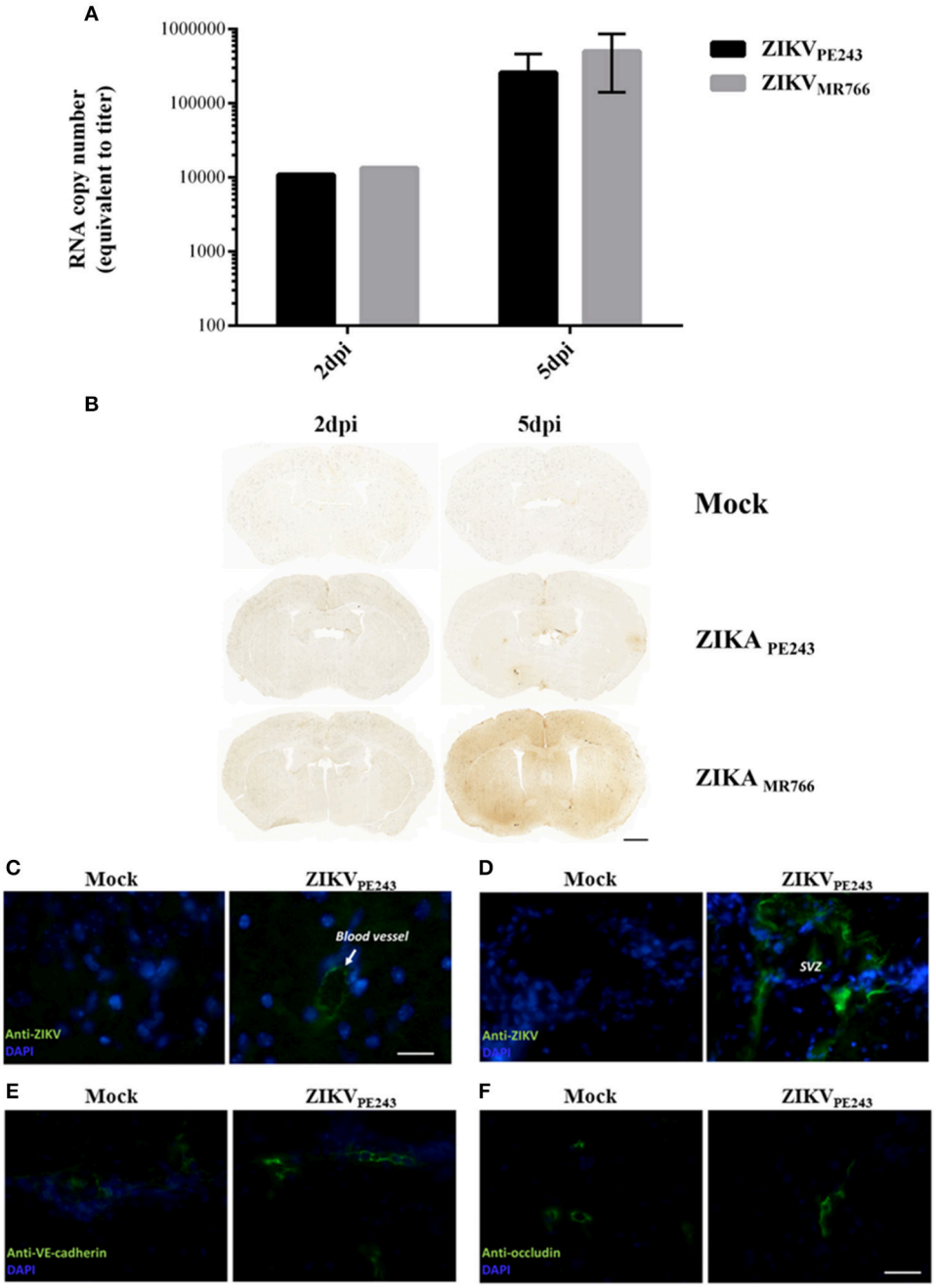

FIGURE 7 | ZIKV reaches mouse brains without disrupting BBB. A129 mice were mock-inoculated or infected with $ZIKV_{PE243}$ or $ZIKV_{MR766}$ (2×10^5 PFU) by i.v. route. **(A)** Virus RNA in the brains obtained from 2 or 5 days infected mice were measured by qRT-PCR. The values indicates the average of RNA copy numbers of four individual mouse infected with the respective viral strain. **(B)** Photomicrographs showing the pattern of immunoglobulin G staining in the brain of young A129 mice infected with $ZIKV_{MR766}$ or $ZIKV_{PE243}$, at 2 or 5 days post infection (dpi). Mice from the control group received an intravenous injection of saline. Scale bar: 1,000 μm. **(C–F)** After 5dpi, mice were transcardially perfused, the brains were harvested, and immunohistochemistry analyses were performed as described. Brain sections were incubated with mouse antibodies anti-4G2 antibody **(C,D)**, anti-VE-cadherin **(E)**, or anti-occludin **(F)**, followed by incubation with AlexaFluor 488-conjugated anti-mouse IgG. Expression of virus E protein and adherens and tight junction were then analyzed using a Zeiss Axio Observer Z1 microscope equipped with an Apotome module.

the brains of mouse experimental models also demonstrated increased levels of IL-6, CCL5, and type I IFNs (Galliez et al., 2016; Tripathi et al., 2017). Therefore, brain endothelial cell activation might contribute to the inflammatory milieu detected upon ZIKV infection. Also, analysis of stillborns tissues revealed the presence of a few inflammatory infiltrates circumventing

the neurons (Mlakar et al., 2016), what might result from the production of chemokines by local infected cells. However, the ability of leukocytes to cross the BBB during infection still needs to be investigated.

Several neurotropic viruses access the CNS as free virions or cell-associated from the bloodstream. Those may use different pathways to gain access to CNS, including direct transport from peripheral nerves, and transcytosis or transinfection. *In vitro* infection of HBMECs and *in vivo* infection of A129 mice with $ZIKV_{PE243}$ did not result in significant BBB disruption, although virus could be clearly detected in the brains. It is in agreement with the fact that ZIKV from Asian lineages did not result in a marked cytophatic effect of HBMECs *in vitro*, and that apical or basolateral infection of HBMECs with ZIKV induced virus release without evidences of disruption of monolayer integrity, which was observed here and in a previous study (Mladinich et al., 2017). Our data also demonstrated that despite the downregulation in metabolism and cell death induced by $ZIKV_{MR766}$, no major disruption of endothelial monolayer occurred *in vitro*, and BBB disruption was not essential for the virus to reach the brain. However, at late time points after infections with $ZIKV_{MR766}$, hemorrhagic points could be detected in the brain sections, suggesting that the prolonged lesion induced by the presence of this virus in the brains may contribute to a late disruption of the BBB. These data also suggest that other mechanisms, but not disruption of endothelial layers in the BBB might be involved in CNS invasion by the virus. Indeed, treatment of infected HBMECs with drugs that inhibited virus replication or transcytosis significantly impaired virus extravasation through cells monolayer in a transwell system.

Chloroquine was previously demonstrated to inhibit cellular infection (Delvecchio et al., 2016), possibly due to increased endosomal pH and prevention of virus uncoating. BFA is an exocytosis inhibitor, and might, therefore, block Flavivirus budding. In fact, HBMEC treatment with both drugs inhibited virus RNA release and extravasation of infectious virus in a transwell system, indicating that active replication was necessary to ZIKV-crossing through BBB. On the other hand, addition of nystatin to the cultures, despite not affecting virus replication levels nor apical RNA release, significantly inhibited virus crossing through the transwell. These data suggest that caveola-mediate traffic might not be essential for ZIKV replication, but may participate in virus basolateral release, or that transcytosis pathway may also take part in the process of virus extravasation.

Neurotropic viruses, such as poliovirus, rabhdovirus, and human herpes virus 1 and 2 were reported to reach the CNS through peripheral nerves (Finke and Conzelmann, 2005; Racaniello, 2006; Diefenbach et al., 2008; Luethy et al., 2016). Axonal transport and dissemination through peripheral nerves might also happen during Flavivirus infection, and it was described that a direct inoculation of WNV in the sciatic nerve of a hamster experimental model promoted limp paralysis (Samuel et al., 2007). However, Flaviviruses usually reach the CNS from the blood. Mouse experimental models demonstrated that YFV17D access the brains mostly hematogenously (Luethy et al., 2016). In addition, WNV were also reported to cross and disrupt BBB, in a way dependent on systemic inflammatory responses (Wang et al., 2004), although a report had demonstrated that BBB disruption was not essential for lethal WNV infection (Morrey et al., 2008). In a mouse model using adapted neurovirulent DENV strain, BBB disruption was observed, with infection of neurons, microglial and endothelial cells, associated to leukocyte infiltration (Velandia-Romero et al., 2012). On the other hand, JEV was reported to infect brain astrocytes, leading to cell activation and production of inflammatory cytokines, VEGF, and metalloproteinases, which then, seemed to affect neighbor endothelial cells, and to disrupt BBB (Chang et al., 2015). In fact, direct effect of JEV in electrical resistance or permeability of cultured endothelial cells were barely observed (Chen et al., 2014). Astrocytes were also demonstrated to be preferentially infected by ZIKV in an *ex vivo* model of organotypic cultures from primary human brain tissue (Retallack et al., 2016). In addition, another study demonstrated that THP-1 cells infected with ZIKV could cross endothelial cells in a transwell system, leading to infection of astrocytes cultured in the basolateral chamber of the transwell (Bramley et al., 2017). Given that astrocytes directly interact with endothelial cells in the brains and that such interaction might be relevant for the formation and organization of the BBB (Janzer and Raff, 1987), infection of these cells after ZIKV crossing through the endothelial layer may contribute to subsequent inflammation and alteration of the barrier.

ZIKV infection of peripheral neurons has never been addressed and dissemination through peripheral nerves might not be the main pathway of virus spreading to CNS, although it cannot be discharged. It is possible then that virus hematogenous dissemination allow virus access to BBB and infection of endothelial cells, promoting virus transcytosis or basolateral release, and infection of brain cells. Viral access to CNS by transcytosis has been demonstrated in other virus infections models, including WNV and JEV and may be a common pathway through which flavivirus reach CNS (Liou and Hsu, 1998; Verma et al., 2009; Dohgu et al., 2012).

Finally, infection of endothelial cells has been demonstrated in other tissues and organs crossed by ZIKV and associated to Zika syndrome, such as placenta, eye, and brain (Noronha et al., 2016; Roach and Alcendor, 2017; Singh et al., 2017; Vermillion et al., 2017). Regarding retinal endothelial cells, increased levels of antiviral and pro-inflammatory cytokine expression was also observed, including IFN-β, IL-6, and CCL5 (Roach and Alcendor, 2017; Singh et al., 2017), similar to what we observed in HBMECs. Activation of endothelial cells may also contribute to alteration of BBB integrity, which was detected at later time points after infection, especially upon infection with $ZIKV_{MR766}$. In fact, we demonstrated that the virus is able to cross the endothelial barrier without disrupting it, which could be an initial step of virus release to CNS, allowing the infection and activation of other cells types and contributing to the amplification of the lesion, as discussed.

In summary, we demonstrated that ZIKV efficiently infect HBMECs, resulting in release of infectious virus particles, what may contribute to virus access to CNS. HBMECs were also activated by the infection, producing inflammatory cytokines and chemokines, which can be relevant for the recruitment and

activation of leukocytes and amplification of the inflammatory response *in vivo*. Those inflammatory mediators might also affect survival, activation and infection of other cells present in the brain. Importantly, endothelial cells are part of the two main barriers to be crossed by ZIKV to cause severe disease—placental and BBB. Fetal endothelium was also demonstrated to be infected by ZIKV in mouse experimental models (Miner et al., 2016), but the direct role of this infection for placental extravasation or fetal vascular alteration was not investigated yet. Therefore, the study of infection of endothelial cells by ZIKV might contribute in further understanding of the mechanisms of virus dissemination and congenital disease, including CNS alterations.

AUTHOR CONTRIBUTIONS

LBA: conceived and supervised the experiments and data analysis. MP, LM, YM: performed and analyzed the *in vitro* experiments. MP, LM, and LBA: wrote the manuscript draft. SC, CL, MR, and MN: developed the methodology for virus production and mouse infection. MP, SC, CL, PF, MB, CF and HP, and PP-C: performed and supervised the *in vivo* experiments. PF, LC, PP-C, FL, and CF: performed image analysis of *in vitro* and *in vivo* assays. PS, PP, AT, and RSA: performed the analyses of negative strand RNA expression and cytokine production by multiplex. MB, AT, MN, RSA, and LBA were responsible for resources, funding acquisition, data interpretation, and write-review and editing. All authors reviewed the manuscript.

ACKNOWLEDGMENTS

This work was supported by CAPES, CAPES/PVE-Program, CNPq, FAPERJ-Rede ZIKA, and FINEP. MP was the recipient of a CNPq fellowship. LM and CL were the recipient of a CAPES fellowship. SC was the recipient of a FAPERJ fellowship. MN is supported by a FAPESP grant #2013/21719-3. MN and MB are a CNPq Fellowship recipient.

The authors wish to thank Dr. Ernesto T. A. Marques Jr (LAVITE, Centro de Pesquisas Aggeu Magalhães-FIOCRUZ, Recife, PE) and Dr. Pedro Vasconcelos for kindly provide ZIKVPE243 and ZIKVBR-SP, respectively. We are also thankful to Dr. Julio Scharfstein (Instituto de Biofísica Carlos Chagas Filho, UFRJ) for kindly provide HBMEC. We also acknowledge Raquel Cirlene and Ronaldo Rocha for technical support.

SUPPLEMENTARY MATERIAL

The Supplementary Material for this article can be found online at: https://www.frontiersin.org/articles/10.3389/fmicb.2017.02557/full#supplementary-material

Supplementary Figure 1 | $ZIKV_{PE243}$ does not induce severe CPE in HBMECs. **(A)** HBMECs were mock-treated or cultured with $ZIKV_{PE243}$ or $ZIKV_{MR766}$, produced in C6/36 cells. Cells were stained with Live/Dead kit and were evaluated by flow cytometry, at the indicated time points. Plots demonstrates a representative experiment of two independent experiments. **(B)** HBMECs were mock-treated (ctrl-) or infected with $ZIKV_{PE243}$ or $ZIKV_{MR766}$. After 48 hpi, cultures were stained with PI (left panel) or TUNEL (right panel) and analyzed by fluorescence microscopy. Triton X-100 and staurosporin were used as positive controls (ctrl+) for PI and TUNEL staining, respectively. **(C,D)** HBMECs **(C)** or Vero cells **(D)** were mock treated or infected with $ZIKV_{PE243}$ or $ZIKV_{MR766}$. After 48 hpi, cells were tripsinized and counted using trypan blue exclusion dye. Data are represented as mean ± *SD* of two independent experiments.

Supplementary Figure 2 | ZIKV reaches mouse brains without disrupting BBB. A129 mice were mock-inoculated or infected with $ZIKV_{PE243}$ or $ZIKV_{MR766}$ (2×10^5 PFU) by i.v. route. As a positive control of BBB disruption, some mice were inoculated with Plasmodium berguei ANKA, a model of cerebral malaria. After 2 or 5 days post infection, mice were i.v. injected with 0.5% Evans blue solution (EB); as a control some mice were injected with PBS (ctrl-). After 1 h, the brains were removed; liver, kidneys and spleen were also removed as controls, and all the organs were photographed for visualization of Evans Blue staining **(A)**. The amount of Evans blue was measured by optical spectroscopy, and the concentration of EB/mg tissue was calculated **(B)**.

REFERENCES

Ballabh, P., Braun, A., and Nedergaard, M. (2004). The blood-brain barrier: an overview: structure, regulation, and clinical implications. *Neurobiol. Dis.* 16, 1–13. doi: 10.1016/j.nbd.2003.12.016

Bayer, A., Lennemann, N. J., Ouyang, Y., Bramley, J. C., Morosky, S., Marques, E. T., et al. (2016). Type III interferons produced by human placental trophoblasts confer protection against Zika virus infection. *Cell Host Microbe* 19, 1–8. doi: 10.1016/j.chom.2016.03.008

Bramley, J. C., Drummond, C. G., Lennemann, N. J., Good, C. A., Kim, K. S., and Coyne, C. B. (2017). A three-dimensional cell culture system to model RNA virus infections at the blood-brain barrier. *mSphere* 2:e00206-17. doi: 10.1128/mSphere.00206-17

Calvet, G., Aguiar, R. S., Melo, A. S., Sampaio, S. A., de Filippis, I., Fabri, A., et al. (2016). Detection and sequencing of Zika virus from amniotic fluid of fetuses with microcephaly in Brazil: a case study. *Lancet Infect. Dis.* 16, 653–660. doi: 10.1016/S1473-3099(16)00095-5

Cao-Lormeau, V. M., Roche, C., Teissier, A., Robin, E., Berry, A. L., Mallet, H. P., et al. (2014). Zika virus, French Polynesia, South Pacific, 2013. *Emerg. Infect. Dis.* 20, 1085–1086. doi: 10.3201/eid2011.141380

Carteaux, G., Maquart, M., Bedet, A., Contou, D., Brugières, P., Fourati, S., et al. (2016). Zika virus associated with meningoencephalitis. *N. Engl. J. Med.* 374, 1595–1596. doi: 10.1056/NEJMc1602964

Chang, C. Y., Li, J. R., Chen, W. Y., Ou, Y. C., Lai, C. Y., Hu, Y. H., et al. (2015). Disruption of *in vitro* endothelial barrier integrity by Japanese encephalitis virus-infected astrocytes. *Glia* 63, 1915–1932. doi: 10.1002/glia.22857

Chanthick, C., Kanlaya, R., Kiatbumrung, R., Pattanakitsakul, S. N., and Thongboonkerd, V. (2016). Caveolae-mediated albumin transcytosis is enhanced in dengue-infected human endothelial cells: a model of vascular leakage in dengue hemorrhagic fever. *Sci. Rep.* 6:31855. doi: 10.1038/srep31855

Chen, C.-J., Ou, Y.-C., Li, J.-R., Chang, C.-Y., Pan, H.-C., Lai, C.-Y., et al. (2014). Infection of pericytes *in vitro* by Japanese encephalitis virus disrupts the integrity of the endothelial barrier. *J. Virol.* 88, 1150–1161. doi: 10.1128/JVI.02738-13

Coelho, S. V. A., Neris, R. L. S., Papa, M. P., Schnellrath, L. C., Meuren, L. M., Tschoeke, D. A., et al. (2017). Development of standard methods for Zika virus propagation, titration, and purification. *J. Virol. Methods* 246, 65–74. doi: 10.1016/j.jviromet.2017.04.011

Cugola, F. R., Fernandes, I. R., Russo, F. B., Freitas, B. C., Dias, J. L., Guimarães, K. P., et al. (2016). The Brazilian Zika virus strain causes birth defects in experimental models. *Nature* 534, 267–271. doi: 10.1038/nature18296

da Conceição, T. M., Rust, N. M., Berbel, A. C., Martins, N. B., do Nascimento Santos, C. A., Da Poian, A. T., et al. (2013). Essential role of RIG-I in the activation of endothelial cells by dengue virus. *Virology* 435, 281–292. doi: 10.1016/j.virol.2012.09.038

Daniels, B. P., and Klein, R. S. (2015). Viral sensing at the blood-brain barrier: new roles for innate immunity at the CNS vasculature. *Clin. Pharmacol. Ther.* 97, 372–379. doi: 10.1002/cpt.75

Delvecchio, R., Higa, L. M., Pezzuto, P., Valadão, A. L., Garcez, P. P., Monteiro, F. L., et al. (2016). Chloroquine, an endocytosis blocking agent, inhibits Zika virus infection in different cell models. *Viruses* 8:322. doi: 10.3390/v8120322

Dick, G. W., Kitchen, S. F., and Haddow, A. J. (1952). Zika virus. I. Isolations and serological specificity. *Trans. R. Soc. Trop. Med. Hyg.* 46, 509–520. doi: 10.1016/0035-9203(52)90042-4

Diefenbach, R. J., Miranda-Saksena, M., Douglas, M. W., and Cunningham, A. L. (2008). Transport and egress of herpes simplex virus in neurons. *Rev. Med. Virol.* 18, 35–51. doi: 10.1002/rmv.560

Dohgu, S., Ryerse, J. S., Robinson, S. M., and Banks, W. A. (2012). Human immunodeficiency virus-1 uses the mannose-6-phosphate receptor to cross the blood-brain barrier. *PLoS ONE* 7:e39565. doi: 10.1371/journal.pone.0039565

Dowall, S. D., Graham, V. A., Rayner, E., Atkinson, B., Hall, G., Watson, R. J., et al. (2016). A susceptible mouse model for Zika virus infection. *PLoS Neglec. Trop. Dis.* 10:e0004658. doi: 10.1371/journal.pntd.0004658

Driggers, R. W., Ho, C. Y., Korhonen, E. M., Kuivanen, S., Jääskeläinen, A. J., Smura, T., et al. (2016). Zika virus infection with prolonged maternal viremia and fetal brain abnormalities. *N. Engl. J. Med.* 374, 2142–2151. doi: 10.1056/NEJMoa1601824

Dudley, D. M., Aliota, M. T., Mohr, E. L., Weiler, A. M., Lehrer-Brey, G., Weisgrau, K. L., et al. (2016). A rhesus macaque model of Asian-lineage Zika virus infection. *Nat. Commun.* 28, 1–9. doi: 10.1038/ncomms12204

Faria, N. R., Azevedo, R. S., Kraemer, M. U., Souza, R., Cunha, M. S., Hill, S. C., et al. (2016). Zika virus in the Americas: early epidemiological and genetic findings. *Science* 352, 345–349. doi: 10.1126/science.aaf5036

Finke, S., and Conzelmann, K. K. (2005). Replication strategies of rabies virus. *Virus Res.* 111, 120–131. doi: 10.1016/j.virusres.2005.04.004

Fujiwara, T., Oda, K., Yokota, S., Takatsuki, A., and Ikehara, Y. (1988). Brefeldin: a causes disassembly of the Golgi complex and accumulation of secretory proteins in the endoplasmic reticulum. *J. Biol. Chem.* 263, 18545–18552.

Galliez, R. M., Spitz, M., Rafful, P. P., Cagy, M., Escosteguy, C., Germano, C. S., et al. (2016). Zika virus causing encephalomyelitis associated with immunoactivation. *Open Forum Infect. Dis.* 3:ofw203. doi: 10.1093/ofid/ofw203

Harmon, B., Schudel, B. R., Maar, D., Kozina, C., Ikegami, T., Tseng, C. T., et al. (2012). Rift Valley fever virus strain MP-12 enters mammalian host cells via caveola-mediated endocytosis. *J. Virol.* 86, 12954–12970. doi: 10.1128/JVI.02242-12

Janzer, R. C., and Raff, M. C. (1987). Astrocytes induce blood-brain barrier properties in endothelial cells. *Nature* 325, 253–257. doi: 10.1038/325253a0

Lanciotti, R. S., Kosoy, O. L., Laven, J. J., Velez, J. O., Lambert, A. J., Johnson, A. J., et al. (2008). Genetic and serologic properties of Zika virus associated with an epidemic, Yap State, Micronesia, 2007. *Emerg. Infect. Dis.* 14, 1232–1239. doi: 10.3201/eid1408.080287

Lazear, H. M., GoVero, J., Smith, A. M., Platt, D. J., Fernandez, E., Miner, J. J., et al. (2016). A mouse model of Zika virus pathogenesis cell host & microbe resource a mouse model of Zika virus pathogenesis. *Cell Host Microbe* 19, 1–11. doi: 10.1016/j.chom.2016.03.010

Liou, M. L., and Hsu, C. Y. (1998). Japanese encephalitis virus is transported across the cerebral blood vessels by endocytosis in mouse brain. *Cell Tissue Res.* 293, 389–394. doi: 10.1007/s004410051130

Lucey, D., Cummins, H., and Sholts, S. (2017). Congenital Zika Syndrome in 2017. *JAMA* 317, 1368–1369. doi: 10.1001/jama.2017.1553

Luethy, L. N., Erickson, A. K., Jesudhasan, P. R., Ikizler, M., Dermody, T. S., and Pfeiffer, J. K. (2016). Comparison of three neurotropic viruses reveals differences in viral dissemination to the centrl nervous system. *Virology* 487, 1–10. doi: 10.1016/j.virol.2015.09.019

Mahad, D., Callahan, M. K., Williams, K. A., Ubogu, E. E., Kivisäkk, P., Tucky, B., et al. (2006). Modulating CCR2 and CCL2 at the blood-brain barrier: relevance for multiple sclerosis. *Pathog. Brain* 129, 212–223. doi: 10.1093/brain/awh655

Martines, R. B., Bhatnagar, J., de Oliveira Ramos, A. M., Davi, H. P., Iglezias, S. D., Kanamura, C. T., et al. (2016). Pathology of congenital Zika syndrome in Brazil: a case series. *Lancet* 6736, 1–7. doi: 10.1016/S0140-6736(16)30883-2

Miner, J. J., and Diamond, M. S. (2016). Mechanisms of restriction of viral neuroinvasion at the blood-brain barrier. *Curr. Opin. Immunol.* 38, 18–23. doi: 10.1016/j.coi.2015.10.008

Miner, J. J., Cao, B., GoVero, J., Smith, A. M., Fernandez, E., Cabrera, O. H., et al. (2016). Zika virus infection during pregnancy in mice causes placental damage and fetal demise article Zika virus Infection during pregnancy in mice causes placental damage and fetal demise. *Cell* 165, 1081–1091. doi: 10.1016/j.cell.2016.05.008

Miranda-Filho, D. B., Martelli, C. M., Ximenes, R. A., Araújo, T. V., Rocha, M. A., Rodrigues, L. C., et al. (2016). Initial description of the presumed congenital Zika syndrome. *Am. J. Public Health* 106, 598–600. doi: 10.2105/AJPH.2016.303115

Mladinich, M. C., Schwedes, J., and Mackow, E. R. (2017). Zika virus persistently infects and is basolaterally released from primary human brain microvascular endothelial cells. *MBio* 8:e00952-17. doi: 10.1128/mBio.00952-17

Mlakar, J., Korva, M., Tul, N., Popović, M., Poljšak-Prijatelj, M., Mraz, J., et al. (2016). Zika virus associated with microcephaly. *N. Engl. J. Med.* 374, 951–958. doi: 10.1056/NEJMoa1600651

Morrey, J. D., Olsen, A. L., Siddharthan, V., Motter, N. E., Wang, H., Taro, B. S., et al. (2008). Increased blood-brain barrier permeability is not a primary determinant for lethality of West Nile virus infection in rodents. *J. Gen. Virol.* 89, 467–473. doi: 10.1099/vir.0.83345-0

Nikolskaia, O. V., de A. Lima, A. P., Kim, Y. V., Lonsdale-Eccles, J. D., Fukuma, T., Scharfstein, J., et al. (2006). Blood-brain barrier traversal by African trypanosomes requires calcium signaling induced by parasite cysteine protease. *J. Clin. Invest.* 116, 2739–2747. doi: 10.1172/JCI27798.

Noronha, L. D., Zanluca, C., Azevedo, M. L., Luz, K. G., and Santos, C. N. (2016). Zika virus damages thehuman placental barrier and presents marked fetal neurotropism. *Mem. Inst. Oswaldo Cruz* 111, 287–293. doi: 10.1590/0074-02760160085

Oliveira Melo, A. S., Malinger, G., Ximenes, R., Szejnfeld, P. O., Alves Sampaio, S., and Bispo de Filippis, A. M. (2016). Zika virus intrauterine infection causes fetal brain abnormality and microcephaly: tip of the iceberg? *Ultrasound Obstet. Gynecol.* 47, 6–7. doi: 10.1002/uog.15831

Racaniello, V. R. (2006). One hundred years of poliovirus pathogenesis. *Virology* 344, 9–16. doi: 10.1016/j.virol.2005.09.015

Rasmussen, S. A., Jamieson, D. J., Honein, M. A., and Petersen, L. R. (2016). Zika virus and birth defects — reviewing the evidence for causality. *N. Engl. J. Med.* 374, 1–7. doi: 10.1056/NEJMsr1604338

Reis, P. A., Estato, V., da Silva, T. I., d'Avila, J. C., Siqueira, L. D., Assis, E. F., et al. (2012). Statins decrease neuroinflammation and prevent cognitive impairment after Cerebral Malaria. *PLoS Pathog.* 8:e1003099. doi: 10.1371/journal.ppat.1003099

Retallack, H., Di Lullo, E., Arias, C., Knopp, K. A., Laurie, M. T., Sandoval-Espinosa, C., et al. (2016). Zika virus cell tropism in the developing human brain and inhibition by azithromycin. *Proc. Natl. Acad. Sci. U.S.A.* 113, 14408–14413. doi: 10.1073/pnas.1618029113

Roach, T., and Alcendor, D. J. (2017). Zika virus infection of cellular components of th eblood-retinal barriers: implications for viral associated congenital ocular disease. *J. Neuroinflamm.* 14:43. doi: 10.1186/s12974-017-0824-7

Rossi, S. L., Tesh, R. B., Azar, S. R., Muruato, A. E., Hanley, K. A., Auguste, A. J., et al. (2016). Characterization of a novel murine model to study Zika virus. *Am. J. Trop. Med. Hyg.* 94, 1362–1369. doi: 10.4269/ajtmh.16-0111

Salinas, S., Schiavo, G., and Kremer, E. J. (2010). A hitchhiker's guide to the nervous system: the complex journey of viruses and toxins. *Nat. Rev. Microbiol.* 8, 645–655. doi: 10.1038/nrmicro2395

Samuel, M. A., Wang, H., Siddharthan, V., Morrey, J. D., and Diamond, M. S. (2007). Axonal transport mediates West Nile virus entry into the central nervous system and induces acute flaccid paralysis. *Proc. Natl. Acad. Sci. U.S.A.* 104, 17140–17145. doi: 10.1073/pnas.0705837104

Saunders, N. R., Dziegielewska, K. M., Møllgård, K., and Habgood, M. D. (2015). Markers for blood-brain barrier integrity: how appropriate is Evans blue in the twenty-first century and what are the alternatives? *Front. Neurosci.* 9:385. doi: 10.3389/fnins.2015.00385

Schuler-Faccini, L., Ribeiro, E. M., Feitosa, I. M., Horovitz, D. D., Cavalcanti, D. P., Pessoa, A., et al. (2016). Possible association between Zika virus infection and microcephaly-Brazil, 2015. *Morb. Mortal Wkly Rep.* 65, 59–62. doi: 10.15585/mmwr.mm6503e2

Singh, P. K., Guest, J. M., Kanwar, M., Boss, J., Gao, N., Juzych, M. S., et al. (2017). Zika virus infects cells lining the blood-retinal barrier and causes chorioretinal atrophy in mouse eyes. *JCI Insight* 2, e923–e940. doi: 10.1172/jci.insight.92340

Srinivasan, B., Kolli, A. R., Esch, M. B., Abaci, H. E., Shuler, M. L., and Hickman, J. J. (2015). TEER measurement techniques for *in vitro* barrier model systems. *J. Lab. Autom.* 20, 107–126. doi: 10.1177/2211068214561025

Tripathi, S., Balasubramaniam, V. R., Brown, J. A., Mena, I., Grant, A., Bardina, S. V., et al. (2017). A novel Zika virus mouse model reveals strain specific differences in virus pathogenesis and host inflammatory immune responses. *PLoS Pathog.* 13:e1006258. doi: 10.1371/journal.ppat.1006258

Tugizov, S. M., Herrera, R., and Palefsky, J. M. (2013). Epstein-Barr virus transcytosis through polarized oral epithelial cells. *J. Virol.* 87, 8179–8194. doi: 10.1128/JVI.00443-13

Velandia-Romero, M. L., Acosta-Losada, O., and Castellanos, J. E. (2012). *In vivo* infectionby a neuroinvasiveneurovirulent dengue virus. *J. Neurovirol.* 18, 374–387. doi: 10.1007/s13365-012-0117-y

Verma, S., Lo, Y., Chapagain, M., Lum, S., Kumar, M., Gurjav, U., et al. (2009). West nile virus infection modulates human brain microvascular endothelial cells tight junction proteins and cell adhesion molecules: transmigration across the *in vitro* blood-brain barrier. *Virology* 385, 425–433. doi: 10.1016/j.virol.2008.11.047

Vermillion, M. S., Lei, J., Shabi, Y., Baxter, V. K., Crilly, N. P., McLane, M., et al. (2017). Intrauterine Zika virus infection of pregnantimmunocompetent mice models transplacental transmission and adverse perinataloutcomes. *Nat. Commun.* 21 145–175. doi: 10.1038/ncomms14575

Wang, T., Town, T., Alexopoulou, L., Anderson, J. F., Fikrig, E., and Flavell, R. A. (2004). Toll-like receptor 3 mediates West Nile virus entry into the brain causing lethal encephalitis. *Nat. Med.* 10, 1366–1373. doi: 10.1038/nm1140

Weaver, S. C., Costa, F., Garcia-Blanco, M. A., Ko, A. I., Ribeiro, G. S., Saade, G., et al. (2016). Zika virus: history, emergence, biology, and prospects for control. *Antiviral Res.* 130, 69–80. doi: 10.1016/j.antiviral.2016.03.010

WHO (2016). Available online at: http://www.who.int/mediacentre/news/statements/2016/emergency-committee-zika-microcephaly/en/

Zhu, Z., Chan, J. F., Tee, K. M., Choi, G. K., Lau, S. K., Woo, P. C., et al. (2016). Comparative genomic analysis of pre-epidemic and epidemic Zika virus strains for virological factors potentially associated with the rapidly expanding epidemic. *Emerg. Microbes Infect.* 5, 1–11. doi: 10.1038/emi.2016.48

Conflict of Interest Statement: The authors declare that the research was conducted in the absence of any commercial or financial relationships that could be construed as a potential conflict of interest.

The reviewer KS and handling Editor declared their shared affiliation.

frontiers in Microbiology

REVIEW
published: 28 March 2019
doi: 10.3389/fmicb.2019.00525

Pathways Exploited by Flaviviruses to Counteract the Blood-Brain Barrier and Invade the Central Nervous System

*Yasmin Mucunã Mustafá†, Lana Monteiro Meuren†, Sharton Vinícius Antunes Coelho† and Luciana Barros de Arruda**

Departamento de Virologia, Instituto de Microbiologia Paulo de Góes, Universidade Federal do Rio de Janeiro (UFRJ), Rio de Janeiro, Brazil

OPEN ACCESS

Edited by:
Gerald Alan Campbell, The University of Texas Medical Branch at Galveston, United States

Reviewed by:
Brian Daniels, Rutgers University, The State University of New Jersey, United States
Vanessa V. Sarathy, The University of Texas Medical Branch at Galveston, United States

***Correspondence:**
Luciana Barros de Arruda
arruda@micro.ufrj.br

†These authors have contributed equally to this work

Specialty section:
This article was submitted to Infectious Diseases, a section of the journal Frontiers in Microbiology

Received: *29 November 2018*
Accepted: *28 February 2019*
Published: *28 March 2019*

Citation:
Mustafá YM, Meuren LM, Coelho SVA and de Arruda LB (2019) Pathways Exploited by Flaviviruses to Counteract the Blood-Brain Barrier and Invade the Central Nervous System. Front. Microbiol. 10:525. doi: 10.3389/fmicb.2019.00525

Human infection by different flaviviruses may cause severe neurologic syndromes, through pathogenic mechanisms that are still largely unknown. Japanese encephalitis virus (JEV), West Nile virus (WNV), Zika virus (ZIKV), yellow fever virus (YFV), dengue virus (DENV), and tick-borne encephalitis virus (TBEV) are believed to reach the central nervous system by a hematogenous route, upon crossing the blood-brain barrier. Although the disruption of BBB during flavivirus infection has been largely evidenced in experimental models, the relevance of BBB breakdown for virus entering the brain was not completely elucidated. *In vitro* models of BBB had demonstrated that these viruses replicated in brain microvascular endothelial cells (BMECs), which induced downregulation of tight junction proteins and increased the permeability of the barrier. Other reports demonstrated that infection of BMECs allowed the basolateral release of infectious particles, without a remarkable cytopathic effect, what might be sufficient for virus invasion. Virus replication and activation of other cells associated to the BBB, mostly astrocytes and microglia, were also reported to affect the endothelial barrier permeability. This event might occur simultaneously or after BMECs infection, being a secondary effect leading to BBB disruption. Importantly, activation of BMECs, astrocytes, and microglia by flaviviruses was associated to the expression and secretion of inflammatory mediators, which are believed to recruit leukocytes to the CNS. The leukocyte infiltrate could further mediate viral invasion through a Trojan horse mechanism and might contribute to BBB breakdown and to neurological alterations. This review discussed the previous studies regarding *in vitro* and *in vivo* models of JEV, WNV, ZIKV, YFV, DENV, and TBEV infection and addressed the pathways for BBB overcome and invasion of the CNS described for each virus infection, aiming to increment the knowledge and stimulate further discussion about the role of BBB in the neuropathogenesis of flavivirus infection.

Keywords: blood-brain barrier, flavivirus, Japanese encephalitis virus, West Nile virus, Zika virus, dengue virus, yellow fever virus, brain microvascular endothelial cells

INTRODUCTION

Flaviviruses encompass arthropod transmitted viruses, which may cause systemic, hemorrhagic, and neurological syndromes. Japanese encephalitis virus (JEV), West Nile virus (WNV), Zika virus (ZIKV), yellow fever virus (YFV), dengue virus (DENV), and tick-borne encephalitis virus (TBEV) are some of the most prevalent flaviviruses associated to human diseases in different regions of the world. Most of the individuals affected by those infections develop asymptomatic or mild manifestations, but these viruses may cause severe neurologic syndromes, once they reach the central nervous system (CNS).

The frequency of neurological manifestations upon flavivirus infection varies considerably depending on the virus. Severe infection by JEV, WNV, TBEV, and congenital ZIKV is associated to encephalitis and other neurological syndromes (Lindquist and Vapalahti, 2008; Melo et al., 2016; Salimi et al., 2016; Samy et al., 2018), whereas the severe disease caused by DENV and YFV are more related to vascular and systemic manifestations (Jennings et al., 1994; Monath and Barrett, 2003; Beck and Barrett, 2015; Halstead and Cohen, 2015; Screaton et al., 2015; Li et al., 2017). Even though these viruses usually do not affect the CNS, a recent surveillance study performed in Brazil reported the presence of laboratory markers of DENV and ZIKV in patients with acute neurological diseases. Among 74 studied cases, 2 patients presented DENV RNA in the CSF and 6 patients showed anti-DENV IgM in the serum. Also, three patients showed ZIKV RNA or IgM in the CSF or in the serum. These data suggest that arboviruses may play a more important role in CNS-associated disease than previously found, at least in endemic countries where the number of infected individuals is very high (Vieira et al., 2018).

All the referred viruses are able to infect neurons, albeit they are not always neuroinvasive (Jennings et al., 1994; Ramos et al., 1998; Chen et al., 2012; Hussmann et al., 2013; Garcez et al., 2016). Viruses can reach the brain through different mechanisms, including peripheral nervous system and axonal transport, and hematogenous route. Although experimental models had previously indicated that some flaviviruses, such as WNV and JEV, disseminated *via* axonal transport or through the olfactory bulb, those models were developed using intrasciatic and intranasal inoculation (Samuel et al., 2007; Yamada et al., 2009), which may not represent their natural infection route. Given the systemic nature of flavivirus infection, and since a disruption of the blood-brain barrier (BBB) is often observed in experimental models of infection, it is believed that crossing this structure is a major mechanism for flavivirus neuroinvasion (Verma et al., 2010; Jurado et al., 2018; Wang et al., 2018).

The BBB is a complex structure, composed by tightly adhered brain microvascular endothelial cells (BMECs), which are associated to pericytes, astrocytes, and microglia. This structure constitutes a barrier between the blood and the CNS parenchyma, acting in the flux regulation of solutes, cells, and pathogens (**Figure 1A**; Ballabh et al., 2004). The cells associated to the BBB express a collection of pattern recognition receptors (PRR) and are able to respond to PAMPs derived from pathogens and to DAMPs released upon CNS damage (Zamanian et al., 2012; da Conceição et al., 2013; Minkiewicz et al., 2013; Wan et al., 2014). Therefore, an inflammatory insult or other pathobiological conditions that affect their metabolism may impact the barrier function (Argaw et al., 2012; Sofroniew, 2015).

BMECs are unique unfenestrated polarized endothelial cells, connected by continuous tight junctions (TJs). The junctions are composed of TJ proteins – claudins and occludin, and of adhesion molecules – E- and VE-cadherins. The TJ complex is stabilized by its association to intracellular cytoskeleton through adaptor proteins, such as zonula occludens (ZO), among others (Chow and Gu, 2015). Those features, in association to the low rate vesicular trafficking of the brain endothelial cells, turn them more resistant to paracellular and transcellular trafficking, in comparison to endothelial cells from other tissues (Obermeier et al., 2013; Siegenthaler et al., 2013; Chow and Gu, 2015). In addition, BMECs express low levels of leukocyte adhesion molecules, limiting the infiltration of immune cells into the brain (Siegenthaler et al., 2013). Virus infection of BMECs may result in cell death or in decreased expression and organization of TJ proteins, directly impacting the integrity of the endothelial monolayer. The activation of the BMECs due to virus replication may also promote the production of mediators that affect the BBB structure and stimulate leukocyte recruitment, including cytokines, such as IL-6 and TNF-α, reactive oxygen and nitrogen species (ROS, NO), and prostaglandins (Schreibelt et al., 2007; da Conceição et al., 2013; Rochfort et al., 2014; Papa et al., 2017; Soe et al., 2017).

BBB endothelial cells are surrounded by the basement membrane, and the structure and function of this core are supported and regulated by adjacent pericytes, astrocytes, and microglia (Chow and Gu, 2015). Astrocytes endfeet covers most of the CNS vasculature, connecting it to the neuronal parenchyma. Therefore, mediators produced upon BMEC activation or after CNS damage affect the function of astrocytes. Also, these cells may be directly infected and activated by viruses (Hussmann et al., 2013; Chang et al., 2015). All the cited stimuli promote a response called astrogliosis, and reactive astrocytes produce cytokines, chemokines, prostaglandins, and nitric oxide (Argaw et al., 2012; Zamanian et al., 2012; Sofroniew, 2015). These mediators modulate angiogenesis, affect TJ proteins expression and organization, restrict or stimulate leukocyte infiltration, and impact neuronal function.

Hence, insults like virus infection and inflammation can stimulate BMECs, astrocytes, and other cells to secrete mediators that will ultimately affect the BBB integrity and CNS function (Fabry et al., 1995; Argaw et al., 2012; Heinemann et al., 2012; Alvarez et al., 2013).

Given the systemic nature of flavivirus infection and the physiological function of the BBB, it is generally believed that BBB disruption is a determinant event preceding viral invasion. A major point supporting this conception is that BMECs, which are the main cell types in the BBB and are susceptible to all neurotropic flaviviruses. Virus replication often induces apoptosis, and several studies suggested that neuroinvasion involved infection of BMECs (Wang et al., 2008a,b; Verma et al., 2009; da Conceição et al., 2013; Lazear et al., 2015; Al-Obaidi et al., 2017; Papa et al., 2017; Patabendige et al., 2018). It is important to notice,

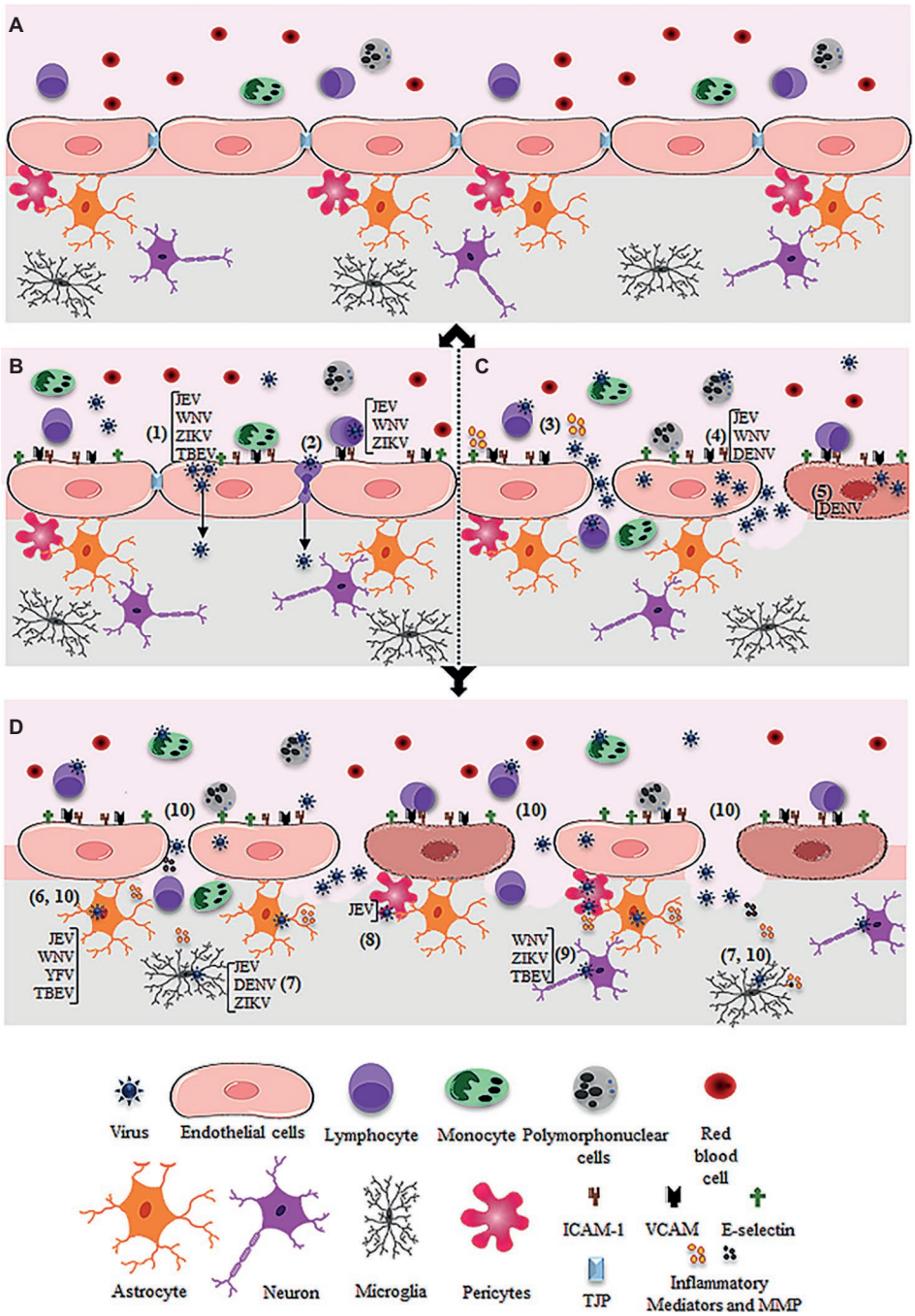

FIGURE 1 | Schematic figure showing possible mechanism of virus entry into the central nervous system through the blood-brain barrier. **(A)** Intact blood-brain barrier is composed by endothelial cell strongly adhered through tight junction proteins (TJP), in association to pericytes, astrocytes, and microglia. The barrier controls the flux of solutes, blood cells (lymphocytes, monocytes, and polymorphonuclear cells), and pathogens from the blood to the central nervous system. **(B)** After systemic infection, some flavivirus reaches the BBB through hematogenous route and may cross the endothelial barrier without remarkable cytopathic effect. JEV, WNV, ZIKV, and TBEV may cross the endothelial barrier as cell-free virus **(1)**. JEV, WNV, and ZIKV were also reported to traverse the endothelial barrier associated to infected leukocytes **(2)**. **(C)** Systemic infection and inflammation and/or the direct infection of brain endothelial cells may induce BBB breakdown, allowing virus invasion of the CNS. Regarding this, systemic inflammation due to activation of immune cells upon infection was associated to the release of inflammatory mediators, which then affect the permeability of the endothelial barrier **(3)**. Also, replication of JEV, WNV, and DENV in the brain endothelial cells may induce downregulation of TJP expression **(4)** and/or cell death **(5)**, promoting the barrier disruption and virus entry. **(D)** After entry into the brain by any of the described pathways **(B and C)**, flaviviruses may infect the astrocytes (as described for JEV, WNV, YFV, TBEV) **(6)**, microglia (as described for JEV, DENV, ZIKV) **(7)**, pericytes (as described for JEV) **(8)**, and neurons (as described for WNV, ZIKV, TBEV) **(9)**. The infection of these cells, especially astrocytes and microglia, induces the release of inflammatory mediators (IL-6, VEGF, TNF-α, IFN-γ, IL-1β and IL-10, MCP-1) and metalloproteinases (MMP2, MMP3, MM9) **(10)**, which mediate the downregulation of adherents and tight junction proteins (TJP), resulting in increased permeability.

however, that due to technical issues inherent to analysis of brain tissues, there are very few studies confirming the infection of BMECs upon human natural infection (Johnson et al., 1985; Ramos et al., 1998). The great majority of the studies were done *in vitro*, with transformed cell lines (da Conceição et al., 2013; Patabendige et al., 2018). Also, since wild-type adult mice were resistant to infection, most of the studies performed *in vivo* used immunodeficient or suckling mice (Velandia-Romero et al., 2012; Daniels et al., 2017; Papa et al., 2017). Therefore, although flavivirus replication in BMEC has been largely demonstrated in experimental models, further analyses of human tissues are critical to further support this hypothesis.

Increasing evidence suggest that flaviviruses can also reach the CNS by crossing the BBB, without barrier breakdown. The basolateral release of infectious particles upon virus replication in BMECs was described in different experimental models, in which no significant cytopathic effect (CPE) had been detected (Verma et al., 2009; Papa et al., 2017). Virus crossing by transcytosis in brain endothelial cells had also been reported (Liou and Hsu, 1998; Papa et al., 2017) and may allow free virus to reach and infect the neurons. Flavivirus may also reach the CNS as cell-associated particles, through a mechanism called "Trojan horse" (Verma et al., 2009). In this context, peripheral-infected leukocytes transmigrate through the endothelial cell layer and release virus within the CNS. The released infectious particles can then infect resident cells. In healthy conditions, the BBB restricts leukocyte infiltration. Therefore, virus invasion through a Trojan horse mechanism requires either a rupture in the BBB structure or alterations of the TJ that allows paracellular migration of the cells. Activation of brain endothelial cells, with increased expression of adhesion receptors and enhanced secretion of chemokines, is also required to attract the infected leukocytes to the brain.

Viral invasion of CNS by all these mechanisms is often followed by leukocyte infiltration. Both virus replication in neurons and the local inflammatory response triggered afterward were reported to be relevant in the neuropathogenesis of flavivirus infection (Roe et al., 2012; Velandia-Romero et al., 2012; Li et al., 2015; Douam et al., 2017; Jurado et al., 2018; Lucas et al., 2018; Wang et al., 2018). Subsequent inflammation elicited after virus invasion of the CNS may also contribute to BBB breakdown and amplify the whole process.

In this review, we will address whether the flaviviruses such as JEV, WNV, ZIKV, YFV, DENV, and TBEV infect BMECs and whether this infection is relevant for the release of infectious particles, able to disseminate through the CNS, and for the disruption of BBB. We will also consider if the infection of other cell types associated to the BBB, such as pericytes, astrocytes, and microglia, triggers cellular activation and the role of this secondary effect for BBB disruption. Finally, we will discuss whether BBB disruption is indeed essential for virus dissemination into the brain.

JAPANESE ENCEPHALITIS VIRUS

Japanese encephalitis virus (JEV) is an important virus agent causing neuropathological disorders in Asia, Australia, and Western Pacific (Samy et al., 2018). Although most individuals infected by JEV present subclinical or febrile mild infection, a small proportion of patients develop encephalitis or meningoencephalitis, which is often fatal or may lead to permanent motor or cognitive deficits (Salimi et al., 2016). Neuroinfection is characterized by disruption of the BBB and extensive inflammation in the brain (Bian et al., 2017; Wang et al., 2018). However, the pathway of JEV entry into the CNS and mechanisms associated to the inflammatory response are not completely elucidated.

JEV is able to infect a variety of cell types present in the BBB, including BMECs, microglia, astrocytes, and pericytes, and *in vitro* infection models have been exploring the effect of viral replication on BBB permeability (Chen et al., 2012, 2014; Chang et al., 2015). Infection of BMECs by JEV did not affect cell viability but resulted in increased permeability of the endothelial monolayer (Lai et al., 2012; Al-Obaidi et al., 2017; Patabendige et al., 2018), suggesting that virus-induced cell death is not the mechanism responsible for BBB disruption and viral invasion. Accordingly, JEV infection of multiple cell types diminished the expression and altered the localization of adherents and tight junction proteins. This effect was also observed when the cells were cultured with virus capsids, instead of infectious particles, suggesting that altered endothelial permeability may happen even in the absence of productive viral replication (Agrawal et al., 2013).

Other studies, however, reported that JEV infection promoted negligible effect on transendothelial electrical resistance (TEER) of rat-derived isolated BMEC, unless they were cultured with other cell types associated to the BBB (Chen et al., 2014; Chang et al., 2015). Among those cells, pericytes and astrocytes are both permissive to JEV replication. Infection of these cells, *in vitro*, induced the release of soluble mediators that degrade tight junction proteins, particularly zonula occludens-1 (ZO-1) (Chen et al., 2014; Chang et al., 2015). Indeed, addition of pericytes or conditioned medium derived from infected pericytes to a culture of BMECs induced endothelial permeability, in a pathway partially dependent on secreted proteases and IL-6 (Chen et al., 2014). Similarly, culture of BMECs with conditioned medium obtained from JEV-infected astrocytes induced the degradation of ZO-1 and claudin-5 and BMEC permeability, in a way dependent on IL-6, VEGF, and metalloproteinases (MMP-2/MMP-9) (Chang et al., 2015).

An *in vitro* model of human BBB, using human BMECs (HBMECs) and astrocyte cell lines, also demonstrated that both cell types were susceptible to JEV (Patabendige et al., 2018). The interaction of endothelial cells with astrocytes was necessary for JEV-induced BBB permeability, and it was associated to increased secretion of inflammatory cytokines. Microglial cells were also activated upon JEV infection *in vitro* and produced inducible nitric oxide synthase (iNOS), IL-1β, IL-6, MCP-1, and TNF-α (Thounaojam et al., 2014), what may contribute to endothelial barrier dysfunction. According to these studies, JEV-induced BBB breakdown seems to be rather a bystander event than to direct virus replication in BMECs. However, JEV interaction with the endothelial cells could initiate the process, by allowing virus access to pericytes, astrocytes,

and microglia, which would, then, secrete mediators that degrade the tight junctions and disrupt the barrier.

Mouse and primate *in vivo* experimental models supported that JEV infection promoted BBB breakdown, leukocyte infiltration, and activation of astrocytes and microglia (Myint et al., 2014; Li et al., 2015; Wang et al., 2018). BBB disruption due to decreased expression of ZO-1 and claudin-5 was detected in JEV-infected mice at the time point when neuropathological syndrome was evident (Li et al., 2015; Wang et al., 2018). In addition, the presence of activated astrocytes and microglia and a robust production of inflammatory cytokines, including TNF-α, IL-6, CCL5, CXCL10, IFN-γ, and CCL2, were detected in the brains of JEV-infected mice (Li et al., 2015; Bian et al., 2017; Patabendige et al., 2018; Wang et al., 2018).

It was also reported that cultivation of an endothelial cell line with brain extracts obtained from JEV-infected mice downregulated the expression of tight junction proteins. In contrast, infection of isolated endothelial cells with JEV did not alter their expression or cell permeability (Li et al., 2015). These data corroborated the hypothesis that infection of endothelial cells *per se* was not responsible for BBB breakdown. Indeed, other findings suggested that the inflammatory response triggered after viral dissemination to CNS promoted BBB permeability and consequent neurological syndrome. First, JEV-infected mice presented virus RNA in the brain from 2 days post infection (dpi), whereas significant BBB disruption was only observed after 4 dpi (Li et al., 2015). Also, treatment of infected mice with neutralizing anti-IFN-γ or anti-CXCL10 antibodies preserved the BBB integrity, with no significant effect on the brain viral load (Li et al., 2015; Wang et al., 2018). Importantly, BBB breakdown was only detected in the mice that developed severe symptoms. These findings support that JEV can reach the CNS independent of BBB disruption, but subsequent events disturb the barrier, which might be a major event related to neurological disease.

Although JEV replication in the brain endothelial cells does not appear to be a major event for virus neuroinvasion, it might be relevant for the subsequent inflammation in the CNS *in vivo*. JEV infection of BMECs promoted the expression of adhesion molecules and secretion of chemokines, enhancing leukocytes adhesion (Lai et al., 2012). However, it should be noticed that leukocyte infiltration is not always deleterious to the host. In this sense, the presence of activated $CD8^+$ T cells in the brains of JEV-infected mice was associated with lower mortality and preservation of the BBB integrity (Jain et al., 2017). Therefore, the profile of activated immune cells that cross the BBB and reach the brain might determine disease outcome.

WEST NILE VIRUS

West Nile virus (WNV) was first isolated in 1937 in Uganda, and during several decades, it was associated to occasional outbreaks in Africa and in the Middle East. Since the decade of 1990, WNV spread to different countries in Europe and Americas, especially United States, and it is now considered one of the most geographically widespread arboviruses in the world. It is estimated that around 80% of the infections are subclinical and most of the symptomatic patients will develop what is called West Nile fever. However, a small proportion of the infected individuals may develop a severe or neuroinvasive disease, leading to encephalitis and meningitis (Sejvar et al., 2003).

There are some hypotheses for WNV neuroinvasion, including the hematogenous and the transneural routes (Suen et al., 2014), and increasing evidence indicate that WNV entry into the CNS is a multistep process employing different mechanism as the infection progresses. Here, we will focus in the studies evaluating CNS invasion after systemic inoculation, which supports the hematogenous pathway of virus entry.

The role of BBB disruption for WNV neuroinvasion and infection-mediated neuropathology is controversial. Several reports demonstrated that WNV infects brain endothelial cells, astrocytes, and neuron cells (Dai et al., 2008; Verma et al., 2010; Hussmann et al., 2013). Direct infection of BMECs induced degradation of tight junction proteins, in a pathway apparently dependent on their endocytosis and lysosomal degradation (Xu et al., 2012). Although endothelial barrier permeability was not directly addressed in this model, disorganization of tight junctions was proposed as a mechanism of BBB disruption and neuroinvasiveness. Other studies, however, indicated that direct infection of BMECs did not result in increased permeability. It is then proposed that viral invasion and neurovirulence are a more complex multistep process involving virus replication in different cell types, along with systemic and neuronal inflammation.

Verma et al. (2009) used an *in vitro* model of BBB, composed of primary HBMEC infected with the neurovirulent strain of WNV (NY99), and they observed that cell-free WNV crossed the endothelial barrier without affecting its integrity. Increased expression of the adhesion molecules VCAM-1 and E-selectin was observed at the peak of WNV replication, suggesting that the infection of endothelial cells might facilitate the migration of leukocytes (Verma et al., 2009). Infiltrating leukocytes could be later associated to virus entry into the brain *via* "Trojan horse" mechanism. Another study demonstrated that WNV virus-like particles (VLPs) were able to cross human umbilical vein endothelial cells (HUVEC) from the apical to the basolateral sides, suggesting that transendothelial migration of WNV may occur independent of viral replication (Hasebe et al., 2010). Comparison between VLPs from high and low virulent strains demonstrated that the first presented a higher migration efficiency in comparison to the latter. ZO-1 expression and endothelial permeability were not altered during VLP transport, and transendothelial migration was inhibited by filipin (Hasebe et al., 2010). These data support the hypothesis that WNV crosses the blood endothelial barrier, in a pathway dependent of raft-associated membrane transport, that causes no direct effect on the barrier integrity. However, this study was performed with HUVECs, and the findings need to be confirmed in brain endothelial cells.

In order to further understand the neuroinvasive differences observed between WNV strains, Hussmann et al. (2013) compared the infection rate of an avirulent WNV lineage (MAD78 strain) to a highly virulent lineage (New York strain), in neurons, astrocytes, and microvascular endothelial cells. Both strains

replicated efficiently in neurons and BMECs. Also, similar levels of infectious particles were detected in the luminal and abluminal chambers of a transwell system with infected BMECs. Thus, the ability of WNV to infect the endothelial cells and to cross the BBB might not be the main responsible for the differential neuroinvasiveness of the virus strains. This diverges with the data obtained with VLP (Hasebe et al., 2010); however, different strains and distinct endothelial cell lines were used in the referred studies. Alternatively, the differences detected with VLPs from distinct strains might be overcome during a productive infection. In the study from Hussmann, the low virulent strain replicated less efficiently in astrocytes, exhibiting a delay in viral genome synthesis and reduced cell-to-cell spread in this cell type. Furthermore, in a transwell system in which infected HBMECs were seed in the luminal chamber, with astrocytes cultured in the abluminal one, there was significant lower virus expression in the astrocytes, indicating that these cells could restrain virus spread within the CNS (Hussmann et al., 2013).

On the other hand, astrocyte activation seems to participate in the rupture of BBB observed during infection. Verma et al. (2010) demonstrated that infection of HBCA astrocyte cell line with WNV upregulated the expression of MMP-1, -3, and -9 along with a downregulation of TIMP-2. Culture of microvascular endothelial cells with supernatants obtained from WNV-infected HBCA diminished the expression of claudin and ZO-1 and increased the permeability of *in vitro* BBB (Verma et al., 2010). All these events were reversed by previous treatment of the supernatants with MMP inhibitors, corroborating the idea that WNV-induced production of MMPs by astrocytes may disrupt the barrier, even when the endothelial cells are not infected.

The relevance of BBB breakdown for virus invasion of CNS, neurovirulence, and lethality of WNV *in vivo* is also controversial. Morrey et al. (2008) and Wang et al. (2004) demonstrated an increased permeability of the BBB upon WNV infection of C57BL/6 mice. In contrast, infection of BALB/c mice did not induce BBB permeability, despite leading to death (Morrey et al., 2008). Those data indicated that WNV entry in the CNS might be independent of BBB breakdown, although viral load in the brains had not been accessed in this model. The hypothesis that BBB permeability may be a consequence and not a cause of the virus entry in the CNS was supported by other *in vivo* study with C57BL/6 mice. In this model, BBB disruption upon WNV infection occurred along the course of infection and not prior to the entry of CNS. BBB breakdown resulted from decreased expression of tight and adherent junction proteins (claudin-1, occludin, ZO-1, and JAM-A; β-catenin and VE-cadherin) and correlated with the peak of WNV titers, increased production of matrix metalloproteinases (MMPs), and leukocyte infiltration in the brain (Roe et al., 2012). Importantly, intracranial inoculation of WNV also induced increased MMP expression and BBB permeability, suggesting that BBB breakdown could be induced by virus replication into the brain (Roe et al., 2012).

Mice deficient in MMP9 expression ($MMP9^{-/-}$ KO mice) were more resistant to infection, in comparison to WT mice, despite presenting equivalent viremia and similar levels of inflammatory cytokines and IFN-α in the circulation. However, $MMP9^{-/-}$ animals presented lower viral load in the brains, accompanied by less BBB permeability, less leukocyte infiltrates, and decreased levels of cytokines in this tissue (Wang et al., 2008a). It is important to notice that despite high viremia, no detectable permeability of the BBB was observed at early time points after infection. Clear BBB breakdown was only detected at late time points, when brain viral titer was already high (Wang et al., 2008a), indicating that virus invasion preceded BBB disruption. These findings and the *in vitro* transwell data support the hypothesis that WNV can migrate through the endothelial cells, what may allow the infection of astrocytes. Astrocytes could be then the cell source of MMP, leading to subsequent BBB breakdown and neuropathology.

Besides or along with virus replication in endothelial brain barrier, leukocyte recruitment appears to be an important event associated to BBB disruption and viral neurovirulence. As previously described, infection of endothelial cell lines with WNV induced increased expression of adhesion molecules (Dai et al., 2008; Roe et al., 2014). Lymphocytes and monocytes showed efficient adhesion and migration through a monolayer of WNV-infected HBMECs. Also, the treatment of WNV-infected endothelial cells with anti-ICAM or anti-VCAM neutralizing antibodies abolished leukocyte adhesion and migration and resulted in decreased endothelial permeability (Roe et al., 2014). Infection of C57BL/6 mice with WNV NY strain also resulted in increased expression of ICAM-1, VCAM-1, and E-selectin in the brain (Dai et al., 2008). ICAM-deficient mice showed similar systemic viral load and inflammatory cytokine levels, in comparison to WT mice. However, $ICAM\text{-}1^{-/-}$ mice presented decreased BBB permeability, with lower leukocyte infiltration, diminished brain viral load and neuronal damage, and increased survival, in comparison to WT mice (Dai et al., 2008).

According to the referred data, it is tempted to speculate that WNV infection of BMECs might be a first essential event occurring after viremia that allows virus transmigration into the CNS. BMEC infection also induced an increased expression of adhesion molecules and production of chemokines, which could contribute to the recruitment of monocytes, lymphocytes, and polymorphonuclear cells to the barrier. The detection of augmented MMP9 expression in the brains after virus replication (Wang et al., 2008a) suggests that subsequent virus infection of other cell types may trigger a secondary BBB disruption that then allows leukocyte infiltration. The latter event would contribute for further virus invasion through a Trojan horse mechanism. This idea is supported by recent mouse experimental data showing that cerebral osteopontin stimulated the infiltration of WNV-infected neutrophils, leading to increased viral burden in the brain and mortality (Paul et al., 2017). Also, virus proteins were detected in the lymphocytes from the brain of WNV-infected mice, suggesting that infiltrating T cells might be a source of virus entering the CNS following a systemic infection (Wang et al., 2008b).

The relevance of the systemic immune response to later BBB breakdown and virus invasion was also sustained by an earlier article accessing the role of innate immune activation for WNV neural disease. The study demonstrated that

TLR3-deficient mice showed lower levels of IL-6, TNF-α, and type I IFN in the blood and in the brains. TLR3-deficient mice were protected from BBB breakdown, viral invasion, leukocyte infiltration, and lethality (Wang et al., 2004), indicating that systemic inflammation was determinant for virus dissemination. After that, several studies have been investigating the role of different elements of innate immune response in the protection or enhancement of WNV neurovirulence. It was reported that signal transduction mediated by type III or type I IFN receptors was important for the maintenance of BBB integrity and for controlling WNV neuroinvasion (Lazear et al., 2015; Miner et al., 2015; Daniels et al., 2017). *In vitro* infection of different cell types demonstrated that IFN-λ addition or depletion did not significantly affect WNV replication. Still, systemic WNV infection of mice deficient in IFN-λ receptor (Ifnlr1$^{-/-}$) resulted in higher virus concentration in the brain and spinal cord, despite similar viral load in the blood, spleen and other systemic tissues (Lazear et al., 2015). The only difference detected between WT and Ifnlr1$^{-/-}$ mice was an increased BBB permeability in the latter. In addition, using a transwell model of BBB, it was demonstrated that IFNLR signal in BMEC increased barrier resistance. These data indicated that, although IFN-λ did not inhibit virus replication *in vitro* or *in vivo*, it increased barrier integrity and protected mice from the neurological effects caused by WNV infection. Importantly, no difference of brain viral load was detected upon intracerebroventricular inoculation of Ifnlr1$^{-/-}$ mice with WNV, supporting the idea that the major protective role of IFN-λ was the maintenance of the barrier strength.

Type I IFN signaling pathway was also reported to be pivotal for the maintenance of BBB integrity, at least in experimental models. Daniels et al. (2014) demonstrated that addition of type I IFN to an *in vitro* culture of murine BMEC infected with WNV preserved BBB integrity and tight junction organization and reduced viral traffic through the endothelial monolayer. Also, BMECs obtained from ifnar$^{-/-}$ mice exhibited a significant reduction in TEER and increased secretion of TNF-α and IL-1β upon WNV infection *in vitro*. It was then suggested that type I IFN might regulate the transendothelial trafficking of WNV by restraining the BBB permeability induced by those cytokines (Daniels et al., 2014). *In vivo* data corroborated these findings, since IFNAR (ifnar$^{-/-}$) or IRF7 (irf7$^{-/-}$) knockout mice infected with WNV presented higher BBB permeability and tight junction dysregulation compared to WT mice. Another mouse experimental model of WNV infection demonstrated that selective depletion of IFNAR in astrocytes resulted in increased BBB permeability, viral neuroinvasion, neuronal cell death, and immunopathology. Importantly, the loss of signaling *via* astrocyte IFNAR led to higher mortality rate of WNV-infected mice due to augmented virus entry, but not to virus replication into the brain (Daniels et al., 2017). These findings corroborated the *in vitro* data showing that the activation of astrocytes was determinant for BBB disruption.

Finally, the relevance of the BBB for WNV neurovirulence was accessed in mice deficient in several TAM receptors. In a study performed by Miner et al. (2015), it was demonstrated that Axl/Mertk-deficient mice exhibited increased BBB permeability and higher viral load and mortality upon subcutaneous infection of WNV, in comparison to wild-type mice (Miner et al., 2015). In contrast, no difference in viral expression in the brain was detected when the virus was inoculated directly in the CNS by intracranial injection. These findings suggest that TAM receptors exert their protective role by preserving BBB integrity and restricting virus invasion of the CNS rather than affecting neuronal replication. Interestingly, it was also showed that Mertk-depleted BMECs were less responsive to IFN-β, indicating that cooperation between TAMR and IFNAR may be a mechanism for endothelial barrier protection (Miner et al., 2015).

ZIKA VIRUS

Zika virus (ZIKV) was first described in Uganda, in 1947, and the first human cases were reported in 1963 (Dick et al., 1952; Simpson, 1964). Very few cases of human infection had been described in Africa and Asia until 2007, when an outbreak occurred at Yap Islands. Another outbreak at French Polynesia was reported in 2013, and from 2015 to 2016, a huge epidemic started in Brazil and spread throughout Americas (Duffy et al., 2009; Musso, 2015; Bogoch et al., 2016; Faria et al., 2016). Since then, ZIKV infection was associated with microcephaly and other neurological manifestations in fetuses and newborns upon vertical transmission, and this is now collectively called Zika congenital syndrome (Melo et al., 2016; Oliveira Melo et al., 2016). Although less frequent, neurological disorders have also been reported in adults, including encephalitis and Guillain-Barre syndrome (Brasil et al., 2016; Carteaux et al., 2016). ZIKV was detected in the post-mortem brains of microcephalic fetuses or stillborns and in the CSF of encephalitic adult (Carteaux et al., 2016; Mlakar et al., 2016), indicating that the virus invades the CNS. Indeed, numerous studies indicated that ZIKV is neurotropic. Viral particles and RNA were detected in the brain of mice inoculated by different pathways (Cugola et al., 2016; Li et al., 2016); in brain organoids infected *in vitro* (Garcez et al., 2016); and in the CSF of infected rhesus monkeys (Dudley et al., 2016). However, the mechanisms associated to brain invasion are still unclear.

Previous evidence indicated that endothelial cells from the BBB are permissive to replication of different ZIKV strains and that the virus may cross the endothelial barrier, without inducing a significant increase in its permeability (Shao et al., 2016; Al-Obaidi et al., 2017; Bramley et al., 2017; Mladinich et al., 2017; Papa et al., 2017; Alimonti et al., 2018). Mladinich et al. (2017) showed that ZIKV (Porto Rico strain PRVABC59) infected and replicated efficiently in primary human brain microvascular endothelial cells (HBMECs). ZIKV was basolaterally released in a transwell system, without inducing a remarkable cytopathic effect (Mladinich et al., 2017). Similarly, Papa et al. (2017) demonstrated that infection of HBMECs with African and Brazilian ZIKV strains ($ZIKV_{MR766}$ and $ZIKV_{PE243}$) resulted in efficient virus replication and basolateral release of infectious particles, which were able to replicate in other cell types seeded separately in a transwell system. It is important

to notice that infection with $ZIKV_{PE243}$ strain did not induce a remarkable CPE and no cell death was detected in the cultures, whereas infection with $ZIKV_{MR766}$ was associated to some level of cytopathic effect. The viruses crossed the endothelial barrier with no apparent increase in permeability, which was further confirmed by the maintenance of tight junction protein expression and localization (Papa et al., 2017). The study suggested that ZIKV might cross the endothelial barrier by endocytosis and exocytosis-dependent replication pathway or by transcytosis. Infection with both strains also induced HBMEC activation and secretion of IL6 and CCL5, what may contribute to the recruitment of leukocytes in an *in vivo* fashion (Papa et al., 2017). Other studies that used brain endothelial cells (i-BMECs) derived from pluripotent stem cell (iPSC) also confirmed that ZIKV (Canadian isolate) infected and traversed the iBMECs, without compromising the BBB (Alimonti et al., 2018). On the other hand, a 3D cell culture system using an HBMEC cell line showed a certain resistance to infection in comparison to conventional 2D culture. However, pretreatment of the cultures with inflammatory cytokines, such as TNF-α, increased virus replication and disorganization of the junctional network, indicating that an inflammatory response triggered *in vivo* might contribute to BBB disruption and ZIKV invasion of the brain. This study also established a transwell culture, in which HBMECs were seeded in the inserts and astrocytes in the abluminal chamber. Using this system, it was demonstrated that HBMECs allowed the migration of infected monocytes, which then enhanced the infection of the astrocytes (Bramley et al., 2017).

In vivo experimental models supported the hypothesis that ZIKV may cross the BBB without severe disruption. In the study from Papa and colleagues using IFNAR-deficient mouse model, the presence of virus RNA was noticed very early after systemic infection, when no BBB disruption had been detected (Papa et al., 2017). Immunostaining revealed the presence of ZIKV envelope protein in blood vessels and in the cells of plexus choroid of subventricular zone, suggesting that brain endothelial cells were indeed infected by the virus. Interestingly, barrier breakdown was detected at later time points upon infection. Given that leukocytes recruitment to the brains seems to be determinant for neuronal lesion and lethality induced by ZIKV (Jurado et al., 2018), one can speculate that later BBB disruption was possibly triggered by the inflammatory response that followed virus replication. Another study comparing different ZIKV strains revealed that, depending on the mouse age, infection with $ZIKV_{MR766}$, but not with $ZIKV_{PE243,}$ resulted in mouse death (Lucas et al., 2018). Evidence of BBB breakdown, including endogenous IgG leakage in the brains and microhemorrhagic lesions, were only detected after infection with $ZIKV_{MR766}$. However, it is still not clear whether BBB breakdown was essential for the neurological disease and death or if it was a marker and a consequence of a severe disease.

It should be considered that the African strain $ZIKV_{MR766}$ was extensively passaged in mouse brains when it was isolated, what could explain its increased replication in the mouse model. Indeed, there are extensive differences between the sequences of $ZIKV_{MR766}$ and the Asian isolates, like $ZIKV_{PE243}$, which were not mouse adapted. Therefore, comparison between different ZIKV isolates might clarify the molecular mechanisms associated to disease or protection, including the contribution of the sequence differences for virulence, tissue tropism, pathology, and immune evasion. Regarding this, the protective response detected after infection with $ZIKV_{PE243}$ strain was associated to specific $CD4^+$ T cells and neutralizing antibody (Lucas et al., 2018), suggesting that a systemic response may affect the amount of virus reaching the BBB and the lesion extension, ultimately affecting the disease outcome.

Jurado and colleagues investigated the role of IFNAR deficiency in hematopoietic and non-hematopoietic cells in a mouse model of ZIKV infection. It was demonstrated that IFN response in non-hematopoietic cells was essential for protection against viral dissemination to the brain, BBB disruption, and ZIKV-induced neuropathology. Virus-induced paralysis was dependent of $CD8^+$ T cells infiltration in the brains, indicating that leukocyte infiltration due to BBB disruption might be a major issue for neuropathogenesis. They also observed that astrocytes were the main cell types infected in the brains of susceptible mice (Jurado et al., 2018). These findings indicated that astrocyte infection after virus crossing through BMECs might be an important contributor of subsequent BBB disruption and lymphocyte infiltration.

ZIKV infection during the embryonic period also impacted vascular function, particularly the BBB (Shao et al., 2016). Inoculation of C57BL/6J or 129S1/SvImJ mice at the embryonic day 14.5 affected mouse neurovascular development, resulting in postnatal microcephaly and brain damage. Analysis of the brains at postnatal period indicated a significant increase in vessel density and diameter in the cerebral cortex, with evidence of leaky blood-brain barrier (BBB). Furthermore, the brains exhibited extensive microglial activation, astrogliosis, and high levels of IL-1β and TNF-α (Shao et al., 2016). Thus, an excessive immune response can also harm the neurovascular development, leading to increased BBB permeability and brain damage.

DENGUE VIRUS AND YELLOW FEVER VIRUS

Dengue virus (DENV) and Yellow fever virus (YFV) viruses are usually associated to systemic and hemorrhagic clinical syndromes, and neurological manifestations are considered sporadic. Although very rare, immunization with YFV may induce encephalitis, and even though it is usually controlled by the host, it represents a clinical concern (Jennings et al., 1994; Monath and Barrett, 2003; Beck and Barrett, 2015; Halstead and Cohen, 2015; Screaton et al., 2015; Li et al., 2017).

YFV neurovirulence has been mostly investigated using laboratory neuroadapted strains and performing intracerebral inoculation in mice; therefore, the exact mechanism through which the virus accesses the brain and whether the viruses are capable to disrupt the blood-brain barrier remains unclear. Adult mice are resistant to systemic inoculation of YFV, and brain damage was only detected when high virus doses were inoculated. For this reason, neurological studies were mostly

performed using intracerebral inoculation (Barrett and Gould, 1986; Liu and Chambers, 2001). Based on these models, it was suggested that YFV accesses the brain tough hematogenous route (Mims, 1957; Luethy et al., 2016). More recent studies have been using mice deficient in IFNAR and/or IFNLR, which are highly susceptible to infection (Luethy et al., 2016; Douam et al., 2017). Douam et al. (2017) demonstrated that IFNAR-deficient mouse presented increased viremia and high viral load in systemic organs, including liver, spleen, and kidney. The viral load in the brain was also higher than the one observed in WT mice, but it did not increase overtime. IFNAR$^{-/-}$ mice also lost weight and displayed clinical manifestations; but both parameters were recovered at later time points after inoculation. In contrast, mice deficient in both IFNAR and IFNLR (ifnar$^{-/-}$ ifnlr$^{-/-}$) succumb to infection. These mice showed enhanced systemic infection and progressive increase of viral load in the brains, associated with evidence of BBB leakage. In both mice models, BBB permeability was only accessed at 5 dpi, whereas virus was already detected at 3 dpi; therefore, it is difficult to determine whether BBB disruption was necessary for virus invasion. Importantly, significant differences in the profile of T cells activation, especially serum IFN-γ levels appeared to influence the disease outcome (Douam et al., 2017).

Regarding DENV infection, increasing number of reports has been demonstrating the potential risk of neurological manifestations, with an incidence rating varying from 0.5 to 20% (Li et al., 2017; Vieira et al., 2018). Encephalitis was reported in children and adults, and virus RNA and anti-DENV IgM were detected in the CSF (Lum et al., 1996; Domingues et al., 2008; Vieira et al., 2018). Analysis of clinical samples obtained from dengue fatal cases also demonstrated the presence of virus RNA or proteins in the CSF and in brain sections, suggesting that DENV may indeed achieve the CNS (Miagostovich et al., 1997; Ramos et al., 1998; Araújo et al., 2011).

Similar to what was observed with other neurotropic viruses, DENV (serotype 2) was able to infect human BMECs, leading to the release of high titers of infectious particles and cell death *in vitro* (da Conceição et al., 2013). hBMEC infection was associated to cellular activation with increased expression of ICAM and enhanced secretion of inflammatory cytokines and chemokines, what may contribute to the recruitment of leukocytes *in vivo* (da Conceição et al., 2013). In another study, Velandia-Romero et al. (2016) evaluated the infection and permeability of primary mouse brain endothelial cells (MBECs), cultured either isolated or with primary astrocytes. The cells were infected with a DENV-4 isolate or with its variant, the neuroadapted strain D4MB-6. It was observed that both DENV strains infected MBECs, but not the astrocytes. MBECs infection altered the structure and function of BBB, affecting the endothelium permeability and the localization of the tight junction proteins ZO-1 and Claudin-1. TJ disorganization then allowed paracellular passing of free virus particles in a transwell system (Velandia-Romero et al., 2016). Microglia was also demonstrated to be susceptible to infection to all DENV serotypes. *In vitro* infection of murine microglia cell line (BV2) with DENV 1–4 resulted in increased expression of proinflammatory cytokines, including TNF-α, IFN-γ, IL-1β and IL-10, MCP-1, and IL-6, and of MMP-2 and MMP-9 (Bhatt et al., 2015). Although it had not been addressed, activation of microglia might contribute to BBB lesion. According to these data, infection of endothelial cells by DENV seems to be more relevant for BBB disruption, when compared to infection by other flaviviruses. Still, virus interaction with other cell types associated to BBB could also affect the barrier integrity.

A major caveat for the study of dengue pathogenesis *in vivo* is the limited susceptibility of small animal models to most DENV isolates. To overcome this issue, seminal papers were developed with mouse-adapted DENV2 strains (D2S10 and D2S20) derived from the parental PL046 isolate (Shresta et al., 2006; Orozco et al., 2012; Prestwood et al., 2012). Immunodeficient mice inoculated with D2S10 strain by systemic routes (i.v. or s.c.) presented virus in neuronal and non-neuronal tissues, showed high levels of inflammatory cytokines, and increased vascular permeability, resembling the main features of severe dengue. Importantly, mouse infection with this strain was lethal with no apparent signs of paralysis (Shresta et al., 2006; Orozco et al., 2012; Prestwood et al., 2012). On the other hand, the mice inoculated with PL046 presented virus only in the brain and spinal cord and exhibited paralysis (Shresta et al., 2006). However, the molecular mechanisms of virus dissemination to the CNS were not addressed in these models.

DENV infection in immunocompetent mice was mostly performed by intracranial inoculation. Those studies were important to evaluate the virus neurotropism but did not access the role of BBB integrity for DENV-induced CNS manifestations. Chaturvedi et al. (1991) were some of the first to report that DENV can destabilize the blood-brain barrier *in vivo*, using an experimental model of mice infected with a DENV2 virus strain. A remarkable increase in BBB permeability and high virus titers in the brains were evidenced when the mice were intracerebrally inoculated. In contrast, systemic (i.p.) infection induced slight alteration in the BBB permeability at late time points after infection, but no virus particles were detected (Chaturvedi et al., 1991). Another study based on intracranial inoculation of different virus isolates indicated that DENV serotype and genotype features may also influence the neurological disease outcome (Souza et al., 2013). However, BBB integrity was not evaluated in this model.

A major increment in the study of DENV neuropathogenesis came from the findings that mice deficient in IFN-α/βR and IFN-γR are highly susceptible and develop high viremia, paralysis, and death (Sarathy et al., 2015). Comparison between A129 (IFN-α/βR −/−) and AG129 (IFNα/β/γR −/−) mice intravenously inoculated with DENV2 demonstrated that IFN-γ signaling was essential to protect the CNS from viral invasion, through a CD8^{+}T cell-mediated response (Prestwood et al., 2012). Mice deficient in IFN-α/βR / IFN-γR / FcγRIIB were also susceptible to systemic infection, and virus was detected in the brains at late time points after infection (Dhole et al., 2016). Although DENV has been extensively detected in the brains and spinal cord upon systemic infection of AG129 mice, the pathway through which flaviviruses reach the CNS was not addressed (Shresta et al., 2004; Prestwood et al., 2012).

Velandia-Romero et al. (2012) developed another model of DENV infection *in vivo*, using suckling BALB/c mice (2–21 postnatal days) infected with the neuroadapted strain of DENV-4 (D4MB-6). Intraperitoneal inoculation of mice at 14 or 21 days after birth did not result in any clinical signs or mortality. In contrast, mice inoculated at 2 and 7 postnatal days developed fatal encephalitis accompanied by paralysis and postural instability. BBB leakage and increased viral replication in the brains were detected and correlated with the clinical outcome (Velandia-Romero et al., 2012). However, BBB integrity was only evaluated at 6 days post infection, whereas virus replication was already detected in the brains at 3 dpi. Therefore, it is hard to determine whether the barrier disruption was essential or not for virus invasion of the CNS. Importantly, DENV antigen was detected in endothelial cells and in the microglia of the mice that developed neurological manifestations. Activated phenotype of the infected cells, astrocytosis, and leukocyte infiltration, close to hemorrhagic focuses, were also evidenced (Velandia-Romero et al., 2012). These findings suggested that virus-BBB interaction might be relevant to DENV neuropathogenesis.

DENV dissemination was also accessed in a primate model of DENV infection with antibody-dependent enhancement (ADE) (Vasconcelos et al., 2016). *Callithrix penicillate* primates were subcutaneously infected with DENV3, followed by treatment with anti-DENV2 antibodies to mimic ADE. After several inoculations, virus antigen and microglia activation were detected in the brains, along with evidence of inflammation. Although the infection by DENV in the absence of ADE had not been explored, these findings supported the hypothesis that DENV is able to reach the CNS. However, infection of brain endothelial cells or BBB integrity was not investigated in this model.

All the referred data indicate that DENV may potentially infect brain endothelial cells, activate those and other cells associated to the BBB, and cause neurological manifestations. However, except for the few studies with human fatal cases, most findings were achieved with limited experimental models. The use of small animal models is an alternative to bypass the technical complications of human studies. However, it has been largely demonstrated that different flaviviruses evade interferon response in human but not in mouse cells (Ashour et al., 2010; Grant et al., 2016). Therefore, the dissemination of these viruses to the CNS after systemic infection has been mostly observed in immunodeficient mice. Although the relative resistance of adult wild-type mice to neurological disease caused by flaviviruses is a major caveat, some researchers claim that IFNAR-deficient mice might be a relevant model, since the IFN response in human cells is normally counteracted by these viruses. Still, there are several gaps in the comprehension of the pathway through which DENV reaches the brain that worth to be investigated.

TICK-BORNE ENCEPHALITIS VIRUS

Tick-borne encephalitis virus (TBEV) is part of another complex of flaviviruses, which are not transmitted by mosquitoes, and it is present in Europe and Asia, with an estimation of 10,000 to 15,000 cases per year (Kellman et al., 2018). Most infections are asymptomatic or are associated to a mild flu-like syndrome. However, in some individuals, the initial symptoms are followed by a second phase, characterized by neurological manifestations ranging from mild meningitis to severe encephalomyelitis. Up to 40% of these cases result in long-term neurological sequelae following encephalitis (Holzmann, 2003).

Like the other flaviviruses described here, the pathogenesis of tick-borne encephalitis in humans is not completely determined, but *in vitro* and *in vivo* infection models have been unveiling some aspect of the infection. Once the TBEV reaches the CNS, neurons are believed to be the primary target of virus replication. *In vitro* assays demonstrated that the virus is cytopathic and productively replicate and disseminate in primary human neurons and in human neural cell lines (Růzek et al., 2009; Bílý et al., 2015). Astrocytes were also reported to be susceptible to TBEV replication, but resistant to virus-induced cytopathic effect. Rat primary astrocytes were productively and persistently infected by TBEV, but no cytotoxicity was observed until 14 dpi (Potokar et al., 2014). Similarly, Palus et al. (2014) demonstrated that infection of primary human astrocytes (HBCAs) by TBEV resulted in sustained intracellular viral load and release of infectious particles, with no CPE or cell death until 15 dpi. Despite the lower frequency of infected cells in the culture, astrocyte activation was clearly evidenced by increased expression of glial fibrillary acidic protein (GFAP), higher mRNA expression of inflammatory cytokines and chemokines, and enhanced production of MMP-9 (Palus et al., 2014). These findings suggested that astrocytes infection with TBEV could affect BBB integrity by the release of proinflammatory cytokines and MMP. However, like other neurotropic viruses, TBEV induced the expression of type I IFN in astrocytes, which restricts the infection efficiency. Abrogation of IFN response by using astrocytes from IFNAR-deficient mice or by adding neutralizing antibodies to the cultures rendered mouse astrocytes more susceptible to TBEV infection, with increased virus replication and dissemination, and diminished cell viability (Lindqvist et al., 2016). In addition, infection of cells in the presence of supernatants obtained from infected astrocytes induced ISG expression and limited TBEV infection, supporting the hypothesis that IFN released by astrocytes upon TBEV infection might limit viral dissemination (Lindqvist et al., 2016).

Still, the pathways by which TBEV reaches astrocytes and neurons were not determined. It was only recently demonstrated that TBEV replicate in human BMECs (Palus et al., 2017). *In vitro* assays comparing lower and higher neuroinvasive lab strains of TBEV demonstrated that both strains productively replicated in HBMECs but did not induce remarkable CPE at the time points analyzed (Palus et al., 2017). Importantly, TBEV infection did not affect the expression or localization of tight junction proteins nor the expression of adhesion molecules. Also, the viruses were able to transmigrate through the endothelial barrier *in vitro*, without enhancing its permeability (Palus et al., 2017).

In vivo experimental mouse models demonstrated that subcutaneous infection with TBEV promoted neurological signs and death (Růžek et al., 2011). Kinetic analysis of virus dissemination and BBB integrity indicated that infectious particles

were detected in the brain only after 7 dpi, simultaneously with the decrease of viremia. BBB disruption was not observed during the viremic phase of the infection, and it was only detected after 10 dpi. At this time point (10 dpi), the clinical symptoms were most evident, and the mice started to die. Taken together, these data indicated that infection of endothelial cells by TBEV does not affect the integrity of BBB. Also, although virus-endothelial cell interaction might be relevant for virus transmigration and invasion of the CNS, these events seem to not require a significant disruption of the BBB. The impact on the BBB structure is possibly rather a consequence of the brain infection, but it is still determinant for disease severity (Růžek et al., 2011).

CONCLUDING REMARKS

Several flaviviruses are potentially neurotropic and neurovirulent, but the knowledge regarding the mechanisms of neuropathogenesis is very incipient for most of them. Also, the pathway through which flaviviruses reach the CNS is still unclear. Given the systemic nature of the initial infections caused by JEV, WNV, ZIKV, DENV, YFV, and TBEV, it is believed that they reach the brain mainly through a hematogenous route. Indeed, hemorrhagic focuses or other evidence of BBB leakage are often observed upon infection, indicating that viruses might cross the endothelial brain barrier to reach the CNS and cause neurological syndromes. *In vitro* experimental models have demonstrated that different viruses productively infect brain endothelial cells and induce cell death, what could be a major contributor to BBB damage and virus crossing. However, the role of BBB disruption for viral invasion is controversial, and increasing evidence suggest that flaviviruses can traverse the endothelial barrier by transcellular pathways. In either case, viruses could then access other cells associated to the BBB, such as pericytes, astrocytes, and microglia. Infection of these cells might induce cellular activation and release of proteases and other mediators that affect TJ organization and BBB integrity. Barrier breakdown could be, then, a secondary effect due to the inflammatory response into the brain. Still, BBB damage seems to be essential for neuropathology, by further increasing the local viral load, leukocyte infiltration, and inflammation. Different pathways proposed for flaviviruses entering the brain through the BBB are depicted in **Figure 1**. The scheme suggests that flaviviruses may reach the CNS by cell-free virus transcytosis through the endothelial cells or by transmigration of infected leukocytes into the CNS. Both mechanisms would allow the release of infectious virus into the brain that could then infect BBB-associated cells and neurons. Either pathway will be followed by an inflammatory response. Inflammation, virus replication in endothelial cell, and/or cells associated to the barrier would then trigger BBB leakage.

It is important to consider that most of the studies regarding the role of endothelial cell infection and BBB disruption for neuroinvasion and disease were performed *in vitro* or in mouse experimental models. *In vitro* assays were fundamentally developed using human transformed cell lines or primary cells from rodents, which are not natural hosts of these infections. Furthermore, wild-type adult mice usually control systemic infection by flaviviruses and do not develop neurological manifestation. For this reason, *in vivo* assays aimed to explore neurological syndromes were formally performed by intracranial inoculation. Systemic inoculation and investigation of virus invasion to the CNS in experimental models have been restricted to immunodeficient or suckling mice. Those are susceptible to virus dissemination, invasion of the CNS, and neuronal damage. It is important to point that even in these models, the phenomena are usually evaluated at fixed time point after infection, which does not give a clear picture of the sequence of events preceding CNS damage. Also, a detailed analysis of the specific cells infected by the viruses was poorly performed in *in vivo* models.

The investigation regarding flavivirus neuroinvasion upon natural human infection is also very incipient. It probably reflects the inefficient or delayed diagnosis of the patients, which restricts the number of available samples with confirmed infection by flaviviruses. Clear investigation of the cells infected in the blood-brain barrier and CNS parenchyma requires good quality pathological analysis or cell isolation, followed by phenotypic or molecular evaluation of infection and activation. The inherent difficulty for tissue obtention for these analyses, associated to the low number of available samples, has been restricting the research to molecular diagnosis and confirmation of virus invasion of the CNS. Hence, whether brain endothelial cells are targeted by flavivirus infection and whether this event, associated or not with BBB breakdown, is relevant for virus invasion and neuropathogenesis upon natural human infection are still opening questions in the field.

Finally, the experimental models have been unveiling several specific issues regarding flavivirus neuroinvasion, significantly improving the knowledge about these neglected diseases. However, systematic experiments designed to evaluate whether brain endothelial cells are indeed infected *in vivo* and to investigate the kinetics and relevance of the BBB breakdown are still need to be performed. Also, effort should be taken to improve flavivirus diagnosis and to strengthen the interaction between physicians and researchers, aiming to better understand the events followed flavivirus infection that leads to neuroinvasion and neurologic diseases in humans. Full comprehension of these mechanisms would identify specific molecular targets and stimulate the development of new medications against flavivirus neurological syndromes, ultimately benefitting the patients.

AUTHOR CONTRIBUTIONS

YM, LM, SC, and LA wrote the review. LA revised the figure and final text.

FUNDING

This study was financed in part by the Coordenação de Aperfeiçoamento de Pessoal de Nível Superior - Brasil (CAPES) - Finance Code 001. This work was also supported by FINEP, CNPq, and FAPERJ. LM, and SC are the recipients of a CNPq fellowship. YM is the recipient of a CAPES fellowship.

REFERENCES

Agrawal, T., Sharvani, V., Nair, D., and Medigeshi, G. R. (2013). Japanese encephalitis virus disrupts cell-cell junctions and affects the epithelial permeability barrier functions. *PLoS One* 8, 1–16. doi: 10.1371/journal.pone.0069465

Alimonti, J. B., Ribecco-Lutkiewicz, M., Sodja, C., Jezierski, A., Stanimirovic, D. B., Liu, Q., et al. (2018). Zika virus crosses an in vitro human blood brain barrier model. *Fluids Barriers CNS* 15, 1–9. doi: 10.1186/s12987-018-0100-y

Al-Obaidi, M. M. J., Bahadoran, A., Har, L. S., Mui, W. S., Rajarajeswaran, J., Zandi, K., et al. (2017). Japanese encephalitis virus disrupts blood-brain barrier and modulates apoptosis proteins in THBMEC cells. *Virus Res.* 233, 17–28. doi: 10.1016/j.virusres.2017.02.012

Alvarez, J. I., Katayama, T., and Prat, A. (2013). Glial influence on the blood brain barrier. *Glia* 61, 1939–1958. doi: 10.1002/glia.22575

Araújo, F. M., Brilhante, R. S., Cavalcanti, L. P., Rocha, M. F., Cordeiro, R. A., Perdigão, A. C., et al. (2011). Detection of the dengue non-structural 1 antigen in cerebral spinal fluid samples using a commercial ayavailable enzyme-linked immunosorbent assay. *J. Virol. Methods* 177, 128–131. doi: 10.1016/j.jviromet.2011.07.003

Argaw, A. T., Asp, L., Zhang, J., Navrazhina, K., Pham, T., Mariani, J. N., et al. (2012). Astrocyte-derived VEGF-A drives blood-brain barrier disruption in CNS inflammatory disease. *J. Clin. Invest.* 122, 2454–2468. doi: 10.1172/JCI60842

Ashour, J., Morrison, J., Laurent-Rolle, M., Belicha-Villanueva, A., Plumlee, C. R., Bernal-Rubio, D., et al. (2010). Mouse STAT2 restricts early dengue virus replication. *Cell Host Microbe* 8, 410–421.

Ballabh, P., Braun, A., and Nedergaard, M. (2004). The blood–brain barrier: an overview: structure, regulation, and clinical implications. *Neurobiol. Dis.* 16, 1–13. doi: 10.1016/j.nbd.2003.12.016

Barrett, A. D. T., and Gould, E. A. (1986). Comparison of neurovirulence of different strains of yellow fever virus in mice. *J. Gen. Virol.* 67, 631–637. doi: 10.1099/0022-1317-67-4-631

Beck, A. S., and Barrett, A. D. (2015). Current status and future prospects of yellow fever vaccines. *Expert Rev. Vaccines* 14, 1479–1492. doi: 10.1586/14760584.2015.1083430

Bhatt, R. S., Kothari, S. T., Gohil, D. J., D'Souza, M., and Chowdhary, A. S. (2015). Novel evidence of microglial immune response in impairment of dengue infection of CNS. *Immunobiology* 220, 1170–1176. doi: 10.1016/j.imbio.2015.06.002

Bian, P., Ye, C., Zheng, X., Yang, J., Ye, W., Wang, Y., et al. (2017). Mesenchymal stem cells alleviate encephalitis virus-induced neuroinflammation and mortality. *Stem. Cell Res. Ther.* 8, 1–13. doi: 10.1186/s13287-017-0486-5

Bílý, T., Palus, M., Eyer, L., Elsterová, J., Vancová, M., and Růžek, D. (2015). Electron tomography analysis of tick-borne encephalitis virus infection in human neurons. *Sci. Rep.* 5:10745. doi: 10.1038/srep10745

Bogoch, I. I., Brady, O. J., Kraemer, M. U., German, M., Creatore, M. I., Kulkarni, M. A., et al. (2016). Anticipating the international spread of Zika virus from Brazil. *Lancet* 387, 335–336. doi: 10.1016/S0140-6736(16)00080-5

Bramley, J. C., Drummond, C. G., Lennemann, N. J., Good, C. A., Kim, K. S., and Coyne, C. B. (2017). A three-dimensional cell culture system to model RNA virus infections at the blood-brain barrier. *mSphere* 2, 1–18. doi: 10.1128/mSphere.00206-17

Brasil, P., Sequeira, P. C., Freitas, A. D. A., Zogbi, H. E., Calvet, G. A., de Souza, R. V., et al. (2016). Guillain-Barré syndrome associated with Zika virus infection. *Lancet* 387:1482. doi: 10.1016/S0140-6736(16)30058-7

Carteaux, G., Maquart, M., Bedet, A., Contou, D., Brugières, P., Fourati, S., et al. (2016). Zika virus associated with meningoencephalitis. *N. Engl. J. Med.* 374, 1595–1596. doi: 10.1056/NEJMc1602964

Chang, C. Y., Li, J. R., Chen, W. Y., Ou, Y. C., Lai, C. Y., Hu, Y. H., et al. (2015). Disruption of in vitro endothelial barrier integrity by Japanese encephalitis virus-infected astrocytes. *Glia* 63, 1915–1932. doi: 10.1002/glia.22857

Chaturvedi, U. C., Dhawan, R., Khanna, M., and Mathur, A. (1991). Breakdown of the blood-brain barrier during dengue virus infection of mice. *J. Gen. Virol.* 72, 859–866. doi: 10.1099/0022-1317-72-4-859

Chen, S. T., Liu, R. S., Wu, M. F., Lin, Y. L., Chen, S. Y., Tan, D. T., et al. (2012). CLEC5A regulates Japanese encephalitis virus-induced neuroinflammation and lethality. *PLoS Pathog.* 8, 1–18. doi: 10.1371/journal.ppat.1002655

Chen, C. J., Ou, Y. C., Li, J. R., Chang, C. Y., Pan, H. C., Lai, C. Y., et al. (2014). Infection of pericytes in vitro by Japanese encephalitis virus disrupts the integrity of the endothelial barrier. *J. Virol.* 88, 1150–1161. doi: 10.1128/JVI.02738-13

Chow, B. W., and Gu, C. (2015). The molecular constituents of the blood-brain barrier. *Trends Neurosci.* 38, 598–608. doi: 10.1016/j.tins.2015.08.003

Cugola, F. R., Fernandes, I. R., Russo, F. B., Freitas, B. C., Dias, J. L., Guimarães, K. P., et al. (2016). The Brazilian Zika virus strain causes birth defects in experimental models. *Nature* 534, 267–271. doi: 10.1038/nature18296

da Conceição, T. M., Rust, N. M., Berbel, A. C. E. R., Martins, N. B., do Nascimento Santos, C. A., Da Poian, A. T., et al. (2013). Essential role of RIG-I in the activation of endothelial cells by dengue virus. *Virology* 435, 281–292. doi: 10.1016/j.virol.2012.09.038

Dai, J., Wang, P., Bai, F., Town, T., and Fikrig, E. (2008). Icam-1 participates in the entry of West Nile virus into the central nervous system. *J. Virol.* 82, 4164–4168. doi: 10.1128/JVI.02621-07

Daniels, B. P., Holman, D. W., Cruz-Orengo, L., Jujjavarapu, H., Durrant, D. M., Klein, R. S., et al. (2014). Viral pathogen-associated molecular patterns regulate blood-brain barrier integrity via competing innate cytokine signals. *mBio* 5, 1–13. doi: 10.1128/mBio.01476-14

Daniels, B. P., Jujjavarapu, H., Durrant, D. M., Williams, J. L., Green, R. R., White, J. P., et al. (2017). Regional astrocyte IFN signaling restricts pathogenesis during neurotropic viral infection. *J. Clin. Invest.* 127, 843–856. doi: 10.1172/JCI88720

Dhole, P., Nakayama, E. E., Saito, A., Limkittikul, K., Phanthanawiboon, S., Shioda, T., et al. (2016). Sequence diversity of dengue virus type 2 in brain and thymus of infected interferon receptor ko mice: implications for dengue virulence. *Virol. J.* 13, 1–8. doi: 10.1186/s12985-016-0658-4

Dick, G. W. A., Kitchen, S. F., and Haddow, A. J. (1952). Zika virus, I: isolations and serological specificity. *Trans. R. Soc. Trop. Med. Hyg.* 46, 509–520. doi: 10.1016/0035-9203(52)90042-4

Domingues, R. B., Kuster, G. W., Onuki-Castro, F. L., Souza, V. A., Levi, J. E., and Pannuti, C. S. (2008). Involvement of the central nervous system in patients with dengue virus infection. *J. Neurol. Sci.* 267, 36–40. doi: 10.1016/j.jns.2007.09.040

Douam, F., Soto Albrecht, Y. E., Hrebikova, G., Sadimin, E., Davidson, C., Kotenko, S. V., et al. (2017). Type III interferon-mediated signaling is critical for controlling live attenuated yellow fever virus infection in vivo. *mBio* 8, 1–22. doi: 10.1128/mBio.00819-17

Dudley, D. M., Aliota, M. T., Mohr, E. L., Weiler, A. M., Lehrer-Brey, G., Weisgrau, K. L., et al. (2016). A rhesus macaque model of Asian-lineage Zika virus infection. *Nat. Commun.* 7, 1–9. doi: 10.1038/ncomms12204

Duffy, M. R., Chen, T. H., Hancock, W. T., Powers, A. M., Kool, J. L., Lanciotti, R. S., et al. (2009). Zika virus outbreak on Yap Island, federated states of micronesia. *N. Engl. J. Med.* 360, 2536–2543. doi: 10.1056/NEJMoa0805715

Fabry, Z., Topham, D. J., Fee, D., Herlein, J., Carlino, J. A., Hart, M. N., et al. (1995). TGF-beta 2 decreases migration of lymphocytes in vitro and homing of cells into the central nervous system in vivo. *J. Immunol.* 155, 325–332.

Faria, N. R., Azevedo, R. D. S. D. S., Kraemer, M. U. G., Souza, R., Cunha, M. S., Hill, S. C., et al. (2016). Zika virus in the Americas: early epidemiological and genetic findings. *Science* 352, 345–349. doi: 10.1126/science.aaf5036

Garcez, P. P., Loiola, E. C., da Costa, R. M., Higa, L. M., Trindade, P., Delvecchio, R., et al. (2016). Zika virus impairs growth in human neurospheres and brain organoids. *Science* 352, 816–818. doi: 10.1126/science.aaf6116

Grant, A., Ponia, S. S., Tripathi, S., Balasubramaniam, V., Miorin, L., Sourisseau, M., et al. (2016). Zika virus targets human STAT2 to inhibit type I interferon signaling. *Cell Host Microbe* 19, 882–890.

Halstead, S. B., and Cohen, S. N. (2015). Dengue hemorrhagic fever at 60 years: early evolution of concepts of causation and treatment. *Microbiol. Mol. Biol. Rev.* 79, 281–291. doi: 10.1128/MMBR.00009-15

Hasebe, R., Suzuki, T., Makino, Y., Igarashi, M., Yamanouchi, S., Maeda, A., et al. (2010). Transcellular transport of West Nile virus-like particles across human endothelial cells depends on residues 156 and 159 of envelope protein. *BMC Microbiol.* 10:165. doi: 10.1186/1471-2180-10-165

Heinemann, U., Kaufer, D., and Friedman, A. (2012). Blood-brain barrier dysfunction, TGFβ signaling, and astrocyte dysfunction in epilepsy. *Glia* 60, 1251–1257. doi: 10.1002/glia.22311

Holzmann, H. (2003). Diagnosis of tick-borne encephalitis. *Vaccine* 21(Suppl. 1), S36–S40. doi: 10.1016/S0264-410X(02)00819-8

Hussmann, K. L., Samuel, M. A., Kim, K. S., Diamond, M. S., and Fredericksen, B. L. (2013). Differential replication of pathogenic and nonpathogenic strains of West Nile virus within astrocytes. *J. Virol.* 87, 2814–2822. doi: 10.1128/JVI.02577-12

Jain, N., Oswal, N., Chawla, A. S., Agrawal, T., Biswas, M., Vrati, S., et al. (2017). CD8 T cells protect adult naive mice from JEV-induced morbidity

via lytic function. *PLoS Negl. Trop. Dis.* 11, 1–25. doi: 10.1371/journal.pntd.0005329

Jennings, A. D., Gibson, C. A., Miller, B. R., Mathews, J. H., Mitchell, C. J., Roehrig, J. T., et al. (1994). Analysis of a yellow fever virus isolated from a fatal case of vaccine-associated human encephalitis. *J. Infect. Dis.* 169, 512–518. doi: 10.1093/infdis/169.3.512

Johnson, R. T., Burke, D. S., Elwell, M., Leake, C. J., Nisalak, A., Hoke, C. H., et al. (1985). Japanese encephalitis: immunocytochemical studies of viral antigen and inflammatory cells in fatal cases. *Ann. Neurol.* 18, 567–573.

Jurado, K. A., Yockey, L. J., Wong, P. W., Lee, S., Huttner, A. J., and Iwasaki, A. (2018). Antiviral CD8 T cells induce Zika virus associated paralysis in mice. *Nat. Microbiol.* 3, 141–147. doi: 10.1038/s41564-017-0060-z

Kellman, E. M., Offerdahl, D. K., Melik, W., and Bloom, M. E. (2018). Viral determinants of virulence in tick-borne flaviviruses. *Viruses* 10:E329. doi: 10.3390/v10060329

Lai, C. Y., Ou, Y. C., Chang, C. Y., Pan, H. C., Chang, C. J., Liao, S. L., et al. (2012). Endothelial Japanese encephalitis virus infection enhances migration and adhesion of leukocytes to brain microvascular endothelia via MEK-dependent expression of ICAM 1 and the CINC and RANTES chemokines. *J. Neurochem.* 123, 250–261. doi: 10.1111/j.1471-4159.2012.07889.x

Lazear, H. M., Daniels, B. P., Pinto, A. K., Huang, A. C., Vick, S. C., Doyle, S. E., et al. (2015). Interferon-λ restricts West Nile virus neuroinvasion by tightening the blood-brain barrier. *Sci. Transl. Med.* 7, 1–24. doi: 10.1126/scitranslmed.aaa4304

Li, G. H., Ning, Z. J., Liu, Y. M., and Li, X. H. (2017). Neurological manifestations of dengue infection. *Front. Cell. Infect. Microbiol.* 7, 1–13. doi: 10.3389/fcimb.2017.00449

Li, F., Wang, Y., Yu, L., Cao, S., Wang, K., Yuan, J., et al. (2015). Viral infection of the central nervous system and neuroinflammation precede blood-brain barrier disruption during Japanese Encephalitis virus infection. *J. Virol.* 89, 5602–5614. doi: 10.1128/JVI.00143-15

Li, C., Xu, D., Ye, Q., Hong, S., Jiang, Y., Liu, X., et al. (2016). Zika virus disrupts neural progenitor development and leads to microcephaly in mice. *Cell Stem Cell* 19, 120–126. doi: 10.1016/j.stem.2016.10.017

Lindquist, L., and Vapalahti, O. (2008). Tick-borne encephalitis. *Lancet* 371, 1861–1871. doi: 10.1016/S0140-6736(08)60800-4

Lindqvist, R., Mundt, F., Gilthorpe, J. D., Wölfel, S., Gekara, N. O., Kröger, A., et al. (2016). Fast type I interferon response protects astrocytes from flavivirus infection and virus-induced cytopathic effects. *J. Neuroinflammation* 13:277. doi: 10.1186/s12974-016-0748-7

Liou, M. L., and Hsu, C. Y. (1998). Japanese encephalitis virus is transported across the cerebral blood vessels by endocytosis in mouse brain. *Cell Tissue Res.* 293, 389–394. doi: 10.1007/s004410051130

Liu, T., and Chambers, T. J. (2001). Yellow fever virus encephalitis: properties of the brain-associated T-cell response during virus clearance in normal and gamma interferon-deficient mice and requirement for CD4+ lymphocytes. *J. Virol.* 75, 2107–2118. doi: 10.1128/JVI.75.5.2107-2118.2001

Lucas, C. G., Kitoko, J. Z., Ferreira, F. M., Suzart, V. G., Papa, M. P., Coelho, S. V., et al. (2018). Critical role of CD4+ T cells and IFNγ signaling in antibody-mediated resistance to Zika virus infection. *Nat. Commun.* 9, 1–12. doi: 10.1038/s41467-018-05519-4

Luethy, L. N., Erickson, A. K., Jesudhasan, P. R., Ikizler, M., Dermody, T. S., and Pfeiffer, J. K. (2016). Comparison of three neurotropic viruses reveals differences in viral dissemination to the central nervous system. *Virology* 487, 1–10. doi: 10.1016/j.virol.2015.09.019

Lum, L. C., Lam, S. K., Choy, Y. S., George, R., and Harun, F. (1996). Dengue encephalitis: a true entity? *Am. J. Trop. Med. Hyg.* 54, 256–259. doi: 10.4269/ajtmh.1996.54.256

Melo, A. S., Aguiar, R. S., Amorim, M. M., Arruda, M. B., Melo, F. O., Ribeiro, S. T., et al. (2016). Congenital Zika virus infection: beyond neonatal microcephaly. *JAMA Neurol.* 73, 1407–1416. doi: 10.1001/jamaneurol.2016.3720

Miagostovich, M. P., Ramos, R. G., Nicol, A. F., Nogueira, R. M., Cuzzi-Maya, T., Oliveira, A. V., et al. (1997). Retrospective study on dengue fatal cases. *Clin. Neuropathol.* 16, 204–208.

Mims, C. A. (1957). The invasion of the brain by yellow fever virus present in the blood of mice. *Br. J. Exp. Pathol.* 38, 329–338.

Miner, J. J., Daniels, B. P., Shrestha, B., Proenca-Modena, J. L., Lew, E. D., Lazear, H. M., et al. (2015). The TAM receptor Mertk protects against neuroinvasive viral infection by maintaining blood-brain barrier integrity. *Nat. Med.* 21, 1464–1472. doi: 10.1038/nm.3974

Minkiewicz, J., de Rivero Vaccari, J. P., and Keane, R. W. (2013). Human astrocytes express a novel NLRP2 inflammasome. *Glia* 61, 1113–1121. doi: 10.1002/glia.22499

Mladinich, M. C., Schwedes, J., and Mackow, E. R. (2017). Zika virus persistently infects and is basolaterally released from primary human brain microvascular endothelial cells. *MBio* 8, 1–17. doi: 10.1128/mBio.00952-17

Mlakar, J., Korva, M., Tul, N., Popović, M., Poljšak-Prijatelj, M., Mraz, J., et al. (2016). Zika virus associated with microcephaly. *N. Engl. J. Med.* 374, 951–958. doi: 10.1056/NEJMoa1600651

Monath, T. P., and Barrett, A. D. (2003). Pathogenesis and pathophysiology of yellow fever. *Adv. Virus Res.* 60, 343–395. doi: 10.1016/S0065-3527(03)60009-6

Morrey, J. D., Olsen, A. L., Siddharthan, V., Motter, N. E., Wang, H., Taro, B. S., et al. (2008). Increased blood-brain barrier permeability is not a primary determinant for lethality of West Nile virus infection in rodents. *J. Gen. Virol.* 89, 467–473. doi: 10.1099/vir.0.83345-0

Musso, D. (2015). Zika virus transmission from French Polynesia to Brazil. *Emerg. Infect. Dis.* 21:1887. doi: 10.3201/eid2110.151125

Myint, K. S., Kipar, A., Jarman, R. G., Gibbons, R. V., Perng, G. C., Flanagan, B., et al. (2014). Neuropathogenesis of Japanese encephalitis in a primate model. *PLoS Negl. Trop. Dis.* 8, 1–11. doi: 10.1371/journal.pntd.0002980

Obermeier, B., Daneman, R., and Ransohoff, R. M. (2013). Development, maintenance and disruption of the blood-brain barrier. *Nat. Med.* 19, 1584–1596. doi: 10.1038/nm.3407

Oliveira Melo, A. S., Malinger, G., Ximenes, R., Szejnfeld, P. O., Alves Sampaio, S., and Bispo de Filippis, A. M. (2016). Zika virus intrauterine infection causes fetal brain abnormality and microcephaly: tip of the iceberg? *Ultrasound Obstet. Gynecol.* 47, 6–7. doi: 10.1002/uog.15831

Orozco, S., Schmid, M. A., Parameswaran, P., Lachica, R., Henn, M. R., Beatty, R., et al. (2012). Characterization of a model of lethal dengue virus 2 infection in C57BL/6 mice deficient in the alpha/beta interferon receptor. *J. Gen. Virol.* 93, 2152–2157. doi: 10.1099/vir.0.045088-0

Palus, M., Bílý, T., Elsterová, J., Langhansová, H., Salát, J., Vancová, M., et al. (2014). Infection and injury of human astrocytes by tick-borne encephalitis virus. *J. Gen. Virol.* 95, 2411–2426. doi: 10.1099/vir.0.068411-0

Palus, M., Vancova, M., Sirmarova, J., Elsterova, J., Perner, J., and Ruzek, D. (2017). Tick-borne encephalitis virus infects human brain microvascular endothelial cells without compromising blood-brain barrier integrity. *Virology* 507, 110–122. doi: 10.1016/j.virol.2017.04.012

Papa, M. P., Meuren, L. M., Coelho, S. V., Lucas, C. G., Mustafá, Y. M., Lemos Matassoli, F., et al. (2017). Zika virus infects, activates, and crosses brain microvascular endothelial cells, without barrier disruption. *Front. Microbiol.* 8, 1–17. doi: 10.3389/fmicb.2017.02557

Patabendige, A., Michael, B. D., Craig, A. G., and Solomon, T. (2018). Brain microvascular endothelial-astrocyte cell responses following Japanese encephalitis virus infection in an in vitro human blood-brain barrier model. *Mol. Cell. Neurosci.* 89, 60–70. doi: 10.1016/j.mcn.2018.04.002

Paul, A. M., Acharya, D., Duty, L., Thompson, E. A., Le, L., Stokic, D. S., et al. (2017). Osteopontin facilitates West Nile virus neuroinvasion via neutrophil "Trojan horse" transport. *Sci. Rep.* 7, 1–11. doi: 10.1038/s41598-017-04839-7

Potokar, M., Korva, M., Jorgačevski, J., Avšič-Županc, T., and Zorec, R. (2014). Tick-borne encephalitis virus infects rat astrocytes but does not affect their viability. *PLoS One* 9, 1–12. doi: 10.1371/journal.pone.0086219

Prestwood, T. R., Morar, M. M., Zellweger, R. M., Miller, R., May, M. M., Yauch, L. E., et al. (2012). Gamma interferon (IFN-γ) receptor restricts systemic dengue virus replication and prevents paralysis in IFN-α/β receptor-deficient mice. *J. Virol.* 86, 12561–12570. doi: 10.1128/JVI.06743-11

Ramos, C., Sánchez, G., Pando, R. H., Baquera, J., Hernández, D., Mota, J., et al. (1998). Dengue virus in the brain of a fatal case of hemorrhagic dengue fever. *J. Neurovirol.* 4, 465–468. doi: 10.3109/13550289809114548

Rochfort, K. D., Collins, L. E., Murphy, R. P., and Cummins, P. M. (2014). Downregulation of blood-brain barrier phenotype by proinflammatory cytokines involves NADPH oxidase-dependent ROS generation: consequences for interendothelial adherens and tight junctions. *PLoS One* 9:e101815. doi: 10.1371/journal.pone.0101815

Roe, K., Kumar, M., Lum, S., Orillo, B., Nerurkar, V. R., and Verma, S. (2012). West Nile virus-induced disruption of the blood-brain barrier in mice is characterized by the degradation of the junctional complex proteins and

increase in multiple matrix metalloproteinases. *J. Gen. Virol.* 93, 1193–1203. doi: 10.1099/vir.0.040899-0

Roe, K., Orillo, B., and Verma, S. (2014). West Nile virus-induced cell adhesion molecules on human brain microvascular endothelial cells regulate leukocyte adhesion and modulate permeability of the in vitro blood-brain barrier model. *PLoS One* 9, 1–12. doi: 10.1371/journal.pone.0102598

Růžek, D., Salát, J., Singh, S. K., and Kopecký, J. (2011). Breakdown of the blood-brain barrier during tick-borne encephalitis in mice is not dependent on CD8+ T-cells. *PLoS One* 6:e20472. doi: 10.1371/journal.pone.0020472

Růzek, D., Vancová, M., Tesarová, M., Ahantarig, A., Kopecký, J., and Grubhoffer, L. (2009). Morphological changes in human neural cells following tick-borne encephalitis vírus infection. *J. Gen. Virol.* 90, 1649–1658. doi: 10.1099/vir.0.010058-0

Salimi, H., Cain, M. D., and Klein, R. S. (2016). Encephalitic arboviruses: emergence, clinical presentation, and neuropathogenesis. *Neurotherapeutics* 13, 514–534. doi: 10.1007/s13311-016-0443-5

Samuel, M. A., Wang, H., Siddharthan, V., Morrey, J. D., and Diamond, M. S. (2007). Axonal transportmediates West Nile virus entry into the central nervous system and induces acute flaccid paralysis. *PNAS* 104, 17140–17145. doi: 10.1073/pnas.0705837104

Samy, A. M., Alkishe, A. A., Thomas, S. M., Wang, L., and Zhang, W. (2018). Mapping the potential distributions of etiological agent, vectors, and reservoirs of Japanese Encephalitis in Asia and Australia. *Acta Trop.* 188, 108–117. doi: 10.1016/j.actatropica.2018.08.014

Sarathy, V. V., Infante, E., Li, L., Campbell, G. A., Wang, T., Paessler, S., et al. (2015). Characterization of lethal dengue virus type 4 (DENV-4) TVP-376 infection in mice lacking both IFN-α/β and IFN-γ receptors (AG129) and comparison with the DENV-2 AG129 mouse model. *J. Gen. Virol.* 96, 3035–3048. doi: 10.1099/jgv.0.000246

Schreibelt, G., Kooij, G., Reijerkerk, A., van Doorn, R., Gringhuis, S. I., van der Pol, S., et al. (2007). Reactive oxygen species alter brain endothelial tight junction dynamics via RhoA, PI3 kinase, and PKB signaling. *FASEB J.* 21, 3666–3676. doi: 10.1096/fj.07-8329com

Screaton, G., Mongkolsapaya, J., Yacoub, S., and Roberts, C. (2015). New insights into the immunopathology and control of dengue virus infection. *Nat. Rev. Immunol.* 15, 745–759. doi: 10.1038/nri3916

Sejvar, J. J., Haddad, M. B., Tierney, B. C., Campbell, G. L., Marfin, A. A., Van Gerpen, J. A., et al. (2003). Neurologic manifestations and outcome of West Nile virus infection. *JAMA* 290, 511–515. doi: 10.1001/jama.290.4.511

Shao, Q., Herrlinger, S., Yang, S. L., Lai, F., Moore, J. M., Brindley, M. A., et al. (2016). Zika virus infection disrupts neurovascular development and results in postnatal microcephaly with brain damage. *Development* 143, 4127–4136. doi: 10.1242/dev.143768

Shresta, S., Kyle, J. L., Snider, H. M., Basavapatna, M., Beatty, P. R., and Harris, E. (2004). Interferon-dependent immunity is essential for resistance to primary dengue virus infection in mice, whereas T- and B-cell-dependent immunity are less critical. *J. Virol.* 78, 2701–2710. doi: 10.1128/JVI.78.6.2701-2710.2004

Shresta, S., Sharar, K. L., Prigozhin, D. M., Beatty, P. R., and Harris, E. (2006). Murine model for dengue virus-induced lethal disease with increased vascular permeability. *J. Virol.* 80, 10208–10217. doi: 10.1128/JVI.00062-06

Siegenthaler, J. A., Sohet, F., and Daneman, R. (2013). 'Sealing off the CNS': cellular and molecular regulation of blood-brain barriergenesis. *Curr. Opin. Neurobiol.* 23, 1057–1064. doi: 10.1016/j.conb.2013.06.006

Simpson, D. I. (1964). Zika virus infection in man. *Trans. R. Soc. Trop. Med. Hyg.* 58, 335–338. doi: 10.1016/0035-9203(64)90200-7

Soe, H. J., Khan, A. M., Manikam, R., Samudi Raju, C., Vanhoutte, P., and Sekaran, S. D. (2017). High dengue virus load differentially modulates human microvascular endothelial barrier function during early infection. *J. Gen. Virol.* 98, 2993–3007. doi: 10.1099/jgv.0.000981

Sofroniew, M. V. (2015). Astrocyte barriers to neurotoxic inflammation. *Nat. Rev. Neurosci.* 16, 249–263. doi: 10.1038/nrn3898

Souza, K. P., Silva, E. G., de Oliveira Rocha, E. S., Figueiredo, L. B., de Almeida-Leite, C. M., Arantes, R. M., et al. (2013). Nitric oxide synthase expression correlates with death in an experimental mouse model of dengue with CNS involvement. *Virol. J.* 10:267. doi: 10.1186/1743-422X-10-267

Suen, W. W., Prow, N. A., Hall, R. A., and Bielefeldt-Ohmann, H. (2014). Mechanism of West Nile virus neuroinvasion: a critical appraisal. *Viruses* 6, 2796–2825. doi: 10.3390/v6072796

Thounaojam, M. C., Kaushik, D. K., Kundu, K., and Basu, A. (2014). MicroRNA-29b modulates Japanese encephalitis virus-induced microglia activation by targeting tumor necrosis actor alpha-induced protein 3. *J. Neurochem.* 129, 143–154. doi: 10.1111/jnc.12609

Vasconcelos, B. C., Vieira, J. A., Silva, G. O., Fernandes, T. N., Rocha, L. C., Viana, A. P., et al. (2016). Antibody-enhanced dengue disease generates a marked CNS inflammatory response in the black-tufted marmoset *Callithrix penicillata*. *Neuropathology* 36, 3–16. doi: 10.1111/neup.12229

Velandia-Romero, M. L., Acosta-Losada, O., and Castellanos, J. E. (2012). In vivo infection by a neuroinvasive neurovirulent dengue virus. *J. Neurovirol.* 18, 374–387. doi: 10.1007/s13365-012-0117-y

Velandia-Romero, M. L., Calderón-Peláez, M. A., and Castellanos, J. E. (2016). In vitro infection with dengue virus induces changes in the structure and function of the mouse brain endothelium. *PLoS One* 11, 1–20. doi: 10.1371/journal.pone.0157786

Verma, S., Kumar, M., Gurjav, U., Lum, S., and Nerurkar, V. R. (2010). Reversal of West Nile virus-induced blood-brain barrier disruption and tight junction proteins degradation by matrix metalloproteinases inhibitor. *Virology* 397, 130–138. doi: 10.1016/j.virol.2009.10.036

Verma, S., Lo, Y., Chapagain, M., Lum, S., Kumar, M., Gurjav, U., et al. (2009). West Nile virus infection modulates human brain microvascular endothelial cells tight junction proteins and cell adhesion molecules: transmigration across the in vitro blood-brain barrier. *Virology* 385, 425–433. doi: 10.1016/j.virol.2008.11.047

Vieira, M. A. D. C. E. S., Costa, C. H. N., Linhares, A. D. C., Borba, A. S., Henriques, D. F., Silva, E. V. P. D., et al. (2018). Potential role of dengue virus, chikungunya virus and Zika virus in neurological diseases. *Mem. Inst. Oswaldo Cruz* 113:e170538. doi: 10.1590/0074-02760170538

Wan, W., Chen, H., and Li, Y. (2014). The potential mechanisms of Aβ-receptor for advanced glycation end-products interaction disrupting tight junctions of the blood-brain barrier in Alzheimer's disease. *Int. J. Neurosci.* 124, 75–81. doi: 10.3109/00207454.2013.825258

Wang, P., Dai, J., Bai, F., Kong, K. F., Wong, S. J., and Montgomery, R. R. (2008a). Matrix metalloproteinase 9 facilitates West Nile virus entry into the brain. *J. Virol.* 82, 8978–8985. doi: 10.1128/JVI.00314-08

Wang, T., Town, T., Alexopoulou, L., Anderson, J. F., Fikrig, E., and Flavell, R. A. (2004). Toll-like receptor 3 mediates West Nile virus entry into the brain causing lethal encephalitis. *Nat. Med.* 10, 1366–1373. doi: 10.1038/nm1140

Wang, K., Wang, H., Lou, W., Ma, L., Li, Y., Zhang, N., et al. (2018). IP-10 promotes blood-brain barrier damage by inducing tumor necrosis factor alpha production in Japanese encephalitis. *Front. Immunol.* 9, 1–14. doi: 10.3389/fimmu.2018.01148

Wang, S., Welte, T., McGargill, M., Town, T., Thompson, J., Anderson, J. F., et al. (2008b). Drak2 contributes to West Nile virus entry into the brain and lethal encephalitis. *J. Immunol.* 181, 2084–2091. doi: 10.4049/jimmunol.181.3.2084

Xu, Z., Waeckerlin, R., Urbanowski, M. D., van Marle, G., and Hobman, T. C. (2012). West Nile virus infection causes endocytosis of a specific subset of tight junction membrane proteins. *PLoS One* 7, 1–11. doi: 10.1371/journal.pone.0037886

Yamada, M., Nakamura, K., Yoshii, M., Kaku, Y., and Narita, M. (2009). Brain lesions induced by experimental intranasal infection of Japanese encephalitis virus in piglets. *J. Comp. Pathol.* 141, 156–162. doi: 10.1016/j.jcpa.2009.04.006

Zamanian, J. L., Xu, L., Foo, L. C., Nouri, N., Zhou, L., Giffard, R. G., et al. (2012). Genomic analysis of reactive astrogliosis. *J. Neurosci.* 32, 6391–6410. doi: 10.1523/JNEUROSCI.6221-11.2012

Conflict of Interest Statement: The authors declare that the research was conducted in the absence of any commercial or financial relationships that could be construed as a potential conflict of interest.

Title: DEVELOPMENT OF STANDARD METHODS FOR ZIKA VIRUS PROPAGATION, TITRATION, AND PURIFICATION

Authors: Sharton Vinicius Antunes Coelho, Rômulo Leão Silva Neris, Michelle Premazzi Papa, Laila Castro Schnellrath, Lana Monteiro Meuren, Diogo A. Tschoeke, Luciana Leomil, Brunno Renato Farias Verçoza, Milene Miranda, Fabiano L. Thompson, Andrea Thompson Da Poian, Thiago Moreno L. Souza, Fabiana Avila Carneiro, Clarissa R. Damaso, Iranaia Assunção-Miranda, Luciana Barros de Arruda

PII: S0166-0934(17)30123-4
DOI: http://dx.doi.org/doi:10.1016/j.jviromet.2017.04.011
Reference: VIRMET 13241

To appear in: *Journal of Virological Methods*

Received date: 21-2-2017
Revised date: 9-4-2017
Accepted date: 14-4-2017

Please cite this article as: Coelho, Sharton Vinicius Antunes, Neris, Rômulo Leão Silva, Papa, Michelle Premazzi, Schnellrath, Laila Castro, Meuren, Lana Monteiro, Tschoeke, Diogo A., Leomil, Luciana, Verçoza, Brunno Renato Farias, Miranda, Milene, Thompson, Fabiano L., Da Poian, Andrea Thompson, Souza, Thiago Moreno L., Carneiro, Fabiana Avila, Damaso, Clarissa R., Assunção-Miranda, Iranaia, de Arruda, Luciana Barros, DEVELOPMENT OF STANDARD METHODS FOR ZIKA VIRUS PROPAGATION, TITRATION, AND PURIFICATION.Journal of Virological Methods http://dx.doi.org/10.1016/j.jviromet.2017.04.011

DEVELOPMENT OF STANDARD METHODS FOR ZIKA VIRUS PROPAGATION, TITRATION, AND PURIFICATION

Running title: ZIKV propagation and purification

Sharton Vinicius Antunes Coelho[1#], Rômulo Leão Silva Neris[1#], Michelle Premazzi Papa[1], Laila Castro Schnellrath[2], Lana Monteiro Meuren[1], Diogo A. Tschoeke[3], Luciana Leomil[3], Brunno Renato Farias Verçoza[4], Milene Miranda[5], Fabiano L. Thompson[3], Andrea Thompson Da Poian[6], Thiago Moreno L. Souza[5,7], Fabiana Avila Carneiro[4], Clarissa R. Damaso[2], Iranaia Assunção-Miranda[1*], Luciana Barros de Arruda[1*]

[1]Departamento de Virologia, Instituto de Microbiologia Paulo de Góes, Universidade Federal do Rio de Janeiro (UFRJ), Rio de Janeiro, RJ, Brasil

[2]Instituto de Biofisica Carlos Chagas Filho (IBCCF). Universidade Federal do Rio de Janeiro (UFRJ), Rio de Janeiro RJ, Brasil

[3]Departamento de Genética. Instituto de Biologia. Universidade Federal do Rio de Janeiro (UFRJ), Rio de Janeiro RJ, Brasil

[4]NUMPEX - Núcleo Multidisciplinar de Pesquisas, Polo Avançado de Xerém, Universidade Federal do Rio de Janeiro (UFRJ), Duque de Caxias, RJ, Brazil

[5]Laboratório de Imunofarmacologia, Instituto Oswaldo Cruz (IOC), Fundação Oswaldo Cruz (Fiocruz), Rio de Janeiro, RJ, Brazil

[6]Instituto de Bioquímica Médica Leopoldo de Meis, Universidade Federal do Rio de Janeiro (UFRJ), Rio de Janeiro, RJ, Brasil

[7]National Institute for Science and Technology on Innovation on Neglected Diseases (INCT/IDN), Center for Technological Development in Health (CDTS), Fiocruz, Rio de Janeiro, RJ, Brazil

* To whom correspondence should be addressed:

- Instituto de Microbiologia Paulo de Góes, Universidade Federal do Rio de Janeiro. CCS, Bloco I, lab. I-SS-048; lab. I-SS-055. Av. Carlos Chagas Filho, 373. Cidade Universitária, Rio de Janeiro, RJ, Brazil, 21941-902. Tel.: (5521) 2560-8344 (ext. 117); Fax: (5521) 2560-8344; E-mail: arruda@micro.ufrj.br, iranaiamiranda@micro.ufrj.br.

#These authors equally contributed to this work

Highlights

- Standard protocols for propagation and titration of Zika virus strains were established
- The susceptibility of different cell types to Zika virus infection was determined

- Developed a protocol for virus purification leading to optimal yields and purity

Abstract – 198 words; text – 4035 words

ABSTRACT

The emergence of Zika virus (ZIKV) infection has stimulated several research groups to study and collaborate to understand virus biology and pathogenesis. These efforts may assist with the development of antiviral drugs, vaccines and diagnostic tests, as well as to promote advancements in public health policies. Here, we aim to develop standard protocols for propagation, titration, and purification of Asian and Brazilian ZIKV strains, by systematically testing different cell types, kinetics, multiplicity of infection and centrifugation protocols. ZIKV produces a productive infection in human, non-human primate, and rodents-derived cell lines, with different efficacies. The highest yield of ZIKV-AFR and ZIKV-BR infectious progeny was obtained at 7 days post infection in C6/36 cells (7×10^7 and 2×10^8 PFU/ml, respectively). However, high titers of ZIKV-AFR could be obtained at earlier time points in Vero cells (2.5×10^7 PFU/ml at 72hpi), whereas ZIKV-BR titers reached 10^8 PFU/ml at 4dpi in C6/36 cells. High yield of purified virus was obtained by purification through a discontinuous sucrose gradient. This optimized procedure will certainly contribute to future studies of virus structure and vaccine development. Beyond the achievement of efficient virus propagation, the normalization of these protocols will also allow different laboratories around the world to better compare and discuss data regarding different features of ZIKV biology and disease, contributing to more efficient collaborations and progression in ZIKV research.

Keywords: Zika virus; virus propagation; virus purification; standard protocols

INTRODUCTION

Zika disease, caused by Zika virus (ZIKV) infection, has recently emerged as a global health concern, being reported in more than 60 countries around the world (WHO, 2016). The urgent need of reliable diagnostic tests, virus control measures, and efficient surveillance programs has gathered researchers with different expertise in a huge effort to further understand ZIKV biology.

Zika virus (ZIKV) is an arthropod-borne virus (arbovirus), from *Flaviviridae* family, genus *Flavivirus*, which is transmitted by mosquitoes from *Aedes* genus. The virus was first isolated in 1947, in Uganda, and, until 2007, very few human cases had been described, all were associated with mild clinical symptoms (Dick, et al., 1952). After human-associated outbreaks occurred in Micronesia and Pacific Islands, in 2007 and 2013, ZIKV spread throughout the Americas, causing a large outbreak, especially in Brazil (Lanciotti, et al., 2008; Hayes, 2010; Cao-Lormeau, et al., 2014; Faria, et al., 2016). As virus circulation scaled up, a broader spectrum of clinical manifestations has been reported. Severe neurological symptoms, such as microcephaly and other malformations have been reported after congenital infection (Oliveira Melo, et al., 2016; Rasmussen, et al., 2016, Melo, et al., 2016). Also, meningoencephalitis and Guillain-Barré syndrome were associated with ZIKV infection in adults (Carteaux, et al., 2016; Brasil, et al., 2016). Importantly, other forms of transmission were confirmed or are being investigated, including maternal-fetal, sexual, posttransfusion and posttransplant, and even direct contact (Martines, et al., 2016; Calvet, et al., 2016; Mlakar, et al, 2016; D'Ortenzio, et al., 2016; Davidson, et al., 2016; Tang, et al., 2016; Nicastri, et al., 2016; Musso, et al., 2014; Musso, et al., 2015; Barjas-Castro, et al., 2016; Nogueira, et al., 2017; Swaminathan, et al., 2016).

ZIKV is enveloped and contains a single-stranded positive-sense genome. Two different ZIKV lineages have been epidemiologically characterized, African and Asian. The African ZIKV is an ancestral strain, whereas the Asian lineage is currently circulating and causing the epidemic outbreak in the Americas (Weaver, et al., 2016; Calvet, et al., 2016; Zhu, et al., 2016).

The necessity of a global effort to study different aspects of ZIKA biology, including specialist and non-specialist scientific community, demands the establishment of standard protocols. However, the yield of low-titer ZIKV stocks in cell culture may be a hurdle for expanding the range of experimental approaches. Additionally, the use of concentrated and purified ZIKV as a source of virus stock would minimize cross-interference of cellular molecules secreted from cells during infection, or even from constitutive cell contamination, as was described with *A.* a*lbopictu*s C6/36 cells line (Chen, et al., 2004). Therefore, purified virus stocks may be more suited for some experimental strategies than the use of infected-cell supernatants, particularly, those studies involving vaccine development, animal models and host-cell interaction assays. The establishment and standardization of routine protocols to propagate, titrate, and purify ZIKV particles, as well as the investigation of susceptible and permissive cell lines, will be, then, very helpful to overcome the current experimental problems and to optimize ZIKV research. Here, we determined the kinetics and optimal multiplicity of infection to propagate virus stocks and evaluated ZIKV infection in nine different cell lines. These cell lines represent epithelial, endothelial and glial cells, from lung, kidney and brain tissues, derived from insect (C6/36), humans (HBMEC, A549, U87, and HeLa), non human primates (Vero, LLCM-K2), and rodents (BHK-21, C6). Moreover, we established a protocol for virus particles purification leading to optimal yields and purity.

The standardization of reliable protocols may expedite the study of ZIKV biology and contribute to efficient Zika-study networks.

MATERIALS AND METHODS

Cell lines

C6/36 mosquito cell line (ATCC-CLR1660; kindly given by Dr. Andrea T. Da Poian, Instituto de Bioquímica Médica, UFRJ) were cultured at 28°C in Leibovitz (L-15) medium (Life Technologies) supplemented with 0.3% of tryptose phosphate broth, 0.75% sodium bicarbonate, 0.2% of L-glutamine (Sigma-Aldrich, St Louis, MO), 10% FBS (Life Technologies) and nonessential amino acids. Vero (ATCC-CCL81; kindly given by Dr. Amilcar Tanuri, Instituto de Biologia, UFRJ), LLC-MK2 (ATCC-CCL7), and A549 (ATCC-CCL-185) cells were cultured in DMEM high glucose, supplemented with L-glutamine and 5% fetal bovine serum (Life Technologies, Grand Island, NY). U87-MG (ATCC-HTB14; kindly given by Dr. Amilcar Tanuri) and C6 glioma (ATCC-CCL107) cells were cultured with the same culture medium supplemented with 1 mM non-essential amino acids. HBMEC (human brain microvascular endothelial cells; kindly provided by Dr. Dennis Grab, The Johns Hopkins University, MD, USA) (Nikolskaia, et al., 2006) were cultured in M199 supplemented with L-glutamine and 5% fetal bovine serum. All cells, except for C6/36, were maintained at 37°C with 5% CO_2. Mycoplasma-free conditions of cell cultivation were routinely certified by checking the presence of cytoplasmic DNA in a fluorescence microscope, using DAPI probe (Santa Cruz Biotechnology), and by PCR, using a mixture of oligonucleotides for the specific detection of mycoplasmas, as previously described (Freshney, 2005).

Virus

ZIKV strain MR766 (ZIKV-AFR, ATCC VR1838) was kindly provided by Dr. Amilcar Tanuri (Instituto de Biologia, UFRJ).

ZIKV-BR_{PE} was isolated from a febrile case in the state of Pernambuco, Brazil and was kindly provided by Dr. Ernesto T.A. Marques Jr. (Centro de Pesquisas Aggeu

Magalhães, FIOCRUZ, PE) (gene bank ref. number KX197192). ZIKV-BR_{SP} was distributed as part of ZIKA FAPESP NETWORK and it was kindly provided by Dr. Mauricio L. Nogueira (FAMERP, SP) (Faria, et al., 2016). Both ZIKV-BR samples were obtained after 3-4 passages in C6/36 cells and metagenomics analysis was performed by our group after six passages in C6/36 cell line, as described therafter.

Metagenomics and genome assembly

ZIKV samples (2 x 10^5 PFU) in 300 µl was filtered through 0.22 µm membranes, followed by RNA extraction (QIAamp Viral RNA Mini Kit, Qiagen). To remove any residual DNA, the samples were treated with RNase-free DNAse, according to manufacturer's instructions (DNAse RNAse-free Set, Qiagen®) Double-stranded cDNA libraries were constructed by Truseq Stranded total RNA LT (Illumina®) with Ribo-zero treatment, according to the manufacturer´s instruction. The library size distribution was assessed using 2100 Bioanalyzer (Agilent®) with High Sensitive DNA kit (Agilent®), and the quantification was performed with 7500 Real-time PCR System (Applied Biosystems®) with KAPA Library Quantification Kit (Kapa Biosystems). Paired-end sequencing (2 x 300 bp) was done with MiSeq Reagent kit v3 (Illumina®). The sequences were analyzed using the PRINSEQ software to remove reads smaller than 50 bp and those with Phred quality score of < 20. Paired-End reAd merger (PEAR) software was used to merge and extend the paired-end Illumina reads using the default parameters (Schmieder and Edwards, 2011a; Zhang, et al., 2014). The extended reads were analyzed with Deconseq program, against the Human Genome Database, with Identity and Coverage cutoff of 70%, to remove human RNA sequences (Schmieder and Edwards, 2011b). Non-human reads were analyzed against all GenBank viral genomes (65,052 sequences) with BLAST software using 1e-5 e-value cutoff. The sequences rendering a genome were assembled with SPAdes 3.7.1 software (Nurk, et al., 2013) followed by a reassemble with

CAP3 program (Huang and Madan, 1999). The metagenomic results are demonstrated as Supplementary Data.

Cell infection

Cells were cultured overnight in their respective culture medium and supplements for complete adhesion, until 70% confluence was obtained. Then, each cell type was infected with the different ZIKV samples, using MOIs from 0.01 to 0.25, in the absence of FCS, for 90 min, with gentle agitation, for virus adsorption. Media were removed, and substituted by the appropriate culture medium, supplemented with 2% FCS (C6/36, Vero, HBMEC, LLC-MK2 cells) or 7% FCS (A549, C6, HeLa cells). Infected cell cultures were observed daily for possible cytopathic effects (CPE). Cells and supernatants were harvested when about 70% CPE was observed, or at the indicated time points. To perform temporal analyses of ZIKV replication in VERO and C6/36 cells, culture supernatants were collected on the indicated days and replaced with proportional fresh medium.

Plaque assay

Samples obtained at different time points post-infection were titrated by plaque assay. Vero cells were plated, in 24-well plates, at the concentration of 4 x 10^4 cells/500µl/well, and cultured overnight for complete adhesion. Then, medium was removed, cells were washed with PBS, and incubated with serial dilutions of virus samples, in FCS-free medium. After 90-min incubation under slight agitation, medium was removed, cells were washed with PBS, and cultured with different concentration of carboxy-methil-cellulose (CMC), supplemented with 1% FCS. After 5 days, cells were fixed overnight with 4% formaldehyde and stained with 1% violet crystal for 1 h. Plaques were counted and virus yield was calculated and expressed as PFU/ml.

Analysis of viral replication by qRT-PCR

C6/36 cells were infected with the indicated MOI of ZIKV-BR_{PE} for 7 days, as described. The supernatant was harvested and RNA was extracted using TRIZOL reagent (Life Technologies), according to the manufacturer's instructions, using 300 µl of supernatant and 1 ml Trizol. Treatment with DNAse I (Ambion, Thermo Fischer) was performed to remove genomic DNA contamination and first strand cDNA was synthesized using High-Capacity cDNA Archive Kit (Applied Biosystems), according to the manufacturer's instructions. cDNAs were tested with quantitative real-time PCR using a StepOnePlus Real-time PCR system and Taqman Master Mix Reagents (Applied Biosystems), using primers and probe specific for the E sequence, as described by Lanciotti et al (Lanciotti, et al., 2008). The supernatants was titrated by plaque assay to perform a standard curve and determine the equivalent PFU.

Virus purification

C6/36 cells (10^8) were infected with ZIKV-BR_{PE} (MOI=0.01) for 7 days and the supernatant was harvested and clarified to remove cellular debris by centrifugation at 700 *g* for 20 min at 4ºC. The supernatant was then centrifuged at 150,000 *g* for 2.5 h at 4ºC, using a 45Ti rotor (Beckman). The supernatant was discarded and 200 µl of 3E buffer (0.12 M tris-base, 0.06 M sodium acetate, 3 mM EDTA), pH 7.4, was added to the pellet, which was incubated overnight at 4ºC to resuspend virus pellet without agitation and minimize loss of viral particle integrity. The resuspended pellet was than ultracentrifuged in a discontinuous 10-60% sucrose gradient at 116,000 *g* for 1.5 h at 4ºC, using a SW41 rotor (Beckman). The gradient fractions were identified as upper (up), middle, two purified fractions (FP#1 and FP#2), and the lower fraction (bottom), and collected in an approximate volume ratio of 1:4:1:1:5 (ml). Sucrose was removed from purified fractions by centrifugation in centrifugal filter units (Amicon Ultra-15 3000 NMWL, Merck Millipore) with PBS at 7,500 *g* at 4° C for 30 min, adding PBS at 10 min intervals. The

virus was stored at -80°C. Each fraction obtained from the gradient was titrated by plaque assay, as previously described. In addition, fractions were also analyzed by electrophoresis in SDS-polyacrylamide gel stained with Coomassie Blue-R.

Electron Microscopy

Electron microscopy analyzes were performed using the negative contrast technique. ZIKV purified samples were fixed with 2.5% glutaraldehyde (Sigma-Aldrich) in 0.1 M sodium cacodylate buffer, pH 7.3, for 30 min. Then, 10 µl of the samples were dropped gently on copper grids, previously coated with Formvar film (Ted Pella), where they remained for 2 min for adherence of the ZIKV on the film. The drop was gently dried with filter paper, followed by negative staining with 5% uranyl acetate for 30 sec and, then, gently dried with filter paper. The images were obtained in transmission electron microscope FEI Tecnai Spirit operating at 120 kV.

Statistical analyses

Data were analyzed using the GraphPad Prism software (GraphPad Software, San Diego, CA, USA). Comparisons among groups were performed by two way ANOVA; p values <0.05 were considered statistically significant.

RESULTS

Replication kinetics of ZIKV-AFR and ZIKV-BR$_{PE}$ in Vero and C6/36 cell lines

Standardization of the stock titers and replication kinetics of ZIKV, in mammalian and mosquito cell lines are necessary to study the virus biology. Initially, we evaluated the best conditions to determine virus titers by plaque assay, using Vero cells. Cells at 70-80% confluence were infected with different dilutions of the virus stock, and incubated with different concentrations of CMC for 5 days. After fixing with formaldehyde and staining with violet crystal, we detected clear and homogeneous plaques when cells were cultured with 1.5% CMC. Infected Vero cells cultured with 1% CMC generated irregular, comet-like plaques; and monolayers incubated with 3% CMC generated very small plaques, which were difficult to count with consistency (Figure 1). We also performed the titration assay at different days post-infection and with higher cell confluence, but the results were not clear nor reproducible (data not shown).

Once we established that 5 days of infection and 1.5% CMC were the best conditions for plaque assay, we started to determine the best protocol to propagate ZIKV in mammalian (Vero) and mosquito (C6/36) cell lines. We also compared two different virus isolates, the prototype ZIKV MR766 strain, from African lineage (ZIKV-AFR), and the Brazilian ZIKV isolate from Pernambuco, which was previously sequenced and belongs to Asian lineage (ZIKV-BR$_{PE}$) (Way, et al., 1976; Donald, et al., 2016).

Vero cells were infected with different MOIs, from 0.1 to 0.01 and supernatants were harvested at 3 days post-infection (dpi), when 70% CPE was detected in the culture. The efficiency of virus replication increased as the MOI was reduced. ZIKV-AFR showed higher replication rates in this cell type when compared with ZIKV-BR$_{PE}$, with titers above 10^7 PFU/ml at MOI 0.01 (Figure 2A). To confirm that ZIKV infection has reached

the highest titer at 3 dpi, cells were infected with both ZIKV strains, at MOI 0.01, and supernatants were harvested after 2, 3 and 4 dpi (Figure 2B). Cell morphology and CPE were also evaluated daily, as shown in Figure 2C. Titers of ZIKV-AFR were almost 10^7 PFU/ml at 2 dpi already, reaching a peak on day 3, and a small decrease later on, when most of the cells were dead (Figures 2B and 2C). On the other hand, ZIKV-BR_{PE} showed a slower replication kinetic when compared with ZIKV-AFR, reaching the highest titer (3×10^6 PFU/ml) only at 4 dpi. Although CPE was detected at this time point, the cells were still adhered to the flask, whereas in the ZIKV-AFR-infected cultures, most of the cells had already detached (Figure 2C).

Similar assays were performed using freshly thawed C6/36 cells,., in which both ZIKV-AFR and ZIKV-BR_{PE} produced high levels of infectious virus particles, when cells were infected at MOI 0.01 (Figure 3A). The differences detected due to infection with different MOIs were much less prominent, in comparison to what was observed during infection of Vero cells with both ZIKV strains. In addition, cytopathic effect was barely detected until 7 dpi, and at 10 dpi, around 70-80% of the monolayer was intact (Figure 3C). We harvested supernatants from cells infected with either ZIKV-AFR or ZIKV-BR_{PE} at 4 to 10 dpi, and analyzed virus titers by plaque assay. Infection with ZIKV-BR_{PE} resulted in higher virus titers at 4 dpi, despite no obvious CPE formation (Figure 3B and 3C). After this time point, 50% medium was replaced by fresh culture medium, and supernatants were harvested at 7 and 10 dpi. Virus titers were very similar at subsequent time points, indicating that high-yield ZIKV-BR_{PE} stocks can be obtained as early as 4 dpi in C6/36 cells. Infection with ZIKV-AFR also resulted in high virus titer, but only at 7 dpi (Figure 3B).

These data indicated that both cell lines are useful for virus propagation, yielding approximately 10^7-10^8 PFU/ml, when a MOI of 0.01 was used. Interestingly, higher titers

of ZIKV-AFR were obtained at earlier time point in Vero cells (10^7 PFU/ml at 3 dpi), , whereas ZIKV-BR_{PE} replication showed a faster and higher replication rate in C6/36 cells (10^8 PFU/ml in 4 days). Therefore, the time point for harvesting the cell supernatant should be different according to the virus strain and cell line. To investigate whether these differences were specifically related to the virus isolate, we compared two different Brazilian ZIKV isolates – ZIKV-BR_{PE} (previously used) and ZIKV-BR_{SP}. Both isolates showed similar replication kinetics and yield of infectious progeny in C6/36 and Vero cells (Figures 4A-D).

We then established a correlation between the production of infectious ZIKV particles and the detection of virus genome using, respectively, the plaque assay protocol described here and qRT-PCR described by Lanciotti (Lanciotti, et al., 2008). Supernatants from ZIKV-BR_{PE}-infected cells were used to perform a virus titration curve, ranging from 10^3 to 10^8 PFU, and tested by quantitative real time RT-PCR; the correlation between PFU and Ct numbers is shown in Figure 4E.

Susceptibility of different cell lines to ZIKV replication

After confirming C6/36 and Vero cells as standard cell models for virus propagation, we analyzed the susceptibility of distinct cell types, obtained from different tissues and host species, to the Brazilian ZIKV strain. Cell lines from human origin (A549, HBMEC, U87, HeLa), primates (LLC-MK2), rat (C6) and hamster (BHK-21) were evaluated. In order to compare the replication efficiency between the cell lines, we normalized the infection protocol using MOI 0.1 and harvested the supernatants at 3 dpi. In cases where we could not observe any evidence of CPE at this time point, cells were maintained for longer periods. Since those cells may be cultured at different concentrations to achieve confluence and may show distinct proliferation and survival kinetics under their specific culture conditions, we calculated the PFU/cell ratio,

considering the initial cell numbers at the time of infection. Among the mammalian cell lines tested in this work, human lung epithelial (A549) and human brain microvascular endothelial cells (HBMEC) showed the highest rates of extracellular progeny production, above 1 PFU/cell. However, none of them reached the progeny production of the invertebrate cell line C6/36 (16 PFU/cell), which further increased to 468 PFU/cell at 7 dpi. All other cell lines tested, including brain-tumor derived cells, were poorly permissive to virus replication showing very low progeny yields in comparison to A549, HBMEC, C6/36, and Vero cells (Table 1).

Standardization of ZIKV purification method

Finally, we set up a protocol to purify ZIKV, allowing the production of virus stocks highly concentrated and free of most cell contaminants. For this purpose C6/36 cells, which gave the highest virus yield, were infected with ZIKV-BR_{PE} at MOI 0.01. After 7 days, virus was purified from the cell supernatant using a discontinuous 10-60% sucrose gradient, as described in Methods. Purified ZIKV could be clearly detected as an opaque band in the centrifugation tube, which was then defined as the purified fraction (PF) (Figure 5A). For further analyses, different gradient fractions were defined (Figure 5A) and carefully collected for analysis by SDS-polyacrylamide gel electrophoresis. A protein band with the expected mass of the viral E glycoprotein was enriched in the purified fraction (Figure 5B). To determine the presence of infectious ZIKV particles along the gradient fractions, all fractions were titrated by plaque assay. Indeed, despite the presence of ZIKV in all

fractions, the purified fraction showed titers higher than 10^9 PFU/ml (Figure 5C) and the efficiency of infectious virus recovery was determined to be higher than 65% (Table 2). Analysis of the purified fraction by electron microscopy confirmed the enrichment of

intact purified virus of approximate 50 nm size (Figure 5D), as previously described (Kostyuchenko, et al., 2016).

DISCUSSION

Autochthonous transmissions of ZIKV have been reported in Brazil since 2015 followed by rapid virus spread to other American countries (Faria, et al., 2016; Zanluca, et al., 2015; Campos, et al., 2015). The acuteness of the outbreaks and the severe neurological effects of the infection compelled the scientific community to invest efforts in the study of various aspects of ZIKV biology. Many research groups involved in ZIKV research came from different backgrounds, mostly outside the flavivirus field, needing to overcome the obstacles imposed by the generation of low-titer virus stocks, a well-known feature of the flaviviruses (Maramorosch and McIntosh, 1994).

In the present work, we determined routine protocols to propagate, titrate and purify ZIKV, using mosquito and mammalian cell lines. C6/36 and Vero cells have been used for virus propagation, but different laboratories would use diverse protocols, resulting in different yields of virus stocks. Research groups that have not worked with ZIKV or other flaviviruses would need to obtain standard protocols. Our goal was to determine the appropriate cell lines and infection conditions to obtain optimal virus titers in a reproducible fashion. For that purpose, we tested cell confluence, MOI and replication kinetics of ZIKV from African and Asian lineages. ZIKV-AFR used in this study was the African isolate prototype MR766, which was originally propagated in Vero cells (Way, et al., 1976). In fact, this strain was best propagated in this cell type, with the production of more than 10^7 PFU/ml at 2 dpi.. On the other hand, the two Brazilian strains (Asian lineage) analyzed in this study replicated best in mosquito C6/36 cells. However, if one needs to compare different virus strains, it will be desirable to use viruses that originated or propagated from the same cell source. Therefore, we established that a 4-

day infection of Vero cells, and 7 day-infection of C6/36 cells, using MOI of 0.01, provide similar titers for both ZIKV strains. It is important to note that infection with ZIKV did not induce a remarkable CPE in C6/36 cells, and high virus yields were obtained even when cell morphology and adherence to the flasks were similar to mock-infected controls. In addition, we detected that C6/36 infection produced highest yields when the cells were used freshly after thawing.

Virus-induced CPE also differed when Vero cells were infected with ZIKV-AFR or ZIKV-BR$_{PE}$. In the latter case the cells adhered to the flasks for longer period, although presented a more round morphology. These subtle details may also help researchers to analyze whether the cell type is adequate for virus propagation.

Importantly, we evaluated ZIKV replication in a few cell lines, from different tissues and host species, and detected two human cell types – HBMEC and A549 - which produced high virus titers upon infection. Interestingly, virus replication in brain-tumor derived cells from rat or human origin produced negligible titers. ZIKV-AFR replicated better in primate cells than the Brazilian strain, probably reflecting prior virus adaptation to non-human primate cells. In this context, it is noteworthy that infection of mosquito C6/36 cells with ZIKV-BR generated the highest progeny production among all tested cell lines.

Finally, ZIKV purification was achieved by sedimentation through a sucrose gradient with a recovery efficiency higher than 65%. The recovery of purified ZIKV was confirmed by SDS-acrylamide gel electrophoresis, electron microscopy, and titration of all fractions. High yields and purity of purified virus are essential for studies on virus structure and virus interaction with cellular components. A previous study had described a method for ZIKV (French Polynesia strain H/PF/2013) purification using a sucrose cushion centrifugation followed by a continuous potassium tartrate gradient (Sirohi, et

al., 2016). This method also allowed high yield of purified ZIKV, but required the use of a Vero cell lineage that overexpressed protease furin, different from the cell line used in the present work, C6/36, which is routinely used by several groups. In addition, we were able to obtain enriched virus fractions using less C6/36 cells than Vero because the mosquito cells produce the highest yield of extracellular infectious virus among all tested cell lines.

In summary, we developed detailed protocols that may help researchers from different areas of expertise to study ZIKV biology and pathogenesis. Our study might contribute to further establish ZIKV networks around the world to control this infection.

ACKNOWLEDGMENTS

This work was supported by CAPES, CAPES/PVE-Program, CNPq, FAPERJ-Rede ZIKA, and FINEP. SVAC was the recipient of a FAPERJ fellowship. RLSN and MPP were recipients of CNPq fellowships. LCS was the recipient of a CAPES fellowship. CD and ATP are recipients of CNPq research fellowships.

The authors wish to thank Dr. Ernesto T. A. Marques Jr (LAVITE, Centro de Pesquisas Aggeu Magalhães-FIOCRUZ, Recife, PE), and Dr. Mauricio Lacerda Nogueira (Faculdade de Medicina de Ribeirão Preto-FAMERP, São José do Rio Preto, SP) for kindly provide ZIKV-$BR_{PE,}$ and ZIKV-BR_{SP}, respectively. The authors also wish to thank Dr. Amilcar Tanuri (Instituto de Biologia, UFRJ, RJ, Brazil) for kindly provide ZIKV-AFR, Vero and U87-MG cell lines; and Dr. Andrea T. Da Poian (Instituto de Bioquímica Médica, UFRJ, RJ, Brazil) for kindly provide C6/36 cell line. We thanks CENABIO (Centro Nacional de Biologia Estrutural e Bioimagem, UFRJ, RJ, Brazil) for support with the electron microscopy. We also acknowledge Sidnei Gomes da Costa, Raquel Cirlene and Ronaldo Rocha for technical support.

The authors declare no conflicts of interest.

REFERENCES

1. Barjas-Castro, M.L., Angerami, R.N., Cunha, M.S., Suzuki, A., Nogueira, J.S., Rocco, I.M., Maeda, A.Y., Vasami, F.G., Katz, G., Boin, I.F., Stucchi, R.S., Resende, M.R., Esposito, D.L., de Souza, R.P., da Fonseca, B.A., Addas-Carvalho, M., 2016. Probable transfusion-transmitted Zika virus in Brazil. Transfusion. **56**, 1684-8.

2. Brasil, P., Sequeira, P.C., Freitas, A.D., Zogbi, H.E., Calvet, G.A., de Souza, R.V., Siqueira, A.M., de Mendonca, M.C., Nogueira, R.M., de Filippis, A.M., Solomon, T., 2016. Guillain-Barré syndrome associated with Zika virus infection. Lancet, **387**, 1482.

3. Calvet, G., Aguiar, R.S., Melo, A.S., Sampaio, S.A, De Filippis, I., Fabri, A., Araujo, E.S., De Sequeira, P.C., De Mendonça, M.C., De Oliveira, L., Tschoeke, D.A., Schrago, C.G., Thompson, F.L., Brasil, P., Dos Santos, F.B., Nogueira, R.M., Tanuri, A., De Filippis, A.M., 2016. Detection and sequencing of Zika virus from amniotic fluid of fetuses with microcephaly in Brazil: A case study. Lancet Infect. Dis. **16**, 653–660.

4. Campos, G.S., Bandeira, A.C., Sardi, S.I., 2015. Zika Virus Outbreak, Bahia, Brazil. Emerg Infect Dis. **21**, 1885-6.

5. Cao-Lormeau, V.M., Roche, C., Teissier, A., Robin, E., Berry, A.L., Mallet, H.P., Sall, A.A., Musso, D., 2014. Zika virus, French Polynesia, South Pacific, 2013. Emerg Infect Dis. **20**, 1960.

6. Carteaux, G., Maquart, M., Bedet, A., Contou, D., Brugières, P., Fourati, S., Cleret de Langavant, L., De Broucker, T., Brun-Buisson, C., Leparc-Goffart, I., Mekontso Dessap, A., 2016. Zika Virus Associated with Meningoencephalitis. New Engl J Med, **374**, 1595-6.

7. Chen, S., Cheng, L., Zhang, Q., Lin, W., Lu, X., Brannan, J., Zhou, Z.H., Zhang, J., 2004. Genetic, biochemical, and structural characterization of a new densovirus isolated from a chronically infected Aedes albopictus C6/36 cell line. Virology. **318**, 123-33.

8. Davidson, A., Slavinski, S., Komoto, K., Rakeman, J., Weiss, D., 2016. Suspected Female-to-Male Sexual Transmission of Zika Virus - New York City, 2016. MMWR Morb Mortal Wkly Rep. **65**, 716-7.

9. Dick, G,W., Kitchen, S.F., Haddow, A.J., 1952. Zika virus. I. Isolations and serological specificity. Trans. R. Soc. Trop. Med. Hyg. **46**, 509-520.

10. Donald, C.L., Brennan, B., Cumberworth, S.L., Rezelj, V.V., Clark, J.J., Cordeiro, M.T., Freitas de Oliveira França, R., Pena, L.J., Wilkie, G.S., Da Silva Filipe, A., Davis, C., Hughes, J., Varjak, M., Selinger, M., Zuvanov, L., Owsianka, A.M., Patel, A.H., McLauchlan, J., Lindenbach, B.D., Fall, G., Sall, A.A., Biek, R., Rehwinkel, J., Schnettler, E., Kohl, A. 2016. Full Genome Sequence and sfRNA Interferon Antagonist Activity of Zika Virus from Recife, Brazil. PLoS Negl Trop Dis. **10(10)**:e0005048.

11. D'Ortenzio, E., Matheron, S., Yazdanpanah, Y., de Lamballerie, X., Hubert, B., Piorkowski, G., Maquart, M., Descamps, D., Damond, F., Leparc-Goffart, I., 2016. Evidence of Sexual Transmission of Zika Virus. N Engl J Med. **374**, 2195-8.

12. Faria, N.R., Azevedo, R.S., Kraemer, M.U., Souza, R., Cunha, M.S., Hill, S.C., Thézé, J., et al., 2016. Zika virus in the Americas: Early epidemiological and genetic findings. Science. **352**, 345-349.

13. Freshney, R.I., 2005. Culture of Animal Cells: A Manual of Basic Technique and Specialized Applications, 5th Edition. John Wiley & Sons, Inc., Hoboken, New Jersey. pp. 315-317

14. Hayes, E.B., 2009. Zika Virus Outside Africa. Emerg Infect Dis. **15**, 2007–2010.

15. Huang, X., Madan, A., 1999. CAP 3: A DNA sequence assembly program. Genome Res. **9**, 868–877.

16. Kostyuchenko, V.A., Lim, E.X., Zhang, S., Fibriansah, G., Ng, T.S., Ooi, J.S., Shi, J., Lok, S.M., 2016. Structure of the thermally stable Zika virus. Nature. **533**, 425-8.

17. Lanciotti, R.S., Kosoy, O.L., Laven, J.J., Velez, J.O., Lambert, A.J., Johnson, A.J., Stanfield, S.M., Duffy, M.R., 2008. Genetic and serologic properties of Zika virus associated with an epidemic, Yap State, Micronesia, 2007. Emerg Infect Dis. **14**, 1232–1239.

18. Maramorosch, K., McIntosh, A.H., 1994. Arthropod Cell Culture Systems. CRC Press; 1st edition (June 3, 1994)

19. Martines, R.B., Bhatnagar, J., de Oliveira Ramos, A.M., Davi, H.P., Iglezias, S.D., Kanamura, C.T., Keating, M.K., Hale, G., Silva-Flannery, L., Muehlenbachs, A.1., Ritter, J., Gary, J., Rollin, D., Goldsmith, C.S., Reagan-Steiner, S., Ermias, Y.1., Suzuki, T., Luz, K.G., de Oliveira, W.K., Lanciotti, R., Lambert, A., Shieh, W.J., Zaki, S.R., 2016. Pathology of congenital Zika syndrome in Brazil: a case series. The Lancet, **6736**, 1–7.

20. Melo, A.S., Aguiar, R.S., Amorim, M.M., Arruda, M.B., Melo, F.O., Ribeiro, S.T., Batista, A.G., Ferreira, T., Dos Santos, M.P., Sampaio, V.V., Moura, S.R., Rabello, L.P., Gonzaga, C.E., Malinger, G., Ximenes, R., de Oliveira-Szejnfeld, P.S., Tovar-Moll, F., Chimelli, L., Silveira, P.P., Delvechio, R., Higa, L., Campanati, L., Nogueira, R.M., Filippis, A.M., Szejnfeld, J., Voloch, C.M., Ferreira, O.C. Jr, Brindeiro, R.M., Tanuri, A., 2016. Congenital Zika Virus Infection: Beyond Neonatal Microcephaly. JAMA Neurol. **73**, 1407-1416.

21. Mlakar, J., Korva, M., Tul, N., Popović, M., Poljšak-Prijatelj, M., Mraz, J., Kolenc, M., Resman, Rus, K., Vesnaver Vipotnik, T., Fabjan Vodušek, V., Vizjak, A., Pižem, J., Petrovec, M., Avšič Županc, T., 2016. Zika Virus Associated with Microcephaly. New Engl J Med., **374**, 951–8.

22. Musso, D., Nhan, T., Robin, E., Roche, C., Bierlaire, D., Zisou, K., Shan Yan, A., Cao-Lormeau, V.M., Broult, J., 2014. Potential for Zika virus transmission through blood transfusion demonstrated during an outbreak in French Polynesia, November 2013 to February 2014. Euro Surveill. **19**, 1-3.

23. Musso, D., Roche, C., Robin, E., Nhan, T., Teissier, A., Cao-Lormeau, V.M., 2015. Potential sexual transmission of Zika virus. Emerg Infect Dis. **21**, 359-61.

24. Nicastri, E., Castilletti, C., Liuzzi, G., Iannetta, M., Capobianchi, M.R., Ippolito, G., 2016. Persistent detection of Zika virus RNA in semen for six months after symptom onset in a traveller returning from Haiti to Italy, February 2016. Euro Surveill. **21**, 1-4.

25. Nikolskaia, O.V., de A Lima, A.P., Kim, Y.V., Lonsdale-Eccles, J.D., Fukuma, T., Scharfstein, J., Grab, D.J. 2006. Blood-brain barrier traversal by African trypanosomes requires calcium signaling induced by parasite cysteine protease. J Clin Invest.;**116(10)**:2739-47.

26. Nogueira, M.L., Estofolete, C.F., Terzian, A.C., Mascarin do Vale, E.P., da Silva, R.C., da Silva, R.F., Ramalho, H.J., Fernandes Charpiot, I.M., Vasilakis, N., Abbud-Filho, M., 2017. Zika Virus Infection and Solid Organ Transplantation: A New Challenge. Am J Transplant. **17**, 791-795

27. Nurk, S., Bankevich, A., Antipov, D., Gurevich, A.A., Korobeynikov, A., Lapidus, A., Prjibelski, A.D., Pyshkin, A., Sirotkin, A., Sirotkin, Y., Stepanauskas, R., Clingenpeel, S.R., Woyke, T., McLean, J.S., Lasken, R., Tesler, G., Alekseyev, M.A., Pevzner, P.A. 2013. Assembling single-cell genomes and mini-metagenomes from chimeric MDA products. J Comput Biol, **20**, 714–737.

28. Oliveira Melo, A.S., Malinger, G., Ximenes, R., Szejnfeld, P.O., Alves Sampaio, S., Bispo de Filippis, A.M., 2016. Zika virus intrauterine infection causes fetal brain abnormality and microcephaly: Tip of the iceberg? Ultrasound Obstet Gynecol, **47**, 6–7.

29. Rasmussen, S.A., Jamieson, D.J., Honein, M.A., Petersen, L.R., 2016. Zika Virus and Birth Defects — Reviewing the Evidence for Causality. New Engl J Med, **374**, 1–7.

30. Schmieder, R., Edwards, R., 2011a. Fast identification and removal of sequence contamination from genomic and metagenomic datasets. PLoS ONE. **6**, 1-11.

31. Schmieder, R., Edwards, R., 2011b Quality control and preprocessing of metagenomic datasets. Bioinformatics, 2011. **27**, 863–864.

32. Sirohi, D., Chen, Z., Sun, L., 2016. The 3.8Å resolution cryo-EM structure of Zika Virus. Science. **352**, 467–470.

33. Swaminathan, S., Schlaberg, R., Lewis, J., Hanson, K.E., Couturier, M.R., 2016. Fatal Zika Virus Infection with Secondary Nonsexual Transmission. N Engl J Med. 2016. **375**, 1907-1909.

34. Tang, W.W., Young, M.P., Mamidi, A., Regla-Nava, J.A., Kim, K., Shresta, S., 2016. A Mouse Model of Zika Virus Sexual Transmission and Vaginal Viral Replication. Cell Rep. **17**, 3091-3098.

35. Way, J.H., Bowen, E.T., Platt, G.S., 1976. Comparative studies of some African arboviruses in cell culture and in mice. J. Gen. Virol. **30**, 123-130.

36. Weaver, S.C., Costa, F., Garcia-Blanco, M.A., Ko, A.I., Ribeiro, G.S., Saade, G., Shi, P.Y., Vasilakis, N., 2016. Zika virus : History , emergence , biology , and prospects for control. Antiviral Res. **130**, 69–80.

37. WHO, 2016. http://www.who.int/mediacentre/news/statements/2016/emergency-committee-zika-microcephaly/en/

38. Zanluca, C., Melo, V.C., Mosimann, A.L., Santos, G.I., Santos, C.N., Luz, K., 2015. First report of autochthonous transmission of Zika virus in Brazil. Mem Inst Oswaldo Cruz. **110**, 569-72.

39. Zhang, J., Kobert, K., Flouri, T., Stamatakis, A., 2014. PEAR: A fast and accurate Illumina Paired-End reAd mergeR. Bioinformatics. **30**, 614–620.

40.Zhu, Z., Chan, J.F., Tee, K.M., Choi, G.K., Lau, S.K., Woo, P.C., Tse, H., Yuen, K.Y., 2016. Comparative genomic analysis of pre-epidemic and epidemic Zika virus strains for virological factors potentially associated with the rapidly expanding epidemic. Emerg Microbes Infect. **5**, 1-11.

FIGURE LEGENDS

Figure 1: Standardization of the titration protocol. ZIKV-BR_{PE} stocks were inoculated in Vero cells, which were cultured with the indicated CMC concentrations. After 5 days, cultures were fixed and stained with crystal violet and plaques were counted.

Figure 2: Replication of ZIKV strains in Vero cells. ZIKV-BR_{pe} or ZIKV AFR were inoculated at the indicated MOI in Vero cells. **(A)** At 3 dpi, the supernatants were harvested and plaque assay was performed. **B-C)** ZIKV-BR_{PE} or ZIKV AFR were inoculated at MOIs of 0.01 in Vero cells. After the indicated dpi, the supernatants were titrated by plaque assay **(B)** and CPE was evaluated by optical microscopy **(C)**. *$p<0.05$

Figure 3: ZIKV strains replication in C6/36cells. A) ZIKV-BR_{PE} or ZIKV AFR were inoculated at the indicated MOIs in C6/36 cells. After 7 days p.i., the supernatants were harvested and plaque assay was performed. **B-C)** ZIKV-BR_{PE} or ZIKV AFR were inoculated at MOIs of 0.01 in C6/36 cells. After the indicated time points p.i., the supernatants were titrated by plaque assay **(B)** and CPE was evaluated by optical microscopy **(C)**.

Figure 4: Different brazilian ZIKV strains show similar replication level and kinetic both in C6/36 and Vero cells. A-B) ZIKV-BR_{PE} or ZIKV-BR_{SP} were inoculated at the indicated MOIs in C6/36 **(A)** or Vero **(B)** cells. After 7 dpi., the supernatants were harvested and viral replication was evaluated by plaque assay. **C-D)** ZIKV-BR_{PE} or ZIKV-BR_{SP} were inoculated with a MOIs 0.01 in C6/36 **(C)** or Vero **(D)** cells. After the indicated time points p.i., the supernatants were titrated by plaque assay. **E)** Correlation between the production of infectious viral particles titrated by plaque assay and the Ct values obtained by qRT-PCR of the supermatant of C6/36 cells infected with ZIKV-BR_{PE}.

Figure 5: ZIKV purification. A) ZIKV-BR_{PE} were centrifuged over a discontinuous sucrose gradient, as described in Methods, and the indicated fractions were collected in an approximated volume ratio of 1:4:1:1:5 (mL). A concentrated virus layer was clearly distinguished and marked as purified fraction (PF) #1 and #2. **B)** All fractions obtained after sucrose gradient centrifugation were analyzed by SDS-PAGE; a band of 55kDa, corresponding to ZIKV E protein is indicated. **C)** All fractions obtained after sucrose gradient centrifugation were titrated in Vero cells. **D)** Purified fractions were observed by TEM. Bars indicate 100nm (left) or 50nm (right). Arrows indicate ZIKV particles.

Table 1: ZIKV replication in different cell types

Cell line	**Cell type/organ**	**Host**	**PFU/ml**	**PFU/cell**
C6/36	Larva / whole	*Aedes albopictus*	5×10^6	16 (464.7*)
HBMEC	Endothelial / Brain	Human	4.5×10^5	3.6
A549	Epithelial / Lung	Human	8.45×10^5	1.14
Vero	Epithelial / Kidney	*African green monkey*	2.2×10^5	0.33
LLCMK-2**	Epithelial / Kidney	*Rhesus monkey*	2.5×10^3	0.0125
BHK-21	Fibroblast / Kidney	Hamster	1.15×10^2	0.00034
U87	Glial / Brain	Human	6.25 x 10	0.0000806
C6	Glial / Brain	Rat	4.75 x10	0.000067
HeLa	Epithelial/cervix	Human	2.75 x 10	0.000042

*7 days

**7 days. LLC-MK2 did not produce detectable PFU at 3 days p.i.

Table 2: Efficiency of ZIKV recovery during the purification procedure

Initial Titer	1.8×10^7 PFU/ml
Initial Volume	300 ml
Initial PFU input	$300 \times 1.8 \times 10^7$ = **5.4×10^9 PFU**
Purified Fraction #1 Titer	2.3×10^9 PFU/ml
Purified Fraction #2 Titer	1.35×10^9 PFU/ml
Volume of Purified fractions	1 ml/each PF
Total PFU in Purified fractions	$2.3 \times 10^9 + 1.35 \times 10^9$ = **3.65×10^9 PFU**
Purification Efficiency (total purified/total input)*100	67.6%

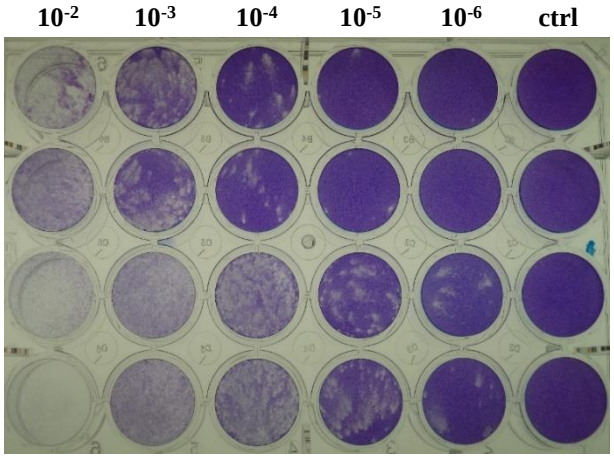

1% CMC

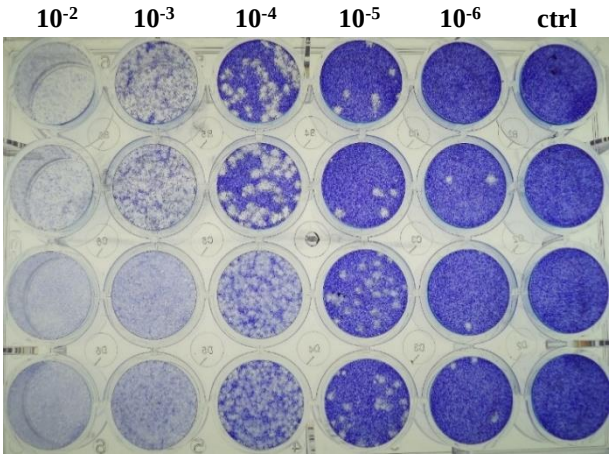

1.5% CMC

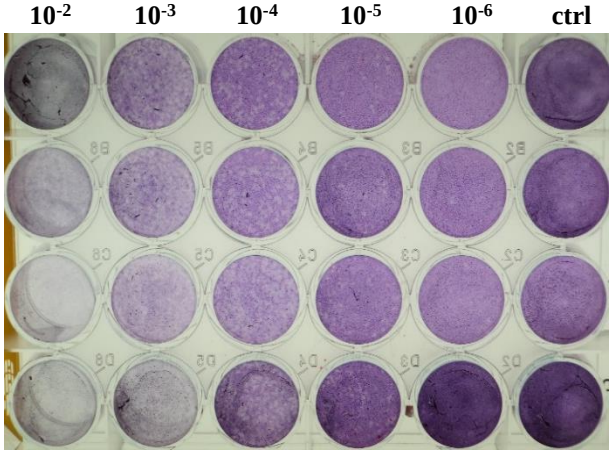

3% CMC

Figure 1

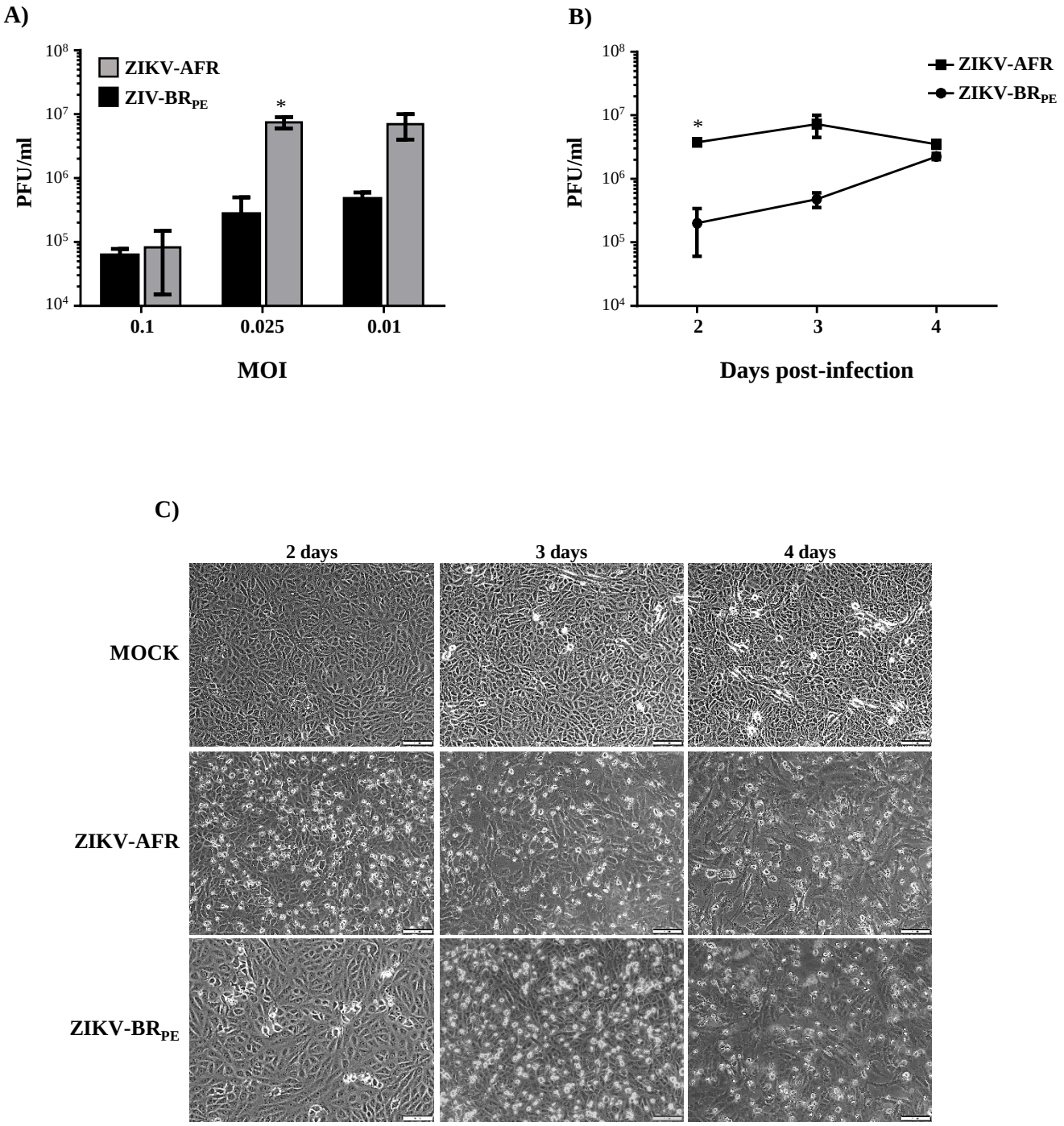
A)
ZIKV-AFR
ZIV-BR$_{PE}$
PFU/ml
10^8
10^7
10^6
10^5
10^4
*
0.1
0.025
0.01
MOI
B)
ZIKV-AFR
ZIKV-BR$_{PE}$
PFU/ml
*
2
3
4
Days post-infection
C)
2 days
3 days
4 days
MOCK
ZIKV-AFR
ZIKV-BR$_{PE}$

Figure 2

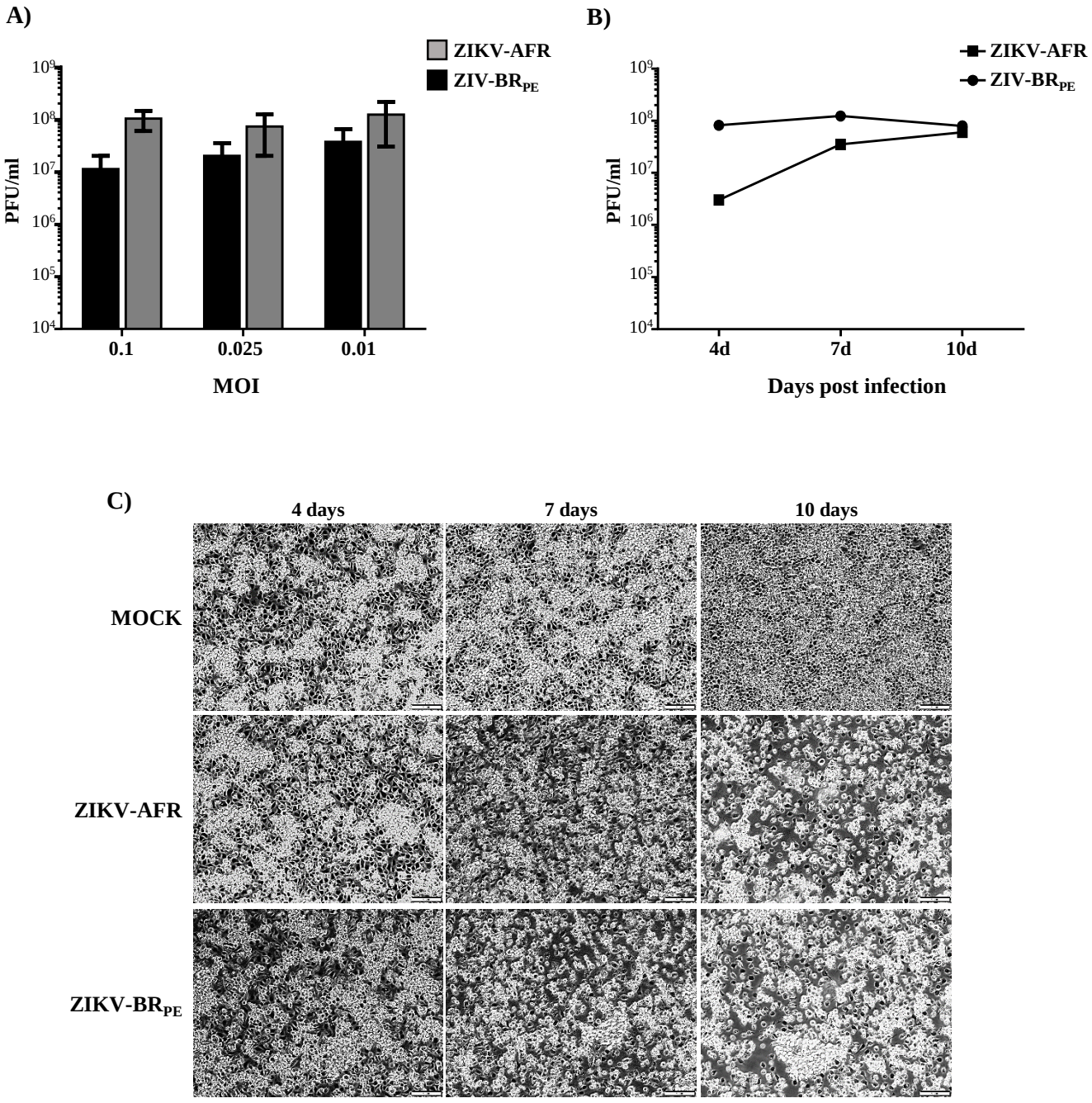
A)
ZIKV-AFR
ZIV-BR$_{PE}$
PFU/ml
10^9
10^8
10^7
10^6
10^5
10^4
0.1
0.025
0.01
MOI
B)
ZIKV-AFR
ZIV-BR$_{PE}$
PFU/ml
4d
7d
10d
Days post infection
C)
4 days
7 days
10 days
MOCK
ZIKV-AFR
ZIKV-BR$_{PE}$

Figure 3

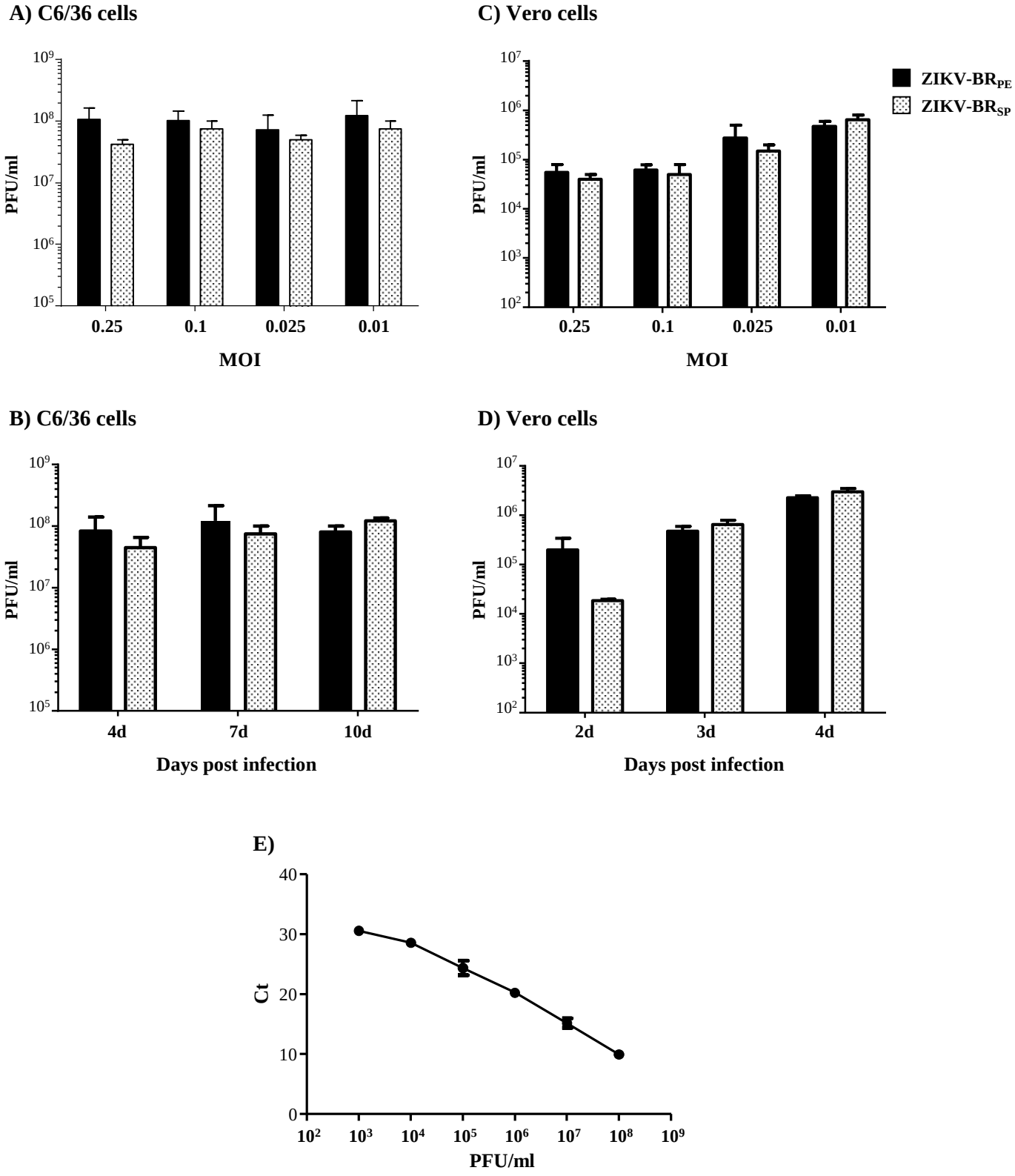
A) C6/36 cells
C) Vero cells
ZIKV-BR$_{PE}$
ZIKV-BR$_{SP}$
PFU/ml
MOI
0.25
0.1
0.025
0.01
B) C6/36 cells
D) Vero cells
Days post infection
4d
7d
10d
2d
3d
4d
E)
Ct
PFU/ml

Figure 4

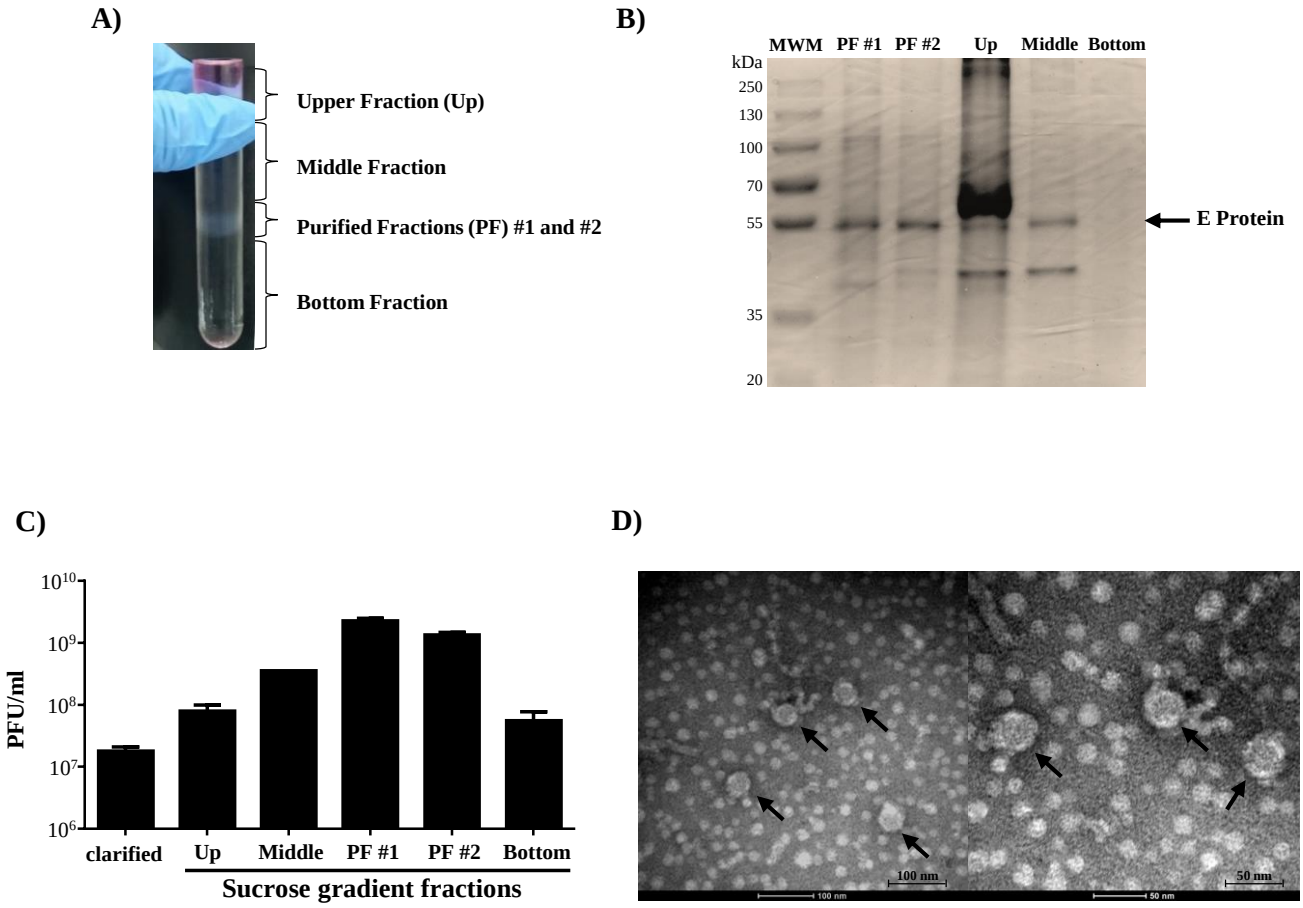
A)
Upper Fraction (Up)
Middle Fraction
Purified Fractions (PF) #1 and #2
Bottom Fraction
B)
MWM
PF #1
PF #2
Up
Middle
Bottom
kDa
250
130
100
70
55
35
20
E Protein
C)
PFU/ml
10^{10}
10^{9}
10^{8}
10^{7}
10^{6}
clarified
Up
Middle
PF #1
PF #2
Bottom
Sucrose gradient fractions
D)
100 nm
50 nm

Figure 5

PLOS | NEGLECTED TROPICAL DISEASES

RESEARCH ARTICLE

Viral immunogenicity determines epidemiological fitness in a cohort of DENV-1 infection in Brazil

Tauyne Menegaldo Pinheiro[1], Mânlio Tasso de Oliveira Mota[1], Aripuanã Sakurada Aranha Watanabe[1¤a], Joice Matos Biselli-Périco[1¤b], Betânia Paiva Drumond[2], Milene Rocha Ribeiro[1], Danila Vedovello[1], João Pessoa Araújo, Jr.[3], Paulo Filemon Paolucci Pimenta[4], Bárbara Aparecida Chaves[4,5], Mayara Marques Carneiro da Silva[6], Izabella Cristina Andrade Batista[7], Michelle Premazzi Papa[8], Lana Monteiro Meuren[8], Carolina Gonçalves de Oliveira Lucas[8], Flavio Lemos Matassoli[8], Laura Helena Vega Gonzales Gil[6], Adriana Bozzi[7], Carlos Eduardo Calzavara-Silva[7], Luciana Barros de Arruda[8], Danielle da Glória de Souza[9], Mauro Martins Teixeira[10], Nikos Vasilakis[11], Maurício Lacerda Nogueira[1]*

1 Laboratório de Pesquisa em Virologia, Departamento de Doenças Dermatológicas, Infecciosas e Parasitárias, Faculdade de Medicina de São José do Rio Preto, SP, Brazil, **2** Laboratório de Vírus, Instituto de Ciências Biológicas, Universidade Federal de Minas Gerais, Belo Horizonte, MG, Brazil, **3** Laboratório de Virologia, Departamento de Microbiologia e Imunologia, Instituto de Biociências, Universidade Estadual Paulista Júlio de Mesquita Filho, Botucatu, SP, Brazil, **4** Laboratório de Entomologia Médica, Centro de Pesquisas René Rachou, Fiocruz, Belo Horizonte, MG, Brazil, **5** Programa de Pós-Graduação em Medicina Tropical, Universidade do Estado do Amazonas (UEA) e Fundação de Medicina Tropical Dr. Heitor Vieira Dourado (FMT-HVD), Manaus, AM, Brazil, **6** Departamento de Virologia, Centro de Pesquisas Aggeu Magalhães, Fiocruz, Recife, PE, Brazil, **7** Laboratório de Imunologia Celular e Molecular, Centro de Pesquisas René Rachou, Fiocruz, Belo Horizonte, MG, Brazil, **8** Laboratório de Genética e Imunologia das Infecções Virais, Departamento de Virologia, Instituto de Microbiologia Prof. Paulo de Góes, Universidade Federal do Rio de Janeiro, RJ, Brazil, **9** Departamento de Microbiologia, Instituto de Ciências Biológicas, Universidade Federal de Minas Gerais, Belo Horizonte, MG, Brazil, **10** Laboratório de Imunofarmacologia, Departamento de Bioquímica e Imunologia, Instituto de Ciências Biológicas, Universidade Federal de Minas Gerais, Belo Horizonte, MG, Brazil, **11** Department of Pathology, Center for Biodefense and Emerging Infectious Diseases, Institute of Human Infections and Immunity, Center for Tropical Diseases, University of Texas Medical Branch, Galveston, United States of America

¤a Current address: Laboratório de Virologia, Departamento de Parasitologia, Microbiologia e Imunologia, *Universidade Federal de Juiz de Fora*, *MG*, *Brazil*.
¤b Current address: Departamento de Biologia, Instituto de Biociências, Letras e Ciências Exatas, Universidade Estadual Paulista Júlio de Mesquita Filho, São José do Rio Preto, SP, Brazil.
* mauriciolnogueira@gmail.com

Citation: Pinheiro TM, Mota MTdO, Watanabe ASA, Biselli-Périco JM, Drumond BP, Ribeiro MR, et al. (2018) Viral immunogenicity determines epidemiological fitness in a cohort of DENV-1 infection in Brazil. PLoS Negl Trop Dis 12(5): e0006525. https://doi.org/10.1371/journal.pntd.0006525

Editor: William B. Messer, Oregon Health and Science University, UNITED STATES

Received: November 22, 2017

Accepted: May 14, 2018

Published: May 29, 2018

Data Availability Statement: All relevant data are within the paper and its Supporting Information files

Funding: This work is funded by Fundacao de Amparo a Pesquisa do Estado de Sao Paulo (FAPESP), Grants # 2012/11733-6 and 2013/21719-3 to MLN and 2015/22750-7 to TMP and by INCT-Dengue/CNPq. MLN and MMT are CNPq Fellows. NV is supported by a NIH/NIAID Grant # U01 AI115577. The funders had no role in study

Abstract

The dynamics of dengue virus (DENV) circulation depends on serotype, genotype and lineage replacement and turnover. In São José do Rio Preto, Brazil, we observed that the L6 lineage of DENV-1 (genotype V) remained the dominant circulating lineage even after the introduction of the L1 lineage. We investigated viral fitness and immunogenicity of the L1 and L6 lineages and which factors interfered with the dynamics of DENV epidemics. The results showed a more efficient replicative fitness of L1 over L6 in mosquitoes and in human and non-human primate cell lines. Infections by the L6 lineage were associated with reduced antigenicity, weak B and T cell stimulation and weak host immune system interactions, which were associated with higher viremia. Our data, therefore, demonstrate that reduced

design, data collection and analysis, decision to publish, or preparation of the manuscript.

Competing interests: The authors have declared that no competing interests exist.

viral immunogenicity and consequent greater viremia determined the increased epidemiological fitness of DENV-1 L6 lineage in São José do Rio Preto.

Author summary

Since 2008 L6 is the endemic lineage that has circulated in SJRP. In 2010, the L1 lineage was first identified in the city. For a period, both lineages co-circulated, and then in 2013, L1 began to diminish until it was no longer detected in the population. Differences in replicative fitness are usually the main factor for clade replacement (CR) in DENV epidemics. However, despite the better viral fitness of the emerging lineage, the absence of CR could not be explained by these differences alone. Here, we combine epidemiological, phylogenetic, molecular and immunological analyses to provide a more precise understanding of the role of fitness in lineage dynamics with the persistence of L6 even after the introduction of L1 without CR. Differences in immune responses elicited by DENV-1 L1 and L6 lineages (genotype V), but not viral fitness in mosquito or human cells, explain the dynamics of circulating DENV in a city of Brazil.

Introduction

The spread of dengue (DENV) over the past several decades has made this arbovirus infection a major public health concern of global impact [1,2]. The disease has a complex epidemiological pattern and a high economic impact globally and is considered hyperendemic, *i. e*. dengue fever has a high incidence and/or prevalence rate affecting all groups equally [3,4]. Worldwide, it is estimated that 390 million new DENV infections occur annually [1], and this number will likely increase with the creation of new vector habitats due to climate change [5]. Because of their wide distribution, particularly in urban and peri-urban environments in tropical and subtropical regions, mosquitoes of the *Aedes* genus are the main vectors of this disease [6,7]. DENV can lead to a wide spectrum of clinical manifestations that are classified by the World Health Organization (WHO) as *dengue without warning signs*, *dengue with warning signs* and *severe dengue* [8]. Previous infections with a heterologous type are usually, but not exclusively, associated with progression to more severe disease [1].

There are four genetically distinct serotypes of DENV (DENV-1 to -4) that share similar epidemiological features [6]. Each serotype is divided into distinct groups defined as genotypes, which in turn subdivided in different lineages [9,10]. The circulation of the virus is characterized by frequent lineage turnover, in which a lineage of circulating viruses is usually replaced by a new lineage, a well-documented phenomenon known as clade replacement (CR). CR can lead to an increase in the number of cases and in the severity of the disease [10–17]. In previous CR events, an established lineage circulating for a number of years in a given population is replaced when a new lineage is introduced. This replacement is usually followed by the extinction of the previous lineage after a period of co-circulation of both lineages [10–17].

Since the mid-1980s, DENV-1 has been circulating in Brazil. All Brazilian DENV-1 isolates described to date belong to genotype V, which is subdivided into three distinct clades (lineages 1, 3 and 6) [18–20]. These lineages were introduced into Brazil at different times, and CR or the co-circulation of different lineages has been observed in the country [18–20]. This pattern

of co-circulation of different lineages was also observed in São José do Rio Preto (SJRP), São Paulo, Brazil.

Here, we combine phylogenetic, molecular and immunological analyses to describe the epidemiological dynamics of two Brazilian DENV-1 lineages (L1 and L6) circulating in SJRP from 2008 to 2015 to provide a more precise understanding of the role of fitness in lineage dynamics with the persistence of L6 even after the introduction of L1 without CR.

The reduced immunogenicity of L6, which contributed to B and T cell-specific immune response evasion, appears to have played a prominent role in its dominance over time.

Results

Phylogenetic analysis

We used 20 envelope sequences (1,485 nucleotides) of DENV-1 isolates obtained from patients in SJRP, from 2008 to 2012, for the phylogenetic analyses. The results indicated that the isolates were subdivided into two lineages within genotype V. Isolates 59/2011, 287/2011, 354/2011, 395/2011, 422/2011, 430/2011, 437/2011, 442/2011, 492/2012 and 516/2012 were grouped within one lineage previously called L1 or lineage II [13,18] the most recent common ancestor (MRCA) for those species dates back to approximately 2008 (95% BCI = 2006–2009). Ten isolates from SJRP were grouped in another lineage, previously called L6 or lineage I [13,18]: 365/2008, 09/2009, 88/2010, 64/2011, 205/2011, 384/2011, 387/2011, 484/2012, 531/2012 and 552/2012. These isolates share an MRCA from approximately 2007 (2006–2008) (Fig 1A).

When deduced protein envelope sequences were analyzed, a total of four amino acid (aa) substitutions were observed between the two groups of isolates from SJRP. Those aa substitutions were observed at positions 338, 394 (located in domain III), 428 and 436 (located in the stem loop region). The aa observed in SJRP isolate sequences within L1 were as follows: 338, serine; 394, arginine; 428, valine; and 436, valine; whereas SJRP isolates within L6 presented leucine, lysine, leucine and isoleucine residues, respectively. A comparison between the complete genome sequences of the L1 and L6 lineages from SJRP (287/2011 and 484/2012, respectively) revealed 56 aa differences (Fig 1B).

The L6 lineage was first identified in SJRP in 2008, and the L1 lineage was detected only in 2010. These two lineages of DENV-1, genotype V, co-circulated in SJRP from 2010 until 2012. Based on sequencing or genotyping analysis by Taqman-based qPCR, 64 serum samples were identified as infected by L1 from 2010 to 2012, whereas 102 samples obtained from 2008 to 2015 were identified as L6, resulting in a total of 166 discriminated samples. In SJRP, L6 became the dominant circulating lineage after 2013 (Fig 1C).

Viral fitness in viral dominance

Replicative fitness in vitro. To determine whether better viral fitness in the L6 lineage could explain its dominance in our study area, we assessed the viral replication of L1 and L6 isolates *in vitro*.

Initially, we tested two strains of each lineage and compare the quantification by flow cytometry and qRT-PCR. The results were very similar for both strains (S1 Fig). As qRT-PCR is a fast and reliable method, it was used for quantification of the viruses. One strain was chosen as prototype for each lineage, 287/11 for L1 lineage and 484/12 for L6 lineage.

In mosquito cell lines (C6/36 and Aag-2), L1 viruses had higher replication rates than L6 viruses by approximately one $\log_{10}$. Viral replication of L1 and L6 was also assayed in non-human primate cell lines (Vero E6 and LLC-MK2), in which similar results were obtained. Likewise, in a human cell line (HepG2), L1 viruses again demonstrated higher viral replication (Fig 2A).

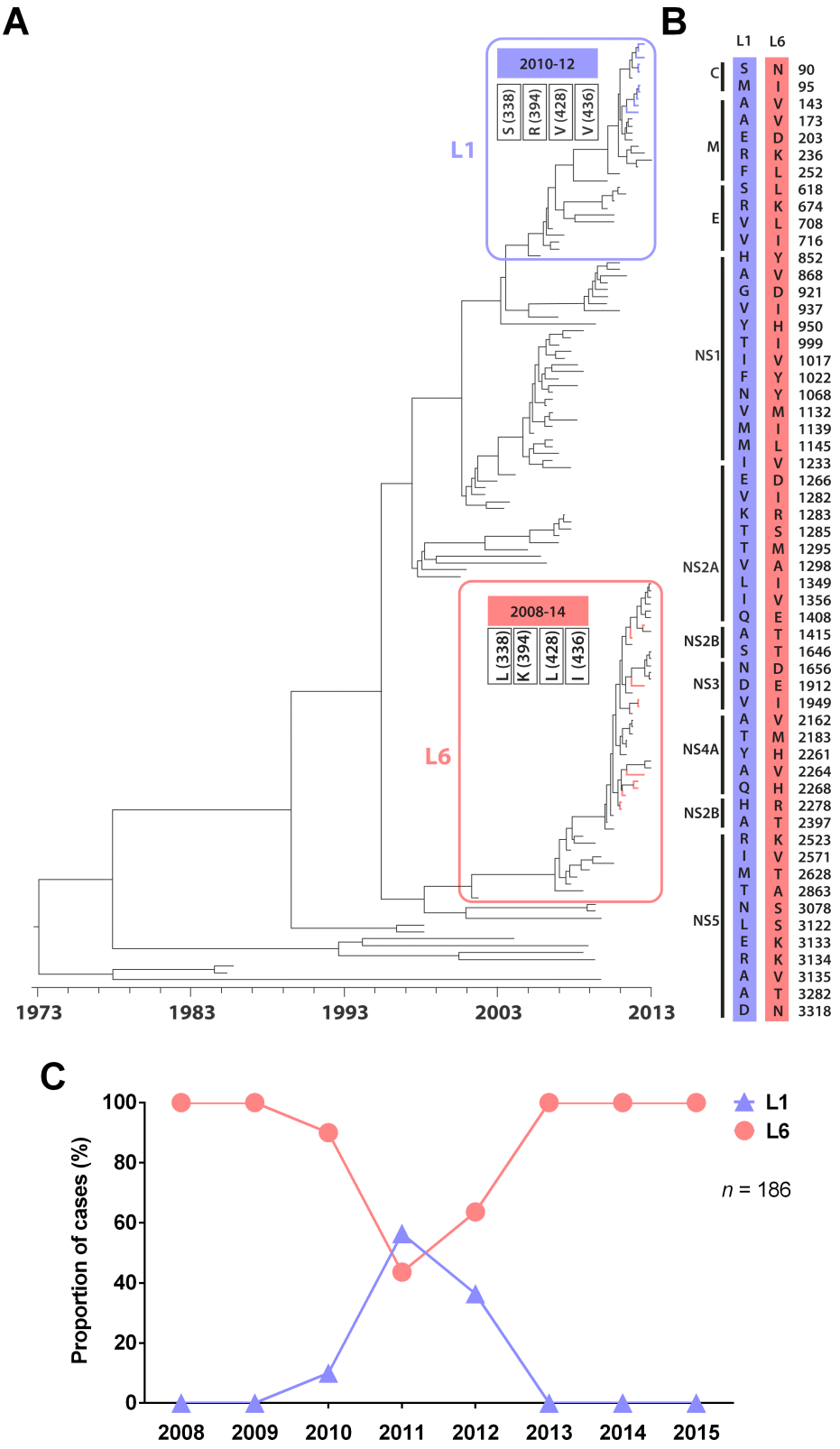

Fig 1. Evolutionary relationship between DENV-1 isolates and co-circulation of the two lineages from SJRP. (A) Phylogenetic tree of DENV-1 after Bayesian inference based on envelope nucleotide sequences with aa substitutions, characterizing the L1 and L6 lineages from SJRP, which are shown in blue and red, respectively. (B) Comparison of

amino acid substitutions between the representative complete genome sequences of L1 and L6 lineages from SJRP (287/2011 and 484/2012, respectively). (C) Circulation of DENV-1 lineages (L1 and L6) in SJRP from 2008 to 2015 based on sequencing and genotyping data.

https://doi.org/10.1371/journal.pntd.0006525.g001

The immunological status of the population could interfere with the propagation of viruses through an antibody-dependent enhancement (ADE) phenomenon [2]. Neutralizing antibody induced by previous heterologous infection can also interfere with DENV replication in vivo in an acute infection [21].

We tested 96 sera from symptomatic DENV-1 (L1 or L6)-infected patients for anti-dengue IgG antibodies to identify differences in the presence of prior heterologous exposure to DENV infection in both patient populations. Cross-reactive immunity can interfere with the risk of a second infection for a specific lineage of DENV-1, but primary (negative IgG) or secondary (positive IgG) DENV infections were similar in both groups ($P = 0.1339$; Fig 2B). Due to L6 persistence, we would have expected L6 viruses to replicate more efficiently (better replicative fitness) than L1 viruses. Therefore, an additional factor, such as transmission potential by the vector, could have been a contributor and were, therefore, investigated.

Replicative fitness in mosquitoes and coinfections. For a virus lineage to establish a fitness advantage over others, it must be able to infect and disseminate in mosquitoes at a higher rate, thus establishing a higher transmission potential [16]. We infected *Ae. aegypti* mosquitoes from two populations: PPCampos (captive) and Dom Pedro (wild). Consistent with the results obtained in C6/36 and Aag-2 cells, we observed that both lineages infected the mosquitos, resulting in a greater number of genome copies of L1 viruses. Indeed, the levels of L1 viruses were greater than those of L6 viruses in either the bodies or the heads after single infections in PPCampos (Fig 3A) and Dom Pedro (Fig 3B) mosquitoes.

Next, we calculated the infection rate (IR), disseminated infection rate (DIR) and vector competence (VC) for each lineage. These calculations again demonstrated an advantage of L1 viruses (range: 85 to 100%; Fig 3C) over L6 viruses (range: 30 to 80%; Fig 3D).

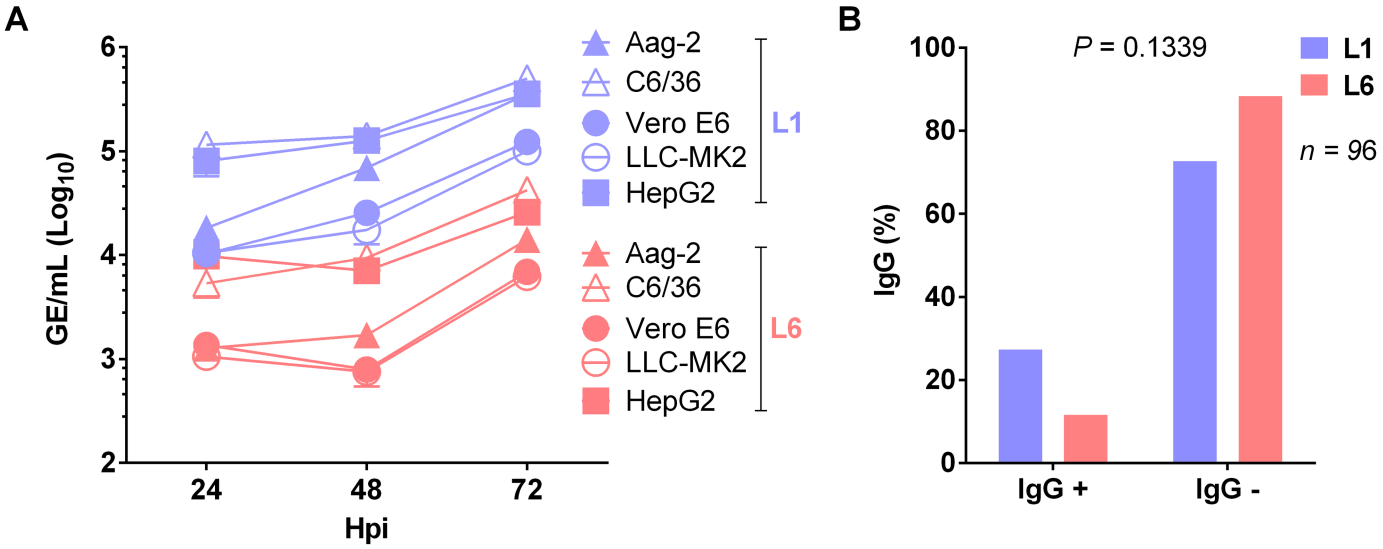

Fig 2. Replicative fitness in cell culture and cross-reactive immunity of DENV-1 lineages. (A) Growth curves of L1 or L6 isolates infected at an MOI of 0.1 in mosquito (C6/36 and Aag-2), human (HepG2) and non-human primate (Vero E6 and LLC-MK2) cell lines ($P \leq 0.05$, Student's T test). (B) Proportion of L1 or L6 DENV-1 cases classified as primary (negative IgG) or secondary (positive IgG) DENV infections (Fisher's exact test).

https://doi.org/10.1371/journal.pntd.0006525.g002

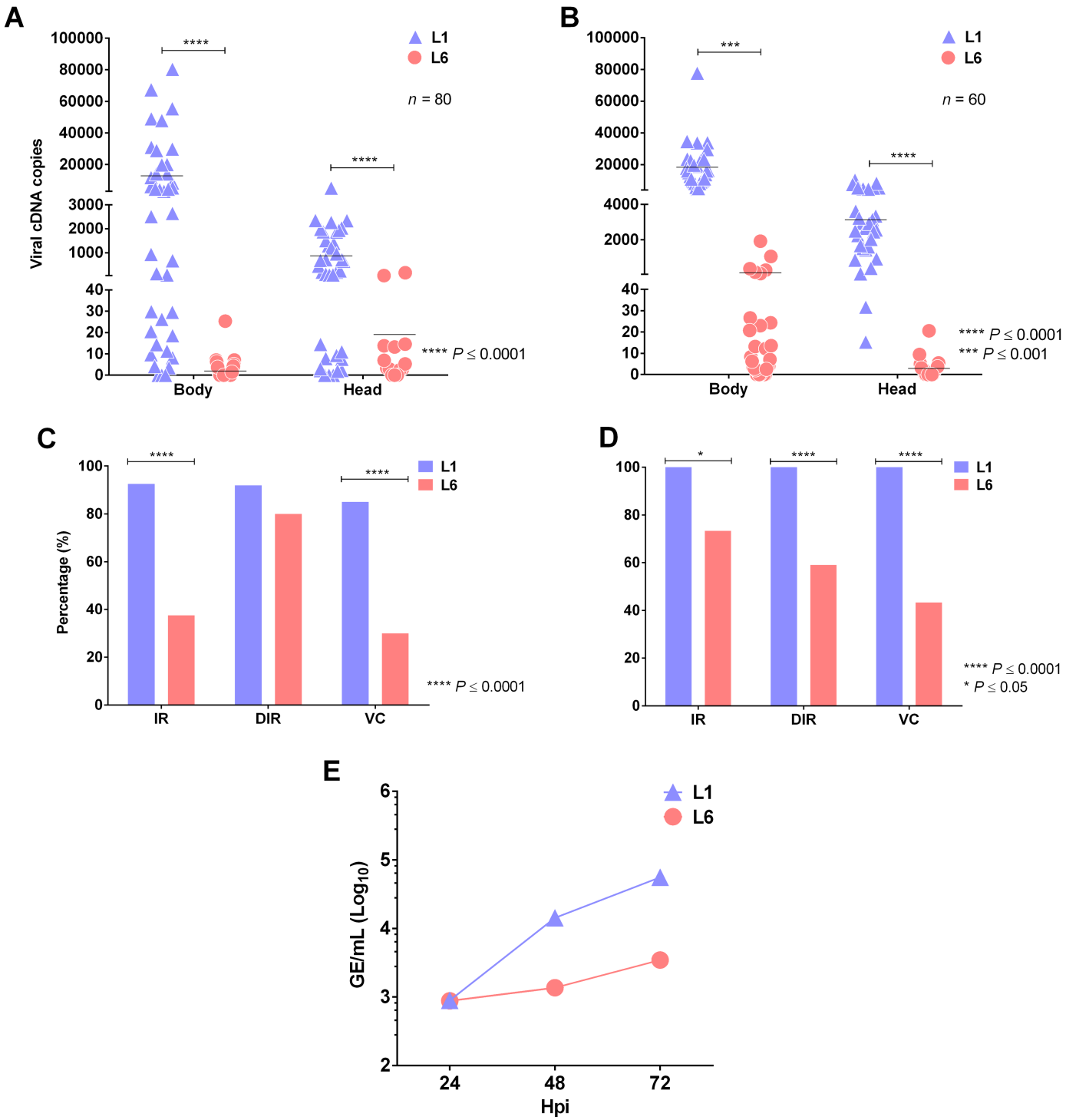

Fig 3. Replicative fitness in mosquitoes under selective pressure of DENV-1 lineages. (A and B) Viral cDNA copy number of L1 or L6 viruses in PPCampos. (A) and Dom Pedro (B). (C and D) Proportion of the infection rate (IR), disseminated infection rate (DIR) and vector competence (VC) of L1 or L6 viruses in PPCampos (C) and Dom Pedro (D). (E) Coinfection of L1 and L6 isolates in Aag-2 cells (MOI = 0.1) (Student's T test).

https://doi.org/10.1371/journal.pntd.0006525.g003

After analyzing the viral replication of lineages in cell culture and mosquitoes, our results suggested that L1 displayed improved viral fitness, contradicting our epidemiological findings.

However, caution should be exercised when interpreting *in vitro* experimental outcomes because they could fail to represent the complexity of natural transmission cycles, and differences in fitness can be demonstrated under forms of selective pressure such as coinfection [16]. To examine the potential of coinfection to explain our results, we performed a viral competition assay in which Aag-2 cells and mosquitoes were coinfected with L1 and L6 isolates and the relative amount of each virus was quantified. When present in culture concomitantly, L1 viruses replicated approximately one log faster than L6 viruses in Aag-2 cells, a statistically significant difference, except at 24 hours post infection (hpi) ($P = 0.6081$; Fig 3E and S4 Fig). These results suggest that viral-related factors or viral-specific fitness do not account for the dominance of the circulating L6 lineage without replacement by L1.

Epidemiological fitness in viral dominance

Subgenomic flavivirus RNA and interferon response. DENV-2 lineages can inhibit type I interferon responses via subgenomic flavivirus RNA (sfRNA) production. In DENV-2, the greater expression of sfRNA relative to genomic RNA (gRNA) can be responsible for improved fitness [15]. Thus, higher sfRNA:gRNA production ratios could have accounted for the epidemiological fitness of DENV-1 in our population.

Evaluation of the sfRNA:gRNA ratio in HepG2 cells showed that the sfRNA:gRNA ratio in cells infected with L6 was 10-fold higher than that in cells infected with L1 ($P \leq 0.001$; Fig 4A). The type I IFN antiviral response was measured to assess whether this mechanism could account for the epidemiological fitness of the DENV-1 lineages. In the supernatants of HepG2

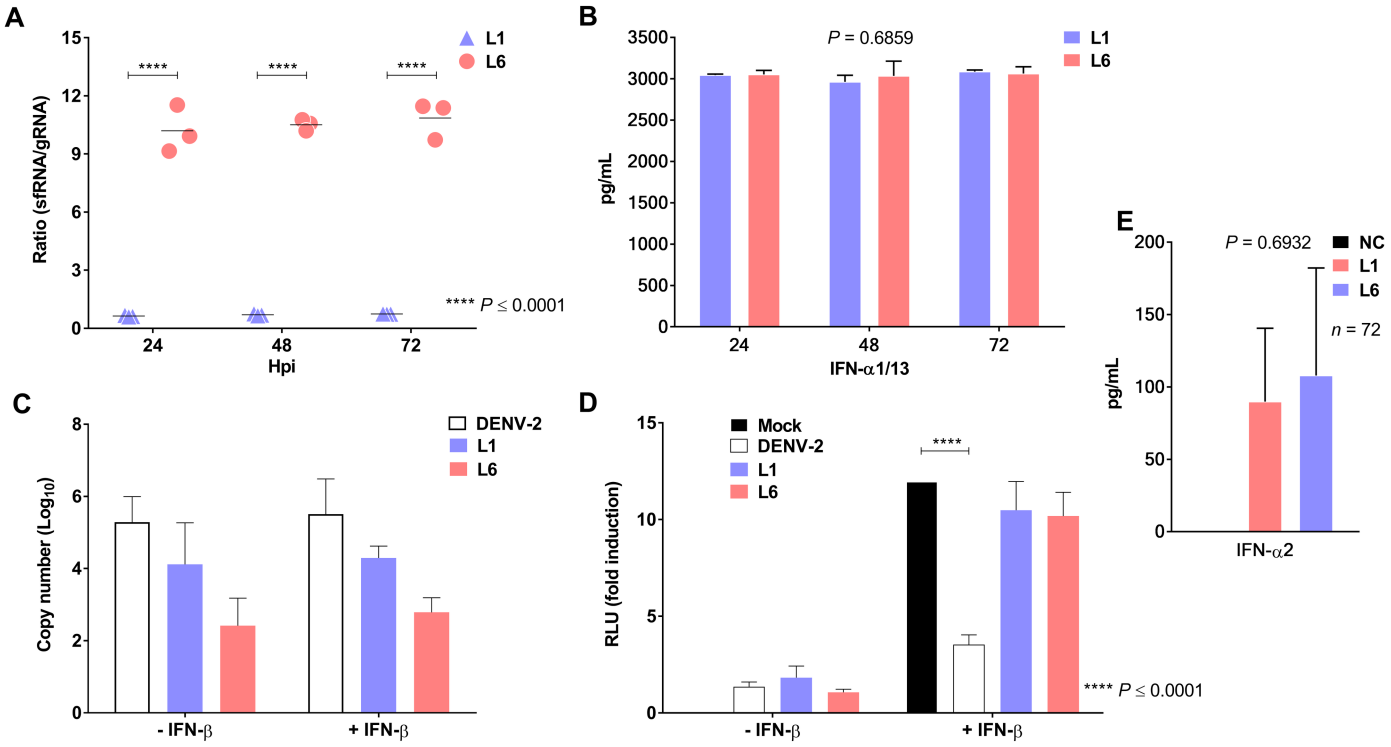

Fig 4. sfRNA and expression of type I interferon antiviral responses by DENV-1 lineages. (A) Ratio of sfRNA:gRNA in HepG2 cells infected with L1 or L6 viruses at an MOI of 1.0 (Student's T test). (B) Quantification of IFN-α1/13 production in supernatants of HepG2 cells by an ELISA (Chi-squared test). (C) Viral cDNA copy number of DENV-2, L1 or L6 viruses in HBMECs (before or after treatment with IFN-β) using real-time PCR. (D) IFN-induced luciferase activity in HBMECs that were mock-treated or infected with DENV-2, L1 or L6 DENV-1 in the presence or absence of IFN-β (Student's T test). (E) Quantification of IFN-α2 production in negative controls and L1 or L6 DENV-1-infected patients using the Luminex assay (Mann-Whitney test).

https://doi.org/10.1371/journal.pntd.0006525.g004

cells, IFN-α1/13 levels were similar in both lineages ($P = 0.6859$; Fig 4B). To verify whether IFN signaling was impaired during infection, HBMEC-ISRE-Luc cells were infected with DENV-2 (strain 16681) and the L1 or L6 DENV-1 lineages, in the presence or absence of IFN-β (Fig 4C). The IFN response was reduced only in HBMEC-ISRE-Luc cells infected with DENV-2. Neither L1 nor L6 inhibited the IFN-induced response upon endothelial cell infection (Fig 4D). IFN-α2 was also measured in naturally infected human sera and, consistent with the results obtained in cell culture, there were no differences in IFN-α2 production between patients infected with either L1 or L6 ($P = 0.6932$; Fig 4E). According to our findings, both lineages were unable to inhibit IFN expression or the IFN-induced response. Thus, the proposed model for epidemiological fitness based on sfRNA [15] does not apply to these DENV-1 lineages.

Cytokine profiles. Because viral fitness and suppression of the type I IFN response could not account for our epidemiological findings, we focused on evaluating the immune responses in patients infected with either lineage of DENV-1. The most immunogenic lineage would be replaced in a given population because enhanced immune responses would result in decreased viral loads and a lower chance of transmission in humans. Initially, sera from 72 patients presenting with dengue without warning signs, infected with either L1 or L6 lineages, were tested for 29 cytokines, chemokines, adhesion molecules and growth factors.

The levels of various molecules were detectable in the serum samples, but only the levels of cytokines IL-1RA, IL-12p40, IL-7, IL-17a, IL-13, EGF, VEGF and CCL11 (Fig 5A–5G) showed differences between the serum of patients infected with the L1 lineage and those infected with the L6 lineage. Whereas the levels of IL-12p40, IL-7, IL-17a and VEGF were elevated in patients infected with L1, the levels of IL-1RA, IL-13, EGF and CCL11 were greater in patients infected with L6. None of the other tested molecules showed significant differences (S3 Fig).

Antigenicity and adaptive immune response. Previous studies [22] hypothesized that lineages with lower antigenic potential could have better epidemiological fitness. Thus, we conducted an *in silico* analysis using 20 DENV-1 sequences that had been previously clustered into the L1 and L6 lineages to verify potential antigenic differences in polyprotein. We found that four aa substitutions in the sequences grouped in the L1 lineage increased the B and T epitope antigenic scores. Sequences clustered into L6 displayed diminished antigenicity (Fig 6A); therefore, L1 would trigger the immune system in a more effective manner.

To confirm *in vivo* the reduced antigenicity observed for the L6 sequences using bioinformatics, eight-week-old male C57BL/6 mice were immunized with L1 and L6 isolates, and spleen cells were collected to analyze B and T cell activation by flow cytometry. B cell activation was measured by analyzing $CD21^+/CD40^+$ expression, and L6 did not appear to activate B cells (Fig 6B). An analysis of CD4 and CD8 expression demonstrated that L1 induced a much higher frequency of activated $CD4^+/CD69^+$ (Fig 6C) and $CD8^+/CD25^+$ cells (Fig 6D) than L6, indicating prominent T cell activation.

To confirm whether the L1 and L6 isolates would differentially stimulate human leukocytes, PBMCs from 11 healthy donors were mock-treated or infected with each isolate and B and T lymphocyte activation was analyzed; anti-DENV serology was performed in 9 donors to determine whether they were dengue naive or had been previously infected; serum was not available for 2 donors. Among those 9, seven were dengue naive, one showed anti-DENV IgG (but we could not evaluate the serotype nor whether there was primary or secondary infection), and one showed inconclusive serology result.

B cell activation was evaluated by measuring total IgM levels in culture supernatants. We observed that L1 induced slightly higher, but not significant levels of IgM, in comparison to L6 (Fig 6E). Regarding CD38 and HLA-DR expression on T cells, we observed that 8 donors showed a higher T cell activation in response to L1 than to L6 isolates; those included six

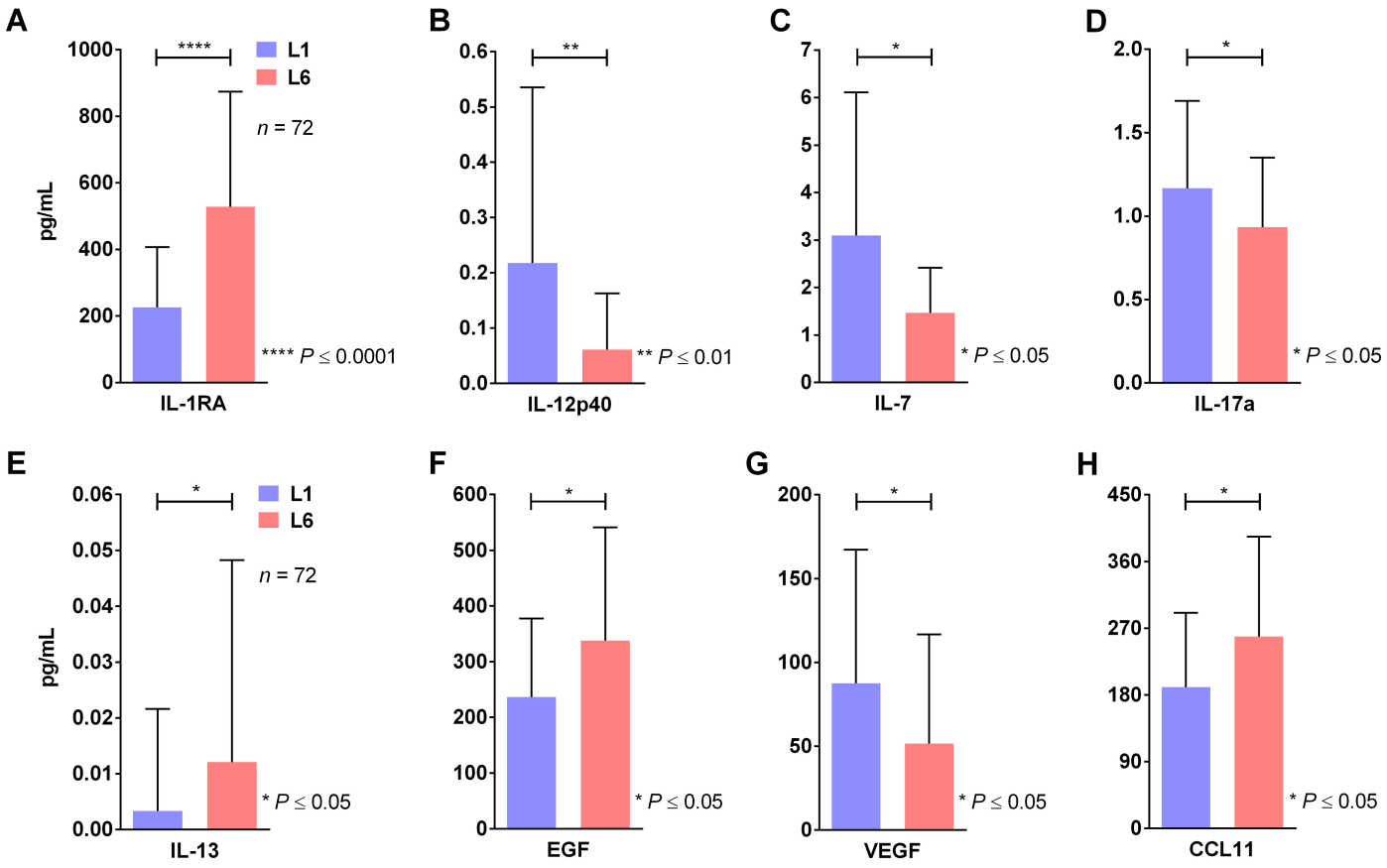

Fig 5. Quantification of cytokines, chemokines, adhesion molecules and growth factors showing significant differences in L1 or L6 DENV-1-infected patients. (A) IL-1RA. (B) IL-12p40. (C) IL-7. (D) IL-17a. (E) IL-13. (F) EGF. (G) VEGF. (H) CCL11. (Mann-Whitney test). See also S3 Fig.

https://doi.org/10.1371/journal.pntd.0006525.g005

dengue naive and two with undetermined serology. Four donors showed a slightly higher response induced by L6; those included two dengue naive, one dengue positive, and one inconclusive (Fig 6F and 6G).

We also measured the levels of IFN-γ, IL-6 and IL-8 in PMBC culture. Analysis of the cytokines secreted demonstrated that both lineages induced high levels of IFN-γ and IL-6; but higher levels were detected in L1-infected cells. On the other hand, L6-infected cells showed increased IL-8 (S2 Fig).

Because effective innate and adaptive immune responses would eventually translate into the control of viral replication, we evaluated the levels of virus in serum samples of patients infected with the L1 or L6 DENV-1 lineages from 2008 to 2014. As shown in Fig 7, the levels of virus in patients infected with L6 were 3.5-fold higher in serum than in patients infected with L1 viruses ($P \leq 0.001$).

Discussion

To understand the forces that drive DENV epidemics, it is crucial to develop efficient control methods for this disease. The introduction of new lineages and CR is important for maintenance of the disease in a given population. CR is a well-documented event that occurs in many epidemics when a new DENV strain emerges and displaces the endemic strain, even between viruses of the same serotypes and genotypes. This process usually causes an increase in both

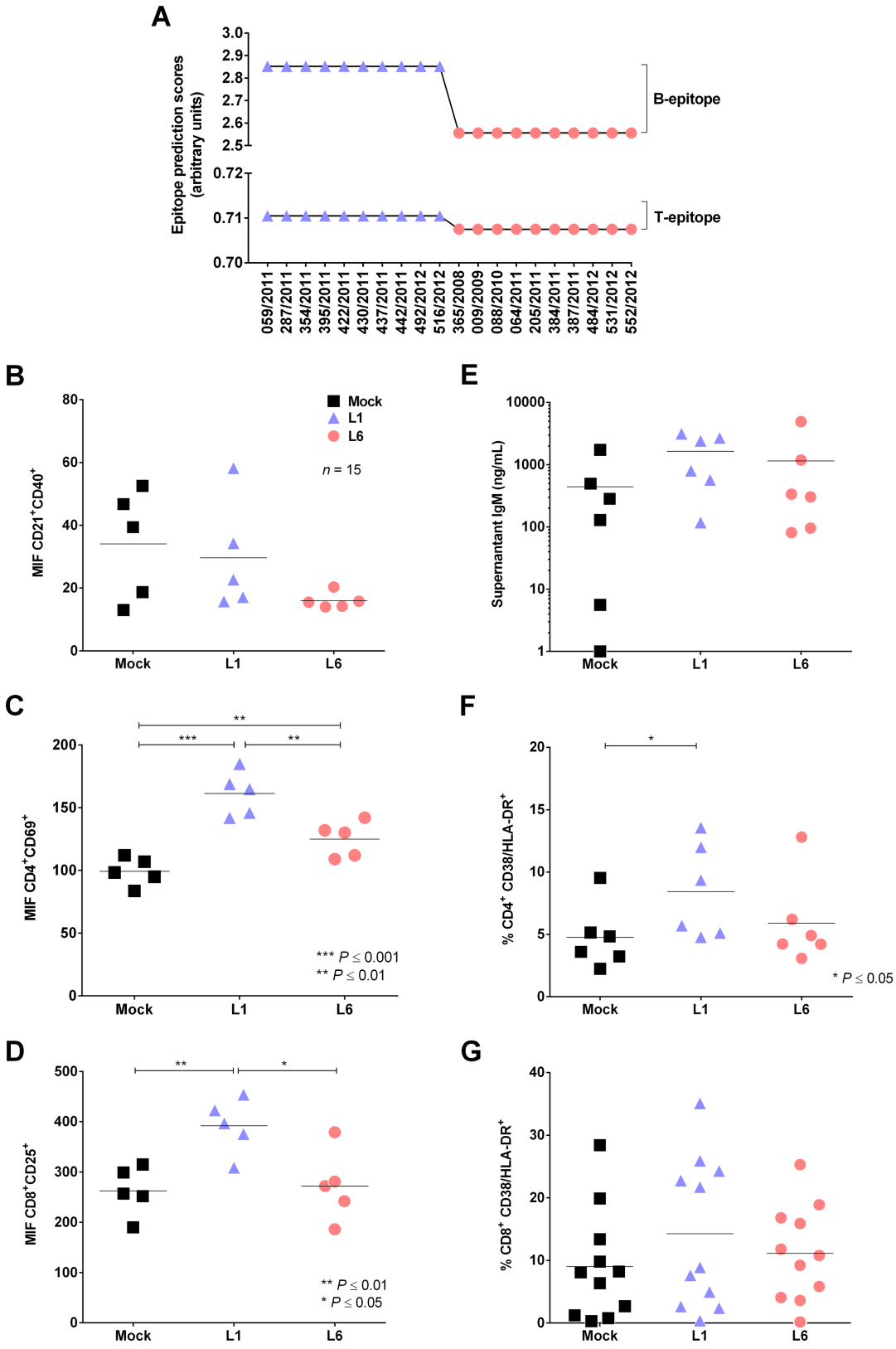

Fig 6. Rank of antigenicity, B and T cell activation and viral load of DENV-1 lineages. (A) Twenty DENV-1 sequences from SJRP (L1 and L6) subjected to B and T antigenicity prediction and classified according to their immunogenic potential. (B, C

and D) Analysis of B (B), CD4 (C) and CD8 T (D) cell activation in C57BL/6 at 7 days post-infection by flow cytometry (Student's T test). (E, F and G) Average and individual data for IgM levels by an ELISA (E); CD4 (F) and CD8 T (G) cell activation frequency obtained in PBMCs from healthy donors by flow cytometry (Student's T test).

https://doi.org/10.1371/journal.pntd.0006525.g006

the number of cases and the severity of the disease [15,16]. Although relatively common, the forces that dictate whether CR will occur are not completely understood. Genetic variations may alter viral fitness; however, the interplay of this factor with epidemiological factors has not been defined.

Since 2008, the L6 lineage of DENV-1 (genotype V) has circulated in SJRP. The duration of the circulation of this lineage in the population allowed us to consider it an endemic lineage. In mid-2010, a different Brazilian lineage arose: L1. This newly introduced lineage appeared to have improved viral fitness compared to L6; thus, L1 was expected to replace L6 as the dominant strain. From the emergence of the L1 lineage until 2012, the epidemics in SJRP appeared to follow the path of other epidemics, and the CR event would occur. However, the L1 lineage did not displace L6, but rather both co-circulated without a clear predominance. L1 started to decline until its complete disappearance in 2013. This finding raised questions about differences in the fitness between the lineages, which were investigated by our group.

Lineages of the same serotype may present different characteristics in transmissibility, virulence and antigenic properties, some of which may lead to increased fitness and could be related to a greater epidemic potential [15,16,23]. The viral fitness is defined by *the capacity of a virus to produce infectious progeny in a given environment, whereas the capacity of a virus to become dominant in a given region has been called epidemiological fitness* [15]. The latter is determined by a combination of factors, including the genetics of the viral strain, transmission potential by the vector and human system interactions [24]. Investigations of the factors involved in lineage replacement have revealed important implications for advancing our understanding of DENV epidemiology, evolutionary dynamics and control [11].

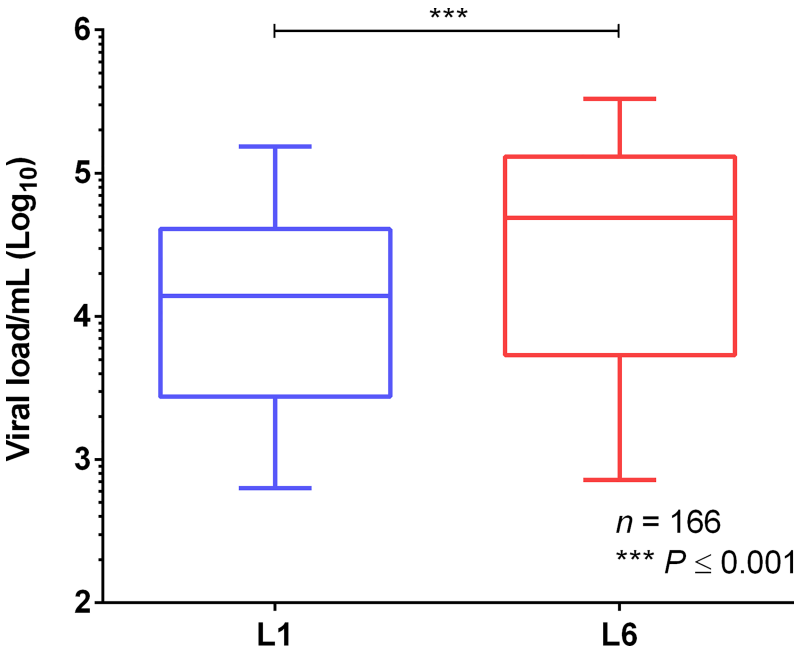

Fig 7. Viral load quantification of DENV-1-infected patients using real-time PCR.

https://doi.org/10.1371/journal.pntd.0006525.g007

Viral fitness is an important contributing factor to CR and, on some occasions, it can account for the persistence of the strain. In other DENV epidemics, improved replicative fitness of the emerging strain has been responsible for the dominance of the newer lineage. For example, the replicative fitness advantage of the NI-2B lineage over the NI-1 lineage in *Ae. aegypti* could have contributed to the CR event, resulting in the dominance of NI-2B in Managua [16]. Replacement of the NI-1 lineage by the NI-2B lineage was also associated with an increase in disease severity.

In the SJRP epidemic, differences in the replicative fitness could have accounted for the persistence of L6 even after the introduction of the new lineage (L1). However, the L1 had higher replication rates than L6 in mosquito, human and non-human primate cell lines. It also had an increased fitness in two different populations of *Ae. aegypti* mosquitoes and thus could have a higher potential for transmission than L6. Unfortunately, it was not possible to analyze viral levels in mosquitos collected at that time. In theory, the coinfection of vectors with both lineages can result in competition and can accurately represent the natural transmission cycles. However, the superior viral fitness of L1 in mosquito cell culture indicates that coinfections do not have any effect on viral fitness. In fact, all tests conducted by our group revealed superior viral fitness of L1, *in vitro* or *in vivo*. Therefore, the better replicative fitness L1 would induce its dominance and not its replacement by L6. Some studies theorize that *in vitro* infections can sometimes fail to predict the actual dynamics of DENV epidemics [16]. Therefore, differences in replicative fitness did not explain the observed pattern of L6 persistence.

Evasion of interferon responses by the virus could be a factor underlying the maintenance of the L6 lineage in the population. This has been identified as a determinant of epidemiological fitness in the lineage dominance of DENV-2 (PR-2B) in Puerto Rico [15]. During flavivirus infections, short flavivirus RNAs (sfRNAs) are produced by the incomplete degradation of viral RNA by the host-cell exonuclease Xrn1. These sfRNAs are associated with the pathogenesis of flaviviruses [25]. The high expression of sfRNAs could have inhibited type I interferon responses and facilitated evasion of the immune response. In a study conducted in Puerto Rico, the PR-2B lineage produced elevated expression of subgenomic flavivirus RNA (sfRNA) relative to genomic RNA (gRNA) during replication. Notably, sfRNA could bind TRIM25 and inhibit the IFN response. Thus, higher sfRNA:gRNA ratios are associated with superior epidemiological fitness [15]. Although L6 had higher sfRNA:gRNA ratios than L1, which in turn could increase its epidemic potential, it did not appear to be related to IFN inhibition, as previously reported [15]. Both lineages appeared to be incapable of inhibiting the IFN response and produced similar levels of type I IFN *in vitro* and *in vivo*, suggesting this was not the mechanism underlying the differences observed.

Previous antibody immunity to dengue could also play a role in epidemic dynamics. For example, the immunological status of the population could interfere with L1 propagation through an antibody-dependent enhancement (ADE) phenomenon. Waning immunity due to a prior DENV infection can alter the outcome of the present infection, as observed in Nicaragua [2]. High titers of pre-infection cross-reactive neutralizing antibodies drastically reduce the probability of a severe disease in a second infection, although this protective effect is not observed against all DENV serotypes [26]. However, no significant differences in the frequency of anti-dengue IgG antibodies were found in our patients.

Because previously reported mechanisms were unable to explain the persistence of L6, we evaluated various aspects of the immune response in order to provide an alternative explanation to our findings. To assess possible differences in immunological responses, a panel of 29 cytokines, chemokines, adhesion molecules and growth factors were measured in plasma of patients. Dengue infection was associated with the increase of several cytokines in serum of patients. Overall infection with the L6 lineage was associated with greater increases of cytokines with

anti-inflammatory (IL-1RA and IL-13) or Th2-like activity (IL-13 and CCL11). In contrast, infection with the L1 lineage was associated with greater increase of cytokines with Th1/Th17–like activity (IL-12 and IL-17) and IL-7, a cytokine that promotes lymphocyte development in the thymus and maintains survival of naive and memory T cell homeostasis in the periphery. The exact role of these cytokines in the context of dengue infection is not precisely know but these results clearly show that the L1 lineage had a tendency to generate immune responses usually associated with resistance to dengue infection whereas the L6 lineage the tendency to generating cytokines with anti-inflammatory activity or that block Th1/Th17 responses.

The latter studies suggested that immune responses to L1 were enhanced and more pro-inflammatory and led us to investigate in greater detail adaptive immune responses in patients infected with the L1 or L6 lineages. *In silico* analysis suggested that the L1 lineage was potentially more immunogenic than the L6 lineage. These predictions were confirmed by studies in mice that showed increased immunogenicity of L1, as assessed by greater B and T cell activation. Unfortunately, we did not have access to PBMCs derived from L1 or L6 infected patients, and only the sera were available. Therefore, it was not possible to assess directly T cell recall responses to L1 and L6 viruses. However, experiments in human PMBCs infected with either lineage showed that the L1 lineage induced stronger responses than those infected with L6 viruses. Altogether, he data suggest that different DENV isolates might induce distinct levels of B and T cell activation. L1-induced response was mostly associated to IFN-γ production, whereas L6 induced activation was driven to inflammatory IL-8 secretion. Distinct T cell phenotype and function, with increased T cells activation and IFN-γ production might then be associated to disease control [27–30]. Altogether, these studies suggest that the adaptive immune responses in infected individuals triggered by L1 were stronger than those triggered by L6.

Our prediction would be that differences in immune response would necessarily have to associate with altered viral loads, if these responses were to affect the likelihood of one strain to override the other. Indeed, patients infected with the L6 lineage, the one with significantly decreased immune activation, were those with the higher viral loads. We would expect that the high viral L6 loads would enhance the probability of transmission of the L6 lineage to the vector and, consequently, to another host.

The current dogma indicates that, after infection with a certain DENV serotype, only a heterologous DENV serotype can cause infection in the same individuals. However, studies using non-human primates have indicated that new inoculations with either the same or different genotypes of DENV-2 can cause a persistent boost in neutralizing antibodies [31]. Because L6 only weakly stimulates B and T cells, it may not increase immunological memory, nor may it induce the development of neutralizing antibodies in sufficient titers to protect against a new exposure. Although further work with specific experiments are needed to strengthen this evidence, it appears that neutralizing antibodies may quickly control infections, preventing more severe disease; however, they may not avoid future infections. A similar mechanism has been proposed for studies in Nicaragua [31] and may provide an explanation for the maintenance of L6 for such a long period in the population. High viral loads of L6 enhance the probability of vector transmission of the L6 lineage. However, despite the better replicative fitness, the L1 lineage appears to elicit a stronger immune response, preventing broader propagation of this lineage due to the extinction of the susceptible population.

Based on our data, the absence of CR together with the superior epidemiological fitness of L6 in SJRP was a result of the human immune system functioning as a bottleneck that favored the L6 lineage to achieve a broader distribution, even with lower viral fitness. The model is summarized in Fig 8. The inability of the L1 lineage to replace the endemic L6 lineage in this city shows that the interplay between replicative, immunological and epidemiological features that affect the dynamics of viral propagation is far more complex than previously suspected. In

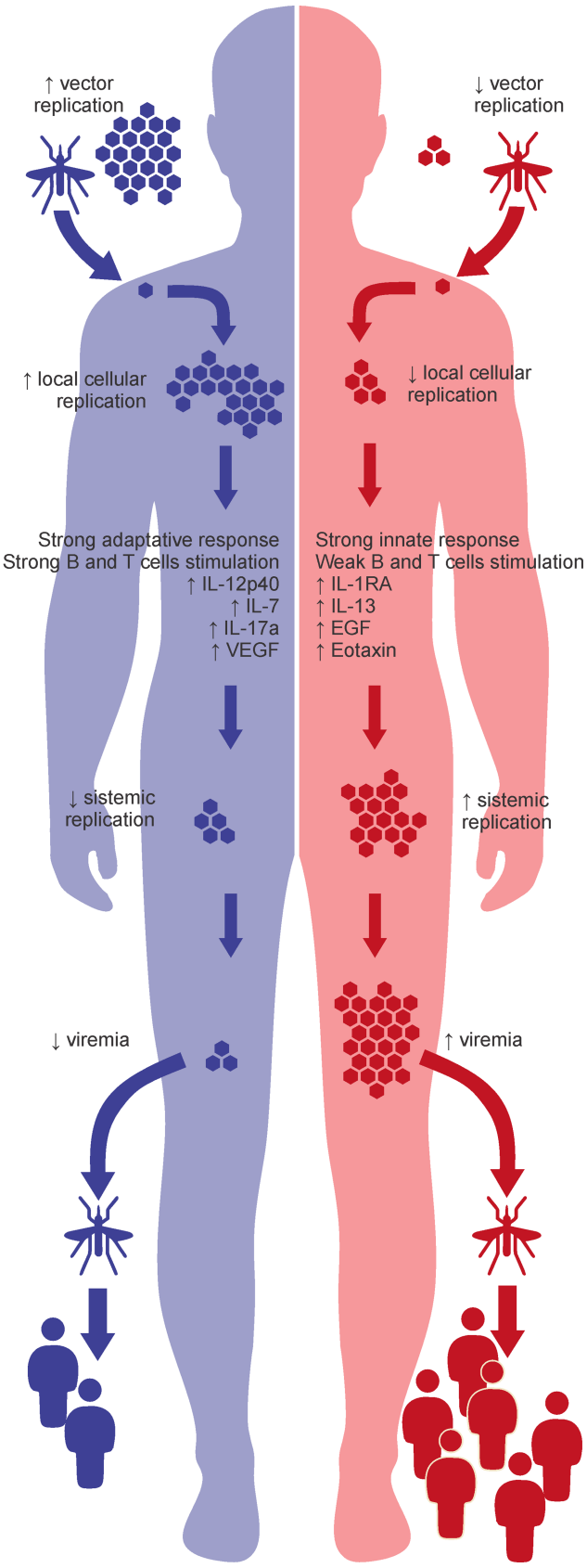
↑ vector replication
↓ vector replication
↑ local cellular replication
↓ local cellular replication
Strong adaptative response
Strong B and T cells stimulation
↑ IL-12p40
↑ IL-7
↑ IL-17a
↑ VEGF
Strong innate response
Weak B and T cells stimulation
↑ IL-1RA
↑ IL-13
↑ EGF
↑ Eotaxin
↓ sistemic replication
↑ sistemic replication
↓ viremia
↑ viremia

Fig 8. Proposed model for L6 lineage (red) dominant circulation without L1 lineage replacement (blue) in the SJRP population, with the main differences found between the two DENV-1 lineages.

https://doi.org/10.1371/journal.pntd.0006525.g008

this case, the lower viral immunogenicity for B and T cells associated with host immunological factors counteracts the superior viral fitness, contributing to the lineage dominance.

Materials and methods

Ethics statement

The panel of 186 DENV-1 viruses used in the present study was collected from symptomatic patients from 2008 to 2015 in a public healthcare facility in SJRP (São Paulo, Brazil) as part of the flavivirus and hantavirus surveillance program in the city. This study was reviewed and approved by the Human Research Ethics Committee of Faculdade de Medicina de São José do Rio Preto (CAAE: 02078812.8.00005414).

All the samples are obtained from an existing collection in the laboratory (LPV-Dengue 2008–2015) and all of them were already anonymized.

Blood samples (buffy coats) from healthy donors were obtained anonymously from the Hemotherapy Service at the Hospital Universitário Clementino Fraga Filho (HUCFF) of Universidade Federal do Rio de Janeiro (UFRJ). The study protocol was approved by the Experimental Ethics Committee of UFRJ (Permit Number: IMPPG 025), and the review board waived the need for informed patient consent.

All animal work was performed in accordance with the Fiocruz Animal Use Committee (protocol P-60/14-4; license number LW-30/15). Fiocruz personnel are required to adhere to applicable federal, state, local and institutional laws and policies governing animal research, including the regulations from the Brazilian Council of Animal Use Control (CONCEA - 3rd Edition, published at Sep, 26, 2016), Federal Law 11794/08 and Protocols for Animal Use—Oswaldo Cruz Research Foundation (ISBN: 85-7541-015-6).

Samples

We observed predominantly dengue without warning signals. All the samples used in this study were collected untill 5 days of the *symptoms* onset. The serum samples were subjected to molecular biological and serological diagnostic tests for dengue. Initially, DENV infection was confirmed using reverse transcription-PCR (RT-PCR) and multiplex nested PCR (M-N-PCR) assays as described previously [32], which distinguishes the four serotypes. Ninety-six DENV-1-positive samples were tested for anti-dengue IgG antibodies, as recommended by the SERION ELISA classic Dengue IgG test kit (Virion Serion).

DENV envelope gene sequence amplification and analysis

Twenty DENV-1-positive samples were used to amplify the envelope gene sequence, followed by nucleotide sequencing using the Sanger-based method with a previously described primer [33]. Viral RNA was extracted using the QIAamp Viral RNA Mini kit (Qiagen) as recommended by the manufacturer. First-strand cDNA was synthesized using the Superscript III First Strand Synthesis System (Invitrogen) following the manufacturer's instructions with primer d1a16. PCR was performed to amplify a 1,855-bp fragment, of which 1,485 bp corresponded to the entire DENV-1 E gene. The reaction consisted of 2 μL of cDNA, 5 μL of 10X Accutaq LA buffer, 2.5 μL of dNTPs (10 mM/μL), 1 μL of DMSO 2%, 1 μL of primers d1s3 and d1a17 (10 μM), 0.5 μL of Accutaq LA DNA polymerase (5 U/μL; Sigma-Aldrich) and DEPC-treated water. The reactions were submitted to the following cycle conditions: 98˚C for 30 sec,

followed by 30 cycles of 94˚C for 15 sec, 50˚C for 20 sec and 68˚C for 1 min and 30 sec. A final extension step was performed at 68˚C for 10 min.

An analysis of the amplicons was performed by electrophoresis on a 1% agarose gel. The PCR product (40 μL) was purified using 2.8 μL of 3 M sodium acetate and 1.2 μL of cold absolute ethanol. The samples were stored overnight at -20˚C or for 1 h at -80˚C and subsequently centrifuged at 16,100 x g for 20 min. The pellet was washed with 200 μL of 70% ethanol and centrifuged at 16,100 x g for 10 min. The dried pellet was resuspended in 20 μL of Milli-Q water. Twenty nanograms of purified PCR products were used as templates in 20 μL of cycle sequencing reactions using 2 μL of 1X Sequencing buffer, 2 μL of BigDye Terminator v.3.0 (Applied Biosystem), 1 μL of forward and reverse primers (3.2 μM) (see S1 Table) and DEPC-treated water; these samples were submitted to 96˚C for 1 min followed by 25 cycles of 96˚C for 10 sec, 50˚C for 5 sec and 60˚C for 4 min. Precipitation of sequencing reactions was performed using ethanol/EDTA as recommended by the BigDye Terminator kit v.3.0 (Applied Biosystems) protocol. The samples were resuspended in 10 μL of Hi-Di Formamide (Applied Biosystems) and analyzed with ABI PRISM 3130 equipment (Applied Biosystems).

The quality of the sequences was analyzed using Sequencing Analysis 5.2 software (Applied Biosystems). The consensus sequence was edited using Accelrys Gene v.2.5 (Accelrys). Nucleotide sequences were then aligned with the previously published E gene sequence from GenBank (GU131863.1) using MEGA 6.0.6 Molecular Evolutionary Genetics Analysis (http://en.bio-soft.net/tree/MEGA.html).

To obtain insight into the genetic relationship among DENV-1 strains, envelope sequences obtained from different DENV-1 isolates from SJRP and other geographic sites were aligned using ClustalW [34], taking into account the codon sequences. Amino acid sequences were predicted, and substitution patterns were analyzed. Phylogenetic and coalescent analyses were conducted using BEAST package v.1.8 with Markov Chain Monte Carlo (MCMC) algorithms [35]. Input files for BEAST were generated using BEAUTI v.1.8.1 [35], and the year each strain was isolated/obtained was used as a calibration point. Analyses were performed using the General Time Reversible nucleotide substitution model with four gamma categories (GTR + 4G), the Bayesian Skyline method [36] and a relaxed (uncorrelated lognormal) molecular clock. Two independent runs (100 million chains, discarding the first 10 million steps) were run, and parameters and trees were sampled every 10,000 steps. The convergence of parameters was checked with Tracer v1.6.0 [37], and uncertainties were addressed as 95% Bayesian Credible Intervals (BCI). Using Tree Annotator v. 1.8.1 [38], a maximum clade credibility (MCC) tree was generated and then visualized in Figure Tree v. 1.4.2 [38].

In addition, full-length sequences of viral RNA genomes from SJRP were sequenced using next-generation sequencing with Illumina **MiSeq System (Illumina)** as described previously [39]. Briefly, isolates were subjected to RNA extraction using the QIAamp Viral RNA Mini kit (Qiagen), followed by quantification using a PicoDrop (Picodrop Limited). RNA was treated with DNAse I (Sigma-Aldrich), and reverse transcription-PCR was performed with random primers (50 ng; Invitrogen) using the High Capacity cDNA Reverse Transcription kit (Applied Biosystems), according to the manufacturer's instructions. After sequencing, the obtained sequences were assembled and edited using Geneious v.7.1.4 (Biomatters Ltda), and polyprotein sequences were aligned and translated to compare aa substitutions. Two sequences (287/2011 and 484/2012) were selected to represent the L1 and L6 lineages, respectively.

Genotyping

When it was not possible to obtain an amplicon of the envelope gene region or complete genomic sequences, lineage discrimination of DENV-1-positive samples was performed using the

TaqMan Real-Time PCR genotyping assay and the AgPath-ID One-Step RT-PCR kit (Applied Biosystems) with two primers and probe sets for the envelope (2021_F, 2021_R and 2021_P1) and NS5 (8587_F, 8587_R and 8587_P2) regions, as shown in S2 and S3 Tables.

For the genotyping assay validation, twenty samples previous grouped into L1 or L6 lineages by phylogenetic analyses were selected and the experimental validation was performed under blind conditions. All of the samples used were correctly discriminate.

The One-Step qRT-PCR reaction was performed using two different master mixes and consisted of 7 μL of RNA sample, 12.5 μL of 2X RT-PCR buffer, 1 μL of forward and reverse primers (20 μM), 0.75 μL of probe (10 μM), 1 μL of 25X RT-PCR enzyme mix and nuclease-free water in a total volume of 25 μL per reaction. To identify the L1 lineage, primers 2021_F and 2021_R and probe 2021_P1 were used; 8587_F, 8587_R and 8587_P2 were used for lineage L6 identification. The reactions were subjected to the following cycle conditions, with data collections at 60˚C: 50˚C for 10 min, 95˚C for 10 min, 60˚C for 30 sec and 95˚C for 10 min, followed by 50 cycles of 95˚C for 15 sec and 60˚C for 1 min. A final extension step was conducted at 60˚C for 30 sec. Genotyping was performed using human sera and standardized samples (to provide standard curves) to allow the relative quantification of virus levels. All qRT-PCR reactions were performed using a StepOne Real-Time PCR System (Applied Biosystems).

Cells and viruses

Peripheral blood mononuclear cells (PBMCs) were obtained after centrifugation of buffy coat samples over a ficoll-hypaque gradient. Moreover, human brain microvascular endothelial cells (HBMECs) were stably transfected with the reporter vector pISRE-Luc-Hygro containing an NdeI-Bst1107 site of pISRE-Luc (Stratagene) and cloned into vector pCEP4 (Invitrogen). Cells then referred to as HBMEC-ISRE-Luc were kindly provided by Dr. Laura Helena Vega Gonzales Gil, CPqAM, FIOCRUZ, Recife-PE, Brazil. Both human primary cells were cultured in RPMI-1640 medium (Cultilab) supplemented with 10% fetal calf serum (FCS; Gibco) (complete medium) at 37˚C in a 5% CO_2 atmosphere.

Mosquito, human and non-human primate cell lines were also used for the *in vitro* assays. C6/36 cells (ATCC) were cultured in Leibovitz's medium (L-15; Cultilab) and Aag-2 (kindly provided by Dr. João Trindade Marques, UFMG, Brazil) in Schneider's insect medium (Sigma-Aldrich) at 28˚C. Vero E6 and LLC-MK2 cells (ATCC) were cultured in Minimum Essential Medium (MEM; Cultilab) and HepG2 cells (ATCC) in Dulbecco's Modified Eagle's Medium (DMEM; Cultilab) at 37˚C in a 5% CO_2 atmosphere. All culture mediums were supplemented with 1% fetal bovine serum (FBS; Gibco) for maintenance or 10% for expansion, excluding Aag-2, for which 8% FBS, 10 U/mL of penicillin, 10 g/mL of streptomycin and 250 μg/mL of amphotericin B were used (Gibco).

Initially, samples were selected to represent each lineage, and viral isolation was performed based on previous investigations [40]. Briefly, viruses selected from L1 or L6 DENV-1 human sera were diluted 1:10 in L-15 and used to inoculate C6/36 cells, which were then incubated at 28˚C for 7–10 days. Successful isolation was confirmed by RT-PCR of the culture supernatant, as previously described for the sequencing reaction, followed by PCR. PCR was performed to amplify an 1,855-bp fragment using 2 μL of cDNA, 5 μL of 10X buffer, 2 μL of dNTPs (10 mM/μL), 2 μL of primers d1s3 and d1a17 (10 μM), 1 μL $MgCl_2$, 0.25 of Taq DNA polymerase (5 U/μL; Sigma-Aldrich) and DEPC-treated water. The reactions were subjected to the following cycle conditions: 94˚C for 2 min, followed by 30 cycles of 94˚C for 45 sec, 56˚C for 45 sec and 72˚C for 45 sec. A final extension step was performed at 72˚C for 10 min. Amplification was confirmed by electrophoresis on a 1.5% agarose gel.

Titration was determined by flow cytometry to calculate the number of infectious particles/mL (IP/mL), as described previously [41] with modifications, using FACSCalibur (BD Biosciences) equipment. The adaptations were cells fixed in 4% paraformaldehyde and permeabilized with 0.1% triton X-100. Viral stocks from the third passage were used for the experiments.

Growth curves

Approximately $0.05x10^6$ cells (C6/36, Aag-2, Vero E6, LLC-MK2 and HepG2) were plated in each well of a 24-well plate 24 h prior to infection. Five cell lines were infected with L1 or L6 isolates at a multiplicity of infection (MOI) of 0.1 for 1:30 h in triplicates. The cells were then washed with 1X phosphate-buffered saline (PBS) to remove unabsorbed virus and then incubated in 1 mL of maintenance medium. The supernatants were harvested at 24, 48 and 72 hpi for relative quantification using the SYBR Green Real-Time PCR assay with the GoTaq qPCR Master Mix kit (Promega) and primers Den_F (5'-TTAGAGGAGACCCCTCCC-3') and Den_R2 (5'-GAGACAGCAGGATCTCTGG-3'), as previously described [42]. Total RNA was extracted using TRIzol (Invitrogen) according to the manufacturer's protocol. First-strand cDNA was synthesized using the Superscript III First Strand Synthesis System (Invitrogen) following the manufacturer's instructions with primer Den_R2. The qRT-PCR reaction was also performed according to the manufacturer's protocol.

The results were obtained using a standard curve and analyzing the melting curve (~ 85˚C) to approximately CT 35, according to the minimum information for the publication of quantitative real-time PCR experiments (MIQE).

Mosquito infection

Ae. aegypti eggs from populations PPCampos (captive; maintained approximately 15 years in an insectary at the Laboratório de Entomologia Médica, CPqRR, FIOCRUZ, Belo Horizonte-MG, from Campos dos Goytacazes-RJ) and Dom Pedro (wild; collected in 2014 in district Dom Pedro of Manaus-AM) were used in this study according to a previous description [43]. Briefly, the larvae were hatched in an insectary at a temperature of 28˚C and relative humidity of 80%, and infections were performed using 3 to 5-day-old female mosquitoes (Dom Pedro from the F2 generation) using a glass feeding device containing 2/3 of blood mouse (*Mus musculus*) and 1/3 of C6/36 cells suspension infected with either L1 or L6 lineages.

The mean viral titer used for infection with L1 or L6 isolates was 5×10^5 $TCID_{50}$/mL. Infected PPCampos (n = 80) and Dom Pedro (n = 60) females were maintained in cages with 10% glucose solution until day 14 after the experimental infection (complete extrinsic incubation period). They were then dissected, and total RNA was extracted from their bodies and heads (with attached salivary glands) using TRIzol (Invitrogen) as described previously [40], followed by one-step qRT-PCR [43].

The infection rate (IR) was then calculated as the individual proportion of all experimentally infected mosquitoes, in which DENV was detected in the body. Similarly, the vector competence (VC) was calculated, in which DENV was detected in the head (indicating the virus escaped the midgut barrier, completing its life cycle). However, the disseminated infection rate (DIR) is the proportion of DENV-infected mosquito heads of all infected mosquitoes with virus dispersed in the body (DIR = VC/IR).

Viral competition assays

Aag-2 cells were coinfected with L1 and L6 isolates mixed at an equal ratio (1:1) at an MOI of 0.1, and the supernatants were harvested at 24, 48 and 72 hpi, as previously described for the growth curves. Total RNA was extracted using TRIzol (Invitrogen) according to the

manufacturer's instructions, and the relative amounts of L1 and L6 viruses in each dual infection were calculated based on the developed genotyping assay.

Investigation of sfRNA:gRNA ratios and IFN responses

HepG2 cells were infected at an MOI of 1.0, and the supernatants and cells were harvested at 24, 48 and 72 hpi. The sfRNA:gRNA ratio of the cells was obtained by real-time PCR using GoTaq qPCR Master Mix (Promega) with primers D1GSF, D1SF and D1GSR (described in S4 Table).

Cells total RNA was extracted using TRIzol (Invitrogen) according to the manufacturer's protocol. First-strand cDNA was synthesized using M-MLV Reverse Transcriptase (Invitrogen) following the manufacturer's instructions with primers D1GSR. The qRT-PCR reaction was performed using two different mixes, and it consisted of 5 μL of cDNA, 12.5 μL of 2X GoTaq qPCR Master Mix, 2 μL of forward and reverse primers (10 μM), 0.25 μL of CXR reference dye and nuclease-free water to a final volume of 25 μL per reaction. To quantify gRNA, primers D1GSF and D1GSR were used; otherwise, D1SF and D1GSR were used for sfRNA quantification. The reactions were subjected to the following cycle conditions, with data collected at 55˚C and 60˚C: 95˚C for 5 min, followed by 40 cycles of 95˚C for 15 sec and 55˚C for 1 min. A final dissociation step was conducted at 60–95˚C. The results were obtained using a standard curve and by analyzing the melting curve (~ 84.5˚C) to approximately CT 35. Quantification of gRNA and sfRNA levels was performed as described previously [44].

In addition, IFN-α1/13 production was measured in the supernatants of infected HepG2 as recommended for sample cultures by the Human IFNA1/Interferon Alpha-1/13 ELISA Kit (RAB0541; Sigma-Aldrich).

Analysis of IFN-stimulated response by ISRE expression in HBMEC reporter cell line

HBMEC-ISRE-Luc cells were mock-treated or infected with DENV-2 (strain 16681), L1 or L6 DENV-1, in the presence or absence of IFN-β (1000 U– 2 ng/mL; PeproTech). After 48 hpi, the cells were lysed using cell culture lysis reagent (CCLR; Promega), and the supernatants were collected after centrifugation. The luciferase activity was measured by mixing 20 μL of cell lysate with 50 μL of Luciferase Assay Reagent (Promega), and the light produced was measured using a GloMax 96 Microplate Luminometer (Promega). The results are shown in relative light units (RLUs).

Cytokine production

Seventy-two samples of DENV-1 human sera (L1 or L6) were subjected to a selected panel to measure cytokines, chemokines, adhesion molecules and growth factors (EGF, VEGF, TNF-β, TNF-α, MIP-1β, MIP-1α, MCP-1, IP-10, IL-17, IL-15, IL-13, IL-12 (p70), IL-12 (p40), IL-10, IL-8, IL-7, IL-6, IL-5, IL-3, IL-2, IL-1RA, IL-1β, IL-1α, IFN-γ, IFN-α2, GM-CSF, G-CSF and CCL11) using the MILLIPLEX MAP Human Cytokine/Chemokine Magnetic Bead Panel–Premixed 29 Plex–Immunology Multiplex Assay (HCYTMAG-60K-PX29; Millipore) by the Luminex system in the MAGPIX instrument, according to the manufacturer's instructions.

Antigenicity prediction

In silico analyses of the putative antigenic potential of L1 and L6 lineages were performed as previously described [21]. Briefly, 20 amino acid sequences encoding the DENV-1 polyprotein were first aligned using the Multalin interface (http://multalin.toulouse.inra.fr/multalin/

multalin.html) with default parameters. The consensus sequence coding for Capsid, Envelope and NS1 proteins was submitted to the BepiPred 1.0 server (http://www.cbs.dtu.dk/services/BepiPred/) for Linear B epitope prediction. The consensus sequence coding for DENV-1 polyprotein was run into the NetCTL server (http://www.cbs.dtu.dk/services/NetCTL/) to predict T-cell epitopes. Both algorithms were run using default settings. The Allele Frequency Net Database (http://www.allelefrequencies.net/) was used to select the most predominant HLA classes in the Southeast of Brazil and to set up the NetCTL server. The mean value of the epitope propensity scores for each sequence was then classified and plotted according to its potential immunogenicity.

B and T cell activation

Eight-week-old male C57BL/6 mice were divided into 3 groups (5 animals/group) and intraperitoneally immunized with $5x10^5$ IP per mouse of DENV-1: L1 (group 1) or L6 (group 2). Mock C6/36 injections in L-15 medium (group 3) were used as controls. At 7 days p.i., the spleens from each group of mice were extracted, immersed in cold RPMI 1640 medium (Cultilab) and macerated. After centrifugation at 377 x g for 10 min, the erythrocytes were lysed in 9 mL of cold water. Lysis was stopped by adding 1 mL of 1.5 M PBS. The spleen cells were collected after centrifugation and resuspended in 1 mL of RPMI supplemented with 10% FBS (Gibco). To assess viability, an aliquot of cells was diluted 1:20 in 0.4% Trypan Blue solution (Invitrogen) and counted using a Neubauer chamber. A panel of monoclonal antibodies (Becton Dickinson, USA) specific for $CD4^+$, $CD8^+$ and $CD21^+$ lymphocyte subsets and activation markers (CD25, CD69, CD28 and CTLA-4) was then used for cell staining (see S5 Table).

Briefly, $1x10^6$ spleen cells were distributed in 96-well polystyrene conical bottom microwell plates and centrifuged at 377 x g for 10 min. After 30 min of incubation with the antibodies at 4˚C, the cells were washed twice with 0.15 M PBS and fixed in 2% paraformaldehyde in PBS. Flow cytometry acquisition of 30,000 events/tube and analysis were performed using FACSCalibur (BD Biosciences) equipment. Distinct gating strategies were used to analyze the lymphocyte subsets ($CD4^+$, $CD8^+$ T-cell subsets and $CD21^+$ B cells) with FlowJo software. The T lymphocyte $CD8^+$ and $CD4^+$ subsets were selected from the $CD3^+$ cell population, and B lymphocytes were selected using the $CD21^+$ marker. The frequency of cells was determined using quadrant statistics. Limits for the quadrant markers were always set based on negative populations and isotype controls. To analyze the $CD8^+$ lymphocytes, the quadrants were always set for CD8 high populations to avoid including CD8 low NK cells. The results were expressed as percentages of cells for the different gated lymphocyte subpopulations analyzed. The expression of activation markers was evaluated inside each lymphocyte population by measuring the mean intensity fluorescence (MIF), which represents the number of molecules per cell.

The human PBMCs ($2x10^5$ cells) were cultured with L1 or L6 DENV-1 at an MOI of 1.0 for 2 h. Control cultures were performed using supernatant from noninfected C6/36 cells (mock-infected). At 48 hpi, the cells were harvested and incubated with CD38-APC, HLA-DR-FITC and CD3-Pacific Blue (eBiosciences). The frequency of $CD38^+$/HLA-DR^+ among the total PBMCs, $CD4^+$ or $CD8^+$ cells for the analysis of PBMC activation was determined by flow cytometry using FACSCalibur (BD Biosciences) equipment and FlowJo software. Additionally, after 12 days of culture, the supernatants were harvested and the IgM or IgG levels were analyzed by capture ELISA. Briefly, the ELISA plates were incubated with anti-human IgM or IgG antibodies at 3 mg/mL (Sigma-Aldrich) overnight at 4˚C. The plates were blocked with PBS containing 10% FCS for 2 h at 37˚C and washed with PBS-0.05% Tween 20 (PBS-T), and serial dilutions of the supernatant samples were added and incubated overnight at 4˚C. Serial dilutions of purified human IgM or IgG were also added to generate a standard curve. The plates

were incubated with alkaline phosphatase (AP)-conjugated anti-human IgM or IgG (1 mg/mL; Invitrogen) for 2 h at 37˚C, washed and developed using pNPP substrate (Sigma-Aldrich). The reaction was read at 405 nm using an ELISA reader (Bio-Rad Laboratories). Also, the secretion levels of IFN-γ, IL-6 and IL-8 were evaluated by ELISA, according to manufacturer's protocol (PeproTech).

Statistical analysis

The comparative analysis of the two lineages was performed using Student's T test and Chi-squared test. Fisher's exact test was used to compare proportions, and the Mann-Whitney non-parametric test was also applied. P values ≤ 0.05 were considered significant. All analyses were performed using GraphPad Prism version 6.01.

Accession numbers

The envelope sequences of the DENV-1 isolates analyzed in this study are in GenBank under the following accession numbers: KT438562, KT438564, KT438565, KT438566, KT438567, KT438568, KT438569, KT438570, KT438571, KT438572, KT438573, KT438574, KT438575, KT438576, KT438577, KT438578, KT438579, KT438581, KT438582 and KT438583. Additional genomic sequences used in the aa substitutions analysis can be found as GenBank: KP188543 and KP188540.

Supporting information

S1 Fig. Comparative quantification of growth curves of two strains of either L1 or L6 lineage infected at an MOI of 0.1 in *Ae. albopictus* cell line (C6/36). (A) Quantification of cells by flow cytometry-based assay. (B) Quantification of supernatants by qRT-PCR method.
(TIF)

S2 Fig. Evaluation of cytokines in human leukocytes (PBMCs) cultured with L1 or L6 DENV-1 at an MOI of 1.0 and analyzed by capture ELISA. (A, B, C and D) Average and individual data levels for IFN-γ (B), IL-6 (C) and IL-8 (D) production (Wilcoxon test).
(TIF)

S3 Fig. Quantification of cytokines, chemokines, adhesion molecules and growth factors that were not significantly different in L1 or L6 DENV-1-infected patients. (A) IL-1α, IL-1β, IL-2, IL-3, IL-5, IL-6, IL-10, IL-12p70, IL-15, IFN-γ, TNF- α and TNF- β. (B) IL-8, IP-10, MCP-1, MIP-1α, MIP-1β, G-CSF and GM-CSF (Mann-Whitney test).
(TIF)

S4 Fig. Mosquitoes coinfection with different L1:L6 ratios. Dom Pedro mosquitoes were fed with different L1:L6 ratios. Fourteen dpi viral cDNA copy numbers were determined in the body and head of the mosquitoes by Taqman-based qPCR (Student's T test).
(TIF)

S1 Table. Names and sequences of sense and antisense primers with amplicons used in the sequencing reactions.
(DOCX)

S2 Table. Names and sequences of sense and antisense primers with amplicons used for genotyping.
(DOCX)

S3 Table. Name, identified lineage and sequence of probes used for genotyping.
(DOCX)

S4 Table. Names and sequences of sense and antisense primers with amplicons used for the quantification of sfRNA and gRNA levels.
(DOCX)

S5 Table. Monoclonal antibodies and activation markers used for immunostaining and flow cytometry analysis.
(DOCX)

Acknowledgments

The authors thank S.M. Oliani and L.R. Azevedo for their facilities and technical assistance in the Luminex assay. We are grateful to L.S. Ullmann for her assistance in the generation of the genomic data. We also thank V.V. Costa and Z.M. Garcia for experimental assistance and comments on this work.

Author Contributions

Conceptualization: Tauyne Menegaldo Pinheiro, Mânlio Tasso de Oliveira Mota, Aripuanã Sakurada Aranha Watanabe, Joice Matos Biselli-Périco, João Pessoa Araújo, Jr., Carlos Eduardo Calzavara-Silva, Luciana Barros de Arruda, Danielle da Glória de Souza, Mauro Martins Teixeira, Nikos Vasilakis, Maurício Lacerda Nogueira.

Data curation: Mauro Martins Teixeira, Maurício Lacerda Nogueira.

Formal analysis: Mânlio Tasso de Oliveira Mota, Betânia Paiva Drumond, João Pessoa Araújo, Jr., Paulo Filemon Paolucci Pimenta, Laura Helena Vega Gonzales Gil, Carlos Eduardo Calzavara-Silva, Luciana Barros de Arruda, Danielle da Glória de Souza, Nikos Vasilakis, Maurício Lacerda Nogueira.

Funding acquisition: Mauro Martins Teixeira, Nikos Vasilakis, Maurício Lacerda Nogueira.

Investigation: Tauyne Menegaldo Pinheiro, Mânlio Tasso de Oliveira Mota, Aripuanã Sakurada Aranha Watanabe, Joice Matos Biselli-Périco, Milene Rocha Ribeiro, Danila Vedovello, Bárbara Aparecida Chaves, Mayara Marques Carneiro da Silva, Izabella Cristina Andrade Batista, Michelle Premazzi Papa, Lana Monteiro Meuren, Carolina Gonçalves de Oliveira Lucas, Flavio Lemos Matassoli, Adriana Bozzi, Carlos Eduardo Calzavara-Silva, Luciana Barros de Arruda.

Methodology: Tauyne Menegaldo Pinheiro, Betânia Paiva Drumond, Paulo Filemon Paolucci Pimenta, Laura Helena Vega Gonzales Gil, Adriana Bozzi, Luciana Barros de Arruda, Mauro Martins Teixeira, Nikos Vasilakis, Maurício Lacerda Nogueira.

Project administration: Maurício Lacerda Nogueira.

Resources: João Pessoa Araújo, Jr., Laura Helena Vega Gonzales Gil, Maurício Lacerda Nogueira.

Software: João Pessoa Araújo, Jr., Carlos Eduardo Calzavara-Silva.

Supervision: Carlos Eduardo Calzavara-Silva, Maurício Lacerda Nogueira.

Validation: Maurício Lacerda Nogueira.

Writing – original draft: Tauyne Menegaldo Pinheiro, Mânlio Tasso de Oliveira Mota, Betânia Paiva Drumond, Luciana Barros de Arruda, Mauro Martins Teixeira, Nikos Vasilakis, Maurício Lacerda Nogueira.

References

1. Bhatt S, Gething PW, Brady OJ, Messina JP, Farlow AW, et al. (2013) The global distribution and burden of dengue. Nature 496: 504–507. https://doi.org/10.1038/nature12060 PMID: 23563266.
2. OhAinle M, Balmaseda A, Macalalad AR, Tellez Y, Zody MC, et al. (2011) Dynamics of dengue disease severity determined by the interplay between viral genetics and serotype-specific immunity. Sci Transl Med 3: 114ra128. https://doi.org/10.1126/scitranslmed.3003084 PMID: 22190239.
3. Messina JP, Brady OJ, Scott TW, Zou C, Pigott DM, et al. (2014) Global spread of dengue virus types: Mapping the 70 year history. Trends Microbiol 22: 138–146. https://doi.org/10.1016/j.tim.2013.12.011 PMID: 24468533.
4. Teixeira MG, Siqueira JB Jr., Ferreira GL, Bricks L, Joint G (2013) Epidemiological trends of dengue disease in Brazil (2000–2010): A systematic literature search and analysis. PLoS Negl Trop Dis 7: e2520. https://doi.org/10.1371/journal.pntd.0002520 PMID: 24386496.
5. Liu-Helmersson J, Quam M, Wilder-Smith A, Stenlund H, Ebi K, et al. (2016) Climate Change and Aedes Vectors: 21st Century Projections for Dengue Transmission in Europe. EBioMedicine 7: 267–277. https://doi.org/10.1016/j.ebiom.2016.03.046 PMID: 27322480.
6. Chen R, Vasilakis N (2011) Dengue—quo tu et quo vadis? Viruses 3: 1562–1608. https://doi.org/10.3390/v3091562 PMID: 21994796.
7. Guzman MG, Halstead SB, Artsob H, Buchy P, Farrar J, et al. (2010) Dengue: A continuing global threat. Nat Rev Microbiol 8: S7–16. https://doi.org/10.1038/nrmicro2460 PMID: 21079655.
8. Horstick O, Martinez E, Guzman MG, Martin JL, Ranzinger SR (2015) WHO dengue case classification 2009 and its usefulness in practice: An expert consensus in the Americas. Pathog Glob Health 109: 19–25. https://doi.org/10.1179/2047773215Y.0000000003 PMID: 25630344.
9. Holmes EC, Twiddy SS (2003) The origin, emergence and evolutionary genetics of dengue virus. Infect Genet Evol 3: 19–28. PMID: 12797969.
10. dos Santos FB, Nogueira FB, Castro MG, Nunes PC, de Filippis AM, et al. (2011) First report of multiple lineages of dengue viruses type 1 in Rio de Janeiro, Brazil. Virol J 8: 387. https://doi.org/10.1186/1743-422X-8-387 PMID: 21813012.
11. Choudhury MA, Lott WB, Aaskov J (2014) Distribution of fitness in populations of dengue viruses. PLoS One 9: e107264. https://doi.org/10.1371/journal.pone.0107264 PMID: 25222471.
12. Zhang C, Mammen MP Jr., Chinnawirotpisan P, Klungthong C, Rodpradit P, et al. (2005) Clade replacements in dengue virus serotypes 1 and 3 are associated with changing serotype prevalence. J Virol 79: 15123–15130. https://doi.org/10.1128/JVI.79.24.15123-15130.2005 PMID: 16306584.
13. Cunha Mdos P, Guimaraes VN, Souza M, de Paula Cardoso D, de Almeida TN, et al. (2016) Phylodynamics of DENV-1 reveals the spatiotemporal co-circulation of two distinct lineages in 2013 and multiple introductions of dengue virus in Goias, Brazil. Infect Genet Evol 43: 130–134. https://doi.org/10.1016/j.meegid.2016.05.021 PMID: 27223633.
14. Manakkadan A, Joseph I, Prasanna RR, Kunju RI, Kailas L, et al. (2013) Lineage shift in Indian strains of Dengue virus serotype-3 (Genotype III), evidenced by detection of lineage IV strains in clinical cases from Kerala. Virol J 10: 37. https://doi.org/10.1186/1743-422X-10-37 PMID: 23360780.
15. Manokaran G, Finol E, Wang C, Gunaratne J, Bahl J, et al. (2015) Dengue subgenomic RNA binds TRIM25 to inhibit interferon expression for epidemiological fitness. Science 350: 217–221. https://doi.org/10.1126/science.aab3369 PMID: 26138103.
16. Quiner CA, Parameswaran P, Ciota AT, Ehrbar DJ, Dodson BL, et al. (2014) Increased replicative fitness of a dengue virus 2 clade in native mosquitoes: Potential contribution to a clade replacement event in Nicaragua. J Virol 88: 13125–13134. https://doi.org/10.1128/JVI.01822-14 PMID: 25187539.
17. Mendez JA, Usme-Ciro JA, Domingo C, Rey GJ, Sanchez JA, et al. (2010) Phylogenetic history demonstrates two different lineages of dengue type 1 virus in Colombia. Virol J 7: 226. https://doi.org/10.1186/1743-422X-7-226 PMID: 20836894.
18. Drumond BP, Mondini A, Schmidt DJ, Bosch I, Nogueira ML (2012) Population dynamics of DENV-1 genotype V in Brazil is characterized by co-circulation and strain/lineage replacement. Arch Virol 157: 2061–2073. https://doi.org/10.1007/s00705-012-1393-9 PMID: 22777179.
19. Goncalvez AP, Escalante AA, Pujol FH, Ludert JE, Tovar D, et al. (2002) Diversity and evolution of the envelope gene of dengue virus type 1. Virology 303: 110–119. PMID: 12482662.

20. Raghwani J, Rambaut A, Holmes EC, Hang VT, Hien TT, et al. (2011) Endemic dengue associated with the co-circulation of multiple viral lineages and localized density-dependent transmission. PLoS Pathog 7: e1002064. https://doi.org/10.1371/journal.ppat.1002064 PMID: 21655108.

21. Sariol CA, Nogueira ML, Vasilakis N (2018) A Tale of Two Viruses: Does Heterologous Flavivirus Immunity Enhance Zika Disease? Trends Microbiol 26: 186–190. https://doi.org/10.1016/j.tim.2017.10.004 PMID: 29122447.

22. Villabona-Arenas CJ, Mondini A, Bosch I, Schimdt DJ, Calzavara-Silva CE, et al. (2013) Dengue virus type 3 adaptive changes during epidemics in Sao Jose de Rio Preto, Brazil, 2006–2007. PLoS One 8: e63496. https://doi.org/10.1371/journal.pone.0063496 PMID: 23667626.

23. Cologna R, Armstrong PM, Rico-Hesse R (2005) Selection for virulent dengue viruses occurs in humans and mosquitoes. J Virol 79: 853–859. https://doi.org/10.1128/JVI.79.2.853-859.2005 PMID: 15613313.

24. Wargo AR, Kurath G (2012) Viral fitness: definitions, measurement, and current insights. Curr Opin Virol 2: 538–545. https://doi.org/10.1016/j.coviro.2012.07.007 PMID: 22986085.

25. Chapman EG, Costantino DA, Rabe JL, Moon SL, Wilusz J, et al. (2014) The structural basis of pathogenic subgenomic flavivirus RNA (sfRNA) production. Science 344: 307–310. https://doi.org/10.1126/science.1250897 PMID: 24744377.

26. Endy TP, Nisalak A, Chunsuttitwat S, Vaughn DW, Green S, et al. (2004) Relationship of preexisting dengue virus (DV) neutralizing antibody levels to viremia and severity of disease in a prospective cohort study of DV infection in Thailand. J Infect Dis 189: 990–1000. https://doi.org/10.1086/382280 PMID: 14999601.

27. Azeredo EL, Neves-Souza PC, Alvarenga AR, Reis SR, Torrentes-Carvalho A, et al. (2010) Differential regulation of toll-like receptor-2, toll-like receptor-4, CD16 and human leucocyte antigen-DR on peripheral blood monocytes during mild and severe dengue fever. Immunology 130: 202–216. https://doi.org/10.1111/j.1365-2567.2009.03224.x PMID: 20113369.

28. Chaturvedi UC, Agarwal R, Elbishbishi EA, Mustafa AS (2000) Cytokine cascade in dengue hemorrhagic fever: implications for pathogenesis. FEMS Immunol Med Microbiol 28: 183–188. PMID: 10865168.

29. Ho LJ, Hung LF, Weng CY, Wu WL, Chou P, et al. (2005) Dengue virus type 2 antagonizes IFN-alpha but not IFN-gamma antiviral effect via down-regulating Tyk2-STAT signaling in the human dendritic cell. J Immunol 174: 8163–8172. PMID: 15944325.

30. Jain A, Pandey N, Garg RK, Kumar R (2013) IL-17 level in patients with Dengue virus infection & its association with severity of illness. J Clin Immunol 33: 613–618. https://doi.org/10.1007/s10875-012-9855-0 PMID: 23274801.

31. Katzelnick LC, Montoya M, Gresh L, Balmaseda A, Harris E (2016) Neutralizing antibody titers against dengue virus correlate with protection from symptomatic infection in a longitudinal cohort. Proc Natl Acad Sci U S A 113: 728–733. https://doi.org/10.1073/pnas.1522136113 PMID: 26729879.

32. de Morais Bronzoni RV, Baleotti FG, Ribeiro Nogueira RM, Nunes M, Moraes Figueiredo LT (2005) Duplex reverse transcription-PCR followed by nested PCR assays for detection and identification of Brazilian alphaviruses and flaviviruses. J Clin Microbiol 43: 696–702. https://doi.org/10.1128/JCM.43.2.696-702.2005 PMID: 15695666.

33. Christenbury JG, Aw PP, Ong SH, Schreiber MJ, Chow A, et al. (2010) A method for full genome sequencing of all four serotypes of the dengue virus. J Virol Methods 169: 202–206. https://doi.org/10.1016/j.jviromet.2010.06.013 PMID: 20600330.

34. Larkin MA, Blackshields G, Brown NP, Chenna R, McGettigan PA, et al. (2007) Clustal W and Clustal X version 2.0. Bioinformatics 23: 2947–2948. https://doi.org/10.1093/bioinformatics/btm404 PMID: 17846036.

35. Drummond AJ, Suchard MA, Xie D, Rambaut A (2002–2014) BEAST Bayesian Evolutionary Analysis Sampling Trees, Version v1.8.1.

36. Drummond AJ, Rambaut A, Shapiro B, Pybus OG (2005) Bayesian coalescent inference of past population dynamics from molecular sequences. Mol Biol Evol 22: 1185–1192. https://doi.org/10.1093/molbev/msi103 PMID: 15703244.

37. Rambaut A, Suchard MA, Xie W, Drummond AJ (2003–2013) Tracer MCMC Trace Analysis Tool, Version v1.6.0.

38. Rambaut A, Drummond AJ (2002–2014) TreeAnotator v1.8.1 MCMC Output Analysis.

39. Vedovello D, Drumond BP, Marques RE, Ullmann LS, Favaro EA, et al. (2015) First genome sequence of St. Louis encephalitis virus (SLEV) isolated from a human in Brazil. Arch Virol 160: 1189–1195. https://doi.org/10.1007/s00705-015-2378-2 PMID: 25740285.

40. Machado DC, Mondini A, dos Santos Santana V, Yonamine PT, Chiaravalloti Neto F, et al. (2012) First identification of Culex flavivirus (Flaviviridae) in Brazil. Intervirology 55: 475–483. https://doi.org/10.1159/000337166 PMID: 22854125.

41. Lambeth CR, White LJ, Johnston RE, de Silva AM (2005) Flow cytometry-based assay for titrating dengue virus. J Clin Microbiol 43: 3267–3272. https://doi.org/10.1128/JCM.43.7.3267-3272.2005 PMID: 16000446.

42. Chutinimitkul S, Payungporn S, Theamboonlers A, Poovorawan Y (2005) Dengue typing assay based on real-time PCR using SYBR Green I. J Virol Methods 129: 8–15. https://doi.org/10.1016/j.jviromet.2005.05.006 PMID: 15941596.

43. Goncalves CM, Melo FF, Bezerra JM, Chaves BA, Silva BM, et al. (2014) Distinct variation in vector competence among nine field populations of Aedes aegypti from a Brazilian dengue-endemic risk city. Parasit Vectors 7: 320. https://doi.org/10.1186/1756-3305-7-320 PMID: 25015526.

44. Bidet K, Garcia-Blanco MA (2014) Flaviviral RNAs: weapons and targets in the war between virus and host. Biochem J 462: 215–230. https://doi.org/10.1042/BJ20140456 PMID: 25102029.

Archives of Virology
https://doi.org/10.1007/s00705-018-3911-x

ORIGINAL ARTICLE

Zika-virus-infected human full-term placental explants display pro-inflammatory responses and undergo apoptosis

Milene Rocha Ribeiro[1,6] · Jusciele Brogin Moreli[2] · Rafael Elias Marques[3] · Michelle Premazzi Papa[4] · Lana Monteiro Meuren[4] · Paula Rahal[1] · Luciana Barros de Arruda[4] · Antonio Helio Oliani[6] · Denise Cristina Mós Vaz Oliani[6] · Sonia Maria Oliani[1] · Aarthi Narayanan[5] · Maurício Lacerda Nogueira[6]

Received: 3 October 2017 / Accepted: 31 May 2018

Abstract

Zika virus (ZIKV) is a flavivirus that has been highly correlated with the development of neurological disorders and other malformations in newborns and stillborn fetuses after congenital infection. This association is supported by the presence of ZIKV in the fetal brain and amniotic fluid, and findings suggest that infection of the placental barrier is a critical step for fetal ZIKV infection *in utero*. Therefore, relevant models to investigate the interaction between ZIKV and placental tissues are essential for understanding the pathogenesis of Zika syndrome. In this report, we demonstrate that explant tissue from full-term human placentas sustains a productive ZIKV infection, though the results depend on the strain. Viral infection was found to be associated with pro-inflammatory cytokine expression and apoptosis of the infected tissue, and these findings confirm that placental explants are targets of ZIKV replication. We propose that human placental explants are useful as a model for studying ZIKV infection *ex vivo*.

Introduction

Zika virus (ZIKV), a member of the family *Flaviviridae*, is an enveloped, single-strand RNA virus that was the causative agent of major outbreaks in the Americas in 2015 [57, 69]. Its genome has a typical flavivirus architecture and is approximately 11 kb in length. The virus was first isolated from a Rhesus Macaque in 1947 in the Zika forest in Uganda; however, ZIKV infection had been poorly investigated until recently, when numerous infections were reported in more than 60 countries and territories around the world. Major outbreaks have been recorded on the Yap Islands (2007), in French Polynesia (2013), and in Brazil (2015). The virus is primarily transmitted by *Aedes aegypti* mosquitoes, and humans are considered to be amplification hosts, though nonhuman primates may be involved in maintenance of the virus in Africa [68]. In addition, the virus is unique in relation to other flaviviruses such as dengue virus (DENV) in that it may be transmitted by alternative routes, including through sexual and maternal-fetal routes [20, 21, 64, 71].

Most of the cases associated with ZIKV infection are either asymptomatic or present only mild symptoms such as fever, rash, joint pain, and conjunctivitis. Myalgia and headaches have also been reported. In recent outbreaks,

Handling Editor: Tim Skern.

Electronic supplementary material The online version of this article (https://doi.org/10.1007/s00705-018-3911-x) contains supplementary material, which is available to authorized users.

✉ Maurício Lacerda Nogueira
mnogueira@famerp.br

[1] Department of Biology, School of Biosciences, Humanities and the Exact Sciences, São Paulo State University (UNESP), São José do Rio Preto, São Paulo, Brazil

[2] Federal University of São Paulo (UNIFESP), São Paulo, São Paulo, Brazil

[3] Brazilian Biosciences National Laboratory (LNBio), National Center for Research in Energy and Materials (CNPEM), Campinas, São Paulo, Brazil

[4] Paulo de Góes Department of Microbiology, Federal University of Rio de Janeiro (UFRJ), Rio de Janeiro, Brazil

[5] George Mason University, Fairfax, Virginia, USA

[6] Virology Research Laboratory, Department of Dermatological, Infectious, and Parasitic Diseases, São José do Rio Preto School of Medicine (FAMERP), São José do Rio Preto, São Paulo, Brazil

Published online: 06 June 2018

however, ZIKV infection was highly correlated with neurological manifestations, particularly in developing fetuses after congenital infection [4, 9, 44]. In fact, infection of pregnant women has been associated with miscarriage, fetal abnormalities, microcephaly, and other neurological diseases in newborns [41, 53]. The virus has been isolated from multiple bodily fluids from infected individuals, including serum, urine, saliva, and semen [48]. Importantly, the virus has also been detected in amniotic fluid and in the brains of microcephalic newborns and fetuses in cases of stillbirth [7, 46], demonstrating that ZIKV crosses the placenta through an unknown mechanism of action.

Recent studies using experimental mouse models have also indicated that the virus might cross the placental barrier, leading to congenital ZIKV transmission. Systemic infection of pregnant mice resulted in abnormal brain development and microcephaly in the offspring, outcomes that were attributed to viral neurotropism [14, 45, 72]. Infection of trophoblasts and endothelial cells in the placentas of ZIKV-infected mice and nonhuman primates have also been reported [1, 45, 54].

However, most animal models used to study ZIKV infection are deficient in the expression of type I or type I and type II interferon receptors (A129 and AG129, respectively) [2, 45, 59]. Mice that lack components of innate immune responses, including *Mavs*$^{-/-}$, *Irf3*$^{-/-}$, *Irf3*$^{-/-}$*Irf5*$^{-/-}$*Irf7*$^{-/-}$, have also shown susceptibility to ZIKV infection [37]. Although these models are useful for evaluating the efficacy of vaccine candidates and therapies, they may not represent the true effects associated with trans-placental transmission of the virus in immunocompetent individuals, or the conditions in the placenta that favor viral multiplication, including possible local inflammation.

A critical unmet need is a model that can be used to quickly, quantitatively, and effectively screen for functionally relevant countermeasures that may protect the fetus from intrauterine transmission of ZIKV. In this report, we demonstrate that placental explants obtained from full-term placental tissue both support and are affected by ZIKV infection. This tissue may be useful as a model for such experimentation, as well as for the development of treatments against ZIKV infections.

Materials and methods

Cell lines and viruses

Vero cells were cultivated in MEM supplemented with 10% fetal bovine serum, 100 units of penicillin per mL, and 100 µg of streptomycin per mL at 37 °C in a humidified atmosphere containing 5% CO_2. ZIKV-BR (GenBank accession number KU497555; kindly provided by Pedro Vasconcelos, Evandro Chagas Institute, FIOCRUZ, Pará, Brazil) was isolated from a mild case of ZIKV in the state of Paraíba, Brazil, and it was distributed within our local research network project after four passages in C6/36 cells [18]. The DENV-2 strain used was New Guinea C, or NGC (GenBank accession number AF038403). The viruses were propagated and titrated using Vero cells. The viral stock was aliquoted in 100-µL portions and stored at − 80 °C. Titers were determined and titrated using a standard $TCID_{50}$ assay.

Infections in human placental explant cultures

Normal human placenta tissues were obtained from full-term elective cesarean deliveries in cases of non-labor after 38 to 40 weeks of gestation (n = 10) at the Children's and Maternity Hospital of São José do Rio Preto, São Paulo, Brazil, after approval from the local research ethics committee. Placentas were processed within 15 min of delivery. Chorionic villi were dissected into 5-mm sections, and tissues were washed extensively with PBS (1x). Explants were cultured in standard tissue culture plates in DMEM (Cultilab) combined with Ham's F-12 Nutrient Mixture (HAMF-12; Thermo Fisher) and supplemented with 10% FBS (GIBCO), 1% penicillin-streptomycin, and 100 mg of gentamicin per mL. Cultures were maintained at 37 °C in a humidified atmosphere containing 5% CO_2. Twenty-four hours after plating, samples were infected with 1×10^4 TCD_{50} of ZIKV-BR or DENV2. The culture was incubated for 4 hours to allow for virus adsorption. The explants were then washed three times with PBS (1X) for complete removal of the inoculum. The explants were then maintained in DMEM/HAMF-12 with 2% FBS. Culture supernatants from infected and uninfected explants were collected at 0, 3, 6, 12, 24, 72, and 120 hours postinfection (hpi) without the addition of fresh media or washing. Explants were then collected to determine total RNA and were fixed in 4% paraformaldehyde for histology and immunohistochemistry analysis. The culture medium was collected to perform plaque assays and to quantify β-hCG through the use of electrochemiluminescence (Roche Hitachi, Cobas® e411). Some sample tissues that had been cultured for 24 hours were also treated with neutralizing anti-TNF RII/TNFRSF1B antibody (100 ng/mL, R&D Systems, Minneapolis, MN, USA) or TLR-3 ligand polyinosinic:polycytidylic acid, or poly (I:C) (50 µg/mL; Sigma-Aldrich) for 24 hours.

Viral quantification

ZIKV RNA was quantified from culture supernatants using a TaqMan-based qRT-PCR assay (GoTaq ® Probe 1-Step RT-qPCR System, REF AG120) as described previously [35]. DENV2 RNA was analyzed using a SuperScript III Platinum SYBR Green One Step RT-qPCR Kit (REF 1136-059) and

the primers described by Chutinimitkul and colleagues [11]. The primer and probe sequences are described in supplementary Table A1.

Plaque assay

Vero cells were plated at a density of 5×10^5 cells per well in a six-well plate and cultured for 24 hours at 37°C under 5% CO_2. Serial dilutions of supernatant from explant cultures (24 and 72 hpi) were added to each well for 1 hour of incubation. After the medium was removed, infected monolayers were covered with 1.5% carboxymethylcellulose (CMC)/MEM with 2% FSB at a 1:1 ratio. Plaque foci were detected on day 5 after fixation with 10% formalin solution and staining with 2% crystal violet.

Histological analysis

Infected placental tissue sections and their uninfected controls were fixed in 4% buffered formalin for 24 hours, dehydrated in graded ethanol, and embedded in paraffin for histopathological analysis. The samples were stained with hematoxylin and eosin (H&E) and analyzed using a high-power objective (20×) on an Axioskop 2-Mot Plus Zeiss microscope (Carl Zeiss, Jena, Germany). To quantify nuclear fragmentation, 10 random photos were taken of experiments performed in triplicate, and the amount of karyorrhexis was determined for each photo. The mean plus or minus standard deviation per field is shown.

Immunohistochemistry

ZIKV infection and caspase-3 activation were analyzed in the placental explants using immunohistochemistry. Sections of infected placental tissue and the uninfected controls were collected at 72 and 120 hpi. Some samples were also treated with neutralizing anti-TNFRII/TNFRSF1B antibody (R&D Systems, Minneapolis, MN) and harvested at 72 hpi. Serial 3-µm-thick tissue sections were deparaffinized and rehydrated prior to antigen retrieval in citrate buffer at a pH of 6.0. Endogenous peroxide activity was blocked with 3% hydrogen peroxide for 30 minutes, followed by blocking with 10% bovine serum albumin (BSA; Sigma-Aldrich, Missouri, USA) in Tris-buffered saline (TBS) for 2 hours. The slides were incubated with primary mouse antibody against flavivirus E protein (4G2) at a dilution of 1:100, anti-caspase-3 (Abcam, cat. number ab2302) at 1:200, anti-cytokeratin 7 (Dako) at 1:250, or anti-vimentin (Dako) at 1:150 in 10% TBS-BSA for 1 hour at 37 °C, all of which were applied in independent trials. After the washing step, sections were incubated with a secondary antibody (HRP-conjugated anti-mouse or anti-rabbit antibody; Abcan). Positive staining was detected using 3,3′-diaminobenzidine (DAB substrate; Invitrogen, USA). Finally, sections were counterstained with H&E (hematoxylin from InlabConfiança and eosin from AnalytiCals). A negative reaction control was run in the absence of primary antibodies. Analysis was performed using an Axioskop 2-Mot Plus microscope (Carl Zeiss, Jena, Germany) and AxioVision software for densitometric and quantitative analysis. The experiments were each performed in triplicate using samples from three individual donors, and ten fields were quantified in each section. Densitometric analysis was used to determine caspase-3 and 4G2 intensity in sections of placental tissue (40×) on an arbitrary scale from 0 to 255, and the data were expressed as the mean plus or minus standard deviation [6].

Cytokine gene relative expression analysis

RNA from virus-infected explants and uninfected controls was extracted using TRIzol according to the manufacturer's instructions (Life Technologies). Likewise, RNA was extracted within 24 hours from uninfected samples treated with 50 µg of poly (I:C) per mL, as well as from the untreated controls. Cytokine gene relative expression analyses were performed using a SuperScript III Platinum SYBR Green One Step qRT-PCR Kit (Invitrogen; REF 1136-059). The primer sequences for the IL-6, IL-10, IL-1β, TNF-α, IFN-β, IFN-γ, IFN-λ1, and IFN-λ4 cytokines are listed in supplementary Table A2. A comparative ΔΔCt method was used to quantify gene expression levels based on GAPDH Ct values for normalization.

TUNEL assay

Detection of nuclear DNA fragmentation as a morphological marker of the apoptosis process in histological sections was performed using a TUNEL assay. The assay was performed using an In Situ Cell Death Detection Kit (TMR red). After 3 days of infection, 3-mm infected tissue sections and uninfected controls were deparaffinized, hydrated, and rinsed with 0.1 M phosphate buffer (pH 7.4), followed by blocking with 3% BSA and 20% FBS. TUNEL reaction mixture (TdT enzyme fluorescein-labeled nucleotide mix) was added, and the sections were incubated for 60 minutes at 37 °C. For the positive reaction control, the sections were treated with 3U of DNase I per mL for 10 minutes at room temperature. Quantitative analysis was performed using Image-Pro® Plus image analysis software, and fluorescent images of TUNEL-positive cells were captured using an Olympus BX53 microscope system at 40× in red channel detection in the range of 570 to 620 nm. Tests were performed in duplicate, and images of three random fields were acquired from each slide to calculate the mean plus or minus standard deviation.

Data analysis

Data were analyzed using GraphPad Prism software (version 6; GraphPad, CA). Results are expressed as the mean plus or minus standard deviation. Data were analyzed using one-way ANOVA followed by the non-parametric Kruskal-Wallis test (unpaired data) or the Bonferroni correction. Data from a minimum of three independent experiments are presented. Significance was established as $p < 0.05$.

Results and discussion

Placental explants support ZIKV infection

Our goal was to determine whether explants of human placental tissue are a useful model for studying ZIKV infection *ex vivo*. To that end, normal full-term placental tissues were obtained following cesarean section. Chorionic villi were dissected, and the explants (5 mm) were infected with ZIKV-BR or dengue virus 2 (DENV2) for comparison. Immunostaining of the tissues at 72 hpi with the anti-flavivirus antibody 4G2 demonstrated that the tissues were infected by both viruses (Fig. 1a-d). To confirm that placental explants would support a progressive ZIKV infection, culture supernatants from these infected explants were obtained at 0, 3, 6, 12, 24, 72, and 120 hpi, and virus RNA levels were analyzed using RT-qPCR (Fig. 1e). We observed a progressive increase in the ZIKV RNA load as early as 12 hpi, with a peak at 72 hpi. DENV 2 RNA was also detected in placental supernatants until 24 hpi, but RNA levels did not increase at the subsequent time points. Culture supernatants from infected tissues collected at 0 hpi exhibited a viral load of $< 10^1$, and this value was subtracted from those obtained at subsequent time points. Uninfected tissues exhibited no viral load when measured using RT-qPCR.

The release of infectious virus particles at different time points after infection was also evaluated using plaque assay. Accordingly, we observed increased levels of ZIKV plaque-forming units (PFU) in the supernatants of explanted tissues, whereas DENV2 PFU levels decreased at later time points (Fig. 1f).

H&E staining and histological analysis demonstrated that placental tissues infected with ZIKV-BR showed signs of cellular injury, in contrast to uninfected tissues (Fig. 2a-c; additional images can be found in Figure A3 of the Supplementary Information). The presence of trophoblasts in these sections was confirmed by the high expression of the cytokeratin-7 epithelial cell marker (Fig. 2d-f), as well as by the absence of vimentin expression (mesenchymal cell marker) (Fig. 2g-i). In addition, the quantification of nuclear fragmentation revealed a larger amount of karyorrhexis in ZIKV-BR infection than in uninfected and DENV-infected tissues, a finding that suggests that viral replication may indeed be associated with tissue damage (Fig. 2j).

Other studies have demonstrated that placental explant cultures secrete hCG during the process of explant re-epithelization [31, 34, 47, 67]. We evaluated whether ZIKV infection would affect the secretion of b-hCG, a marker of syncytiotrophoblast (SCT) renewal and viability (Fig. 2d-i, k) [32]. ZIKV-infected tissues exhibited lower b-hCG secretion in the culture than the uninfected control (Fig. 2k), a result that suggests lower SCT recovery upon ZIKV infection. Meanwhile, DENV-infected tissues exhibited lower b-hCG secretion after 48 h, thus reducing SCT viability. However, SCTs were found to increase secretion of b-hCG 72 h after infection, suggesting improved SCT recovery. These findings are in accordance with previous studies on experimental mouse models, the results of which have demonstrated the infection of fetal and maternal placental tissues [45]. These and other experimental models have also shown that ZIKV infects various primary human placental cell types and chorionic villus explants, and the data are suggestive of infection occurring via placental and paraplacental virus transmission routes [56, 63]. Previous studies have reported that both cytotrophoblasts (CTBs) and SCTs from chorionic villi exhibit E protein expression upon ZIKV infection; however, only CTBs expressed the nonstructural protein NS3 [63]. In addition, it has been proposed that trophoblasts are resistant to ZIKV replication, based on a study showing that different trophoblast-derived cell lines were permissive to ZIKV, while human primary trophoblasts exhibited low viral RNA levels when compared to other cell types [3]. On the other hand, both macrophages and CTBs obtained from the same tissues were found to be susceptible to ZIKV [56].

An experimental model involving pregnant rhesus monkeys revealed prolonged viremia compared to non-pregnant animals, and the use of this system has provided important data on ZIKV infection in the first and third trimesters. These data show that placentas from late-stage pregnancies are still vulnerable to ZIKV. Therefore, models of infection in full-term explants can be used to recapitulate the second half of pregnancy. Furthermore, full-term explants have the advantage of being easy to obtain after delivery [13, 54].

Our data clearly demonstrate that full-term human placenta explants are permissive to ZIKV and DENV2 infections, which are associated with cell injury. Discrepancies between different studies may be attributed to the time at which the explant was obtained and to the specific ZIKV strain used. It is important to note that immunohistochemical staining and progressive RNA release from cultures indicate that this model can be used to study the dynamics of infection and of host-virus interaction.

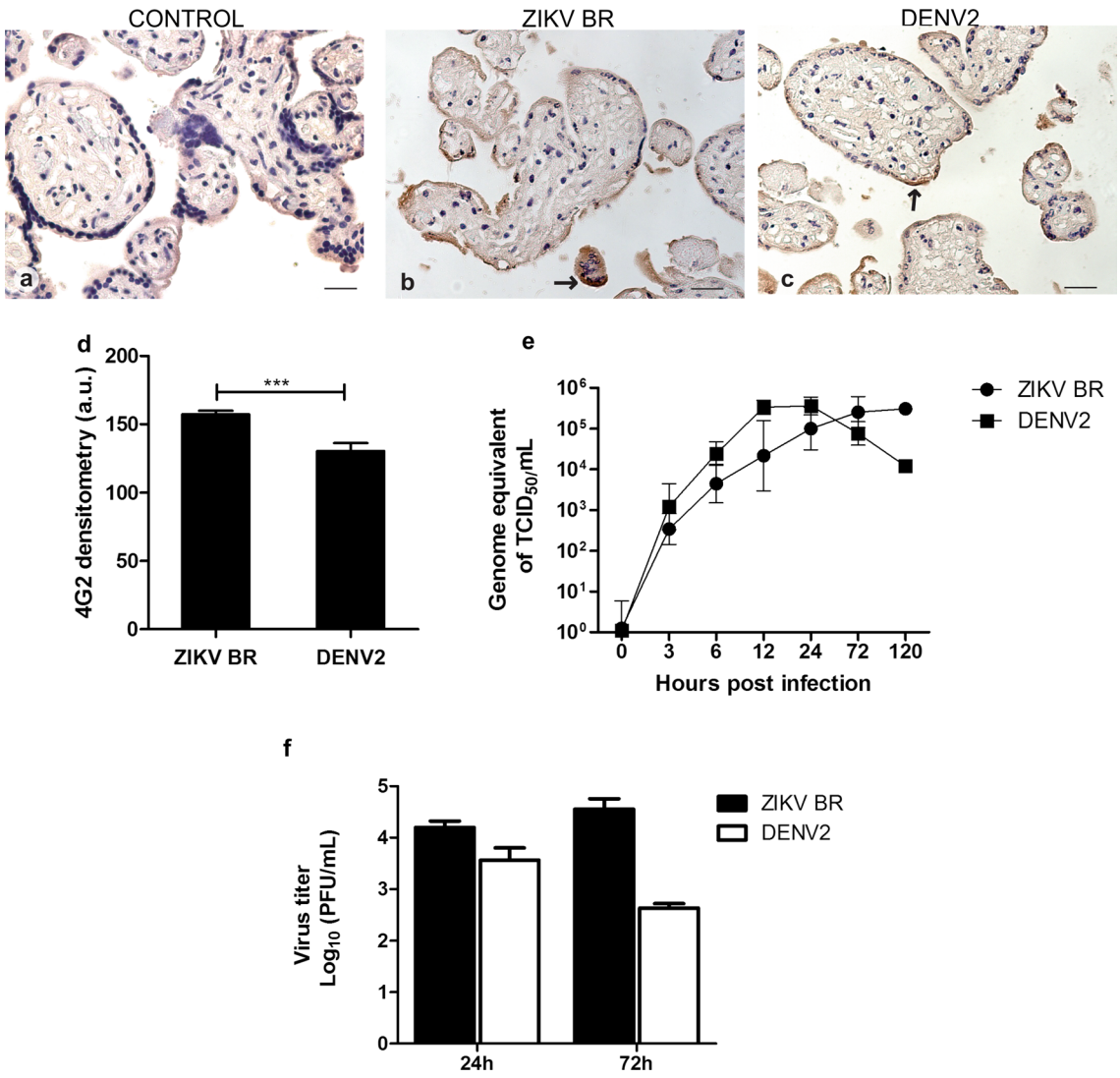

Fig. 1 ZIKV productively infects human placental tissue explants. Placental explants were left uninfected (control) (**a**) or infected with ZIKV (**b**) or DENV (**c**) at 1×10^4 $TCID_{50}$. After 72 hpi, immunohistochemistry staining was performed using the anti-flavivirus 4G2 antibody. Black insets show the details of immunohistochemistry staining. Quantification of 4G2 staining using densitometry in arbitrary units (a.u.) was performed using an Axioskop 2-Mot Plus Microscope (Carl Zeiss, Jena, Germany). The AxioVision software was used for qualitative analysis. Densitometry analysis of the reaction-negative control and of the uninfected samples consistently produced negative results. The data were analyzed using one-way ANOVA followed by the Kruskal-Wallis test; ***, $p < 0.001$ (**d**). Full-term placental explants were left uninfected (controls) or were infected with ZIKV-BR or DENV2 viruses (1×10^4 $TCID_{50}$), and the supernatants were harvested at the time points indicated. RNA extraction and qRT-PCR were performed using specific ZIKV and DENV primers as described in Materials and methods (**e**). The titers of infectious particles in the supernatants were evaluated by plaque assay in Vero cells (**f**). All of the data were obtained from experiments performed in triplicate and are represented as the mean +/− standard deviation. Scale bar: 10 µm

ZIKV infection induces cytokine expression in placental explants

Placental damage and dysfunction caused by viral infection may be a consequence of the viral cytopathic effect or host-mediated pathology [28]. Such conditions alter placental development, restrict fetal growth [42], and may result in neuroinflammation [66]. To determine whether antiviral or inflammatory responses to infection are related to placental dysfunction, we evaluated the expression of interferons (IFNs) and pro-inflammatory cytokines in ZIKV-infected placenta explants.

ZIKV infections in other experimental models have been associated with increased expression of innate immune sensors and interferon-stimulated genes [27]. Also, studies have found purified primary human trophoblasts and trophoblast-derived cell lines to be resistant to ZIKV infection due to the production of type III IFNs (IFN-λ1 and -λ2)

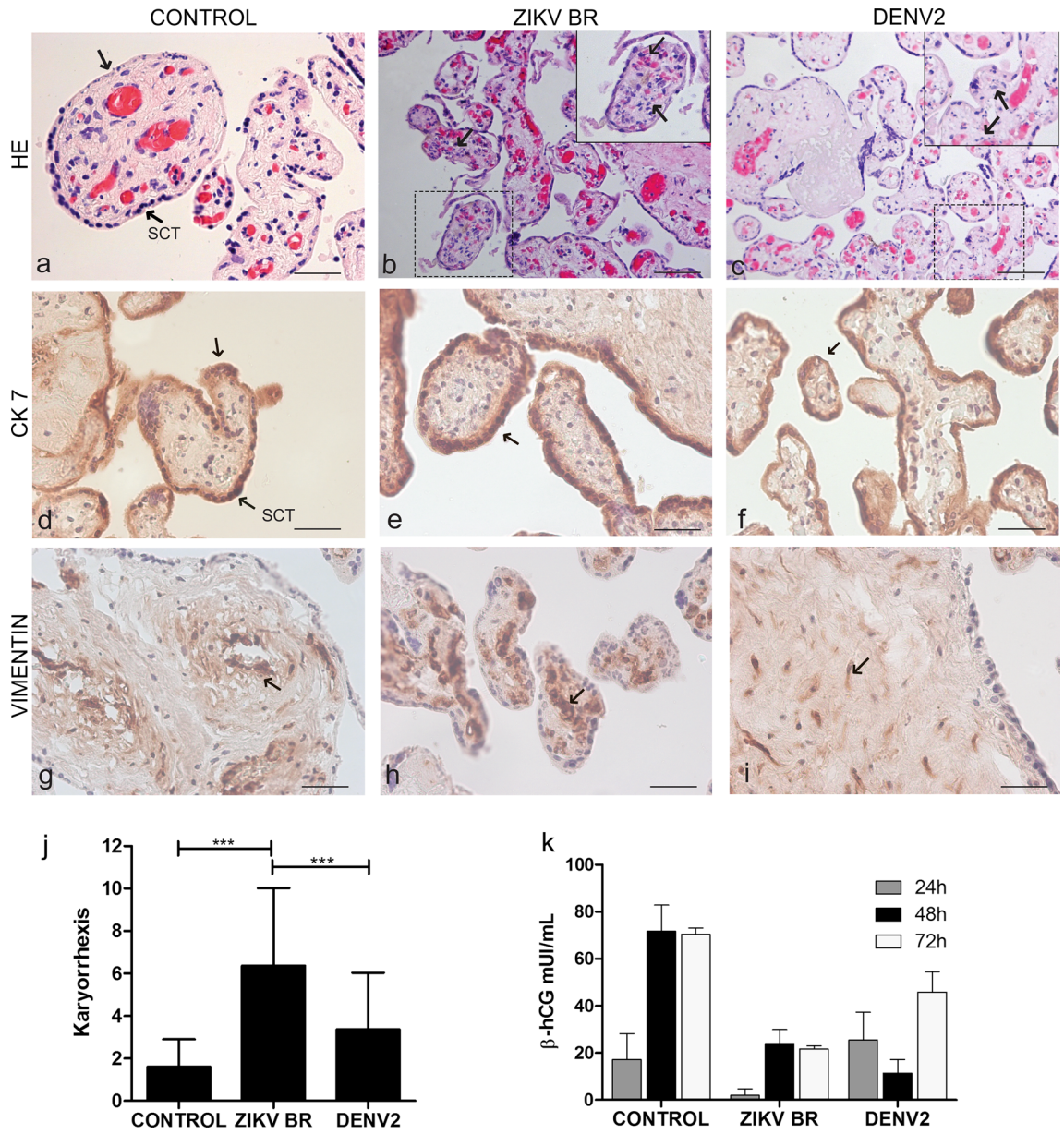

Fig. 2 Histological analysis of infected placental explants. Human placental explants were left uninfected (control) or were infected with ZIKV or DENV. After 72 hpi, immunohistochemistry analysis was performed. The tissues were stained with H&E. Black arrows indicate karyorrhexis, and red arrows point to stromal injury. SCT: syncytiotrophoblasts (**a-c**). Immunohistochemistry analysis of the placental tissues stained with anti-cytokeratin (CK7); black arrows indicate cells stained with anti-cytokeratin (CK7) (**d-f**). Immunohistochemistry analysis of the placental tissues stained with anti-vimentin (mesenchymal cells); black arrows indicate cells stained with anti-vimentin (**g-i**). The graph represents the mean +/− standard deviation of the number of cells per field, with karyorrhexis detected in ten random photos taken from experiments performed in triplicate in the H&E analysis (**j**). The data were analyzed using one-way ANOVA followed by the Bonferroni correction; ***, $p < 0.001$. β-hCG was quantified to determine SCT viability (**k**). Scale bar: 10 µm

[3]. Our experimental model supports ZIKV replication, so we investigated whether and how the relative expression of type I (IFN-β), type II (IFN-γ), and type III (IFN-λ1 and λ4) IFNs would take place in infected placental explants. As a positive control of IFN expression, we cultured explants with poly(I:C) and observed an increase in IFN-β, IFN-λ1, IFN-λ4 and IFN-γ expression at 24 hpi relative to untreated cultures (Fig. 3a). Notably, IFN-λ4 and IFN-γ reached higher levels of expression than IFN-β and IFN-λ1. Placental explants were also infected with ZIKV or DENV or left uninfected, and IFN expression was evaluated at 24 and 72 hpi. ZIKV and DENV infections induced a mild increase in IFN-λ1 and IFN-λ4 expression at 24 hpi; the exception was IFN-λ4 in the case of DENV infection, which did not

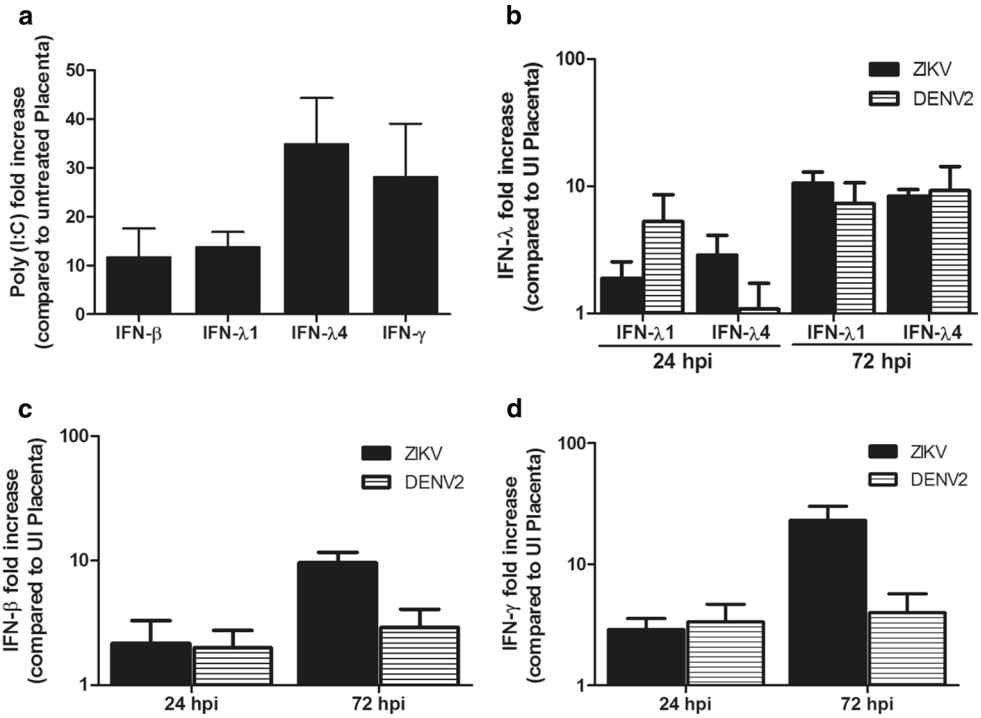

Fig. 3 IFN relative expression in infected placental tissue explants. Explants were cultured with poly(I:C) for 24 hours. RNA was extracted, and the IFN mRNA levels were analyzed by quantitative RT-PCR and normalized using the housekeeping gene GAPDH (**a**). Explants were cultured with ZIKV or DENV for 24 or 72 h. Next, RNA was extracted, and mRNA levels of IFN- λ1 and IFN- λ4 (**b**), IFN- β (**c**), and IFN-γ (**d**) were analyzed by quantitative RT-qPCR and normalized by GAPDH. Results are shown as fold change relative to controls consisting of uninfected tissues and unstimulated poly(I:C). The data shown are representative of at least three independent experiments and are presented as the mean +/− standard deviation

increase (Fig. 3b). At 72 hpi, IFN-λ1 and IFN-λ4 expression in infected explants increased as much as tenfold in the cases of both viral infections. Type III IFNs include IFN-λ1, λ2/λ3, and λ4, all of which seem to induce a similar antiviral response pattern mediated by IFNLR1/IL-10R2 engagement and activation of the JAK-STAT signaling pathway, thus leading to ISG expression [29, 33, 43]. Several studies based on different infectious models have demonstrated that IFN-λ1 and IFN-λ2/λ3 are similarly regulated by IRF-3 and IRF-7 activation. These results strongly suggest that type I and III IFN genes are regulated by a common mechanism. [38].

Despite the differential activation of IFN-λ1 and IFN-λ2, detailed analyses are needed to elucidate the mechanism of this activation. Influenza A virus induces the expression of IFN-λ1 (but not IFN-λ2), although Sendai virus has been found to induce production of high levels of IFN-λ1 and IFN-λ2 [50].

In the infection of both trophoblast cell lines and primary human trophoblasts with ZIKV, the secretion of IFN-λ1 and IFN-λ2 was constitutive. This result demonstrates the important role of interferon-type-III-mediated protection from ZIKV infections at the maternal–fetal interface [3, 12].

IFN-λ4 was discovered more recently, and there is evidence that its expression is regulated by a transduction signaling pathway similar to those regulating other type III IFNs [38, 52]. Our data demonstrated that type III IFNs were produced in the placental explant model and increased over the time points evaluated, and this is consistent with previous data obtained from the use of other placental culture models [3, 12]. The activation of the type III IFN-inducing pathway was further demonstrated by the increased levels of IFN-λ4 mRNA, the expression of which seems not to have been evaluated for ZIKV infection prior to this study. Any discrepancies between our results and those in the literature could be attributed to factors such as the use of different ZIKV strains and the use of a placental explant rather than a single epithelial cell type from the placenta.

ZIKV and DENV2 also induced mild increases in IFNβ expression at 24 hpi, and there was a subsequent significant increase in IFNβ expression at 72 hpi only in the ZIKV-infected explants (Fig. 3c). Interestingly, our results on IFN-γ expression showed a similar pattern, in which only ZIKV infection caused an increase in IFN expression at 72 hpi (Fig. 3d). IFN-γ may induce apoptosis of human primary trophoblasts, mediate proliferation and migration of extravillous cytotrophoblasts (EVCT), and, when in excess, be harmful to pregnancy and to fetal growth [36, 65, 70]. ZIKV NS5 has been found to destabilize STAT2 and suppress the signaling mediated by type I and type III IFN [5, 10, 56]. Therefore, increased levels of IFNs produced to restrict ZIKV infection may be counteracted by the virus while also inducing inflammation and other host responses that could have deleterious effects on pregnancy.

To investigate other aspects of the immune response to ZIKV in placental explants, we assessed the relative expression of IL-1β, IL-6, IL-10, and TNF-α in ZIKV-infected tissues (Fig. 4). Tissues were either stimulated with poly(I:C) or infected with ZIKV or DENV. All groups exhibited increased expression of all of the cytokines evaluated (IL-1β,

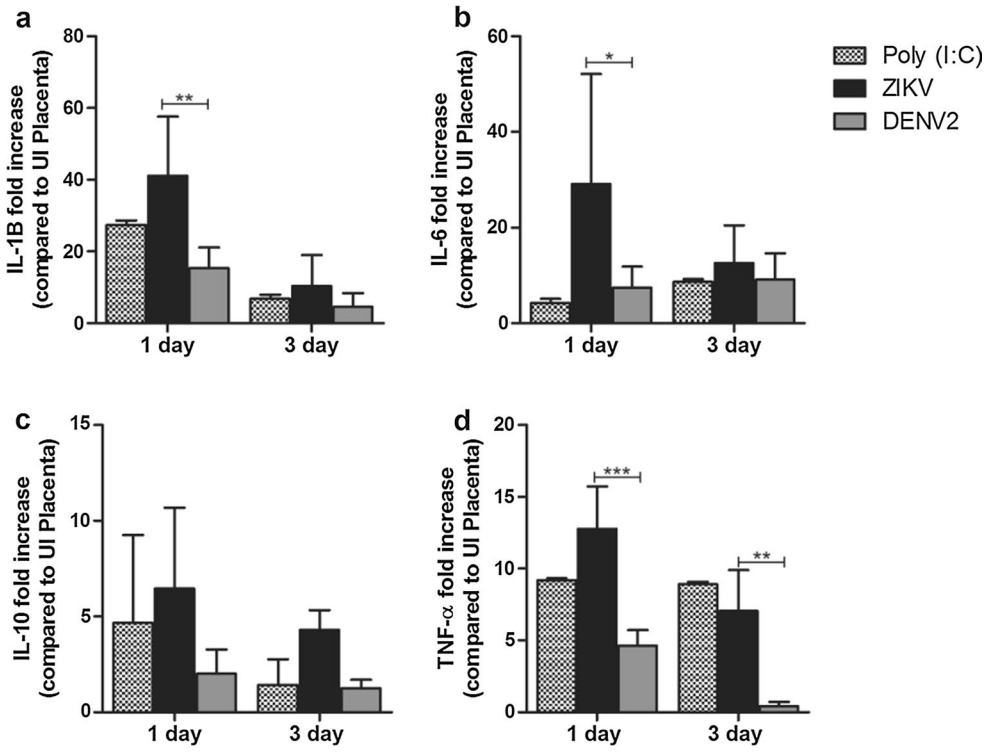

Fig. 4 Cytokine relative expression profiles in placental tissue explants. ZIKV-BR- and DENV2-infected explants were analyzed for cytokine gene expression using RT-qPCR. Uninfected explants (UI) and poly(I:C)-stimulated tissues were analyzed as negative and positive controls, respectively. Unstimulated poly(I:C) and uninfected tissues were used to compare the fold increase. Total RNA was extracted from the explants on days 1 and 3 postinfection. The RNA levels for IL-1β (**a**), IL-6 (**b**), IL-10 (**c**), and TNF-α (**d**) were quantified using gene-specific primers. The analysis was performed using samples obtained in triplicate. Data are represented as the mean +/− standard deviation. One-way ANOVA was performed, followed by Bonferroni correction. *, $p < 0.05$; **, $p < 0.01$; and ***, $p < 0.001$ were considered significant

IL-10, IL-6, and TNF-α) upon infection/stimulation relative to uninfected controls. At 1 day postinfection (dpi), ZIKV-infected explants exhibited significantly higher expression of IL-1β, IL-6, and TNF-α in comparison to DENV2-infected explants (Fig. 4a, b, and d). The expression of pro-inflammatory cytokines such as IL-1β, IL-6, and TNF-α alters the intra-amniotic milieu and is a marker of fetal inflammatory response syndromes. Increased Th1 cytokines have been associated with spontaneous preterm labor and with disruption of fetal tolerance [17, 22, 58]. IL-1β has also been associated with the expression of metalloproteinases and CTB invasion during pregnancy [40, 55]. *In vitro* treatment with IL-1RA impaired trophoblast fusion, viability, and hCG secretion, indicating that IL-1B plays an important role in placental dysfunction and adverse pregnancy outcomes [15, 24]. TNF-α expression during pregnancy is associated with detrimental effects, including gestational hypertension and gestational diabetes mellitus [26, 30, 62]. TNF-α may act directly upon early-term placentas and cause placental pathology, fetal hypoxia, and neurodevelopmental defects in the fetal brain [8]. Also, TNF-α disturbs trophoblast function, leading to decreased cell fusion and reduced expression of hCG [39, 51]. TNFα may also be associated with cell death, as described in other models [23]. IL-10, on the other hand, is typically anti-inflammatory, which often results in tissue protection and is involved in fetal tolerance [19, 60, 61]. ZIKV infection induced the expression of significant levels of pro-inflammatory cytokines, but not of IL-10. This combination could result in pathology and may account for some of the deleterious effects of ZIKV infection during pregnancy.

DENV2 was not able to induce the expression of pro-inflammatory cytokines to the same levels as ZIKV, a difference that may be associated with lower replication efficiency and consequent lower stimulation of the immune system.

ZIKV-infected placental explants undergo apoptosis

To investigate whether ZIKV-induced replication, inflammation, and injury would result in cell death, we performed TUNEL assays 3 days after ZIKV infection to determine whether the explanted tissue underwent apoptosis (Fig. 5). DNase treatment was used as a positive control (Fig. 5a), while untreated, uninfected explants were used as negative control (Fig. 5b). ZIKV-BR-infected samples demonstrated prominent TUNEL staining, which appeared to be quantitatively comparable to the positive control sample (Fig. 5c). DENV infection resulted in lower TUNEL staining (Fig. 5d), which corroborates previous H&E data indicating that DENV2 causes less placental damage in this model.

Apoptosis was further confirmed by immunohistochemistry with cleaved caspase-3 antibodies. ZIKV-BR and DENV2 exhibited increased cleaved caspase 3 staining relative to the uninfected control, which is indicative of apoptotic cell death (Fig. 6a-f). Cleaved caspase 3 expression was higher in ZIKV-infected cultures than in DENV-infected cultures (Fig. 6h). Immunostaining was performed, and the stain was found to cover the

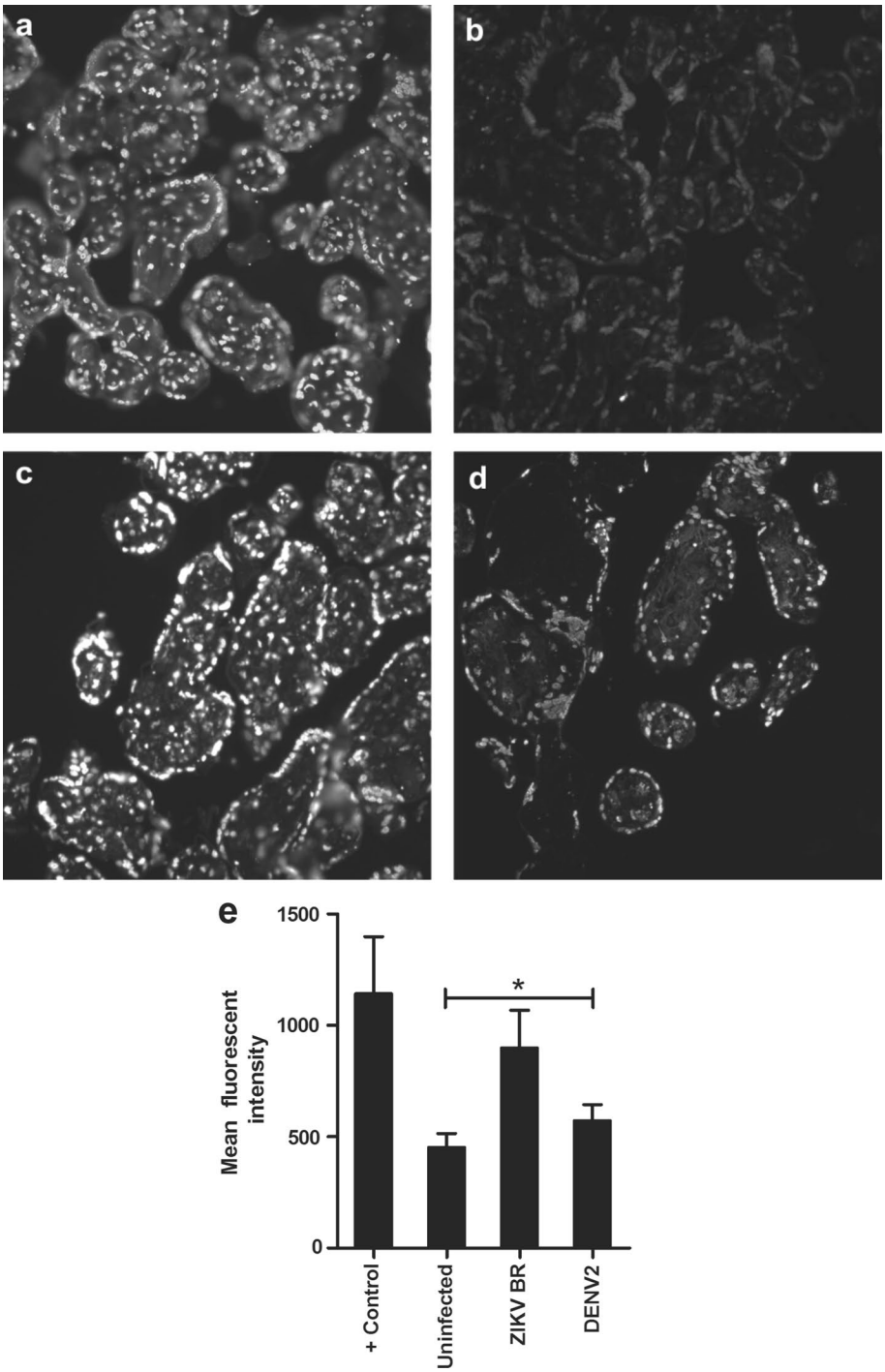

Fig. 5 Evaluation of ZIKV-induced apoptosis in placental explants measured by TUNEL assay. Infected explants on day 3 postinfection and uninfected explants were analyzed by TUNEL assay. Panel **a** represents the DNase-I-treated positive reaction control sample. Panel **b** represents the uninfected sample (control). TUNEL staining of placenta villi sections of ZIKV-BR (**c**) and DENV2-infected (**d**) tissue are shown. The images of TUNEL-positive cells were obtained at a magnification of 40x using an Olympus BX53 microscope system. Quantification was performed by measuring image intensity using Image-Pro® Plus software, version 7.0. One-way ANOVA and the Bonferroni correction were performed to determine statistical significance (*, $p < 0.05$; confidence interval, 95%)

chorionic villi. This result suggests that SCTs may be susceptible to apoptosis via active caspase-3 in ZIKV infections. SCTs cover chorionic villi and play a key role in the innate immune response and recruitment of NK cells [25]. Accordingly, previous studies that have investigated ZIKV tropism in several placental cell types have found ZIKV replication to be associated with abnormal tissue architecture, which could lead to the rupture of the placental barrier [16].

Cleaved-caspase-mediated apoptosis may result from an enhanced inflammatory response, such as the response involved in the TNF-α-TNFR signaling pathway. Because we detected increased expression of TNF-α in placental explants infected with ZIKV, we decided to investigate whether the observed apoptosis could be mediated by this cytokine. ZIKV-infected explants were treated with anti-TNF RII/TNFRSF1B neutralizing antibody, and cleaved caspase-3 activation was evaluated using IHC. Indeed,

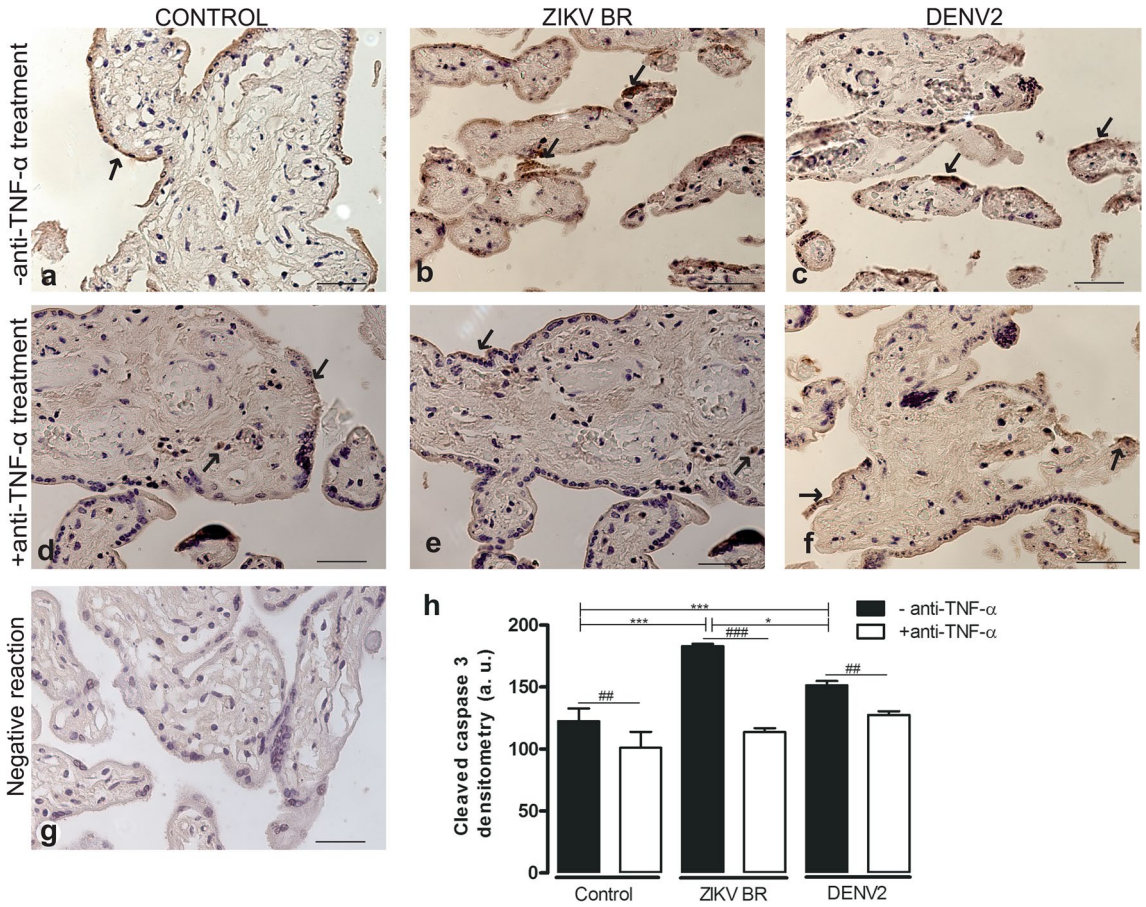

Fig. 6 ZIKV and DENV2 induce caspase-3 activation. Sections were stained with cleaved caspase-3 (**a-f**), as indicated by black arrows. Sections of uninfected samples (control) (**a**), ZIKV-infected tissues (**b**), and DENV2-infected tissues (**c**) are shown. Panels **d**-**f** show sections of uninfected samples (**d**) and ZIKV- or DENV2-infected explants treated with the anti-TNF-α antibody (panels **e** and **f** respectively). Panel **g** shows negative reaction controls in the absence of primary antibodies. Panel **k** shows the quantification densitometry analysis of cleaved caspase-3, which was performed using an Axioskop 2-Mot Plus Microscope (Carl Zeiss, Jena, Germany). AxioVision software was used for the qualitative analysis. One-Way ANOVA was performed to compare untreated groups (controls) to infected groups (*, $p < 0.01$; ***, $p < 0.001$). Two-way ANOVA was performed to compare treated groups to untreated groups with anti-TNF-α antibody ($^{###}$, $p < 0.001$). Scale bar: 10 μm

the anti-TNFR treatment significantly reduced cleaved caspase-3 staining, indicating that TNF-α-mediated apoptosis plays a significant role in tissue damage (Fig. 6d-f). TNFR neutralization also reduced cleaved caspase-3 staining in DENV-infected cultures, suggesting that both viruses are able to induce apoptosis, although lesion extension was found to be more severe when the tissues were infected with ZIKV. Some cell death was still observed after anti-TNFR treatment, suggesting that other mechanisms may also be involved in ZIKV-induced tissue damage. Previous studies have demonstrated that ZIKV infection in human neural progenitors (hNPCs) promotes increased caspase-3 expression, even in the presence of low levels of viral antigens [23]. These findings suggest that this pathway may be induced by ZIKV in different cell types and may be a relevant mechanism associated with congenital abnormalities.

We conclude that our placental tissue explant model is a valuable tool for the study of ZIKV interaction with the human placenta. We observed that placental explants are permissive to and support ZIKV and DENV2 infections for up to 120 hours. Because ZIKV is pathogenic to the human placenta, infected placental explants are amenable to different types of analysis and may therefore serve as a model in future research. Importantly, this model reinforces some critical observations made regarding ZIKV infection in other model systems and in patients [45, 49]. Due to its use of human placentas, this model provides crucial information to be applied to the clinical management of ZIKV infection, as well as to the development of preventive or therapeutic strategies against the deleterious effects of ZIKV on human embryos.

Acknowledgements The authors gratefully acknowledge the Brazilian National Institute of Science and Technology for Dengue Studies (INCT em Dengue), the São Paulo Research Foundation (FAPESP; Grant No. 2013/21719-3 to MLN) and the Brazilian National Research Council (CAPES) for their financial support.

Author contributions MRR and JBM performed the experiments, MRR, JBM, REM, PR, LBA, AN, SMO and MLN analyzed the data, MPP, LMM and LBA contributed reagents/materials/analysis tools, MRR, REM, LBA, SMO, AN and MLN wrote the paper, and PR, LBA, AHO, DMVO, SMO, AN and MLN planned the experiments.

References

1. Adams Waldorf KM, Stencel-Baerenwald JE, Kapur RP, Studholme C, Boldenow E, Vornhagen J, Baldessari A, Dighe MK, Thiel J, Merillat S, Armistead B, Tisoncik-Go J, Green RR, Davis MA, Dewey EC, Fairgrieve MR, Gatenby JC, Richards T, Garden GA, Diamond MS, Juul SE, Grant RF, Kuller L, Shaw DW, Ogle J, Gough GM, Lee W, English C, Hevner RF, Dobyns WB, Gale M, Rajagopal L (2016) Fetal brain lesions after subcutaneous inoculation of Zika virus in a pregnant nonhuman primate. Nat Med 22:1256–1259
2. Aliota MT, Caine EA, Walker EC, Larkin KE, Camacho E, Osorio JE (2016) Correction: Characterization of lethal Zika virus infection in AG129 mice. PLoS Negl Trop Dis 10:e0004750
3. Bayer A, Lennemann NJ, Ouyang Y, Bramley JC, Morosky S, Marques ET, Cherry S, Sadovsky Y, Coyne CB (2016) Type III interferons produced by human placental trophoblasts confer protection against Zika virus infection. Cell Host Microbe 19:705–712
4. Beckham JD, Pastula DM, Massey A, Tyler KL (2016) Zika virus as an emerging global pathogen: neurological complications of Zika virus. JAMA Neurol 73:875–879
5. Bowen JR, Quicke KM, Maddur MS, O'Neal JT, McDonald CE, Fedorova NB, Puri V, Shabman RS, Pulendran B, Suthar MS (2017) Zika virus antagonizes type I interferon responses during infection of human dendritic cells. PLoS Pathog 13:e1006164
6. Brey EM, Lalani Z, Johnston C, Wong M, McIntire LV, Duke PJ, Patrick CW (2003) Automated selection of DAB-labeled tissue for immunohistochemical quantification. J Histochem Cytochem 51:575–584
7. Calvet G, Aguiar RS, Melo AS, Sampaio SA, de Filippis I, Fabri A, Araujo ES, de Sequeira PC, de Mendonça MC, de Oliveira L, Tschoeke DA, Schrago CG, Thompson FL, Brasil P, Dos Santos FB, Nogueira RM, Tanuri A, de Filippis AM (2016) Detection and sequencing of Zika virus from amniotic fluid of fetuses with microcephaly in Brazil: a case study. Lancet Infect Dis 16:653–660
8. Carpentier PA, Dingman AL, Palmer TD (2011) Placental TNF-α signaling in illness-induced complications of pregnancy. Am J Pathol 178:2802–2810
9. Carteaux G, Maquart M, Bedet A, Contou D, Brugières P, Fourati S, Cleret de Langavant L, de Broucker T, Brun-Buisson C, Leparc-Goffart I, Mekontso Dessap A (2016) Zika virus associated with meningoencephalitis. N Engl J Med 374:1595–1596
10. Chaudhary V, Yuen KS, Chan JF, Chan CP, Wang PH, Cai JP, Zhang S, Liang M, Kok KH, Yuen KY, Jin DY (2017) Selective activation of type II interferon signaling by Zika virus NS5 protein. J Virol 91:e00163-17
11. Chutinimitkul S, Payungporn S, Theamboonlers A, Poovorawan Y (2005) Dengue typing assay based on real-time PCR using SYBR Green I. J Virol Methods 129:8–15
12. Corry J, Arora N, Good CA, Sadovsky Y, Coyne CB (2017) Organotypic models of type III interferon-mediated protection from Zika virus infections at the maternal–fetal interface. Proc Natl Acad Sci USA 114:9433–9438
13. Coyne CB, Lazear HM (2016) Zika virus—reigniting the TORCH. Nat Rev Microbiol 14:707–715
14. Cugola FR, Fernandes IR, Russo FB, Freitas BC, Dias JL, Guimarães KP, Benazzato C, Almeida N, Pignatari GC, Romero S, Polonio CM, Cunha I, Freitas CL, Brandão WN, Rossato C, Andrade DG, DeP Faria, Garcez AT, Buchpigel CA, Braconi CT, Mendes E, Sall AA, Zanotto PM, Peron JP, Muotri AR, Beltrão-Braga PC (2016) The Brazilian Zika virus strain causes birth defects in experimental models. Nature 534:267–271
15. Derricott H, Heazell AEP, Greenwood SL, Jones RL (2017) A novel in vitro model of villitis of unknown etiology demonstrates altered placental hormone and cytokine profile. Am J Reprod Immunol. https://doi.org/10.1111/aji.12725
16. El Costa H, Gouilly J, Mansuy JM, Chen Q, Levy C, Cartron G, Veas F, Al-Daccak R, Izopet J, Jabrane-Ferrat N (2016) ZIKA virus reveals broad tissue and cell tropism during the first trimester of pregnancy. Sci Rep 6:35296
17. Elovitz MA, Mrinalini C, Sammel MD (2006) Elucidating the early signal transduction pathways leading to fetal brain injury in preterm birth. Pediatr Res 59:50–55
18. Faria NR, Azevedo RDSD, Kraemer MUG, Souza R, Cunha MS, Hill SC, Thézé J, Bonsall MB, Bowden TA, Rissanen I, Rocco IM, Nogueira JS, Maeda AY, Vasami FGDS, Macedo FLL, Suzuki A, Rodrigues SG, Cruz ACR, Nunes BT, Medeiros DBA, Rodrigues DSG, Queiroz ALN, da Silva EVP, Henriques DF, da Rosa EST, de Oliveira CS, Martins LC, Vasconcelos HB, Casseb LMN, Simith DB, Messina JP, Abade L, Lourenço J, Alcantara LCJ, de Lima MM, Giovanetti M, Hay SI, de Oliveira RS, Lemos PDS, de Oliveira LF, de Lima CPS, da Silva SP, de Vasconcelos JM, Franco L, Cardoso JF, Vianez-Júnior JLDS, Mir D, Bello G, Delatorre E, Khan K, Creatore M, Coelho GE, de Oliveira WK, Tesh R, Pybus OG, Nunes MRT, Vasconcelos PFC (2016) Zika virus in the Americas: early epidemiological and genetic findings. Science 352:345–349
19. Fettke F, Schumacher A, Canellada A, Toledo N, Bekeredjian-Ding I, Bondt A, Wuhrer M, Costa SD, Zenclussen AC (2016) Maternal and fetal mechanisms of B cell regulation during pregnancy: human chorionic gonadotropin stimulates B cells to produce IL-10 while alpha-fetoprotein drives them into apoptosis. Front Immunol 7:495
20. Frank C, Cadar D, Schlaphof A, Neddersen N, Günther S, Schmidt-Chanasit J, Tappe D (2016) Sexual transmission of Zika virus in Germany, April 2016. Euro Surveill. https://doi.org/10.2807/1560-7917.ES.2016.21.23.30252
21. Fréour T, Mirallié S, Hubert B, Splingart C, Barrière P, Maquart M, Leparc-Goffart I (2016) Sexual transmission of Zika virus in an entirely asymptomatic couple returning from a Zika epidemic area, France, April 2016. Euro Surveill. https://doi.org/10.2807/1560-7917.ES.2016.21.23.30254
22. Garcia-Ruíz G, Flores-Espinosa P, Preciado-Martínez E, Bermejo-Martínez L, Espejel-Nuñez A, Estrada-Gutierrez G, Maida-Claros R, Flores-Pliego A, Zaga-Clavellina V (2015) In vitro progesterone modulation on bacterial endotoxin-induced production of IL-1β, TNFα, IL-6, IL-8, IL-10, MIP-1α, and MMP-9 in pre-labor human term placenta. Reprod Biol Endocrinol 13:115
23. Ghouzzi VE, Bianchi FT, Molineris I, Mounce BC, Berto GE, Rak M, Lebon S, Aubry L, Tocco C, Gai M, Chiotto AM, Sgrò F, Pallavicini G, Simon-Loriere E, Passemard S, Vignuzzi M, Gressens P, Di Cunto F (2016) ZIKA virus elicits P53 activation and

genotoxic stress in human neural progenitors similar to mutations involved in severe forms of genetic microcephaly and p53. Cell Death Dis 7:e2440
24. Girard S, Heazell AE, Derricott H, Allan SM, Sibley CP, Abrahams VM, Jones RL (2014) Circulating cytokines and alarmins associated with placental inflammation in high-risk pregnancies. Am J Reprod Immunol 72:422–434
25. Giugliano S, Petroff MG, Warren BD, Jasti S, Linscheid C, Ward A, Kramer A, Dobrinskikh E, Sheiko MA, Gale M, Golden-Mason L, Winn VD, Rosen HR (2015) Hepatitis C virus sensing by human trophoblasts induces innate immune responses and recruitment of maternal NK cells: potential implications for limiting vertical transmission. J Immunol 195:3737–3747
26. Gomes CP, Torloni MR, Gueuvoghlanian-Silva BY, Alexandre SM, Mattar R, Daher S (2013) Cytokine levels in gestational diabetes mellitus: a systematic review of the literature. Am J Reprod Immunol 69:545–557
27. Hamel R, Dejarnac O, Wichit S, Ekchariyawat P, Neyret A, Luplertlop N, Perera-Lecoin M, Surasombatpattana P, Talignani L, Thomas F, Cao-Lormeau VM, Choumet V, Briant L, Desprès P, Amara A, Yssel H, Missé D (2015) Biology of Zika virus infection in human skin cells. J Virol 89:8880–8896
28. Hamilton ST, Scott G, Naing Z, Iwasenko J, Hall B, Graf N, Arbuckle S, Craig ME, Rawlinson WD (2012) Human cytomegalovirus-induces cytokine changes in the placenta with implications for adverse pregnancy outcomes. PLoS One 7:e52899
29. Hamming OJ, Terczyńska-Dyla E, Vieyres G, Dijkman R, Jørgensen SE, Akhtar H, Siupka P, Pietschmann T, Thiel V, Hartmann R (2013) Interferon lambda 4 signals via the IFNλ receptor to regulate antiviral activity against HCV and coronaviruses. EMBO J 32:3055–3065
30. Heazell AE, Buttle HR, Baker PN, Crocker IP (2008) Altered expression of regulators of caspase activity within trophoblast of normal pregnancies and pregnancies complicated by preeclampsia. Reprod Sci 15:1034–1043
31. Helige C, Ahammer H, Hammer A, Huppertz B, Frank HG, Dohr G (2008) Trophoblastic invasion in vitro and in vivo: similarities and differences. Hum Reprod 23:2282–2291
32. Itinteang T, Tan ST, Guthrie S, Tan CE, McIntyre BC, Brasch HD, Day DJ (2011) A placental chorionic villous mesenchymal core cellular origin for infantile haemangioma. J Clin Pathol 64:870–874
33. Kotenko SV, Gallagher G, Baurin VV, Lewis-Antes A, Shen M, Shah NK, Langer JA, Sheikh F, Dickensheets H, Donnelly RP (2003) IFN-lambdas mediate antiviral protection through a distinct class II cytokine receptor complex. Nat Immunol 4:69–77
34. Kurman RJ, Young RH, Norris HJ, Main CS, Lawrence WD, Scully RE (1984) Immunocytochemical localization of placental lactogen and chorionic gonadotropin in the normal placenta and trophoblastic tumors, with emphasis on intermediate trophoblast and the placental site trophoblastic tumor. Int J Gynecol Pathol 3:101–121
35. Lanciotti RS, Kosoy OL, Laven JJ, Velez JO, Lambert AJ, Johnson AJ, Stanfield SM, Duffy MR (2008) Genetic and serologic properties of Zika virus associated with an epidemic, Yap state, micronesia, 2007. Emerg Infect Dis 14:1232–1239
36. Lash GE, Otun HA, Innes BA, Kirkley M, De Oliveira L, Searle RF, Robson SC, Bulmer JN (2006) Interferon-gamma inhibits extravillous trophoblast cell invasion by a mechanism that involves both changes in apoptosis and protease levels. FASEB J 20:2512–2518
37. Lazear HM, Govero J, Smith AM, Platt DJ, Fernandez E, Miner JJ, Diamond MS (2016) A mouse model of Zika virus pathogenesis. Cell Host Microbe 19:720–730
38. Lee HC, Narayanan S, Park SJ, Seong SY, Hahn YS (2014) Transcriptional regulation of IFN-λ genes in hepatitis C virus-infected hepatocytes via IRF-3·IRF-7·NF-κB complex. J Biol Chem 289:5310–5319
39. Leisser C, Saleh L, Haider S, Husslein H, Sonderegger S, Knöfler M (2006) Tumour necrosis factor-alpha impairs chorionic gonadotrophin beta-subunit expression and cell fusion of human villous cytotrophoblast. Mol Hum Reprod 12:601–609
40. Librach CL, Feigenbaum SL, Bass KE, Cui TY, Verastas N, Sadovsky Y, Quigley JP, French DL, Fisher SJ (1994) Interleukin-1 beta regulates human cytotrophoblast metalloproteinase activity and invasion in vitro. J Biol Chem 269:17125–17131
41. Malkki H (2016) CNS infections: mouse studies confirm the link between Zika virus infection and microcephaly. Nat Rev Neurol 12:369
42. McEwan M, Lins RJ, Munro SK, Vincent ZL, Ponnampalam AP, Mitchell MD (2009) Cytokine regulation during the formation of the fetal–maternal interface: focus on cell–cell adhesion and remodelling of the extra-cellular matrix. Cytokine Growth Factor Rev 20:241–249
43. Meager A, Visvalingam K, Dilger P, Bryan D, Wadhwa M (2005) Biological activity of interleukins-28 and -29: comparison with type I interferons. Cytokine 31:109–118
44. Melo AS, Aguiar RS, Amorim MM, Arruda MB, Melo FO, Ribeiro ST, Batista AG, Ferreira T, Dos Santos MP, Sampaio VV, Moura SR, Rabello LP, Gonzaga CE, Malinger G, Ximenes R, de Oliveira-Szejnfeld PS, Tovar-Moll F, Chimelli L, Silveira PP, Delvechio R, Higa L, Campanati L, Nogueira RM, Filippis AM, Szejnfeld J, Voloch CM, Ferreira OC, Brindeiro RM, Tanuri A (2016) Congenital Zika virus infection: beyond neonatal microcephaly. JAMA Neurol 73:1407–1416
45. Miner JJ, Cao B, Govero J, Smith AM, Fernandez E, Cabrera OH, Garber C, Noll M, Klein RS, Noguchi KK, Mysorekar IU, Diamond MS (2016) Zika virus infection during pregnancy in mice causes placental damage and fetal demise. Cell 165:1081–1091
46. Mlakar J, Korva M, Tul N, Popović M, Poljšak-Prijatelj M, Mraz J, Kolenc M, Resman Rus K, Vesnaver Vipotnik T, Fabjan Vodušek V, Vizjak A, Pižem J, Petrovec M, Avšič Županc T (2016) Zika virus associated with microcephaly. N Engl J Med 374:951–958
47. Moser G, Gauster M, Orendi K, Glasner A, Theuerkauf R, Huppertz B (2010) Endoglandular trophoblast, an alternative route of trophoblast invasion? Analysis with novel confrontation co-culture models. Hum Reprod 25:1127–1136
48. Musso D, Gubler DJ (2016) Zika Virus. Clin Microbiol Rev 29:487–524
49. Noronha L, Zanluca C, Azevedo ML, Luz KG, Santos CN (2016) Zika virus damages the human placental barrier and presents marked fetal neurotropism. Mem Inst Oswaldo Cruz 111:287–293
50. Onoguchi K, Yoneyama M, Takemura A, Akira S, Taniguchi T, Namiki H, Fujita T (2007) Viral infections activate types I and III interferon genes through a common mechanism. J Biol Chem 282:7576–7581
51. Otun HA, Lash GE, Innes BA, Bulmer JN, Naruse K, Hannon T, Searle RF, Robson SC (2011) Effect of tumour necrosis factor-α in combination with interferon-γ on first trimester extravillous trophoblast invasion. J Reprod Immunol 88:1–11
52. Pacanowski M, Amur S, Zineh I (2012) New genetic discoveries and treatment for hepatitis C. JAMA 307:1921–1922
53. Panchaud A, Stojanov M, Ammerdorffer A, Vouga M, Baud D (2016) Emerging role of Zika virus in adverse fetal and neonatal outcomes. Clin Microbiol Rev 29:659–694
54. Pantoja P, Pérez-Guzmán EX, Rodríguez IV, White LJ, González O, Serrano C, Giavedoni L, Hodara V, Cruz L, Arana T, Martínez MI, Hassert MA, Brien JD, Pinto AK, de Silva A, Sariol CA (2017) Zika virus pathogenesis in rhesus macaques is unaffected by pre-existing immunity to dengue virus. Nat Commun 8:15674
55. Pontillo A, Girardelli M, Agostinis C, Masat E, Bulla R, Crovella S (2013) Bacterial LPS differently modulates inflammasome gene

expression and IL-1β secretion in trophoblast cells, decidual stromal cells, and decidual endothelial cells. Reprod Sci 20:563–566
56. Quicke KM, Bowen JR, Johnson EL, McDonald CE, Ma H, O'Neal JT, Rajakumar A, Wrammert J, Rimawi BH, Pulendran B, Schinazi RF, Chakraborty R, Suthar MS (2016) Zika virus infects human placental macrophages. Cell Host Microbe 20:83–90
57. Rabaan AA, Bazzi AM, Al-Ahmed SH, Al-Ghaith MH, Al-Tawfiq JA (2017) Overview of Zika infection, epidemiology, transmission and control measures. J Infect Public Health 10:141–149
58. Raghupathy R, Kalinka J (2008) Cytokine imbalance in pregnancy complications and its modulation. Front Biosci 13:985–994
59. Rossi SL, Tesh RB, Azar SR, Muruato AE, Hanley KA, Auguste AJ, Langsjoen RM, Paessler S, Vasilakis N, Weaver SC (2016) Characterization of a novel murine model to study Zika virus. Am J Trop Med Hyg 94:1362–1369
60. Roth I, Corry DB, Locksley RM, Abrams JS, Litton MJ, Fisher SJ (1996) Human placental cytotrophoblasts produce the immunosuppressive cytokine interleukin 10. J Exp Med 184:539–548
61. Roth I, Fisher SJ (1999) IL-10 is an autocrine inhibitor of human placental cytotrophoblast MMP-9 production and invasion. Dev Biol 205:194–204
62. Siwetz M, Blaschitz A, El-Heliebi A, Hiden U, Desoye G, Huppertz B, Gauster M (2016) TNF-α alters the inflammatory secretion profile of human first trimester placenta. Lab Invest 96:428–438
63. Tabata T, Petitt M, Puerta-Guardo H, Michlmayr D, Wang C, Fang-Hoover J, Harris E, Pereira L (2016) Zika virus targets different primary human placental cells, suggesting two routes for vertical transmission. Cell Host Microbe 20:155–166
64. Turmel JM, Abgueguen P, Hubert B, Vandamme YM, Maquart M, Le Guillou-Guillemette H, Leparc-Goffart I (2016) Late sexual transmission of Zika virus related to persistence in the semen. Lancet 387:2501
65. Vargas-Rojas MI, Solleiro-Villavicencio H, Soto-Vega E (2016) Th1, Th2, Th17 and Treg levels in umbilical cord blood in preeclampsia. J Matern Fetal Neonatal Med 29:1642–1645
66. Vermillion MS, Lei J, Shabi Y, Baxter VK, Crilly NP, McLane M, Griffin DE, Pekosz A, Klein SL, Burd I (2017) Intrauterine Zika virus infection of pregnant immunocompetent mice models transplacental transmission and adverse perinatal outcomes. Nat Commun 8:14575
67. Vićovac L, Jones CJ, Aplin JD (1995) Trophoblast differentiation during formation of anchoring villi in a model of the early human placenta in vitro. Placenta 16:41–56
68. Vorou R (2016) Zika virus, vectors, reservoirs, amplifying hosts, and their potential to spread worldwide: what we know and what we should investigate urgently. Int J Infect Dis 48:85–90
69. Wikan N, Smith DR (2016) Zika virus: history of a newly emerging arbovirus. Lancet Infect Dis 16:e119–e126
70. Wilczyński JR, Tchórzewski H, Banasik M, Głowacka E, Wieczorek A, Lewkowicz P, Malinowski A, Szpakowski M, Wilczyński J (2003) Lymphocyte subset distribution and cytokine secretion in third trimester decidua in normal pregnancy and preeclampsia. Eur J Obstet Gynecol Reprod Biol 109:8–15
71. Winkler CW, Woods TA, Rosenke R, Scott DP, Best SM, Peterson KE (2017) Sexual and vertical transmission of Zika virus in anti-interferon receptor-treated Rag1-deficient mice. Sci Rep 7:7176
72. Wu KY, Zuo GL, Li XF, Ye Q, Deng YQ, Huang XY, Cao WC, Qin CF, Luo ZG (2016) Vertical transmission of Zika virus targeting the radial glial cells affects cortex development of offspring mice. Cell Res 26:645–654